

Epithelial Cell-Specific Induction of Activating Transcription Factor 6
Signaling Promotes Intestinal Dysbiosis and Colonic Tumorigenesis

Elena M. Lobner

Vollständiger Abdruck der von der Fakultät Wissenschaftszentrum Weihenstephan
für Ernährung, Landnutzung und Umwelt der Technischen Universität München
zur Erlangung des akademischen Grades eines

Doktors der Naturwissenschaften

genehmigten Dissertation.

Vorsitzende/-r: Prof. Dr. Martin Klingenspor

Prüfende/-r der Dissertation:

1. Prof. Dr. Dirk Haller

2. Prof. Dr. Mathias Heikenwälder

Die Dissertation wurde am 19.12.2017 bei der Technischen Universität München
eingereicht und durch die Fakultät Wissenschaftszentrum Weihenstephan für Ernährung,
Landnutzung und Umwelt am 04.05.2018 angenommen.

ZUSAMMENFASSUNG

Der Begriff “unfolded protein response” (UPR) beschreibt konservierte Signalwege, die wichtig sind für die zelluläre Anpassung an eine gestörte Proteinfaltung und entscheidend für die Zellfunktion sind. Im Darmepithel trägt die Aktivierung der endoplasmatischen Retikulum (ER) UPR zur Pathogenese von Chronisch-entzündlichen Darmerkrankungen (CED) bei. Außerdem könnte die ER UPR das Risiko für Dickdarmkrebs erhöhen. Allerdings gibt es bisher nur begrenzte Beweise dafür, dass die ER UPR direkt zur onkogenen Transformation beiträgt. Gegenstand dieser Doktorarbeit ist, ob eine epithelzellspezifische Aktivierung des „Activating transcription factor 6“ (ATF6), als einem der Hauptvermittler der ER UPR, die Tumorentstehung im Darm begünstigt.

Um die Bedeutung der ATF6-vermittelten ER UPR im Rahmen von Darmkrebs zu erforschen, untersucht meine Arbeit sowohl genetische Veränderungen von ATF6 als auch die Proteinmenge von ATF6 im Darm von Patienten. Dabei zeigte sich eine signifikante Assoziation beider Parameter mit einer schlechten Verlaufsprognose. Um den Effekt einer Aktivierung von ATF6 auf das Darmepithel genauer zu untersuchen, wurde ein neues Mausmodell am Lehrstuhl für Ernährung und Immunologie (Technische Universität München) entwickelt. Diese *nATF6^{IEC}* Maus exprimiert die aktivierte Form von ATF6 (nATF6) spezifisch in Darmepithelzellen durch Villin-Cre vermittelte Rekombination und wurde im Rahmen dieser Promotion erforscht. Dabei zeigte sich die spontane Bildung von Adenomen im Dickdarm von *nATF6^{IEC}* Mäusen, die das Transgen homozygot (tg/tg) exprimieren. Das Auftreten von Tumoren war entzündungsunabhängig und wurde im Alter von 12 Wochen mit einer Inzidenz von 100% beobachtet. Ein signifikanter Verlust mukusgefüllter Becherzellen korrelierte mit einer erhöhten mikrobiellen Durchlässigkeit der Mukus-Schicht. Auffällig waren außerdem mittels 16S rRNA Gen Sequenzierung detektierte Veränderungen der zäkalen Mikrobiota. Die Tumorentstehung und erhöhte Zellteilung konnte sowohl durch Keimfreihaltung als auch durch Antibiotikabehandlung verhindert werden. Umgekehrt induzierte die Assoziierung keimfreier *nATF6^{IEC}* tg/tg Mäuse mit einer präkonditionierten Mikrobiota Dickdarntumore, was den Beitrag mikrobieller Signale zur Entstehung von Darmtumoren unterstreicht. In heterozygoten *nATF6^{IEC}* Mäusen konnte die Tumorentstehung durch die Induktion intestinaler Entzündung ausgelöst werden, was dafür spricht, dass eine Aktivierung von ATF6 auch unter entzündlichen Bedingungen die Tumorgenese fördern kann.

Das *nATF6^{IEC}* Mausmodell liefert wichtige Hinweise darauf, dass eine ATF6 Aktivierung im Darmepithel im Zusammenspiel mit mikrobiellen Signalen die Tumorentstehung fördert. Im Menschen könnte die ATF6-vermittelte ER UPR Aktivierung in Darmepithelzellen einen entzündungsunabhängigen Risikofaktor für die Entstehung von Dickdarmkrebs darstellen und als solcher auch bei CED Patienten eine wichtige Rolle spielen.

ABSTRACT

Unfolded protein responses (UPR) are conserved signaling pathways important for the dynamic adaptation of cells to factors disturbing protein folding and critical for cellular function. Activation of the endoplasmic reticulum (ER) UPR in intestinal epithelial cells (IEC) contributes to the pathogenesis of inflammatory bowel diseases (IBD). Further, it might increase the risk of developing colorectal cancer but the evidence for a direct involvement of ER UPR to oncogenic tissue transformation is limited. This study investigates whether IEC-specific activation of Activating transcription factor 6 (ATF6) as a major mediator of ER UPR promotes intestinal tumorigenesis.

To address the role of ATF6-mediated ER UPR signaling in intestinal disease, the genetic alteration frequency and expression level of ATF6 in colon cancer was analyzed in this thesis and demonstrated a significant association with bad prognosis. To study the effects of ATF6 signaling in more detail, a mouse model referred to as the *nATF6^{IEC}* model was generated at the Chair of Nutrition and Immunology (Technical University Munich). This mouse expresses the activated form of ATF6 (nATF6) specifically in IEC due to Villin-Cre mediated recombination and was investigated within this thesis. *nATF6^{IEC}* mice homozygous (tg/tg) for the transgene spontaneously developed colonic adenomas. This was independent of inflammation, with a tumor incidence of 100 % at 12 weeks of age. Loss of mucin-filled goblet cells was associated with increased microbial penetration of the mucus barrier. 16S rRNA gene sequencing of cecal microbiota revealed a clear separation of bacterial communities according to mouse genotype. Germ-free (GF) housing and antibiotic treatment were shown to prevent epithelial hyper-proliferation and tumor formation. Most importantly, the transfer of a pre-conditioned microbiota into GF recipients re-established the tumorigenic phenotype in *nATF6^{IEC} tg/tg* mice, clearly demonstrating a causal role of microbes in colonic adenoma formation. In heterozygous *nATF6^{IEC}* mice, the induction of inflammation promoted tumor formation, suggesting that ATF6 activation can foster tumorigenesis also under inflammatory conditions.

The *nATF6^{IEC}* model provides clear evidence that ATF6 activation in IEC together with microbial signals promotes tumorigenesis. With respect to human disease, ER UPR activation in IEC could constitute an inflammation-independent risk factor for the development of colorectal cancer, a mechanism which could also promote tumorigenesis in IBD patients.

TABLE OF CONTENTS

ZUSAMMENFASSUNG	I
ABSTRACT	II
TABLE OF CONTENTS	III
1. INTRODUCTION.....	1
1.1 Intestinal mucosal homeostasis - maintenance of exchange and separation	1
1.2 Unfolded protein responses – facilitators of proteostasis	7
1.3 Regulation of the ATF6 arm of ER UPR.....	12
1.4 Contribution of ER UPR to disease pathogenesis.....	15
1.4.1 UPR in intestinal inflammation	15
1.4.2 UPR in cancer	17
1.4.3 Specific contribution of ATF6 signaling to intestinal inflammation and tumorigenesis.....	21
2. STUDY OBJECTIVE	23
3. MATERIAL AND METHODS	24
3.1 Animal experiments, primary cell isolation and culture	24
3.1.1 Generation of the <i>nATF6</i> mouse model	24
3.1.2 Ethics statement, mouse breeding and housing	25
3.1.3 Mouse experiments.....	26
3.1.3.1 Dextran sodium sulfate (DSS)-induced colitis	26
3.1.3.2 Colonoscopy	26
3.1.3.3 Antibiotic treatment	27
3.1.3.4 Bacterial association	27
3.1.3.5 Tamoxifen-induction of nATF6 expression.....	27
3.1.3.6 Isolation of intestinal epithelial cells	28
3.1.3.7 Organoid culture and quantification	28
3.2 Histological methods.....	29
3.2.1 Histology and tissue staining.....	29
3.2.1.1 H&E staining	30

3.2.1.2 Alcian blue/Periodic acid-Schiff (AB/PAS) staining	30
3.2.1.3 High iron diamine-alcian blue (HID-AB) staining	31
3.2.2 Histopathological analysis.....	31
3.2.3 Immunocytochemistry	31
3.2.3.1 Immunohistochemical/-fluorescent stainings.....	31
3.2.3.2 Fluorescence in situ hybridization (FISH).....	33
3.2.4 Electron microscopy	34
3.2.5 Laser capture microdissection	34
3.3 Molecular biological methods	35
3.3.1 Genotyping.....	35
3.3.2 Gene expression analysis.....	36
3.3.3 16S rRNA Sequencing	38
3.3.4 Comparative genomic hybridization (CGH)	39
3.3.5 Western blot analysis	39
3.4 Human cohort	40
3.5 Statistical analysis	41
4. RESULTS.....	42
4.1 ATF6 in colon cancer	42
4.2 Validation and phenotypic description of constitutive <i>nATF6</i> ^{IEC} mice	45
4.2.1 Transgene expression and ER UPR activation in <i>nATF6</i> ^{IEC} mice	45
4.2.2 Intestinal tumor development and reduced survival in <i>nATF6</i> ^{IEC} tg/tg mice	50
4.3 Characterization of the intestine of <i>nATF6</i> ^{IEC} mice	52
4.3.1 Histopathological characterization of tumors as adenomas	52
4.3.2 Alterations in goblet cells and mucus barrier	54
4.3.3 Hyper-proliferative response of enterocytes.....	57
4.3.4 Endoplasmic reticulum dilatation in <i>nATF6</i> ^{IEC} mice.....	59
4.3.5 Intestinal inflammation as a late event of intestinal pathology	61

4.3.6 Effects of CHOP and RAG2 deficiency on tumor formation in <i>nATF6^{IEC}</i> mice	63
4.4 Impact of timing and mode of <i>nATF6</i> expression on intestinal phenotype	65
4.4.1 Presence of tumor development in <i>nATF6^{IEC-OHT}</i> tg/tg mice	65
4.4.2 Absence of tumor development in <i>nATF6</i> x LGR5-Cre ^{ERT2} tg/tg mice.....	67
4.5 Inflammation, wounding and microorganisms as modulators of intestinal tumorigenesis in <i>nATF6^{IEC}</i> mice	71
4.5.1 Increased tumor susceptibility of <i>nATF6^{IEC}</i> tg/wt mice in response to chronic DSS.....	71
4.5.2 Increased tumor susceptibility of <i>nATF6^{IEC}</i> tg/wt mice on the genetic <i>IL10^{-/-}</i> background...72	
4.5.3 Potential effect of mechanical stress on tumor formation.....	74
4.5.4 Bacterial signals as trigger for tumorigenesis in the genetically susceptible host.....	75
5. DISCUSSION	96
5.1 The <i>nATF6^{IEC}</i> mouse – a model to mimic ATF6-specific activation of UPR in IEC.....	97
5.2 The impact of <i>nATF6</i> expression on IEC function.....	98
5.3 Microbial triggers – a prerequisite for the development of intestinal tumors in the <i>nATF6^{IEC}</i> tg/tg mouse?	102
5.4 Conclusion and perspectives	110
6. APPENDIX	114
LIST OF FIGURES	VI
LIST OF TABLES	IX
LIST OF ABBREVIATIONS.....	X
REFERENCES	XII
ACKNOWLEDGEMENTS	XXVI
CURRICULUM VITAE.....	XXVII
PUBLICATIONS AND PRESENTATIONS.....	XXVIII
EIDESSTÄTTLICHE ERKLÄRUNG	XXX

1. INTRODUCTION

1.1 Intestinal mucosal homeostasis - maintenance of exchange and separation

The gastrointestinal tract is an organ system important for the digestive process including ingestion, digestion, absorption and defecation. The intestine, as part of the gastrointestinal tract, is compartmentalized in the small intestine comprising duodenum, jejunum and ileum and the large intestine comprising cecum, colon and rectum. The small intestine has major functions in digestion and absorption while the large intestine is mainly required for electrolyte and water resorption, fermentation and defecation. Nutrient and water exchange with the gut lumen is a major task of the digestive tract and facilitated by a large surface area which in average measures 32 square meters in humans [1]. The gut lumen is one of the densest microbial ecosystems of the human body. Thus, the intestinal interface is constantly confronted with diverse environmental conditions and functions as an important integrator of changes in microbial and metabolite profiles. Besides being responsible for absorption, the intestine needs to resist infection and inhibit microbial translocation across the tissue barrier. Therefore, the intestinal mucosal immune system continuously monitors the intestinal microbiota for the presence of pathogens and is at the same time alert and tolerant to commensals. The intestinal microbiota includes bacteria, archaea, viruses and eukaryotes (yeasts and protozoa) and their combined genomes are referred to as the microbiome [2]. The relative proportions within the intestinal microbiota vary between individuals and are modulated by various factors including age, geographic location and diet [3, 4]. The most dominant microorganisms in the human and murine intestine are bacteria of the phyla *Bacteroidetes* and *Firmicutes* [5, 6]. Further, *Proteobacteria*, *Actinobacteria*, *Verrucomicrobia* and *Fusobacteria* are frequently observed in adults but generally minor constituents [3, 7].

Due to the exposed nature of the intestinal interface, a balanced interaction between the microbiota and the host is critical for intestinal homeostasis and important for intestinal health (Figure 1). The term homeostasis was first described in 1926 by Walter Bradford Cannon [8] and can be defined as “*the maintenance of metabolic equilibrium within an animal by a tendency to compensate for disrupting changes*” [9]. The gut microbiota positively impacts on the host by extracting nutrients from the diet [10] and by producing vitamins [11]. Further, it affects the development and function of the immune system, the intestinal epithelium and its renewal [12-14]. Moreover the microbiota confers protection against pathogens and infection [15-17]. This is achieved by both non-immune-mediated pathways - like production of inhibitory molecules and competition for nutrients - and immune-derived pathways - like the stimulation of the adaptive and innate immune system [17]. The

host in turn provides a habitat and supports the microbiota by providing host-derived nutrients. This is for example evident for the mucus layer which is covering the intestinal surface and serves as a selective microbial habitat and nutrient source [18, 19]. The host further monitors the microbiota by pattern recognition receptors (PRR) [20, 21] and produces antimicrobial peptides (AMP). These AMPs are important to inhibit pathogen colonization and to restrain direct contact of commensal microbes with the epithelium [22-24]. Intestinal homeostasis is affected by the environment and relies on a balance within microbial communities, a balance of host functions and physiology and a balanced interaction of both microbiota and host. What exactly defines a health-promoting intestinal microbiota, also referred to as eubiosis? One of the most discussed factors is the composition of the intestinal microbiota. Though the composition varies significantly between individuals within populations, the intestinal microbiota seems to share a functional core microbiome [3]. A high resilience, plasticity and diversity are believed to be important for a health-promoting intestinal microbiota and to contribute to the control of pathogens [3-5, 25, 26]. Resilience describes the capacity of an ecosystem to recover from modulating perturbations and thus the capacity for self-regeneration. High resilience refers to the attribute of the microbiota to restore its equilibrium after an external perturbation, such as pharmacologic treatment or infection [26]. Studies using short-term controlled feeding further highlight the plasticity of the microbiota since diet can rapidly impact on bacterial groups [27, 28]. A microbiota which is characterized by a high species diversity is believed to be less susceptible to perturbation since well-adapted species out-compete the influx and overgrowth of other species [3, 26]. In contrast to a health-promoting microbiota, a dysbiotic microbiota is believed to contribute to various diseases including inflammatory bowel diseases. Dysbiosis describes a state of the intestinal microbial community which contributes to the manifestation of a disease or to its continuation by a loss of host-microbial balance which cannot be attributed to a single bacterial species [26].

Focusing on the host, a balance of intestinal functions and intestinal physiology depends on the efficient absorption of nutrients and water, the maintenance of an effective barrier and adequate immune regulation. In view of the high renewal rates of the intestine, the continuous intestinal development has to be synchronized with the intestinal functions and tightly controlled to maintain intestinal homeostasis [29]. Both the host and the intestinal microbiota are modulated by changes in environmental conditions. Alterations in food intake and food composition can *e.g.* impact on the microbial composition and the activity of the microbes [30]. Moreover, external influences, such as infection or antibiotic treatment, can promote a disequilibrium in the microbial community. These alterations can modify the availability of bacterial-derived nutrients resulting in metabolic changes or altered host transcription [13].

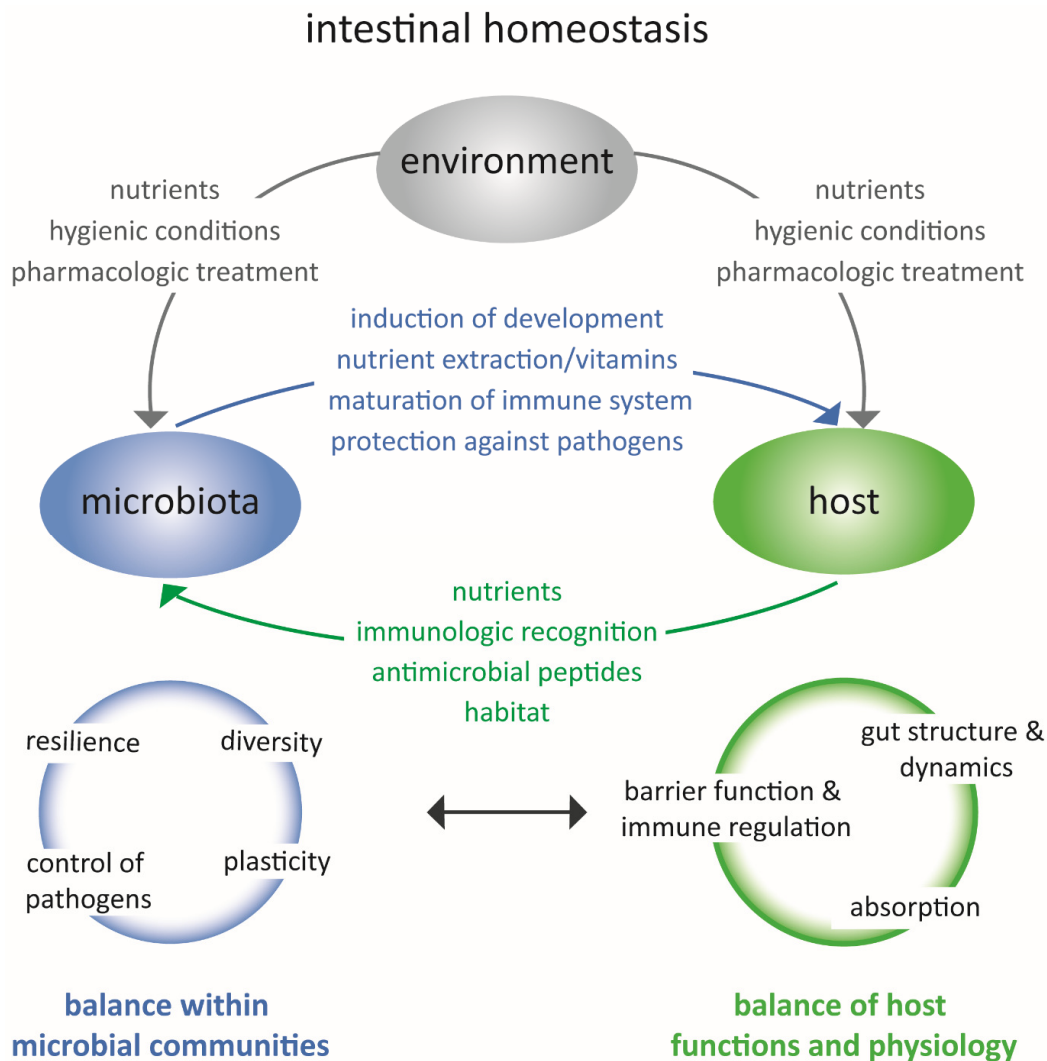


Figure 1: Intestinal homeostasis - an interplay between environment, microbiota and host.

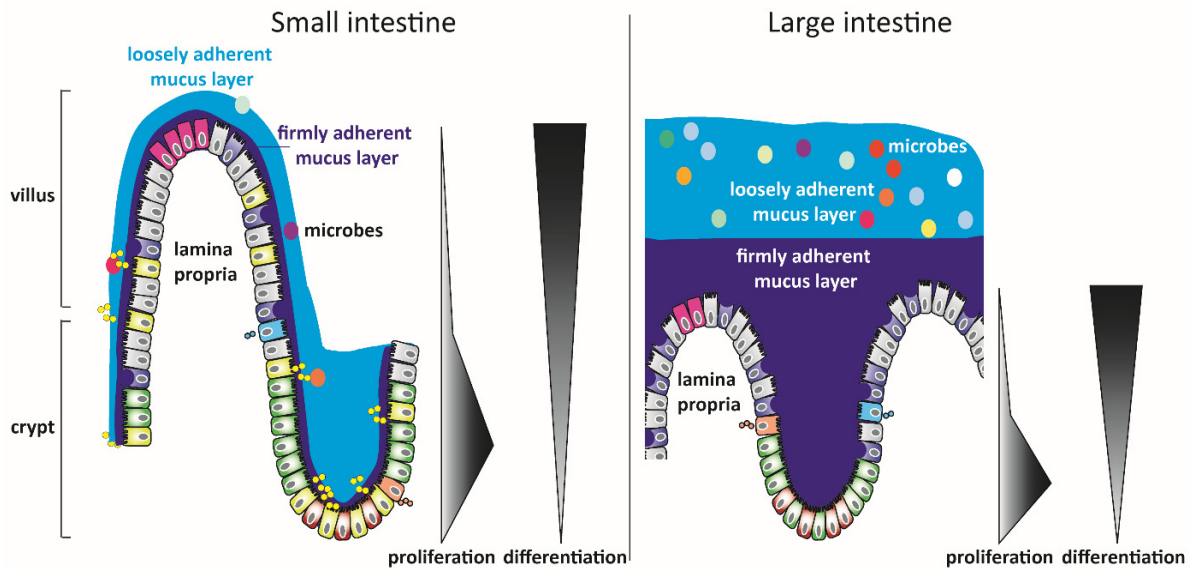
Intestinal homeostasis relies on a fine-tuned interaction between the host and the intestinal microbiota and is influenced by environmental conditions. The interaction between the environment, the microbiota and the host are reciprocal and changes can affect all players. Under homeostatic conditions, a balance within microbial communities and a balance of host functions and physiology allows for “healthy” host-microbial interactions.

To meet all the challenges mentioned before, the intestine is equipped with specialized cells which are integrated in the functional structure of the intestine. Anatomically, the intestine is structured into four layers: mucosa, submucosa, muscularis propria and serosa. The mucosa is the innermost layer and consists of three sheets. A single cell lining of columnar epithelial cells first facing the intestinal lumen attached to a basement membrane overlying the second sheet, the lamina propria, which consists of subepithelial connective tissue and lymph nodes. Underneath is the third sheet referred to as muscularis mucosae. This is a continuous sheet of smooth muscle cells that lies at the base of the lamina propria. The entire mucosa rests on the submucosa, with muscularis propria and serosa beneath [31]. The epithelium of both large and small intestine is folded in such a way to create the crypts of Lieberkühn, with the small intestine having additional finger-like projections

called villi to increase surface area for nutrient uptake. Intestinal epithelial cells (IEC) originate from crypt-based stem cells which give rise to rapidly dividing transit-amplifying cells (TA cells) (Figure 2) [29, 31]. These progenitor cells differentiate into the mature cell types of the epithelium. Upon differentiation, most epithelial cells migrate along the crypt-villus or crypt axis to finally exfoliate into the gut lumen, a process referred to as shedding. With the intestinal epithelium having among the highest mitotic rates in the body, the epithelium is completely renewed every 3-4 or 5-6 days in the small intestine or large intestine, respectively, with the exception of particular long-lived cells [29]. This process is highly dynamic and can be modulated by diverse factors including, amongst others, growth factors [32], luminal nutrition [33] and the intestinal microbiota [34]. The involvement of the microbiota as a modulator of host physiology is for instance evident by an overall reduced epithelial turnover in germ-free (GF) animals [35].

The differentiated cell types of the intestinal epithelium are highly specialized and comprise the most abundant absorptive enterocytes, the secretory Paneth and Goblet cells (GC), Tuft cells, Microfold (M)-cells and enteroendocrine cells (functions and features described in Figure 2). Of importance, numbers, stratification in subpopulations and roles of particular cell types are heterogeneous among the parts of the intestine, which itself reflects different functions of these anatomical structures [36]. Paneth cells for instance - which are important for the production of AMP in the small intestine - are absent from the healthy distal part of the large intestine [37], whereas the presence of goblet cells is more dominant in the large intestine compared to the small intestine. Further, enterocytes have different features according to their location: via striation with numerous actin-rich microvilli enterocytes of the small intestinal villus have a maximized surface area compared to large intestinal enterocytes. Of note, immunological properties of the different intestinal compartments are different as well. This is not only reflected by differences in immune cell composition but also by the presence of M-cells. These cells transcytose luminal particulate antigens to forward them to underlying immune cells. In the small intestine M-cells predominantly overlay Peyer's patches, which are specialized structures of gut-associated lymphoid tissue (GALT) important for immune surveillance [38]. In the colon M-cells are less abundant and are observed in association with isolated lymphoid follicles and colonic patches [39].

Intestinal function relies on both proper absorption and the preservation of a functional barrier to the gut microbiota, which harbors commensals and potential pathogens. Barrier function is achieved by physical, chemical and immunological measures. The separation between microbes and the mucosa aims to reduce the contact to a low number which can still be tolerated by the mucosal immune system and results in a response fine-balanced between tolerance and immune activation.



Symbol	Cell type	Function and Features
	Intestinal stem cell (ISC)	Regeneration of epithelium; long-lived, multipotent
	Transit amplifying (TA) cell	Renewal of epithelial cells; rapidly cycling cells originating from ISCs, differentiate after a finite number of cell divisions
	Enterocyte	Absorption (nutrients, water and bile acids), antigen uptake, processing and presentation
	Goblet cell (GC)	Mucus production; separation of bacteria and host
	Tuft cell	Taste-chemosensory cells suggested to be relevant for the defense against intestinal protozoa and helminth parasites
	Microfold (M)-cell	Phagocytosis and transcytosis of gut lumen (particulate antigens, macromolecules and microorganisms) across the epithelium; delivery to underlying lymphoid tissues (e.g. in Peyer's patches)
	Enteroendocrine cell	Production of gastrointestinal hormones, heterogeneous cells specialized for the secretion of specific hormones (e.g. L cells: glucagon-like peptide 1)
	Paneth cell	Release of antimicrobial substances (e.g. lysozyme, defensins)

Figure 2: Intestinal organization and cell types of intestinal epithelial cells.

The small and large intestine consists of a monolayer of specialized epithelial cells organized in villus-crypt or crypt-villus structures, respectively. Intestinal stem cells are found in the crypt base and give rise to transit amplifying (TA) cells. TA cells have high proliferative capacity and differentiate into specialized epithelial cells after limited rounds of proliferation. These differentiated cells are finally shed into the lumen at the villus tip and crypt top, respectively. The primary functions of the gut are absorption and maintenance of a semi-permeable barrier. Barrier is achieved by physicochemical (e.g. the mucus barrier mainly produced by goblet cells and antimicrobial peptides produced by Paneth cells) and immunological measures (e.g. immune exclusion via secretory IgA mediated by an interplay of M cells and Gut-associated lymphoid tissue).

The intestinal mucus layer serves as a physical as well as a chemical barrier. It can be considered as a three-dimensional hydrophobic matrix covering the intestinal lining composed of the heavily modified Mucin2 (Muc2) as the major structural component in the intestine. This glycoprotein,

among other factors, is produced and secreted by the highly secretory goblet cells, a mechanism which was shown to be under the control of Toll-like receptor recognition of bacterial ligands and inflammasome activation [12, 40]. Of note, the renewal of intestinal mucus even exceeds the rates of epithelial turnover, a mechanism which is suggested to be coupled to expulsion of luminal material [41]. The mucus is organized in two layers, one highly impermeable to bacteria covering the epithelium referred to as the firmly adherent mucus layer, and the loosely adherent mucus layer which serves as a habitat and nutrient source for mucus-adherent commensal bacteria [42] (Figure 2). Whereas the firmly adherent mucus layer is prominent in the large intestine and clearly separates bacteria from the epithelial surface, only a very minor layer is present in the small intestine. Thus, separation of bacteria in the small intestine relies primarily on peristalsis and the activity of antimicrobial peptides and proteins secreted by Paneth cells and enterocytes which are retained and concentrated in the penetrable mucus. The distinct properties of the mucus barrier in the small and large intestine is also evident by distinctive goblet cell subpopulations and differences in the modes of induction of mucus secretion [41].

In the healthy gut the monolayer of polarized IEC further defines a tight barrier for bacteria and macromolecules through close linkage via adherence and tight junction complexes composed of E-cadherin, junctional adhesion molecules, claudins, occludin and tricellulin [43]. As already addressed, the intestinal epithelial lining is permanently renewed, a mechanism which helps to prevent persistent bacterial colonization and thus contributes to expel colonized pathogens [44].

Specialized epithelia further facilitate the delivery of luminal antigen to intestinal lymphoid organs, which is specifically typical to M-cells but was also shown for goblet cells [38, 45], and transcytose secretory IgA (SIgA). SIgA are an additional component of the intestinal mucosal surface relevant for immune exclusion, a mechanism which helps to retain bacteria and toxins in the lumen by binding to them. SIgA are directed against specific mucosal antigens and delivered into the lumen by translocation through IEC via the epithelial polymeric immunoglobulin receptor. Their production is based on (1) the sampling by Peyer's patch M cells, (2) processing by antigen-presenting cells such as dendritic cells, (3) T-cell activation and (4) ultimately B-cell class switch recombination in the GALT [46, 47]. Epithelia are further important players in innate immune recognition through the expression of Pattern-recognition receptors (PRRs), comprising Toll like receptors (TLRs), RIG-I-like receptors and NOD-like receptors that can recognize evolutionary conserved structural motifs produced by microorganisms called pathogen-associated molecular patterns (PAMPs) [48]. Microbial recognition via PRRs was first shown to be important for gut homeostasis by studies of mice deficient in TLRs and signaling adaptors or depleted of key commensal microorganisms [20]. In addition to direct

recognition of conserved structural motifs, a conceptual framework is discussed suggesting that a disruption in homeostasis can be sensed by the host and is critical to mount an immune response [49].

In summary, the intestine has to face one of the most complex environments conceivable. IEC are important mediators of intestinal homeostasis and involved in the modulation of host-microbial interactions. Efficient protein production and secretion is important for this modulatory function as apparent for the synthesis of antimicrobial peptides, cytokines and mucus. Thus, the proper adjustment of protein folding might be fundamental to IEC function and intestinal health.

1.2 Unfolded protein responses – facilitators of proteostasis

A group of highly conserved signaling pathways, termed the unfolded protein response (UPR), are central for the control and maintenance of a homeostatic and productive protein-folding milieu, also referred to as proteostasis. In the endoplasmic reticulum (ER), protein folding is monitored by an ER-specific UPR pathway referred to as ER UPR. The major functions of the ER in eukaryotic cells are calcium storage and release as well as cellular protein trafficking in the secretory pathway. ER protein-folding can be disrupted by environmental, physiological and pathological factors, resulting in ER stress, a condition in which proteins are misfolded or unfolded. The tight control of protein folding is essential for cellular functions. If compared to other compartments, the folding landscape in the ER differs considerably further highlighting the relevance of ER proteostasis. In particular, carbohydrates and a glycosylation machinery are unique to the ER and the macromolecular densities in the ER are 3-6-fold higher than in the cytoplasm [50]. Further, the redox state of the secretory pathway is way more oxidative than that of the cytosol [51] and the free concentration of Ca^{2+} oscillates and can reach up to 1 mM [52, 53]. Triggers for ER stress are diverse and include increased protein synthesis demands, glucose deprivation, redox-, oxidative stress or hypoxia (Figure 3). ER protein stress is first sensed by ER-resident UPR sensors, upon which the signal is transmitted from the ER to the nucleus and the cytoplasm and evokes a response aiming to restore proteostasis within the ER.

Mechanistically, the misfolding of proteins triggers the release of the chaperone Grp78 (Glucose regulated protein 78) from three membrane-attached sensors and signal transducers, PERK (PKR-like ER kinase), IRE-1 (Inositol requiring enzyme 1) and ATF6 (Activating transcription factor 6) which transmit the information to the cytoplasm and the nucleus by activating downstream signal transduction effectors (Figure 3) [54, 55]. PERK in the dimerized and autophosphorylated form phosphorylates the alpha subunit of translation initiation factor 2 (eIF2 α), which inhibits translation

of most mRNAs but promotes the translation of Activating transcription factor 4 (ATF4) and thus the expression of ATF4 target genes [56]. IRE-1 is activated by conformational changes, autophosphorylation and subsequent higher order oligomerization. IRE-1 signals both via its ribonuclease activity and via binding of adaptor proteins like TRAFs (TNF receptor associated factor) [57]. The ribonuclease activity of IRE-1 is responsible for unconventional splicing of *Xbp1* (Xbox-binding protein 1) which functions as an activator of UPR target genes via the unfolded protein response elements (UPRE) [58-60]. Further, it is involved in the degradation of mRNAs by regulated IRE-1-dependent decay of RNAs (RIDD) [59]. ATF6 is a Basic Leucine Zipper Domain (bZIP)-containing transcription factor which is an ER transmembrane protein. Upon release from Grp78 it is transported to the Golgi where it undergoes intramembrane proteolysis via the site 1 and site 2 proteases (S1P and S2P) [61-63]. This allows for the nuclear translocation of the N-terminal fragment of ATF6 (nATF6) and subsequent downstream transcription of target genes via the ER stress elements ERSE and ERSE-II such as Grp78, CCAAT-enhancer-binding protein homologous protein (CHOP) and Xbp1. Transcriptional programs activated by ATF6 increase ER capacity and protein folding, and remove misfolded proteins by ER-associated degradation (ERAD) [58, 60, 64-67].

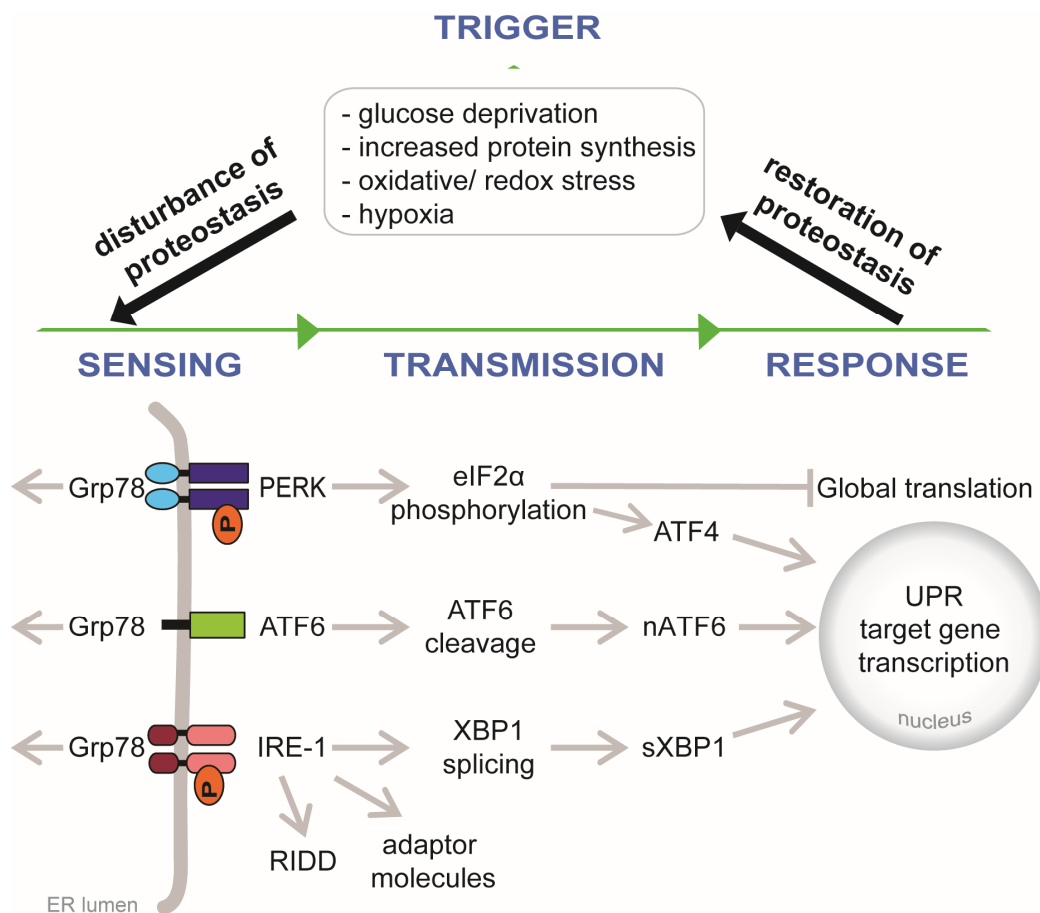


Figure 3: Main principle of ER UPR signaling and detailed signaling.

UPR activation is triggered by disturbances in proteostasis which are sensed, transmitted to the cytoplasm and the nucleus and result in response aiming to restore proteostasis within the ER. In detail, Grp78 is released from three membrane-attached sensors named PERK, IRE-1 and ATF6 to assist the folding of misfolded proteins. The disturbance of proteostasis is signaled via downstream cascades and results in a rapid shutdown of global translation and UPR-driven transcription of target genes involved in the control of ER folding.

The combined action of all three sensors of UPR defines two temporally distinct effector reactions: In an immediate response to diminish ER protein folding load the protein influx into the ER is reduced through phosphorylation of eIF2 α and RIDD. An additional mechanism of UPR induces the release of mRNAs encoding ER-targeted proteins from ribosomes to transiently reduce protein folding stress [68]. The second stage of adaptation is reprogramming of gene expression through UPR-driven transcription factors to increase protein folding and the clearing capacity of the ER. Of importance, excessive and prolonged ER stress can also promote apoptosis [69, 70].

In addition to the already described “reactive mode” of UPR activation triggered by protein stress within the ER, increasing evidence supports a so-called “anticipatory” activation mode of UPR. This mode is independent of protein stress within the ER and is triggered in anticipation of an increased

protein folding demand [71] (Figure 4). Of interest, this mode is even conserved in insects suggesting an important role of this pathway [72]. Anticipatory UPR was first observed for differentiating immune cells which have to synthesize and secrete large amounts of immunoglobulins upon maturation [73, 74]. Further, effectors like mitogenic steroids and peptide hormones like estrogen, VEGF (Vascular endothelial growth factor) or EGF (Epidermal growth factor) were shown to have rapid effects by preactivating the UPR in the absence of ER protein folding stress. Mechanistically, this is regulated by the efflux of calcium ions out of the ER lumen into the cellular space mediated by ER inositol triphosphate (IP3) receptor (IP3R) calcium channel. IP3R itself is activated by binding of IP3, an enzymatic product of the activated phosphorylated form of phospholipase C γ (PLC γ), the central integrator of hormonal action on anticipatory UPR [75-78]. PLC γ is also considered to be downstream of B cell antigen receptor (BCR) mediated anticipatory UPR acting through tyrosine kinases [79].

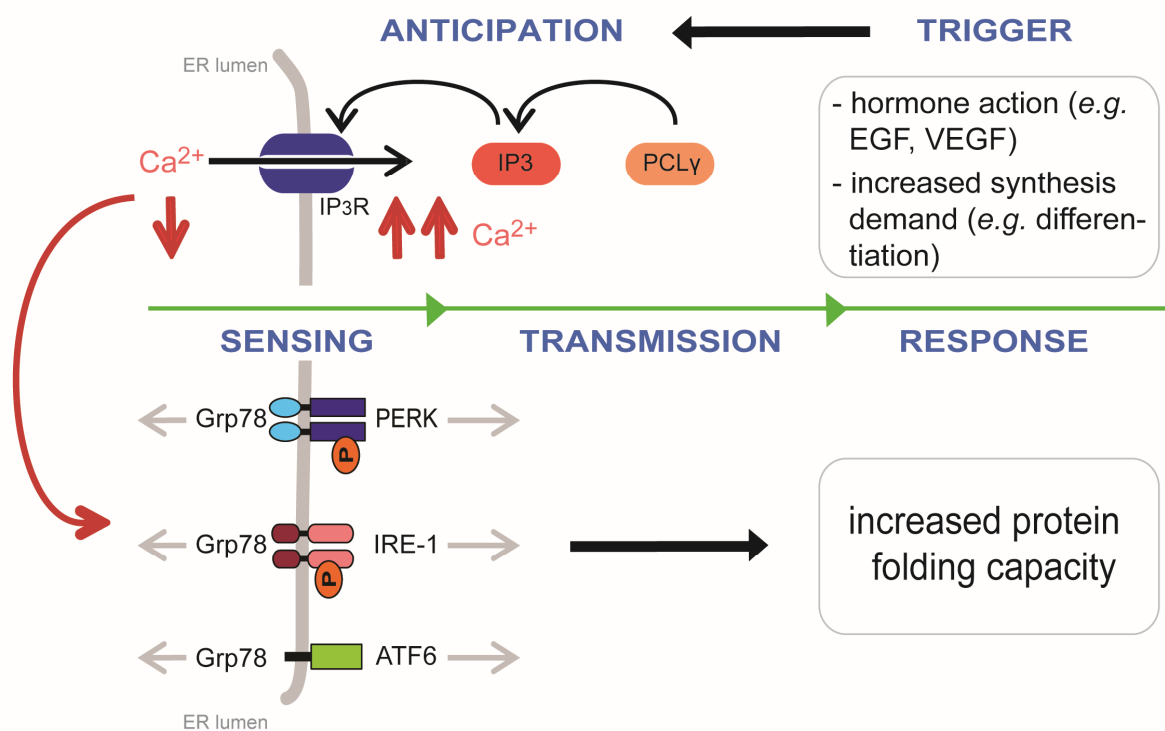


Figure 4: The anticipatory mode of ER UPR.

In contrast to the reactive mode of UPR, the anticipatory mode is not induced by protein folding stress within the ER but triggered in response to hormone action or in anticipation of an increased folding demand. Mechanistically, PLC γ is activated downstream of various pathways and results in the production of IP3. IP3 serves as a ligand which opens the calcium channel IP3R which evokes a rapid efflux of calcium ions into the lumen and a drop of calcium ions in the ER lumen. Low concentrations of calcium within the lumen activate the UPR sensors resulting in signaling and an anticipatory increase in protein folding capacity.

The anticipatory mode of UPR questions the former simplistic view of the UPR as an ER stress driven pathway. Further, the straightforward concept of the UPR as a linear pathway to regulate a well-

defined subset of target genes important for ER proteostasis is currently challenged. A potentially more appropriate concept suggests that UPR target genes and how UPR modifies cellular functions heavily depends on the kind of trigger of UPR (stress-dependent or stress-independent) and the affected cell type. UPR activation results in selective and fine-tuned gene expression programs defined by heterodimerization of transcription factors, crosstalk between the three UPR arms and crosstalk with other signaling pathways [80]. Particularly in disease situations, differential or selective regulation of the three arms of UPR might be relevant [81, 82].

In summary, UPR can be considered an adaptive response to disturbances in proteostasis aiming to restore proteostasis. Yet, the discovery of the anticipatory mode of UPR, cell type specific effects of UPR and context-specific interactions with other signaling pathways suggest a broader function in cellular homeostasis. The impact of UPR on cellular homeostasis and consequentially tissue homeostasis highlights the importance to study the role of UPR in the context of disease development. To consider tissue- and even cell type-specific effects of UPR is critical. Further, selective effects of the distinct UPR arms could be relevant. To pay attention to specific effects of UPR, this study focuses on the importance of ATF6-driven UPR in intestinal epithelial cells and how this impacts on intestinal homeostasis.

1.3 Regulation of the ATF6 arm of ER UPR

As addressed before, the effect of UPR signaling on cellular function depends on the affected cell type and the trigger of UPR activation. Since differential or selective regulation of the three arms of UPR are discussed to promote disease conditions [81, 82], it is critical to understand how the distinct UPR arms are regulated. Increasing evidence indicates that all three UPR arms are modulated by several factors. Since my thesis aims to investigate the contribution of ATF6 activation in IEC to intestinal disease, this chapter will focus on the known regulatory mechanisms for the ATF6-mediated arm of UPR.

As already addressed ATF6 needs to be activated to mediate ATF6-driven UPR. The activation of ATF6 depends on a sequence of events. All of these steps are prone to regulation as illustrated in Figure 5. Modulations can affect (a) the re-location of ATF6 from the ER to the Golgi, (b) the efficient processing of ATF6 within the Golgi and the translocation of the active transcription factor to the nucleus and (c) the transcriptional activation of target genes.

One important regulatory mechanism affecting the re-location of ATF6 is the retention of ATF6 in the ER membrane through its binding to Grp78 via Grp78 binding sites [63]. This interaction masks Golgi localization signals and thus inhibits the transport to the Golgi. In addition to this, ATF6 localization is further regulated by its glycosylation status [83]. ER-resident ATF6 is observed as a constitutively glycosylated protein. Even a single amino acid substitution within an N-linked glycosylation site, which mimics a state of ATF6 partial glycosylation also observed during ER stress, results in increased levels of nATF6 in the nucleus. Of interest this glycosylation status also affects the transactivation activity of nATF6. Besides glycosylation, ATF6 is regulated by the extent of reduction. The reduction of the disulfide bonds between ATF6 monomers is a prerequisite although not sufficient for transport of ATF6 to the Golgi [84]. Upon stress, protein disulfide isomerase PDIA5 seems to be particularly relevant for disulfide bond rearrangement in ATF6 which promotes the transport of ATF6. This activation step seems to be independent of the association between ATF6 and Grp78 [85].

Besides modulation of the re-location of ATF6, the processing of ATF6 in the Golgi can have an influence on the activation of ATF6. Thus, any modulation of the S1P/S2P protease machinery can have an impact. This is specifically important since this protease system is not exclusive to processing of ATF6, but is shared with other ATF6 homologs and SREBP (sterol regulatory element binding proteins) and thus connected to lipid synthesis [61].

Besides this, the potential of nATF6 to drive target gene expression can be modulated. For instance, ATF6 was shown to be phosphorylated by the MAP Kinase p38 (p38 mitogen-activated protein

kinase), which results in increased transactivation of the Grp78 promoter [86]. Further, the binding to different cofactors like the CCAAT binding factor NF-Y/CBF, the transcriptional repressor protein YY1 and TATA-binding was demonstrated [87-89]. Downstream effects of ATF6 might also depend on the respective interaction partners since ATF6 is known to form either homodimers or heterodimers with other transcription factors such as sXBP1 and ATF6 β [90, 91]. This can change the downstream expression profile as evident for XBP1-ATF6 heterodimers and their homodimers [92]. Further, ATF6 itself was identified to possess a quite unique property when compared to other eukaryotic proteins. Within its N-terminus it encodes a region highly homologous to the VN8 region of the herpes simplex viral protein VP16 [93]. This region is relevant to tightly coordinate high transcriptional activity and links this to a high proteasomal degradation resulting in a highly active but unstable transcription factor.

Yet, the precise mechanism of action and how certain proteins like the Calcium-independent phospholipase A2 gamma (iPLA2 γ) [94] or recently identified compounds either positively impact on ATF6 activation (small molecules proteostasis regulators [95]), or function as inhibitors (Ceapins [96, 97]) is often not resolved. Interestingly, even a sensing mechanism which operates within the lipid bilayer of the ER membrane is proposed to trigger the selective activation of ATF6. This selective activation of ATF6 is observed in response to increased membrane protein load [98].

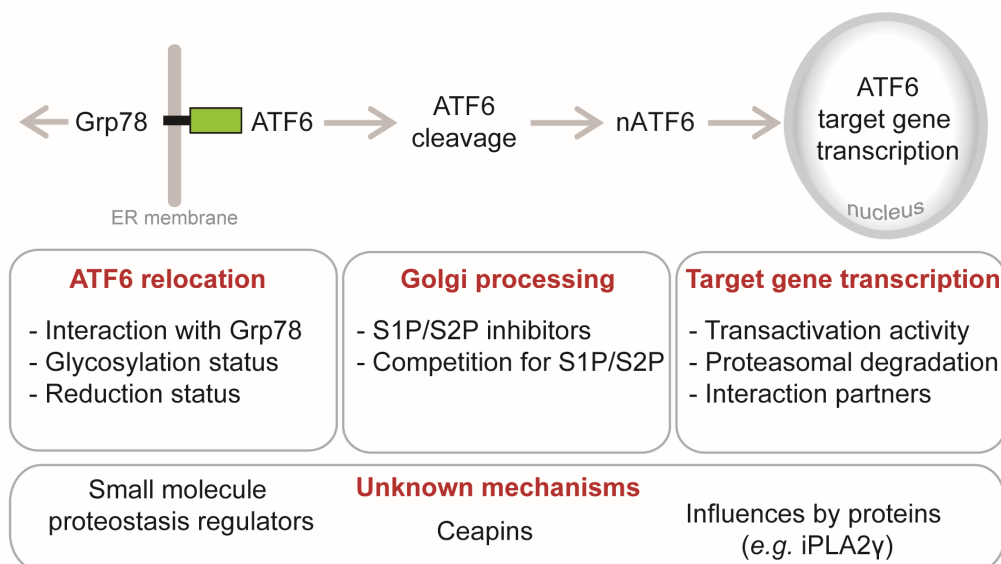


Figure 5: Mechanisms of regulation of ATF6 activation and ATF6-driven target gene expression.

Upon release of Grp78, ATF6 is transported to the Golgi where it is proteolytically processed by S1P and S2P. The N-terminal fragment (nATF6) translocates into the nucleus where it regulates the transcription of ATF6-driven genes. The multi-step activation of ATF6 is influenced by many factors that affect ATF6 relocation to the Golgi, Golgi processing and the degree and nature of target gene transcription. The precise mechanisms how ATF6 is regulated is often unknown.

In addition to regulation of ATF6 activation and ATF6-driven target gene expression the expression of ATF6 itself is modulated by several factors. For example, *ATF6* expression is under the control of specific miRNAs [99] and itself regulates miRNAs to modulate gene expression. This interrelation is for instance described for ATF6-mediated transcription of Calreticulin (Calr) by miR-455 [100].

Although not all regulatory mechanisms have been resolved yet, it is self-evident that signaling via ATF6 can be affected on several levels.

1.4 Contribution of ER UPR to disease pathogenesis

Inappropriate UPR signaling is believed to contribute to a variety of diseases comprising metabolic disease, neurodegenerative disease, inflammatory disease, and cancer (reviewed in [101]). UPR is considerably connected to inflammatory and apoptotic signaling. With respect to inflammatory diseases, the UPR can promote inflammation by enhancing the formation of reactive oxygen species (ROS), triggering nuclear factor- κ B (NF- κ B) and pro-inflammatory gene expression by activator protein 1 (AP1) pathways [102-107]. Further decisive for whether adaptation or apoptosis is the outcome of UPR activation is the nature of the trigger, which arms of UPR are activated and the extent of UPR activation [69]. UPR signaling is linked to apoptosis via (1) IRE-1-mediated activation of TRAF2 (tumor necrosis factor receptor associated factor 2), which activates the ASK1 (apoptosis signal-regulating kinase 1)/JNK (c-Jun amino terminal kinase) kinase cascade, (2) PERK/eIF2 α -dependent induction of the transcriptional factor CHOP and (3) Ca²⁺ release from the ER regulated by Bax (Bcl-2-associated X protein) /Bcl2 (B-cell lymphoma 2) [69].

1.4.1 UPR in intestinal inflammation

In the context of intestinal diseases, our group gave primary evidence that ER UPR activation takes place in IEC of inflammatory bowel disease (IBD) patients and in the colitis model *IL10*^{-/-} as evident by increased expression of Grp78 [108]. IBD are multifactorial, immunologically mediated disorders of chronically relapsing inflammation of the intestine with still unknown etiology. The two major forms of IBD are ulcerative colitis (UC) and Crohn's disease (CD). Both forms share symptoms but differ in location, pathophysiology and depth of inflammation in the intestinal wall. Whereas a continuous inflammation of the mucosal lining of the large bowel is characteristic for UC, inflammation is discontinuous in CD. In contrast to UC, in CD inflammation is observed in any part of the gastrointestinal tract from the mouth to the anus, transmural and characterized by lymphocyte infiltration, granulomas and the risk of stenosis formation. The current concept of disease pathology suggests that the onset of IBD is based on genetic susceptibility, immune dysregulation, microbiota and environmental factors like food, smoking and drugs [109-111]. Genome-wide association studies (GWAS) have identified many genes that may predispose patients to IBD. Large-scale GWAS in cohorts of European descent have identified 163 genetic loci to be associated with IBD [112]. The first trans-ethnic association study of IBD has further implicated 38 additional loci in IBD risk, most of which contribute to both CD and UC [113]. Most genes can be grouped into three major disease-associated pathways: (1) regulation of inflammatory responses (e.g. Interleukin-23 receptor (*IL23R*)), (2) regulation of autophagy (e.g. Autophagy-related protein 16-1 (*ATG16L1*)) and (3) microbial

sensing (e.g. Nucleotide-binding oligomerization domain-containing protein 2 (*NOD2*)) [114]. Focusing on ER function, genetic abnormalities in several genes relevant for ER protein folding and homeostasis like XBP1 [115], AGR2 (Anterior Gradient 2, [116]) and ORMDL3 (Orosomucoid-like 3, [117, 118]) were identified [119].

IEC-specific XBP1 knockout mice support an involvement of IRE-1/XBP1 signaling in intestinal inflammation, since these mice developed spontaneous inflammation of the small intestine, a loss of Paneth cells and showed a significant reduction of goblet cells [115]. Substantial evidence supports the fact that Paneth cell defects in this mouse promote inflammation since Paneth cell specific deletion of XBP1 promotes enteritis similar to a deletion in all IEC [120]. Particularly, exacerbated ER stress in the highly secretory cell types of the IEC like the Paneth and goblet cells seems to promote intestinal inflammation. This is also evident in the *Agr2*^{-/-} mice which develop terminal ileitis and colitis. *Agr2* is an ER disulfide isomerase induced in response to ER stress and was described to be highly relevant for intestinal mucus production [121, 122]. The first observable effect after induction of *Agr2* depletion is rapid Paneth cell hypertrophy and expansion followed by loss of visible mucin-filled goblet cells. Subsequently, decreased enterocyte proliferation and increased apoptosis culminate in intestinal inflammation. *Agr2* deficiency results in a pronounced increase of Grp78 in cells that express goblet cell and Paneth cell lineage markers and intestinal stem/early progenitor cells positive for MSI1 (RNA-binding protein Musashi homolog 1) [121]. Most other models with genetic manipulation of specific components of the UPR - comprising ATF6, p58^{IPK}, IRE-1 β and CHOP - do not spontaneously develop inflammation but have an altered susceptibility towards perturbations in intestinal homeostasis [123-127].

In addition to an association between ER proteostasis modulators and inflammation, there is clear evidence for a role of ER stress provoked by misfolding of secreted proteins in intestinal inflammation. This association is for instance based on observations in two mouse models developed by random mutagenesis termed Eeyore and Winnie. These mice have independent missense mutations in the *Muc2* gene resulting in the accumulation of misfolded Muc2 in goblet cells and consequentially in ER UPR activation [128]. As a consequence, both models spontaneously develop inflammation and have an increased risk for environmentally induced (low dose dextran sodium sulfate (DSS)) inflammation closely remodeling human colitis.

In sum, there is substantial evidence supporting that UPR and ER stress can promote intestinal inflammation in animal models. This observation is supported by the presence of ER stress and UPR activation in IBD patients and detection of genes relevant for ER protein folding in GWAS.

1.4.2 UPR in cancer

UPR activation has been observed in a variety of human tumors including glioma, lymphoma, myeloma and carcinoma of multiple tissues including colon, liver and uterus [129]. Emerging evidence suggests an involvement of UPR in cancer uncoupled from mere protein misfolding. Considering cancer-associated mutations in the genes encoding the three UPR sensors *PERK*, *IRE-1*, and *ATF6* based on the Catalogue of Somatic Mutations in Cancer (COSMIC) database [130], the somatic mutation profiles are distinct, with silent mutations enriched in *IRE-1*, missense mutations enriched in *PERK* and nonsense mutations enriched in *ATF6* [80, 131]. Further, *IRE-1* showed a dominance of in-frame deletions and insertions compared to the other sensors. Of interest, gastrointestinal cancers show the highest rate of somatic mutations considering all three sensors, with a predominance of *ATF6* followed by *IRE-1*. *ATF6* mutations are further frequent in genital, urologic and lung cancer, whereas *PERK* mutations are more pronounced in bone, urologic and lung cancer. *IRE-1* somatic mutations are observed in cancers of the nervous system and gastrointestinal cancers [80].

Independent of genomic alterations in UPR genes, cancer-associated UPR signaling can be induced by cell extrinsic and intrinsic factors (Figure 6). As a result of augmented proliferation, tumor cells are confronted with a hostile tumor microenvironment which is a potent activator of UPR signaling. Hypoxia, evoked by a lack of vascularization and oxygen supply, perturbs redox homeostasis within the ER [132, 133]. Acidosis as a result of increased lactate production based on the Warburg effect also results in UPR activation relevant for cancer cell survival [134, 135]. Furthermore, nutrient deprivation and oxidative stress are activators of the UPR. Exemplarily, a lack of glucose and amino acids activate *PERK* and general control nonderepressible 2 (*GCN2*), resulting in eIF2 α -mediated stop of translation [136, 137].

Besides the cell extrinsic triggers mentioned also cell intrinsic triggers within tumors can activate the UPR. These triggers include transformation-associated proto-oncogene activation or loss of tumor suppressors [138]. Oncogene activation or a loss of tumor suppressors support growth and survival by activating homeostatic processes within the cell that result in maintenance of intracellular metabolites and prevent oxidative stress. One of these pathways effecting on homeostatic processes is the UPR. The UPR is for instance activated in response to the loss of the tumor suppressors tuberous sclerosis complex genes *TSC1* or *TSC2* in cell lines and murine or human tumors [139]. Oncogene-driven UPR activation is known for *c-MYC*, *RAS* (Rat sarcoma), *BRAF* (B-Raf Proto-Oncogene, Serine/Threonine Kinase) and *HER2* (human epidermal growth factor receptor-2) [140-144]. For instance, it was shown that *c-MYC* activates the *PERK/ATF4* arm of UPR as a consequence of

maximized protein load which evokes ER stress. The downstream activation of UPR promotes c-MYC-induced transformation [140]. Further, chromosomal abnormalities as a result of genomic instability and a driving force of tumorigenesis can stimulate the UPR. Aneuploidy, defined as an abnormal number of chromosomes within a cell, was shown to promote proteotoxic stress and UPR activation based on reporter assays for Grp78, ATF6, XBP1 and CHOP [145].

The UPR is an emerging driver of several tumor characteristics necessary for cancer progression which are defined as the hallmarks of cancer (Figure 6) [134]. Major evidence supports a role of UPR in mediating survival and adaptation of cancer cells to stress conditions [146]. A contribution of UPR to initiation and progression of cancer is suggested based on the observation that inhibition or deficiency of PERK interferes with tumor growth and increases animal survival [147-150]. Further, knockdown of XBP1 and ATF6 reduced EGF-stimulated cell proliferation by 30–40% [151]. Of interest, UPR can also promote angiogenesis, which is essential to sustain oxygen and nutrient supply within solid tumors. Angiogenesis modulation was for example demonstrated by direct binding of ATF6 to the VEGF promoter [152, 153] and shown to be under the control of XBP1 and HIF (Hypoxia inducible factor) [154]. In turn, UPR is activated by VEGF via a mechanism involving PCLy likely in an anticipatory fashion [72, 75], suggesting the existence of a positive feedback regulatory loop between UPR and angiogenesis.

The UPR is also connected to the adjustment of metabolic status and thus impacts on the deregulation of cellular energetics. For instance, it is known that inhibition of PERK reduces cancer growth by a concerted impairment of amino acid metabolism and angiogenesis [149]. UPR signaling is further coupled to the hexosamine biosynthetic pathway (HBP) which is the synthetic pathway for a precursor for both O- and N-glycosylation [155, 156]. Hyperglycosylation of proteins as a result of increased HBP is evident in a multitude of tumors and seems to be relevant for different hallmarks including angiogenesis, cell invasion and metastasis (reviewed in [157]). Genomic instability is a major characteristic of cancer cells and a trigger of ER stress and UPR [145]. It is currently under debate whether ER stress may also feedback to genomic instability and DNA damage. Indicative for this is the fact that XBP1 regulates a cluster of target genes linked to DNA damage and repair pathways [158]. Moreover, inactivation of PERK might provoke genomic instability possibly connected to oxidative DNA damage in mammary carcinoma [159]. Cross-talk between the UPR and the tumor protein p53, which has important tumor suppressor functions, has been reported in many studies [160-163]. Tumor dormancy and resistance to treatment is vastly correlated with the UPR. Dormant cells exit active cell division and survive in a quiescent state in which they are also resistant to drug-damaging agents but have the potential to reenter the cell cycle when the conditions are

appropriate [164, 165]. The PERK and IRE-1 arms are known to regulate expression of cyclin D1, thus regulating cell cycle exit [166-168]. A role in survival during dormancy was further attributed to ATF6-Rheb (Ras homolog enriched in brain)-mTOR (mechanistic target of rapamycin) signaling [169].

Tumor-associated inflammation is evident in every neoplastic lesion and could be considered an attempt by the immune system to eradicate tumors. Yet, tumor-associated inflammation can also enhance tumorigenesis and progression and thus supports the acquirement of hallmark capabilities [134]. A critical factor to tumor expansion is the interaction between the tumor and the surrounding stroma. Increasing evidence suggests that UPR is transmittable between cells and transmission from tumor cells to stroma cells interferes with the antitumor inflammatory responses through a mechanism which is not yet clear [170-173]. For instance, transmissible ER stress diminishes antigen processing and presentation and reduces T-cell proliferation of CD8 T cells during cross-priming by dendritic cells [171].

Epithelial-mesenchymal transition (EMT) is a developmental program used by transformed epithelial cells to invade, resist apoptosis and disseminate resulting in metastasis [134]. UPR is linked to invasion and metastasis by the regulation of cell survival during the metastatic cascade, metastatic growth or dormancy by reprogramming tumor cells and actively remodeling the environment (reviewed in [174]). UPR signaling is activated during EMT since cells have to synthesize and secrete extracellular matrix proteins in large quantities. Exemplarily, the PERK-eIF2 α arm of UPR was observed to be activated by EMT. This activation was shown to be indispensable for EMT, since PERK inhibition interfered with the potential of cells to form tumor spheres and migrate in transwell assays [175].

As mentioned before, UPR can have both protective and deleterious outcomes with respect to cell survival. This dual role of UPR is also evident in neoplastic cells either facilitating or suppressing malignant transformation. The high basal UPR in transformed cells makes the cells more susceptible to agents that further augment ER stress and thus drive pro-death functions of UPR. Examples for such agents are proteasome inhibitors like bortezomib. Bortezomib was shown to trigger chronic ER stress, reflected in pronounced activation of PERK, which may promote apoptosis [176]. UPR activation can further have anti-tumor effects by initiation of antitumor immune responses stimulated by aberrant cell surface display of ER proteins like Calreticulin in response to physiological conditions or pharmacological intervention [177, 178]. With respect to treatment approaches, inhibition of pro-survival functions of the UPR in the face of the continued microenvironmental and oncogenic stress is discussed in the development of chemotherapeutics [129].

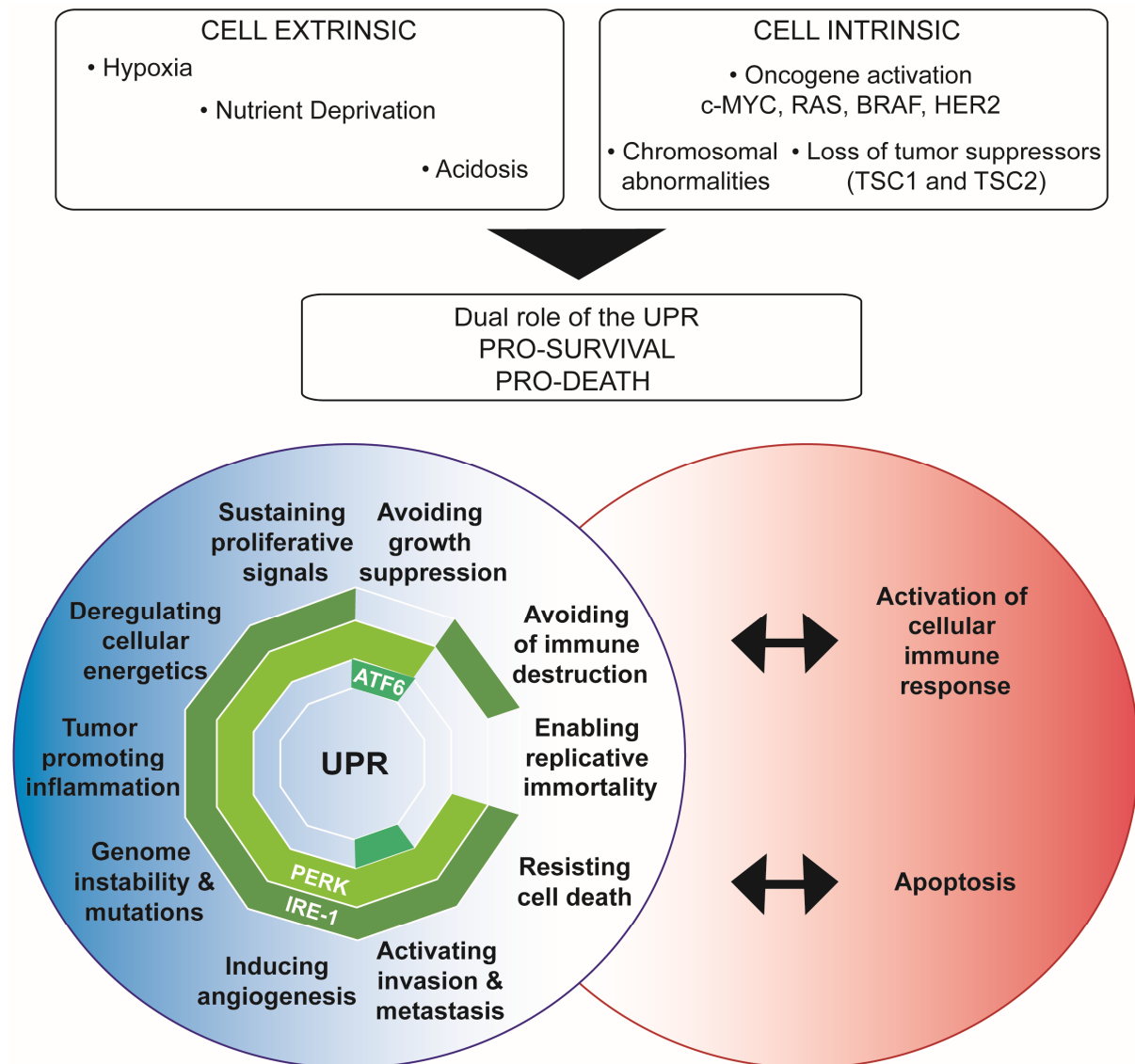


Figure 6: Summary of the role of UPR in cancer.

UPR is activated in tumor cells by extrinsic factors that are mainly evoked by the hostile tumor microenvironment and cell intrinsic factors linked to oncogene activation, loss of tumor suppressors or chromosomal aberrations. The impact of UPR on tumor cells is diverse and can promote survival or cell death. UPR contributes to the hallmarks of cancer (blue circle) [134]. Whereas action of ATF6 is predominantly related to metastasis and dormancy (inner polygon), IRE-1 could be relevant for most processes with the exception of tumor dormancy (outer polygon). The PERK pathway may have more diverse functions in processes related to cancer progression and tumor growth (central polygon) (UPR assignment to hallmarks of cancer adapted from [172]). Besides a contribution of UPR to the hallmarks of cancer, UPR can also have contrary outcomes (red circle).

Overall, UPR is frequently observed in cancer, activated either cell extrinsically or intrinsically. Substantial evidence supports a contribution of UPR to diverse biological capabilities acquired during the multistep development of tumors. Due to its multifaceted roles on cell survival, it is a potential target for cancer therapy.

1.4.3 Specific contribution of ATF6 signaling to intestinal inflammation and tumorigenesis

The current understanding of the role of ATF6 in physiologic and pathologic conditions is based on cell culture as well as mouse models and suggests dominant functions in promoting ER quality control [64, 67]. While ATF6 is dispensable for embryonic and postnatal development - if not combined with ATF6 β or ER co-chaperone p58IPK deficiency - a lack of ATF6 compromises the secretory pathway during ER stress and impairs adaptation to chronic ER stress [64, 90, 179]. A further role of ATF6 was shown through a transgenic mouse model of tamoxifen-induced cardiac-restricted ATF6 activation, demonstrating a protective function of the ATF6 arm by reducing ischemia/reperfusion damage [180, 181].

Animal models proved a link of the ATF6 pathway in IEC and intestinal inflammation. The “woodrat” mouse has hypomorphic mutations in the *Mbtps1* gene resulting in diminished activity of S1P and thus deficient proteolytic activation of ATF6 in the Golgi [127]. Woodrat mice do not develop spontaneous intestinal inflammation but have an increased susceptibility towards the development of colonic intestinal inflammation upon treatment with the detergent DSS. Bone marrow chimeras suggest that this effect is due to non-hematopoietic cells, with IECs being the likely candidates. Considering the involvement of S1P in the activation of many other proteins like ATF6 β , Luman (CAMP Responsive Element Binding Protein 3), OASIS (CAMP Responsive Element Binding Protein 3 Like 1) and SREBPs, these effects could also be independent of ATF6. However, a mouse with a constitutive deletion of total ATF6 also shows a high susceptibility to DSS [124] and there is a big intersection between ER stress chaperone expression in woodrat and *Atf6*^{-/-} mice [182]. This supports that the phenotype observed in woodrat mice indeed depends on a lack of ATF6 activation. Of relevance, it was demonstrated that the anti-inflammatory interleukin 10 interferes with the ER stress response by modulating ATF6 recruitment to the Grp78 promoter [108]. A more indirect link between ATF6 and IBD is based on unbiased GWAS in which *ORMDL3* was associated with the risk to develop CD [118] and UC [117]. This is relevant, since *ORMDL3* was shown to selectively activate the ATF6 arm of UPR in lung epithelia [183, 184].

As evident in Figure 6 there are less indications for a contribution of ATF6 to the hallmarks of cancer compared to the other two arms, although Grp78, an important downstream target gene of ATF6, is frequently found to be overexpressed in tumors [185, 186]. Further, an increased expression of ATF6 on protein level was recently shown in lesions undergoing pre-cancerous atypical change in inflammation-independent (non UC associated) and UC-associated CRC [187]. Of relevance, ATF6 expression was under the detection limit in the normal colonic mucosa but its expression was

significantly elevated with increasing severity of atypia in adenoma. High mRNA expression of ATF6 is positively correlated with head and neck cancer and colorectal cancer primary tumors and the likelihood of patients to develop lymph node metastasis [188] and relapse [169, 189]. Further, ATF6 conveys a survival advantage to D-HEp3 human squamous carcinoma cells upon genotoxic, ER and nutritional stress *in vitro*, as assessed by knockdown experiments [169]. ATF6 over-activation might be linked to chemoresistance of leukemia cells to the chemotherapeutic agent Imatinib, regulated by the protein disulfide isomerase PDIA5 [85]. Further, it supports the survival of dormant tumor cells via Rheb-mTOR signaling without providing a survival benefit in actively dividing cells [169]. Particularly in hepatocellular carcinoma (HCC), ATF6-mediated transcription was suggested to be relevant for transformation by comparing expression profiles of ATF6 transfected cells to poorly differentiated HCC tumors [186, 190]. Still, no direct effect of ATF6 expression on proliferation was demonstrated besides transcriptional regulation of cell-cycle relevant genes. Controversially, a common missense SNP in ATF6 was suggested to impact on susceptibility to HCC which was associated with low expression of ATF6 and downstream target genes [191]. Of interest, in sarcomas the ATF6-encoding q21-23 region is frequently amplified [192]. ATF6 is highly expressed in the respective tumors and also the downstream targets Grp78 and Grp94 are overexpressed. In addition, the inhibition of the S2P protease and consequently inhibition of proteolytic processing of ATF6 and SREBP-1 results in a G1 cell cycle block and apoptosis in liposarcoma [193]. ATF6 could further impact on the expression of micro RNAs indirectly affecting tumorigenesis. For instance it is known, that ATF6 negatively regulates the levels of miR-455 which in turn results in the augmentation of Calreticulin (Calr) expression [100]. Of interest, miR-455 was observed to be downregulated in stage II colon cancer [194] and shown to inhibit proliferation and invasion of colorectal cancer by targeting RAF proto-oncogene serine/threonine-protein kinase [195].

In summary, ATF6 is a transcription factor which mediates one of three arms of the ER UPR. UPR signaling is important for adaptation of proteostasis either in response or anticipatory to protein disturbances and as such important for cell and tissue homeostasis. Maladaptation or deregulated activation of UPR contribute to diverse diseases, including cancer. With respect to the function of IEC, strong evidence points toward a contribution of ER UPR to intestinal inflammation. Inflammation and cancer are interrelated pathologies *e.g.* in view of epidemiology and inflammatory profiles [196]. Since longstanding inflammation promotes colon cancer risk [197, 198] and UPR is suggested to contribute to diverse aspects of tumorigenesis, UPR signaling might also be relevant for intestinal tumorigenesis. The present work focuses on how ATF6-driven UPR affects intestinal epithelial cell homeostasis and how this is connected to intestinal disease.

2. STUDY OBJECTIVE

ER stress and the activation of UPR is suggested to contribute to a variety of pathologies. Yet, there is a lack of understanding how UPR activation impacts on cellular function and cell fate in a tissue- and cell type-specific context. Within the gut, intestinal epithelial cells form an important interface between the gut lumen and the mucosal immune system. Dynamic adaptation to continuously changing conditions is critical for these cells. Consistently, increasing evidence suggests that UPR activation as a cell-intrinsic mechanism for adaptation of proteostasis is important for epithelial function. Profoundly activated, potentially pathological UPR signaling is frequently observed in IEC of IBD patients and in colon cancer, raising the question which properties and particularly which of the three UPR arms contribute to the disruption of intestinal homeostasis culminating in disease. In light of the higher risk of Ulcerative colitis patients to develop colon cancer, the relevance of UPR activation for the development of inflammation and cancer needs to be addressed. Previous work on intestinal inflammation in IL10-deficient mice and IBD patients has suggested a connection between inflammation and the ATF6 arm of UPR. To characterize the particular contribution of this arm, a mouse model – referred to as the *nATF6*^{IEC} mouse – was generated at the Chair of Nutrition and Immunology (Technical University Munich). This *nATF6*^{IEC} mouse expresses the activated form of ATF6 (nATF6) specifically in IEC and should thus mimic IEC-specific activation of the ATF6 arm of UPR. The present work aims to characterize the role of epithelial cell-specific ATF6 expression in the context of intestinal inflammation and tumorigenesis using a novel transgenic mouse model and biopsy material from patients with colorectal cancer.

3. MATERIAL AND METHODS

3.1 Animal experiments, primary cell isolation and culture

3.1.1 Generation of the *nATF6* mouse model

The *nATF6* mouse was generated within the frame of the PHD thesis of Emanuel Berger [199]. The next sections describe the generation of the model, starting with the construction of the cloning vector, the insertion of the *nATF6-HA* transgene into the *ROSA26* locus, the embryonic stem (ES) cell culture, the blastocyst manipulation and the embryo transfer to pseudopregnant mice.

The nuclear fragment of ATF6 coding sequence was amplified from cDNA of embryonic stem cells (C57BL/6; kindly provided by KP Janssen) with primers based on the design of de Almeida et al [200] using a HotStar Hifidelity polymerase (Qiagen) with proof reading activity. After purification, restriction sites were introduced, the fragments were purified and the *HA*-Tag was annealed to the C-terminus. Purified *nATF6-HA* sequences were amplified and ligated into the cloning vector pBluescript-CAG-lox-CAT-lox, which bases on the pBluescript vector backbone (Fermentas). The CAGGS promoter was inserted into the multiple cloning site consisting of a CMV enhancer, a chicken β -actin promoter and a γ -globin splice acceptor for strong constitutive gene expression. The adjacent floxed CAT cassette was replaced by *nATF6-HA*.

Promoter and cDNA fragments were cloned directly from the delivered cloning plasmid into an RMCE exchange vector. The construct contained the CAGGS promoter, a loxP-flanked STOP cassette (Fluc mini ORF and a polyadenylation site), and the *nATF6-HA* open reading frame.

The RMCE ES cell line (derived from mouse strain C57BL/6Ntac-Gt(ROSA)26Sor tm596Arte) was grown on a mitotically inactivated feeder layer comprised of mouse embryonic fibroblasts (MEF) in DMEM High Glucose medium containing 20 % FBS (PAN) and 1200 u/ml Leukemia Inhibitory Factor (Millipore ESG 1107). For manipulation, 2×10^5 ES cells were plated on 3.5 cm dishes in 2 ml medium. For transfection, 3 μ l Fugene6 Reagent (Roche; Catalog No. 1 814 443) was mixed with 100 μ l serum free medium (OptiMEM I with Glutamax I; Invitrogen; Catalog No. 51985-035) and incubated for 5 min at room temperature. 100 μ l of the Fugene/OptiMEM solution was added to the DNA mixture containing 2 μ g circular vector and 2 μ g CAGGS-Flp plasmid. This transfection complex was incubated for 20 min at room temperature and then added dropwise to the cells. From day 2 onwards the medium was replaced daily with medium containing 200 μ g/ml G418 (Geneticin; Invitrogen; Catalog

No. 10131-019). Seven days later, single clones were isolated, expanded and analyzed on the molecular level by Southern blotting according to standard procedures.

After administration of hormones, superovulated Balb/c females were mated with Balb/c males. Blastocysts were isolated from the uterus at dpc 3.5. For microinjection, blastocysts were placed in a drop of DMEM with 15 % FCS under mineral oil. A flat tip, piezo actuated microinjection-pipette with an internal diameter of 12 – 15 micrometer was used to inject 10-15 targeted C57BL/6 N.tac ES cells into each blastocyst. After recovery, 8 injected blastocysts were transferred to each uterine horn of 2.5 dpc, pseudopregnant NMRI females. Chimerism was measured in chimeras (G0) by coat color contribution of ES cells to the Balb/c host (black/white). Highly chimeric mice were bred to strain C57BL/6 females. Germline transmission was identified by the presence of black, strain C57BL/6, offspring (G1).

3.1.2 Ethics statement, mouse breeding and housing

The maintenance and breeding of mouse lines and all experiments were approved by the Committee on Animal Health and Care of the local government body of the state of Upper Bavaria (Regierung von Oberbayern; AZ 55.2-1-54-2532-164-09, 55.2-1-2532-165-12, 55.2-1-54-2531-214-13, 55.2-1-2532-217-14, 55.2-1-54-2532-169-2014) and performed in strict compliance with the EEC recommendations for the care and use of laboratory animals (European Communities Council Directive of November 24, 1986 [86/609/EEC]). Mice were housed under specific pathogen free (SPF) conditions according to the criteria of the Federation for Laboratory Animal Science Associations (FELASA) (12 h light/dark cycles at 24–26°C). Mice were fed a standard diet (autoclaved V1124-300, Ssniff, Soest, Germany) *ad libitum* and were sacrificed by CO₂. Mice were monitored and aborted if a combined score considering weight loss, changes in stool consistency, rectal prolapse and general behavioral and general state of health was reached. Table 1 summarizes all SPF mouse breedings. *nATF6* mice were bred to Villin-Cre mice to achieve IEC specific expression (*nATF6*^{IEC}). All colonies were maintained by breedings in which one breeder was heterozygous for Cre and the other was wild-type for Cre. Mice expressing *nATF6* homozygously (*nATF6*^{IEC} tg/tg) and heterozygously (*nATF6*^{IEC} tg/wt) were compared to control mice derived from the same breeding but without Cre expression (*nATF6*^{IEC} fl/fl). *nATF6*^{IEC} mice were further bred to IL10 (Interleukin 10) -, RAG2 (Recombination activating gene 2) – and CHOP- deficient background.

To generate 4-hydroxytamoxifen inducible mice, *nATF6* mice were bred to Villin-Cre^{ERT2} and LGR5-Cre^{ERT2} mice. All mice used were on the C57BL/6 genetic background.

Table 1: Mouse breedings (SPF).

Mouse breedings	Characteristics	Mode
$nATF6^{IEC}$ ($nATF6 \times Vil-Cre$)	Villin-based expression of nATF6	Constitutive nATF6 expression in IEC
$X IL10^{-/-}$	+ Whole body knockout of IL10	+Constitutive IL10 deficiency
$X RAG2^{-/-}$	+ Whole body knockout of RAG2	+ Constitutive RAG2 deficiency
$X CHOP^{-/-}$	+ Whole body knockout of CHOP	+ Constitutive CHOP deficiency
$nATF6^{IEC-OHT}$ ($nATF6 \times Vil-Cre^{ERT2}$)	Villin-based expression of ATF6	4-hydroxytamoxifen inducible recombination of nATF6 in IEC
$nATF6 \times LGR5-Cre^{ERT2}$	LGR5-based expression of ATF6	4-hydroxytamoxifen inducible recombination of nATF6 in LGR5+ stem cells

$nATF6^{IEC}$ mice were made GF by 2-cell embryo transfer into GF pseudopregnant recipient females (Clean Mouse Facility, University of Bern, Department of Clinical Research). GF mice were housed in 12 h light/dark cycles at 24–26°C, fed a standard diet (autoclaved V1124-300, Ssniff, Soest, Germany) *ad libitum* and were sacrificed by CO₂. Mice were monitored and aborted if a combined score considering weight loss, changes in stool consistency, rectal prolapse and general behavioral and general state of health was reached. Sterility was checked by cultivation of feces in Luria broth (LB) or Wilkins Chalgren agar (WCA) broth (OXOID) and by microscopic observation of Gram-stained fecal smears every 10–14 days and at sampling. A mold-trap was used to indicate the presence of mold. No contaminations were observed during the experiments. Besides for the GF status mice were housed as described for SPF.

3.1.3 Mouse experiments

3.1.3.1 Dextran sodium sulfate (DSS)-induced colitis

12 week (wk) old $nATF6^{IEC}$ tg/wt and $nATF6^{IEC}$ fl/fl male mice were subjected to four cycles of low dosage of DSS (0.5-1 %; 3-5 days; *ad libitum* via drinking water) followed by phases on normal drinking water. Disease activity index (DAI) as a combined score of weight loss (0 (no loss); 1 (1-5 %); 2 (6-10 %); 3 (11-15 %); 4 >15 %), stool consistency (0 (normal); 2 (loose stool); 3 (mild diarrhea); 4 (diarrhea)) and bleeding (0 (no bleeding); 2 (gross bleeding); 3 (gross bleeding > 1 day (d)); 4 (gross bleeding > 2 d)) was assessed (0-4 score points per category; divided by 3).

3.1.3.2 Colonoscopy

To analyze the endoscopic appearance of the colon during DSS-induced colitis, video colonoscopy was performed before the first cycle of DSS, 11 days after each individual cycle of DSS and at the end

of the experiment at the age of 31 wk (46 days after final DSS exposure) (treatment scheme Figure 29A).

Further, macroscopic changes in the colon of *nATF6^{IEC}* mice housed under SPF conditions were visualized over-time in single tg/tg and fl/fl mice by repetitive colonoscopy starting at the age of 8 wk until the age of 40 wk (treatment scheme Figure 31A).

3.1.3.3 Antibiotic treatment

A mixture of vancomycin (0.25 g/l; VWR) and metronidazole (1 g/l; Sigma/Fluka) was administered to *nATF6^{IEC}* tg/tg, tg/wt and fl/fl mice via the drinking water – starting at the age of 6 wk until the age of 12 wk. Antibiotics were prepared fresh twice a week and administered *ad libitum* via drinking water in light-protected bottles. One cohort was directly sampled at the end of this antibiotic treatment (6 wk) whereas a second cohort was put on normal drinking water for an additional 4 weeks (6 wk + 4 wk) (treatment scheme Figure 35A). At sampling, ten-fold dilutions of cecal content (w/v) were prepared by adding appropriate volumes of sterile PBS supplemented with peptone and cysteine (0.05 % w/v each, Fluka) to assess the number of colony forming units (CFU). Dilution series were prepared anaerobically on Wilkins-Chalgren Agar supplemented with L-cysteine and dithioerythritol (0.05 % w/v each). CFU counts were assessed after 2 days of anaerobic growth.

3.1.3.4 Bacterial association

Cecal content from SPF donor *nATF6^{IEC}* mice (tg/tg or fl/fl; age 5 wk) was instantly suspended at 1:10 w/v in filter-sterilized PBS/40 % glycerol, and stored at -80 °C. For gavage, cecal content solutions were centrifuged (3 min, 300 g, 4 °C) to pellet debris, followed by centrifugation (10 min, 8000 g, 4 °C) to collect microbes. This fraction was re-suspended in an equal volume of sterile PBS. Each recipient mouse (tg/tg or fl/fl) was gavaged with 100 µl of the bacterial suspension at the age of 4 weeks (equivalent to 3-5 x 10⁸ bacterial cells per mouse, as determined by THOMA counting chamber). Recipient mice were housed in microbiota-specific isolators and sacrificed at the age of 16 wk (unless abortion criteria as defined in ethical proposals were fulfilled).

3.1.3.5 Tamoxifen-induction of *nATF6* expression

nATF6^{IEC-OHT} and *nATF6* x LGR5 Cre^{ERT2} mice were kept on phytoestrogen-reduced diet (V1154-300 , Sniff, Soest) for three weeks before they were put on 4-hydroxytamoxifen-diet (OHT-diet; CreActive T400 (10 mm, Rad), Genobios, Laval) for one week at the age of 10 wk. After the induction phase,

feed was switched back to phytoestrogen-reduced diet. Mice were sampled at day 4 after the end of induction phase or after 15 weeks (treatment scheme Figure 25A, Figure 27A).

3.1.3.6 Isolation of intestinal epithelial cells

Isolation of primary IEC was performed as previously described [201]. Either intestinal parts were inverted on a needle or the longitudinally opened tissue was transferred to 20 mL Dulbecco's modified Eagle's medium (DMEM; Gibbco) containing 10 % fetal calf serum (FCS), 1 % L-glutamine and 0.8 % antibiotics/antimycotics (IEC isolation medium) supplemented with 1 mM dithiothreitol (Roth), vortexed vigorously for 1 min and incubated (37 °C, 15 min) under continuous shaking. After vortexing for 1 min, the IEC suspension was centrifuged (7 min, 300 g, RT) and the cell pellet resuspended in 5 ml IEC isolation medium. The remaining tissue was vortexed for 1 min and incubated in 20 ml PBS (10 min, 37 °C) containing 1.5 mM EDTA under continuous shaking. After an additional vortexing step, the cell suspension was pelleted by centrifugation. The two IEC suspension fractions were combined and purified by centrifugation through a 20 %/40 % (in medium/PBS) discontinuous Percoll gradient (GE) at 600 g for 30 min. The IEC fraction at the interface between the Percoll phases was collected and washed once with medium and once with PBS. Purified IECs were lysed in urea-containing protein lysis buffer (7 mol l⁻¹ urea, 2 mol l⁻¹ thiourea, 2% CHAPS, 1% DTT (all from Roth, Karlsruhe, Germany) and protease inhibitor (Roche Diagnostics, Mannheim, Germany) or RA1 RNA lysis buffer (Macherey-Nagel) for downstream analysis.

3.1.3.7 Organoid culture and quantification

Colonic crypt organoids were isolated by a sequence of PBS washing steps and collagenase XI digestion. In detail, colonic tissue pieces (smaller than 1 mm) were washed in PBS until the supernatant was clear and then transferred to a collagenase solution (0.4 mg/ml collagenase XI in 40 ml Advanced DMEM /F12 (Invitrogen 12634)). For the first digestion step the tissues were incubated for 9.5 minutes at 37 °C, followed by vigorous shaking for half a minute. After settling of the tissue the supernatant was discarded and fresh collagenase solution was added for digestion step 2 (37 °C, 14.5 minutes). This was again followed by shaking for half a minute and the exchange of supernatant with fresh collagenase solution. Digestion step 3 was conducted for 15 minutes at 37 °C with vigorous shaking for half a minute every 5 minutes, and the exchange of supernatant with fresh collagenase solution. A fourth digestion step analog to step 3 was performed. The supernatant of this step was washed twice in Advanced DMEM/F12, filtered via a 70 µm cell strainer, pelleted by centrifugation at 300 rcf and embedded in Matrigel (BD Biosciences, Franklin Lakes, NJ) for

cultivation similar to previously described [202, 203]. IntestiCult™ Organoid Growth Medium (STEMCELL Technologies, Vancouver, Canada) was used for cultivation. Organoids from *nATF6^{IEC}* tg/tg and fl/fl mice were isolated from SPF or GF housed mice at the age of 20 wk. The organoids were cultured without passaging but regular changes of medium (every 2-3 days) for 7 days and the growth behavior (cyst dimensions and number of budding crypts) was assessed at day 1 and day 7 in at least four individual wells per genotype (treatment scheme Figure 43A). Growth measurements were performed using an Olympus CK X 41 microscope and Olympus cellSens Entry software.

3.2 Histological methods

3.2.1 Histology and tissue staining

For standard histology, the intestine was removed immediately after euthanization and dissected from adjacent tissue. The different parts of the gastrointestinal tract were cut open longitudinally and inspected macroscopically for tumor presence. The tissue was processed as swiss rolls and fixed either in 10 % phosphate buffered formalin, dehydrated (Leica TP1020, Table 2) and embedded in melted paraffin (McCormick; Leica EG1150C) or embedded in optical cutting temperature (OCT) medium without fixation (Richard-Allan Scientific™ Neg-50™; Thermo Fisher).

Table 2: Dehydration and paraffin embedding of FFPE tissue.

Step	Reagent	Time (min)	Step	Reagent	Time (min)
1	70 % EtOH	60	7	100 % EtOH	60
2	70 % EtOH	60	8	100 % EtOH	60
3	80 % EtOH	60	9	Xylene	60
4	96 %EtOH	60	10	Xylene	60
5	96 %EtOH	60	11	Paraffin	60
6	100 % EtOH	60	12	Paraffin	60

For fluorescence *in Situ* hybridization (FISH) analysis, dissected but still longitudinally unopened colonic tubes were rolled to form a closed “swiss roll” and fixed in Carnoy solution overnight (60 % dry MeOH; 30 % dry chloroform; 10 % acetic acid). Dehydration of samples was performed by washes in: dry MeOH (2 times, 30 min); 100 % EtOH (20 and 15 min); xylene/100 % EtOH (1:1) (5 min) and xylene (2 times, 5 min). Dehydrated colonic tissue was submerged in melted paraffin for 20 min and embedded.

3.2.1.1 H&E staining

For H&E staining FFPE tissue sections (2.5-5 μm , Leica RM2255) were deparaffinized and rehydrated in an automated manner (Leica ST5020, Table 3). Staining with hematoxylin (of Mayer) and 0.2% eosin (ethanolic solution; both Medite) was performed (Leica ST5020). Slides were mounted with Histokitt (Roth) and covered with a glass slip (VWR).

Table 3: Deparaffinization, rehydration and H&E staining.

Deparaffinization and Rehydration		
Step	Reagent	Time (min)
1	Xylene	3
2	Xylene	3
3	100 % EtOH	2
4	96 % EtOH	2
5	70 % EtOH	1
H&E staining		
Step	Reagent	Time (min)
6	dH ₂ O	1
7	Hematoxylin	4
8	Running dH ₂ O	2
9	Eosin	2
10	70 % EtOH	1
11	96 % EtOH	1
12	100 % EtOH	1
13	100 % EtOH	1.5
14	Xylene+100 % EtOH	1.5
15	Xylene	2
16	Xylene	2
17	Xylene	various

3.2.1.2 Alcian blue/Periodic acid-Schiff (AB/PAS) staining

FFPE tissue sections were deparaffinized and rehydrated before being stained with alcian blue solution for acidic mucins (1 % v/v in 3 % acetic acid, pH 2.5, 15 min), treated with periodic acid solution (0.5 % v/v, 5 min) and co-stained with Schiff's reagent for neutral mucins (SIGMA ALDRICH, 10 min). Nuclei were then counterstained with hematoxylin, and tissue sections differentiated (0.2 % ammonia water), dehydrated and mounted. The number of goblet cells was calculated as a total number per 100 μm^2 .

3.2.1.3 High iron diamine-alcian blue (HID-AB) staining

FFPE tissue sections were deparaffinized and rehydrated before being stained with freshly prepared high-iron diamine solution (2.33 mg/ml N,N-dimethyl-meta-phenylenediamine (HCl)₂, 389 µg/ml N,N-dimethyl-para-phenylenediamine (HCl) and 102 µg/ml FeCl₃ x 6H₂O) for 16 h at RT. Sections were rinsed with deionized water and stained with alcian blue solution for acidic mucins (1 % v/v in 3 % acetic acid, pH 2.5, 15 min). Nuclei were then counterstained with hematoxylin, and tissue sections differentiated (0.2 % ammonia water), dehydrated and mounted.

3.2.2 Histopathological analysis

H&E stained colonic swiss roll sections were blindly scored for either signs of inflammation (Dr. Sigrid Kisling and Silvia Pitariu) or assessed by a molecular pathologist specialized on molecular oncology of the liver and GI tract (Prof. Dr. Achim Weber, Institute of Pathology, University Zurich and University Hospital Zurich, Switzerland). With focus on inflammation, colonic tissue sections were scored by assessing lamina propria mononuclear cell infiltration, crypt hyperplasia, goblet cell depletion and architectural distortion resulting in a score from 0 to 12. Images were acquired by the Digital microscope M8 (PreciPoint GmbH).

3.2.3 Immunochemistry

3.2.3.1 Immunohistochemical/-fluorescent stainings

For standard immunochemistry FFPE tissue sections of intestinal swiss rolls (2.5-5 µm) mounted on Superfrost Plus slides were deparaffinized and rehydrated. After proteinase k digestion (in case of F4/80: T-2006, Biomedicals) or heat-mediated antigen retrieval with 10 mM Citrate buffer the slides were equilibrated in PBS. In case of immunohistochemical detection, peroxidase quenching was performed (10 min, 3 % H₂O₂). Cryostat sections (5 µm) for HA-tag staining were fixed with 10 % Formalin (15 min, RT) and washed with PBS. Both FFPE and cryostat sections were blocked with a buffer containing 5 % serum of the species in which the secondary antibody was produced (60 min, RT, in a humidified chamber). Primary antibody was incubated overnight at 4 °C followed by 3 washes with PBS and a 1 h incubation with the secondary antibody (fluorochrome or HRP coupled) at RT (Table 4). In case of immunofluorescent staining, nuclei were counterstained with DAPI and mounted. In case of immunohistochemical detection, staining was developed by the use of the HRP substrate DAB, nuclei counterstained with hematoxylin and slides dehydrated and mounted with Aquatex mounting medium (Merck Millipore, Darmstadt, Germany).

For HA-Tag staining of FFPE tissue, a signal amplification protocol of Avidin-Biotin-Complex (ABC) and Tyramid-Signal Amplification (TSA) was applied. On top of the procedures for standard immunofluorescence described before, endogenous peroxidases were blocked by incubation of the tissue sections with 3 % H₂O₂ before blocking with standard blocking buffer. Further, endogenous biotin was blocked with Avidin-Biotin blocking kit (Vector Laboratories, Inc. Burlingame/CA) according to manufacturer's instructions. Further, a biotinylated secondary antibody was used. For ABC amplification, the Vectastain Elite ABC Kit (Vector Laboratories/ Vectastain Elite, Peterborough) was applied according to manufacturer's instructions. To detect and amplify the signal, further TSA was used, in which fluorochrome-labeled tyramides are used as HRP substrate (Individual Cyanine 5 Tyramide Reagent Pack, Perkin Elmer, Boston/ MA).

For simultaneous staining of Grp78 and Ki67, the Ki67 staining was performed as described earlier and developed with the HRP substrate DAB. Consecutively, slides were incubated in 3 % H₂O₂ for 15 minutes to inactivate antibody-bound HRP followed by washes in PBS. Afterwards, sections were stained with Grp78 according to standard procedure, but the signal was developed with the use of HRP green substrate (HRP-Green Solution Set, 42 life sciences GmbH & Co. KG, Bremerhaven, Germany).

Simultaneous staining of Grp78 and AB/PAS was performed by staining Grp78 immunohistochemically as described until the detection of the chromogenic substrate. This was followed by AB/PAS staining starting with the incubation in alcian blue solution.

Table 4: Primary and secondary antibodies used for immunochemical stainings.

Primary Antibody	Manufacturer	Dilution
<u>FFPE tissue:</u>		
Ki67: ab15580	Abcam, Cambridge, UK	1/500-600
E-cadherin: ab76055	Abcam, Cambridge, UK	1/300
Muc2 (H-300): sc-15334	Santa Cruz , Heidelberg, Germany	1/300
Grp78: BiP (C50B12)	Cell Signaling Technology, Danvers, USA	1/200
Grp78: (ET21)	Sigma Aldrich, Taufkirchen, Germany	1/100
CD3: C7930	Sigma Aldrich, Taufkirchen, Germany	1/400
F4/80 BM8	BMA BIOMEDICALS, Dianova Hamburg	1/300
HA-tag	Biozol/Biolegend, Eching, Germany	1/600
GFP	Cell Signaling, Frankfurt, Germany	1/150
<u>Cryo-sectioned tissue:</u>		
HA-Tag: ab9110	Abcam, Cambridge, UK	1/100
Secondary Antibody	Manufacturer	Dilution
Alexa Fluor donkey anti mouse 647	Dianova, Hamburg, Germany	1/300
Alexa Fluor donkey anti mouse 546	Life Technologies, Carlsbad, CA	1/300
Alexa Fluor donkey anti rabbit 488/546	Life Technologies, Carlsbad, CA	1/300
Alexa Fluor donkey anti rabbit 647	Dianova, Hamburg, Germany	1/300
Alexa Fluor donkey anti mouse 488/546/594	Life Technologies, Carlsbad, CA	1/300
donkey anti rabbit, HRP	Dianova, Hamburg, Germany	1/500
donkey anti mouse, Biotin	Dianova, Hamburg, Germany	1/300

Immunohistochemical stainings for pSTAT3 (Cell Signaling 9145), pSTAT1 (Cell Signaling 9167) and RelA (Neo Markers/ Lab Vision Corporation RB 1638-PO) were performed by the Institute of Virology (Prof. Dr. Mathias Heikenwalder, German Research Center for Environmental Health, Helmholtz Center Munich) on the automated IHC/ISH stainer Bond Max (Leica) with EDTA demasking according to manufacturer`s instructions.

3.2.3.2 Fluorescence in situ hybridization (FISH)

Carnoy-fixed paraffin-embedded tissue sections (9 µm) were deparaffinized, rehydrated and fixed in 10 % formalin, before permeabilization in a lysozyme solution (40 mg/ml lysozyme in a filter-sterilized 20 mM Tris/ 2 mM EDTA/ 1.2 % v/v Triton-X100 buffer) for 45 min at 37 °C. Tissue sections were incubated with Cy5-conjugated EUB338 (5'-gct gcc tcc cgt agg agt-3') in 100 µl filter-sterilized hybridization buffer (20 mM Tris/ 0.9 M NaCl and 0.01 % v/v SDS-solution, pH 7.3) overnight at 46°C. Sections were costained with anti-Muc2 (without antigen retrieval) and counterstained with DAPI.

3.2.4 Electron microscopy

Electron microscopy was performed at the Bioimaging Center (Lille, France). Proximal colon tissue was fixed at 4 °C in 2.5 % glutaraldehyde buffered with sodium cacodylate at 0.2 M, pH 7.4. The samples were rinsed four times with sodium cacodylate buffer, postfixed by 1 % OsO₄ (EMS) in the same buffer for 15 min at RT and “en bloc” stained with 2 % uranyl acetate (SPI-Chem) for 15 min in the dark. Subsequently, they were dehydrated using graded acetonitrile (Roth) and embedded in epon-like resin (Embed-812, EMS). Ultrathin sections (90 nm) were cut with a diamond knife (Diatome 45°) on a Leica UC7 ultramicrotome. The sections were mounted on copper grids (hexagonal 150 mesh, Pelanne Instruments). The grids were contrasted with lead nitrate and uranyl acetate according to Reynolds. Images were acquired on a Hitachi H600 transmission electron microscope operated at 75 kV.

3.2.5 Laser capture microdissection

Colonic cryo “swiss rolls” (Microm, Walldorf, Germany) were sectioned (10 µm at 20 °C) and mounted on PET frame slides (MicroDissect, Herborn, Germany) which were pre-treated with RNase ZAP (Sigma-Aldrich, Steinheim, Germany) before use and dried at RT. Slides were stored at -80 °C until use (less than one week). Each slide was stained directly before LMD microscopy using a quick-stain H&E protocol. Briefly, after equilibration to RT (2 min), slides were fixed for 1 min with 70 % (v/v) EtOH, rinsed with Diethylpyrocarbonate (DEPC) water for 30 sec, stained with Harris hematoxylin for 1 min and rinsed with DEPC water for 30 sec. After bluing with 0.1 % (v/v) NH₄OH for 30 sec, slides were counterstained with 2.5 % Eosin for 2 min. Finally, sections were dehydrated in ascending EtOH series (96 %, 100 %) for 30 sec each and air dried at RT for 5 min. Colonic IEC from tumor and non-tumor regions were distinctly cut using the UV laser-cutting system LMD 6000 and the Leica Application Suite software (Leica, Wetzlar, Germany). Cutting was stopped latest 2 hours after equilibration of the slides to RT and dissected IECs were directly lysed in 100 µl RNA lysis buffer (Buffer RLT; Qiagen) and stored at -80 °C. A total area of more than 1 x 10⁶ µm² was cut for each sample and used for RNA isolation.

3.3 Molecular biological methods

3.3.1 Genotyping

Tail cuts or ear punches were lysed in 10 mM Tris-HCl buffer pH 8.0 buffer containing 50 mM KCl, 0.45 % Nonidet P40, 0.45 % Tween 20 and 0.5 mg/mL Proteinase K overnight (O.N.) at 65 °C and inactivated at 95 °C for 10 min. 1 µL of the supernatant was mixed with 10 µl 2x Onetaq DNA polymerase (NEB) and the respective quantity and combination of primers as specified in Table 5 for the different genotyping-PCRs in a final volume of 20 µl (Primer sequence given in Table 6). The different PCR programs for genotyping are defined in Table 7. The PCRs were designed to detect both Wildtype (WT) sequence and knockout (KO)/ transgenic (TG)/ modified (Mod) locus. In case of unknown integration site of the transgene, a DNA control (DNA) was used to test for efficient PCR reaction.

Table 5: Primer combinations and PCR product sizes for genotyping.

PCR	<i>nATF6</i> (<i>Rosa26</i>)	<i>IL10</i> ^{-/-}	Villin- Cre ^{ERT2}	<i>CHOP</i> ^{-/-}	Villin- Cre	LGR5- Cre ^{ERT2}	<i>RAG2</i> ^{-/-}
Primers (nM)	#1342 (125) #1869 (125) #1870 (125)	#1213 (200) #1214 (200) #1215 (200)	#1484 (200) #1485 (200) #1119 (400) #1120 (400)	#2010 (200) #2011 (200) #2012 (200)	#1127 (300) #1128 (300) #1119 (400) #1120 (400)	#2235 (200) #2236 (200) #2237 (200)	#1270 (200) #1271 (200) #1272 (200)
Product size [bp]	WT: 262 Mod.: 300	WT: 200 KO: 450	DNA: 585 TG: 318	WT: 544 KO: 320	DNA: 585 TG: 300	DNA: 298 TG: 174	WT: 263 KO: 350

Table 6: Sequence of genotyping primers.

Primer number	5' - 3' Sequence	Primer number	5' - 3' Sequence
#1342	TCCCTCGTGATCTGCAACT	#2011	CGCCAGGGTTTTCCC
#1869	ATCAGAGCAGCCGATTGTC	#2012	CGCAGGGTCAAGAGTAGTG
#1870	GGCGGATCACAAGCAATAAT	#1127	AAGCCTGGCTCGACG
#1213	GTGGGTGCAGTTATTGTCTTCCCG	#1128	TCGCGAACATCTTCAGG
#1214	GCCTTCAGTATAAAAGGGGGACC	#2235	CTGCTCTCTGCTCCAGT
#1215	CCTGCGTGCAATCCATCTTG	#2236	ATACCCCATCCCTTTGAG
#1484	GACCATATCCACCGAGTCC	#2237	ACTTCAGGGTCACTTGC
#1485	AGGAATGCGATGAAGTAGAGC	#1270	GGGAGGACACTCACTTGCCAG
#1119	CCTTCAGCAAGAGCTGGG	#1271	AGTCAGGAGTCTCCATCTCAC
#1120	GAGACTCTGGCTACTCATCCAGC	#1272	CGGCGGGAGAACCTGCGTGCAA
#2010	ATGCCCTTACCTATCGTGC		

Table 7: PCR program settings for genotyping.

Temp (°C) / Time (sec)		ATF6 (<i>Rosa26</i>)	<i>IL10</i> ^{-/-} / Villin- Cre ^{ERT2} / <i>CHOP</i> ^{-/-}	Villin-Cre	LGR5-Cre ^{ERT2}	<i>RAG2</i> ^{-/-}
Initial Denaturation		94/60	94/60	94/60	94/60	94/60
Denaturation	Cycles: 30 / 35 for <i>IL10</i> ^{-/-}	94/20	94/20	94/15	94/20	94/30
Annealing		58/20	58/20	58/15	55/20	66/20
Extension		68/20	68/30	68/20	68/20	68/30
Final extension		68/60	68/60	68/60	68/60	68/60
Cooling		4/∞	4/∞	4/∞	4/∞	4/∞

3.3.2 Gene expression analysis

RNA of total colonic tissue (out of OCT medium samples) and small or large intestinal IECs was isolated according to manufacturer's instructions (NucleoSpin RNAII kit; Macherey-Nagel GmbH & Co. KG), and measured by Nanodrop spectrophotometer. Isolation of RNA from LMD-dissected tissue was performed using the Rneasy Micro Kit (Qiagen), according to manufacturer's instructions and measured by Quant-iT™ RiboGreen® RNA Assay Kit (Invitrogen, Eugene, USA).

Complementary DNA for qRT-PCR analysis was synthesized from 200-1000 ng RNA using random hexamers and Moloney murine leukemia virus (M-MLV) reverse transcriptase Point Mutant Synthesis System (Promega). qRT-PCR was performed using the LightCycler 480 Universal Probe Library System

(Roche). Calculations ($2^{-\Delta\Delta Ct}$ method, [204]) were normalized to *Gapdh* as housekeeper. Primer sequences and respective probes are listed in Table 8.

Table 8: Primer sequences used for qRT-PCR analyses.

Gene name	PRIMER SEQUENCES; (5' – 3'); LEFT; RIGHT	Upl PROBE
<i>Atf6-endo</i>	GGACGAGGTGGTGTCTAGAG; GACAGCTCTTCGCTTTGGAC	#110
<i>Atf6-total</i>	CCACCAGAAGTATGGGTTTCG; GGTTCTTTATCATCCGCTGCT	#73
<i>Chop</i>	GCGACAGAGCCAGAATAACA; GATGCACTTCTTCTGGAACA	#91
<i>Cxcl10</i>	GCTGCCGTCATTTTCTGC; TCTCACTGGCCCGTCATC	#3
<i>Gapdh</i>	TCCACTCATGGCAAATTCAA; TTTGATGTTAGTGGGGTCTCG	#9
<i>Grp78</i>	CTGAGGCGTATTGGGAAAG; TCATGACATTAGTCCAGCAA	#105
<i>Grp94</i>	CTGTGTGGGATTGGGAACTT; CATGGGGTCATCACTTTCTCT	#53
<i>Ifny</i>	CCTTTGGACCCTCTGACTTG; AGCGTTCATTGTCTCAGAGCTA	#63
IL 22	GTGACGACCAGAACATCCAG; GATCTCTCACTCTCTCAAGC	#94
<i>Il12-p35</i>	CCAGGTGTCTTAGCCAGTCC; GCAGTGCAGGAATAATGTTTCA	#62
<i>Il12-p40</i>	ATCGTTTTGCTGGTGTCTCC; GGAGTCCAGTCCACCTCTACA	#78
<i>Il18</i>	TGTAATGAAAGACGGCACACC; TCTTCTTTGGGTATTGCTTGG	#78
IL-23	CACCAGCGGGACATATGAAT; GTTGTCTTGAGTCCTTGTGG	#47
<i>Il4</i>	CCTGCTCTTCTTTCTCGAATGT; CACATCCATCTCCGTGCAT	#92
<i>Il6</i>	TGATGGATGCTACCAAATGG; TTCATGTACTCCAGGTAGCTATGG	#6
<i>KC (Il8)</i>	AGACTCCAGCCCACTCCAA; TGACAGCGCAGCTCATTG	#83
<i>Mcp1</i>	CATCCACGTGTTGGCTCA; GATCATCTTGCTGGTGAATGAGT	#62
<i>P58ipk</i>	AGAAGACGATTTCAAGAAAGTGC; GCTGAGACTCGGCTTCTCT	#15
<i>Tgfβ</i>	TGGAGCAACATGTGGAAGTCT; CAGCAGCCGGTTACCAAG	#72
<i>Tnfα</i>	TGCCTATGTCTCAGCCTCTTC; GAGGCCATTTGGGAACTTCT	#49
<i>Xbp1s</i>	TGACGAGGTTCCAGAGGTG; TGCACCTGCTGCGGACTCAG	#49
<i>Xbp1u</i>	GCAGCACTCAGACTATGT; GGTCCAACCTGTCCAGAATGCC	#62

Microarray analysis

Microarray analysis was conducted at Wageningen University (Department of Agrotechnology and Food Sciences, Human Nutrition) coordinated by Dr. Mark Boekschoten and processed at the University of Luxembourg (Biomedical Data Science group) by Dr. Enrico Glaab.

Microarray analysis was performed on RNA isolated from colonic IEC of *nATF6^{IEC}* mice and whole tissue of *nATF6^{IEC-OHT}* mice. Colonic IEC were isolated from SPF (n=6 animals per genotype) or GF (n=5 per genotype) housed female *nATF6^{IEC}* mice at the age of 5 wk. Further, RNA isolates of LMD-dissected colonic IEC of tumor versus normal adjacent tissue was analyzed (5 intra-individual

comparisons, age >15 wk). RNA isolated of whole colonic tissue 4 days after the end of tamoxifen induction was used for microarray analysis of *nATF6*^{IEC-OHT} mice (n=3 per genotype). All samples from one sample set were run together. Reverse-transcription, amplification and biotin labeling were performed using the Ambion WT expression kit (ThermoFisher Scientific, Bleiswijk, The Netherlands) for the SPF *nATF6*^{IEC} samples. The GeneChip WT Plus Reagent KIT (Affymetrix, Santa Clara, CA) was used for the GF *nATF6*^{IEC} and *nATF6*^{IEC-OHT} samples and the Ovation Pico SL WTA kit (NuGEN, Leek, The Netherlands) for the tumor versus non-tumor comparison. Labeled RNA samples were hybridized to Gene 1.1 ST arrays (Affymetrix, Santa Clara, CA). Gene chips were visually inspected for irregularities and scanned with Affymetrix GeneTitan instrument.

All microarray gene expression datasets were preprocessed using the Robust Multiarray Analysis (RMA) procedure for background correction, normalization and summarization [205]. Only genetic probes with a minimum average expression larger than the first quartile of the average expressions across all probes were retained for further analysis. Differentially expressed genes were ranked using the empirical Bayes moderated t-statistic [206] and p-value significance scores were adjusted for multiple hypothesis testing using the Benjamini-Hochberg method [207]. Heat maps and dendrogram groupings of genes were generated with the gplots R-package (<http://cran.r-project.org/web/packages/gplots>) and an average linkage hierarchical clustering based on a Pearson correlation distance measure. The genes displayed in these maps were selected by first applying a false-discovery rate (FDR) cut-off (see corresponding figure legends) and then ranking the genes by absolute logarithmic fold-change. Gene expression measurements were then converted to Z-scores and visualized in the maps by a color gradient, where the color darkness is proportional to the absolute Z-score. All statistical analyses were performed in the R Statistical Programming Environment [208].

3.3.3 16S rRNA Sequencing

The DNA isolation, 16S high-throughput sequencing and sequence analysis were conducted as previously described [209]. Briefly, cells were lysed by mechanical lysis and DNA was purified using a column-based procedure. Amplicon libraries (V3/V4 region) were amplified by PCR (25 cycles), purified using the AMPure XP system (Beckmann), pooled in an equimolar amount, and sequenced in paired-end mode (PE275) using a MiSeq system (Illumina, Inc.). Raw sequences were processed using IMNGS (www.imngs.org) based on the UPARSE approach [210]. First, all reads were trimmed to the position of the first base with quality score <3 and then paired. The resulting sequences were size filtered, excluding those with assembled size <300 and >600 nucleotides. Paired reads with expected

error >3 were further filtered out and the remaining sequences were trimmed by ten nucleotides on each side to avoid GC bias and nonrandom base composition. For each sample, sequences were de-replicated and checked for chimeras with UCHIME [211]. Sequences from all samples were merged, sorted by abundance, and operational taxonomic units (OTUs) were picked at a threshold of 97 % similarity. Finally, all sequences were mapped back to the representative sequences resulting in one OTU table for all samples. Further analyses were performed using in-house-developed scripts in the R programming environment.

3.3.4 Comparative genomic hybridization (CGH)

Comparative genomic hybridization (CGH) analysis were performed at the Helmholtz Center Munich by Dr. Kristian Unger (Integrative Biology Group). Tumor and normal tissue regions as classified by histopathological assessment of H&E stained sections were punched from FFPE tissue blocks. Genomic DNA was extracted and purified using the QIAamp® DNA FFPE Tissue kit (QIAGEN) according to the manufacturer`s instructions followed by quantification with the Nanodrop spectrophotometer. DNA quality was assessed by 2 % agarose electrophoresis. DNA from normal tissue of the same mouse was used as reference for the corresponding tumor DNA. For each array, 250 ng of reference DNA was labeled with Cy5, and the same amount of sample DNA was labeled with Cy3 using an oligo array CGH labeling kit (Enzo). The labeled DNA was purified using AMICON ultra-0.5 ml centrifugal filters (Millipore) and hybridized on SurePrint G3 Custom CGH Microarrays (8x60K, AMADID 41078, Agilent) according to the manufacturer`s protocol. After washing and scanning according to the manufacturer`s protocol, resulting data text files were subjected to preprocessing, normalization, and copy-number calling within the statistical platform R (www.R-project.org). Spatial normalization was conducted using the Bioconductor package MANOR and the copy-number status of each array probe was called using the CGHcall package followed by complexity reduction using the CGHregions package. To visually assess the copy-number profiles, karyogram-like plots were generated along mouse ideogrammes using an in-house written function.

3.3.5 Western blot analysis

Total protein concentration of ultrasonicated samples lysed in urea-containing protein lysis buffer was assessed by 660 nm Protein Assay (Pierce) according to the manufacturer`s instructions. Lysates were diluted with 6x sodium dodecyl sulfate buffer and incubated at 95 °C for 5 min. Samples were separated by reducing sodium dodecyl sulfate polyacrylamide gel electrophoresis (SDS-PAGE) and transferred on polyvinylidene difluoride membranes (Immobilon-P membrane, Merck-Millipore,

Darmstadt, Germany) by semi-dry blotting using a semi dry blotting chamber (PeqLab, Erlangen, Germany). After blocking with 5 % milk powder or 3 % ECL Prime Blocking Reagent (Amersham) in 1xTBS/0.1 % Tween-20 (TBST) for 1 h at RT, membranes were incubated in primary antibody diluted in the blocking buffer ON at 4 °C (Table 9). After three washes with TBST, membranes were incubated in blocking buffer with secondary antibody (Table 9) for 1 h at RT followed by three washes with TBST or washes in PBST for near-infrared (NIR) detection. The blots were detected using an enhanced chemiluminescence light-detecting kit (GE Healthcare) or direct NIR detection using an Odyssey imaging system (LI-COR). In case of whole protein detection as loading control, samples were separated by SDS-PAGE, stained by Coomassie and imaged by a calibrated densitometer (GC-800, Biorad). Quantification was performed using Image Studio Lite Version 5.2 (LI-COR).

Table 9: Primary and secondary antibodies used for Western Blot analysis.

Primary Antibody	Manufacturer	Dilution
Grp78: ET21	Sigma Aldrich, Taufkirchen, Germany	1/2000-4000
ATF6: ADI-905-729-100	Enzo Life Sciences, Lausen, Switzerland	1/1000
β -Actin (13E5): #4970	Cell Signaling Technology, Danvers, USA	1/2000
HA-Tag: ab91110	Abcam, Cambridge, UK	1/1000
Phospho-eIF2a	Cell Signaling Technology, Danvers, USA	1/1000
Secondary Antibody	Manufacturer	Concentration
donkey anti rabbit, HRP	Dianova, Hamburg, Germany	1/2000
goat anti rabbit; IR CW800	LI-COR, Lincoln, USA	1/10000-15000

3.4 Human cohort

The use of surgically resected human tissue samples was approved by the Ethics Committee of the Medical Faculty of TUM (#1926/7, and #5428/12) and obtained after prior informed written consent. Tumor tissue from 104 patients with histopathologically confirmed colorectal cancer, who underwent complete surgical resection (R0) between 1988 and 2010 at the Dept. of Surgery, Klinikum rechts der Isar, TUM, was obtained by a pathologist immediately after resection and subsequently shock-frozen and stored in liquid nitrogen until further use. The clinical and histopathological data of the retrospective cohort have been collected and documented as published [212]. Patient age, gender, TNM tumor classification stage and anatomical localization are indicated in Table A 1. Patients with inflammatory bowel disease or neoadjuvant therapy were excluded from the study. Further, samples of histologically confirmed non-diseased colon mucosa from resected

specimen (n=28) were analyzed. Specimens were transferred into liquid nitrogen and stored at -80 °C until further processing. Post-operative follow-up data were available, with a median follow-up of 97 months, as reported previously [213]. Protein lysates were prepared from the frozen tissue lysates essentially as described earlier [214].

The public “The Cancer Genome Atlas TCGA” data set was analyzed for prognostic association of UPR genes with the cBioPortal platform, consisting of 633 CRC samples from 629 patients, of which 541 cases had available follow-up survival documentation [215, 216]. Analysis were performed by Prof. Dr. Klaus-Peter Janssen (Department of Surgery, Technical University Munich, Munich, Germany).

3.5 Statistical analysis

Statistical analyses were performed with R or Graphpad Prism V.6.00/V.7.02 using analysis of variance (ANOVA) followed by pairwise comparison testing (Holm-Sidak, Tukey, Bonferroni correction and Sidak), by Kruskal-Wallis test followed by Dunn`s multiple comparison, Mann-Whitney test, two-sided Welch Two Sample t-test with p-values adjusted by Benjamini-Hochberg-Method or by unpaired two-tailed T-test. Graphics were created using GraphPad Prism V.6.00. and 7.02. Unless otherwise stated, data are presented as mean \pm SD and p-values below 0.05 were considered to be statistically significant ($p \leq 0.05$: *; $p < 0.01$: **; $p < 0.001$: ***; $p < 0.0001$: ****). P-values resulting from multiple-testing were corrected by calculation of the Benjamini-Hochberg False-discovery rate. For visualization of the relationships between bacterial profiles, non-parametrical multiple dimensional scaling plots were computed using the packages *vegan* and *ade4*. Recurrence-free survival (i.e., distant metastasis-free survival) was considered as primary endpoint. Statistical evaluation was performed using IBM® SPSS® Statistics Version 19 (SPSS Inc., IBM Corporation, Somers, New York, USA). In order to derive optimal cut-off values of gene expression levels, maximally selected log-rank statistics performed by R Software version 2.13.0 (R Foundation for Statistical Computing, Vienna, Austria) were used. To consider multiple test issue within these analyses, the R-function *maxstat.test* was employed, as described in detail earlier [213].

4. RESULTS

4.1 ATF6 in colon cancer

To address the question whether UPR signaling is involved in colon cancer, the publically available TCGA CRC (colorectal cancer) dataset consisting of 629 patients was tested for genetic alterations in UPR mediators (Figure 7A, in collaboration with Prof. Dr. Klaus-Peter Janssen, Department of Surgery, Technical University Munich). Genetic alterations comprise somatic gene mutations (whole exome seq.), DNA copy number alterations, mRNA expression changes (microarray) and Protein expression (Reverse phase protein array). The highest frequencies of genetic alterations were observed for ATF6 (7 %), ATF6B (6 %) and XBP1 (7 %). Only ATF6 and ATF6B showed prognostic significance with respect to disease-free survival (p-values 0.039 and 0.041). Most ATF6 and ATF6B alterations were mutually exclusive with a combined frequency of 12 %. With respect to ATF6, alterations with ATF6 up-regulation were significantly associated with bad prognostic impact on disease-free survival (p-value 0.019; Figure 7A and B). In case of genetic alterations classified as ATF6 up-regulated only, alterations resulting in genomic deletion of the ATF6 locus, mRNA and protein down-regulation were excluded.

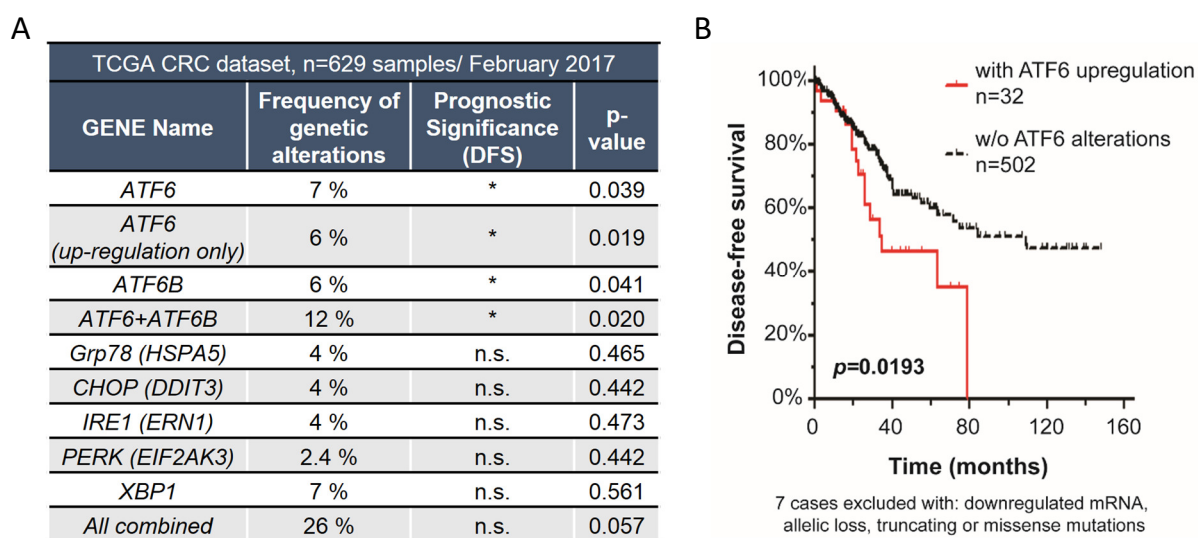


Figure 7: ATF6 alterations have prognostic significance in the TCGA CRC dataset.

(A) Summary of frequency of genetic alteration of UPR mediators and its correlation with the prognostic significance with respect to disease-free survival (DFS) in the TCGA CRC dataset (February 2017) retrieved from cBioPortal. **(B)** Kaplan-Meier analysis for disease-free survival of subjects with ATF6 up-regulation in the TCGA CRC dataset. Analysis were performed by Prof. Dr. Klaus-Peter Janssen, Department of Surgery, Technical University Munich.

Based on the high prognostic significance of genetic alterations classified as ATF6 up-regulated, the protein expression of the activated form of ATF6 (nATF6) was analyzed by Western Blot in tumor tissues of a human cohort consisting of 104 patients (in collaboration with Prof. Dr. Klaus-Peter Janssen, Department of Surgery, Technical University Munich). Among the 104 patient samples analyzed, 83 cases without protein degradation and documented follow-up were retained for further analysis (Table A 1). Cut-off determination by maximally selected log rank statistics was used to stratify patients with high intratumoral ATF6 protein expression levels (threshold: 1.55-fold of mean normal tissue) (Figure 8 B). Kaplan-Meier analysis revealed significantly reduced disease-free survival in CRC patients with aberrant ATF6 expression levels ($p=0.0308$) (Figure 8 A). The subgroup with over-threshold expression comprised 10.8 % of all patients analyzed, and their hazard ratio for developing metachronous metastasis was 4.0 (95 % CI 1.2 to 14.2). Correlation of ATF6 expression levels with clinical and pathological parameters was assessed by Spearman-rho analysis. High ATF6 expression levels were significantly associated with tumor size ($p=0.013$, correlation coefficient: 0.267), as well as with increased patient age ($p=0.033$, correlation coefficient: 0.231). No further significant correlation with staging, grading, nodal status, or mismatch-repair deficiency was observed.

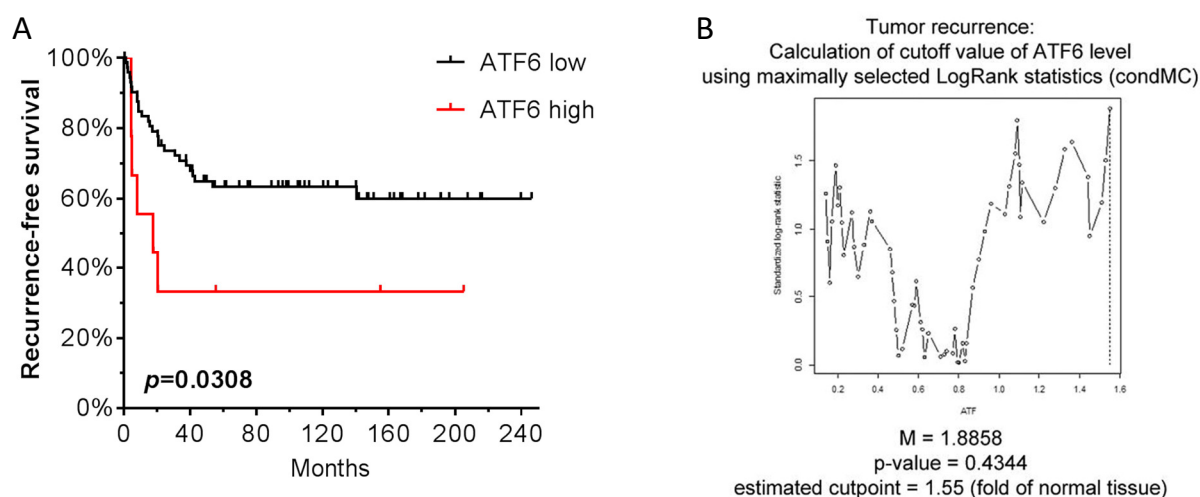


Figure 8: High nATF6 levels have prognostic significance in human colon cancer

(A) Kaplan-Meier analysis for recurrence-free survival of a colon cancer patient collective (104 patients) according to protein expression of the activated form of ATF6. β -Actin was used as a housekeeper for nATF6 expression. **(B)** Determination of cutoff value for nATF6 level using maximally selected LogRank statistics in (condMC, R) (cutoff: 1.55; activated ATF6, fold of mean level in normal colon mucosa; maximum of the log-rank statistics is $M = 1.8858$).

Taken together, these analysis support the hypothesis that ATF6 activation in IEC could be relevant for the development of CRC and is in concert with the recently published finding that ATF6 expression is associated with dysplastic changes in the human colonic mucosa [187]. Considering the

clinical relevance of increased ATF6 expression, a mouse model was generated to study the role of ATF6-driven UPR in IECs. The so-called *nATF6*^{IEC} mouse was designed to express the activated form of ATF6 specifically in IEC.

4.2 Validation and phenotypic description of constitutive *nATF6*^{IEC} mice

4.2.1 Transgene expression and ER UPR activation in *nATF6*^{IEC} mice

To validate the newly generated *nATF6*^{IEC} mouse model the genetic modification and resulting transgene expression was characterized. The rationale behind the *nATF6*^{IEC} genetic modification is to bypass the endogenous activation pathway of ATF6. Endogenous activation of ATF6 is provoked by ER protein stress and results in subsequent transport of ATF6 to the Golgi and its proteolytic formation of the active transcription factor nATF6 (Figure 9A). In the transgenic situation the activated form of nATF6 is expressed independent of ER stress signals. This is achieved by recombination-mediated cassette exchange (RMCE) of a construct into the *Rosa26* locus (Figure 9B). This construct contains the 1.6-kb hybrid promoter composed of the CMV immediate-early enhance, CBA promoter, and CBA intron 1/exon 1 (commonly called the CAGGS promoter), a loxP-flanked STOP cassette (Fluc mini ORF and a polyadenylation site) and the *nATF6-HA* open reading frame. Cre-mediated recombination is required to induce the expression of nATF6-HA due to Cre-mediated removal of a STOP cassette. IEC-specific expression of nATF6-HA is achieved by breeding the mice to Villin (Vil)-Cre mice. For genotyping, DNA isolated from mouse tail or ear was used, detecting the modified *Rosa26* locus and the presence or absence of Vil-Cre (Figure 9C). The *Rosa26* locus was analyzed by primers discriminating the wildtype (WT) and the modified (Mut) *Rosa26* locus. The presence of Vil-Cre was detected by specific primers (Cre^{tg}) and DNA control primers were used in the same reaction to test for successful DNA amplification. The genotype serving as wildtype control, abbreviated by fl/fl, arises from the same breeding as transgenic mice and is characterized by the presence of the Mut *Rosa26* locus, but absence of Vil-Cre. In contrast to that, homozygous (tg/tg) and heterozygous (tg/wt) mice encode two or respectively one allele of the Mut *Rosa26* locus and express the Cre recombinase under the control of the Villin promoter. To test for the expression of the nATF6 transgene, isolated IEC were processed for downstream RNA and protein detection. qRT PCR analysis of colonic and small intestinal IEC using specific primers for the detection of total (endogenous and transgenic) ATF6 confirm high expression of the ATF6 in IEC of the whole intestinal tract of tg/tg and tg/wt animals (Figure 9D). This increased expression is not accompanied by changes in the expression of endogenous ATF6 (Figure 9D) or the ATF6 isoform ATF6 β (Figure 9E). The nATF6 protein is further detectable using Western Blot both by the use of an HA-Tag and ATF6 antibody (Figure 9F). Whereas the HA-Tag antibody solely detects the transgene, the ATF6 antibody further gives a band in the fl/fl control visualizing endogenously expressed and activated ATF6. Immunofluorescent detection of the transgene using the HA-Tag antibody confirms the specific expression of the transgene in IEC with clear localization to the nuclei (Figure 9G).

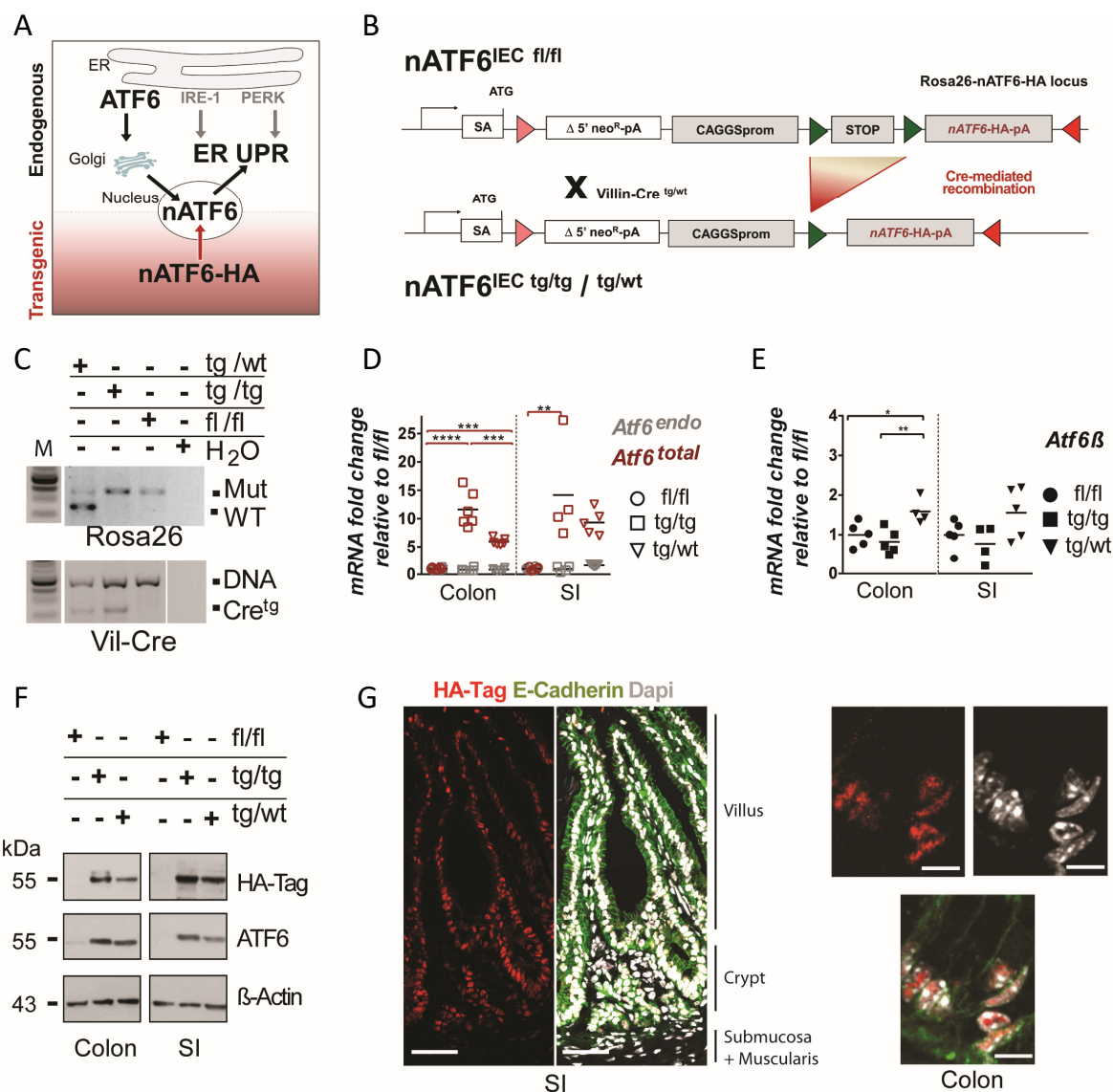


Figure 9: The nATF6^{IEC} mouse model: genetics and ATF6 expression.

(A) Scheme illustrating the endogenous activation pathway of ATF6 (upper part) and expression of the transgene for the activated form of ATF6 (lower part). **(B)** Schematic drawing visualizing the targeting strategy for the newly generated nATF6^{IEC} mouse model and the generation of the Rosa26-nATF6-HA Knock-in allele. A construct containing the 1.6-kb hybrid promoter composed of the CMV immediate-early enhance, CBA promoter, and CBA intron 1/exon 1 (commonly called the CAGGS promoter), a loxP-flanked STOP cassette (Fluc mini ORF and a polyadenylation site), and the nATF6-HA open reading frame was inserted into the ROSA26 locus using recombination-mediated cassette exchange (RMCE). Cre-mediated recombination is achieved by breeding the fl/fl mice to Villin-Cre mice and results in expression of nATF6-HA due to Cre-mediated removal of the STOP cassette. **(C)** Agarose gels demonstrating genotyping results for the modified (Mut) and wildtype (WT) Rosa26 locus and the Cre transgene (Cre^{tg}). A DNA-control (DNA) detecting presence of DNA is used to control for PCR efficiency in case of the Vil-Cre PCR (M: 100 bp marker) **(D)** mRNA levels of colonic and small intestinal IEC for endo (endogenous) and total (transgene + endogenous) Atf6 expression. **(E)** mRNA levels of colonic and small intestinal IEC for Atf6 β expression. **(F)** Western blots of colonic and small intestinal IEC for the activated form of ATF6 using specific antibodies against ATF6 and the HA-epitope. β -Actin served as loading control. **(G)** Transgene localization in the small intestine (SI, ileum, scale bars 50 μ m) and the colon (cellular resolution, scale bars 10 μ m) detected by immunofluorescence. Red: HA-Tag; green: E-Cadherin; white: Dapi. Statistics **(D, E)**: ANOVA followed by pairwise comparison testing (Tukey).

To validate the expression levels of nATF6 present in the *nATF6^{IEC}* tg/tg mouse they were compared to those reached in human tumor samples (Figure 10). Relative to normal tissue adjacent to the tumor a proportion of patients showed similar fold changes as *nATF6^{IEC}* tg/tg mice.

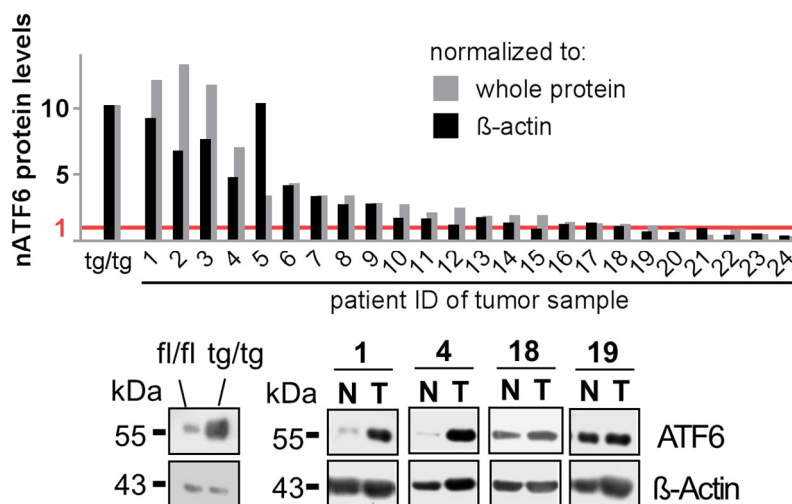


Figure 10: Expression levels of nATF6 in the *nATF6^{IEC}* mouse and tumor tissues.

Comparison between expression levels of nATF6 in the *nATF6^{IEC}* tg/tg mouse relative to the fl/fl mouse and expression in tumor samples relative to normal tissue adjacent to the tumor of the same patient. β -Actin and whole protein, as assessed by Coomassie stain, served as loading control.

To unravel downstream signaling, ER UPR relevant genes were examined in IEC isolates of *nATF6^{IEC}* mice. qRT-PCR analysis showed a substantial increase in the expression of known ATF6 target genes like *Grp78*, *Grp94*, *Chop* and *P58^{IPK}* independent of age and the intestinal site (Figure 11A, B, C). Most target genes did not show statistically significant differences between the expression in tg/tg and tg/wt mice. No significant changes in the splicing of *Xbp1* between tg/tg and fl/fl mice were detected. Focusing on the PERK arm of UPR, no dominant increase in phosphorylated eIF2 α is evident in *nATF6^{IEC}* tg/tg mice (Figure A 1). The analysis of relevant targets of the three arms of ER UPR mediated by PERK, IRE-1/Xbp1 and ATF6 based on microarray analysis point towards a predominant, but not exclusive, activation of ATF6-specific targets (Figure 11D, Figure 12, microarray analysis in cooperation with Dr. Mark Boekschoten (Department of Agrotechnology and Food Sciences, Human Nutrition, Wageningen University) and Dr. Enrico Glaab (Biomedical Data Science group, University of Luxembourg)). Focusing on the expression of the ER UPR chaperone Grp78, Grp78 showed elevated protein levels in IEC, both in tg/tg and tg/wt mice, as analyzed by immunohistochemical detection (Figure 11E) and Western Blot (Figure 11F).

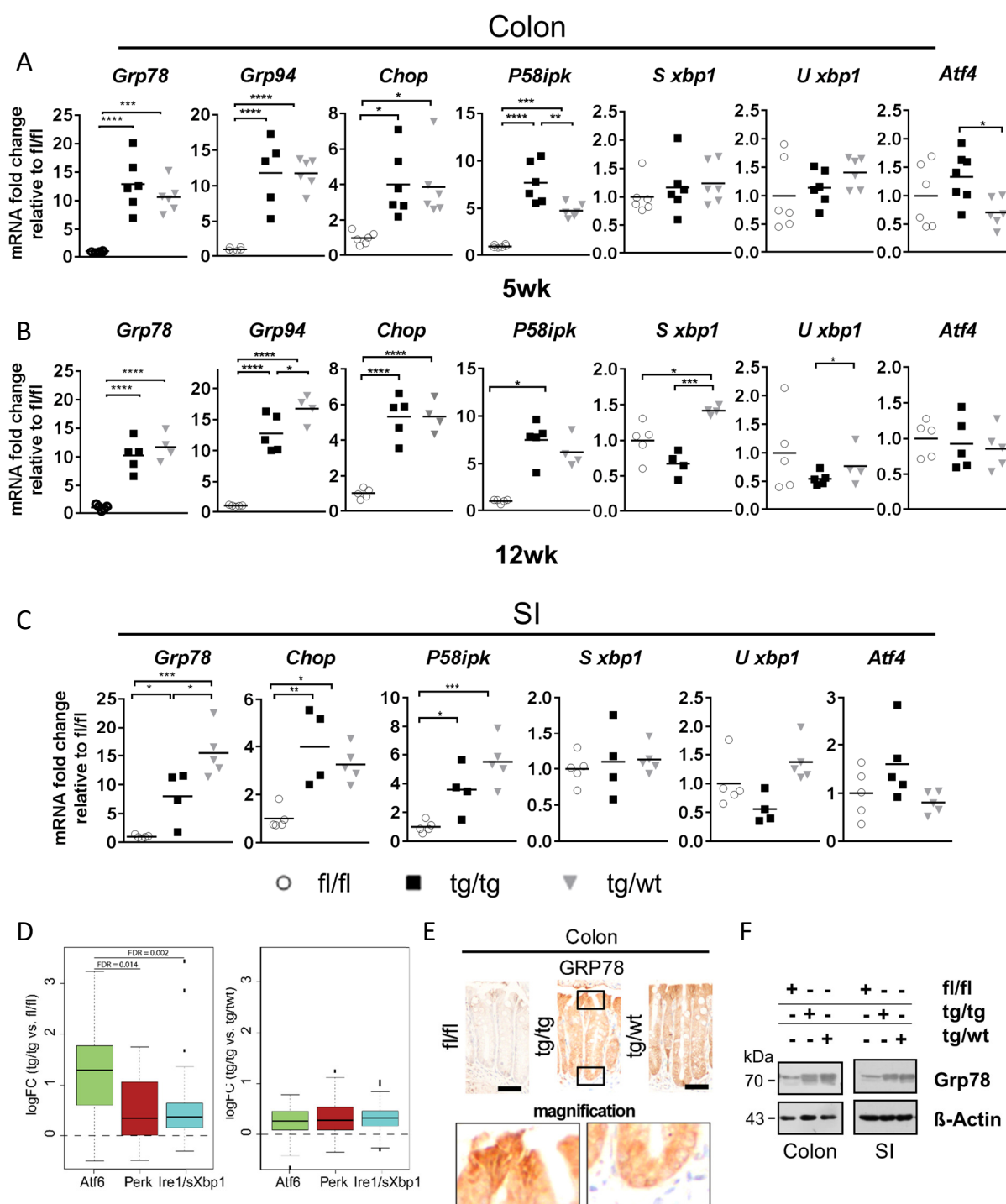


Figure 11: The *nATF6*^{IEC} mouse model: ATF6-driven ER UPR activation in IEC.

(A-B) mRNA expression analysis of colonic IEC for UPR-relevant genes at 5 wk **(A)** and 12 wk **(B)** of age. **(C)** mRNA expression analysis of small intestinal IEC (SI) for UPR-relevant genes at 12 wk of age. **(D)** Median of the expression level of genes independent of significant regulation known to be involved in ATF6, PERK and IRE-1/sXbp1 driven UPR signaling [95] in microarray analysis of colonic IEC at 5 wk of age. In the box plots, bold horizontal lines represent median values and boxes highlight the corresponding interquartile ranges. **(E)** GRP78 protein levels evaluated by immunohistochemical staining (age 12 wk, scale bars 50 μ m). **(F)** Western Blot for GRP78 of colonic and small intestinal IEC at the age of 18 wk. β -Actin served as housekeeper. Statistics **(A-C)**: ANOVA followed by pairwise comparison testing (Tukey) or Kruskal-Wallis test followed by Dunn's multiple comparison test. **(D)** Two-sided Welch Two Sample t-test with p-values adjusted by Benjamini-Hochberg-Method.

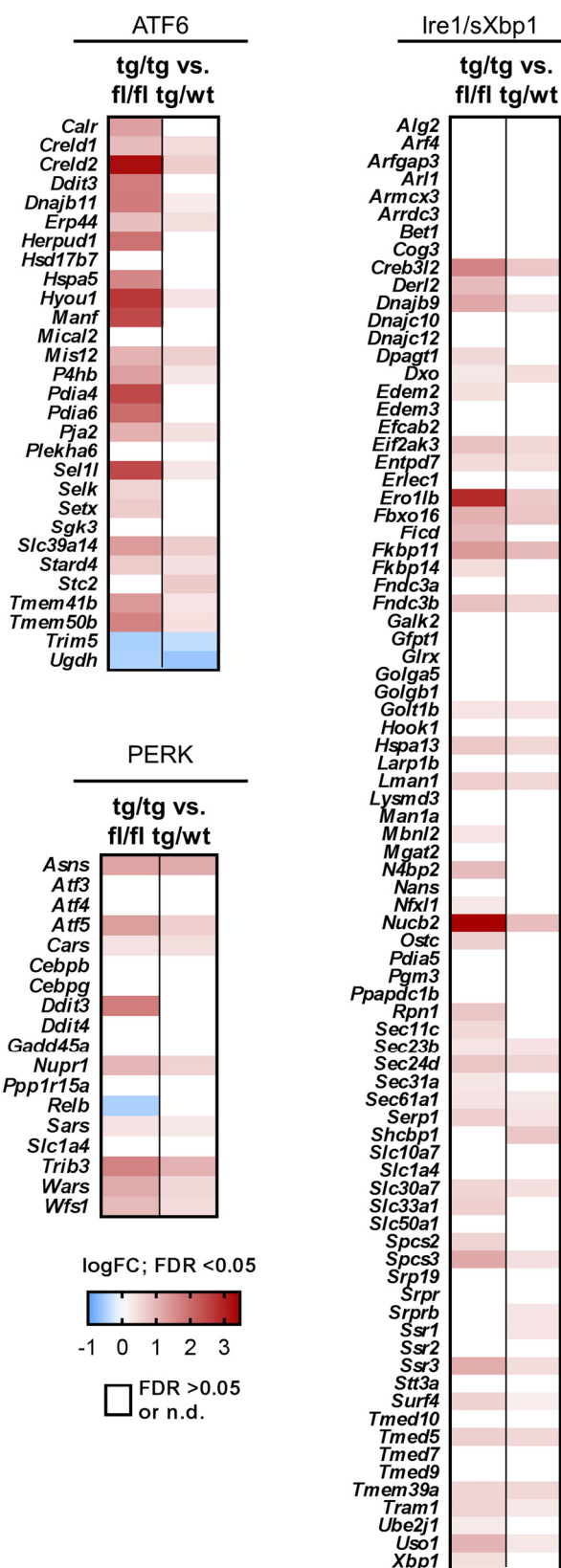


Figure 12: ATF6, PERK and IRE-1/sXBP1 signaling in *nATF6^{EC}* mice.

Heatmap illustration of genes involved in ATF6, PERK and IRE-1/sXBP1 signaling based on microarray analysis of SPF mice. Gene sets are adapted from [95]. Each rectangle color-codes the logFC between tg/tg vs. fl/fl or tg/tg vs. tg/wt, respectively. Genes not significantly regulated (FDR < 0.05) or not detected are color-coded in white.

4.2.2 Intestinal tumor development and reduced survival in *nATF6^{IEC} tg/tg* mice

To phenotypically characterize the *nATF6^{IEC}* mice, they were housed for one year under specific pathogen-free (SPF) conditions. Homozygous mice spontaneously developed large intestinal tumors (Figure 13A). This was associated with a significantly reduced overall survival of *nATF6^{IEC} tg/tg* mice (Figure 13B). In contrast, *fl/fl* and *tg/wt* mice remained tumor-free even at the age of 1 year.

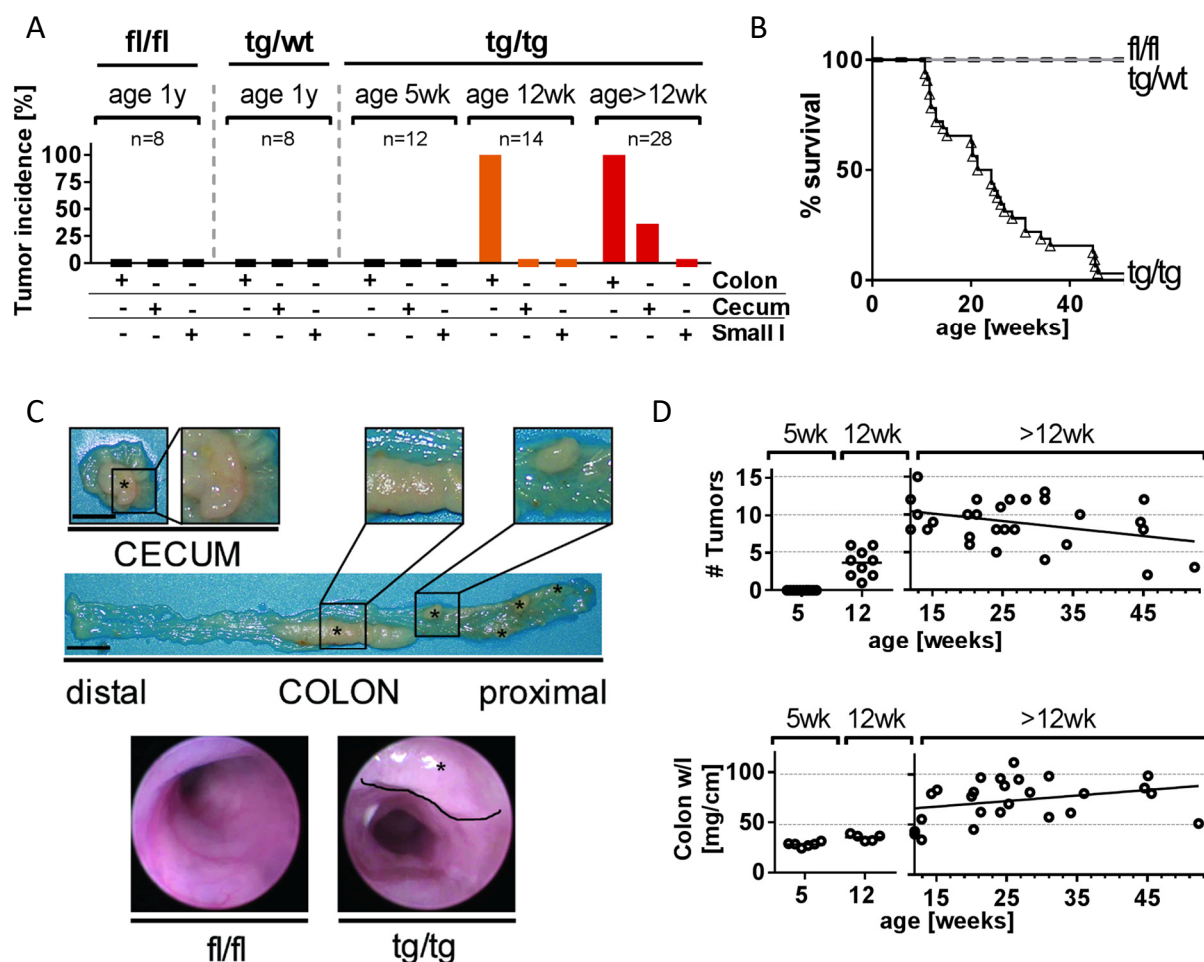


Figure 13: Spontaneous large intestinal tumor formation in *nATF6^{IEC} tg/tg* mice.

(A) Tumor incidence in percentage at different age time points for the *fl/fl*, *tg/tg* and *tg/wt* genotype in the colon, cecum and small intestine (Small I). **(B)** Kaplan-Meier survival analysis of *fl/fl*, *tg/tg* and *tg/wt* mice over 1 year in SPF housing conditions (number of mice: *fl/fl* 8; *tg/tg* 32; *tg/wt* 8). Mouse survival is based on ethical criteria for experimental endpoint. **(C)** Representative macroscopic image of the appearance of cecal and colonic tumors in the *tg/tg* mouse (scale bars 1 cm); asterisks indicate tumors (upper panel). Endoscopic appearance of the colon in *fl/fl* and *tg/tg* mice; tumor indicated by asterisk and dashed line (lower panel). **(D)** Time-dependent analysis of the tumor numbers and tumor volume as analyzed by colon weight/length ratio in *tg/tg* mice.

With respect to the time course of disease, tg/tg mice were classified into pre-tumor (5 wk of age), early-tumor (12 wk) and late-tumor (>12 wk) stages. While no tumors were observed in tg/tg mice at the age of 5 weeks, tumor incidence was 100 % in the colon at the age of 12 weeks (Figure 13A). At late-tumor stage, one third of tg/tg mice also developed cecal tumors. Small intestinal tumors were never observed. Macroscopically, tumors were seen as raised areas of thickened epithelium that resulted in a constricted luminal area in the proximal to mid part of the colon (Figure 13C). Tumor formation was mainly restricted to the mid to proximal end of the colon and the cecum. Tumor volume, as measured indirectly via colon weight/length ratio, correlated with age, but tumor numbers did not (Figure 13D).

4.3 Characterization of the intestine of *nATF6*^{IEC} mice

4.3.1 Histopathological characterization of tumors as adenomas

Histopathological examination of intestinal tumors (T) vs. non-tumor regions (N) revealed that tg/tg mice developed adenomas with low to focal high-grade dysplasia (Figure 14A, B; in cooperation with Prof. Dr. Achim Weber, Institute of Pathology, University Zurich and University Hospital Zurich). Dilated crypts (d) were evident in most tg/tg colonic sections.

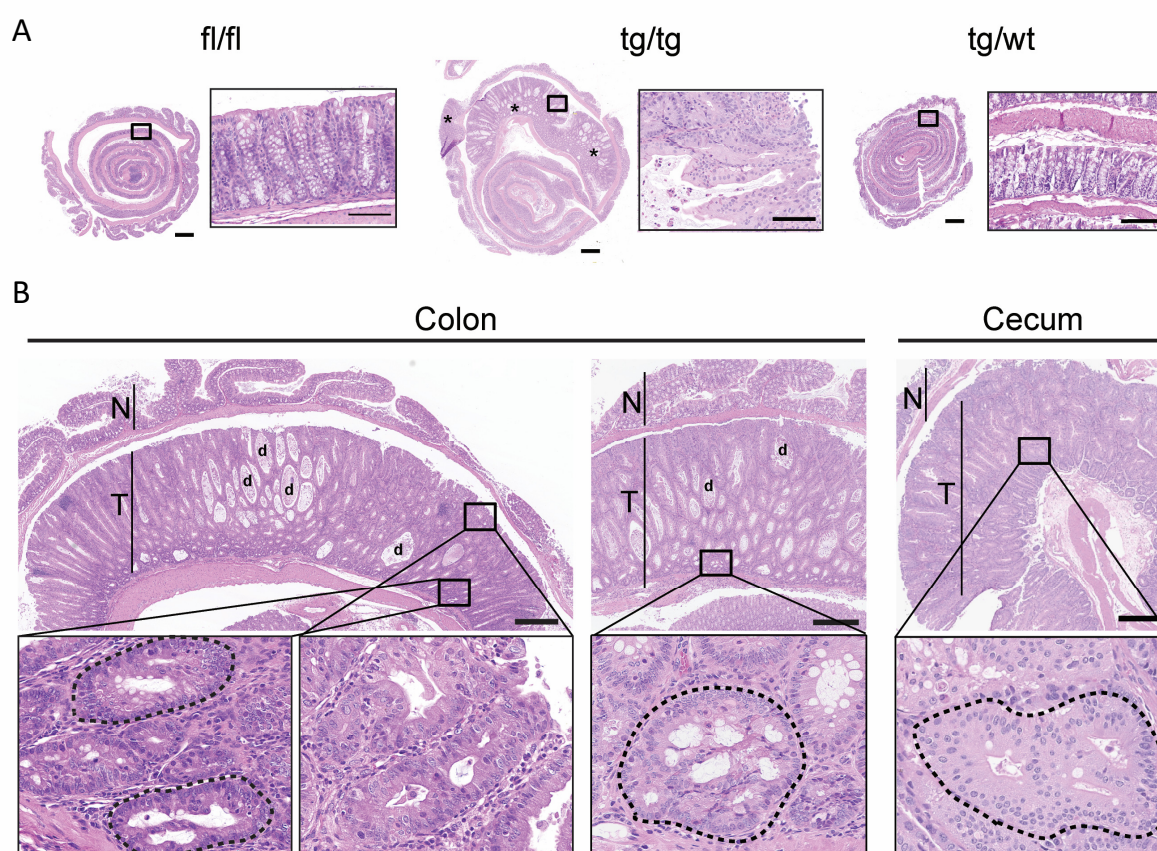


Figure 14: Histopathological characterization of tumors in the *nATF6*^{IEC} tg/tg mouse as adenomas with low to focal high grade dysplasia.

(A) Representative H&E stained sections of colonic swiss rolls (scale bars 1 mm) and corresponding higher magnifications (rectangles; scale bars 200 μ m) are shown for all three genotypes. Indicated by asterisks are tumor regions in the tg/tg section. **(B)** Exemplary pictures of H&E stained tumor regions (T) and non-tumor regions (N) (scale bars 500 μ m). Tumors are classified as adenomas with low to focal high-grade dysplasia. Magnified regions indicate cribriform structures with back to back glands and loss of goblet cells. D: dilated crypts, circled areas: cribriform structures.

To characterize the genomic makeup of these adenomas, array-based comparative genomic hybridization (CGH) was used to compare tumor-derived genomic DNA to a reference genomic DNA from the normal tissue of the respective mouse (in collaboration with Dr. Kristian Unger Integrative Biology Group, Helmholtz Center Munich). The karyogram shown in Figure 15 highlights genomic

imbalances between the tumor genomes in reference to the normal tissue of eight individual mice for chromosomes 1-19. Red indicates a gain and blue a loss in the tumor sample. Most mice showed only marginal alterations with respect to instability of the tumor genome, although some tumor samples (extracted from mouse no. 147) were characterized by more pronounced genomic alterations dominated by losses.

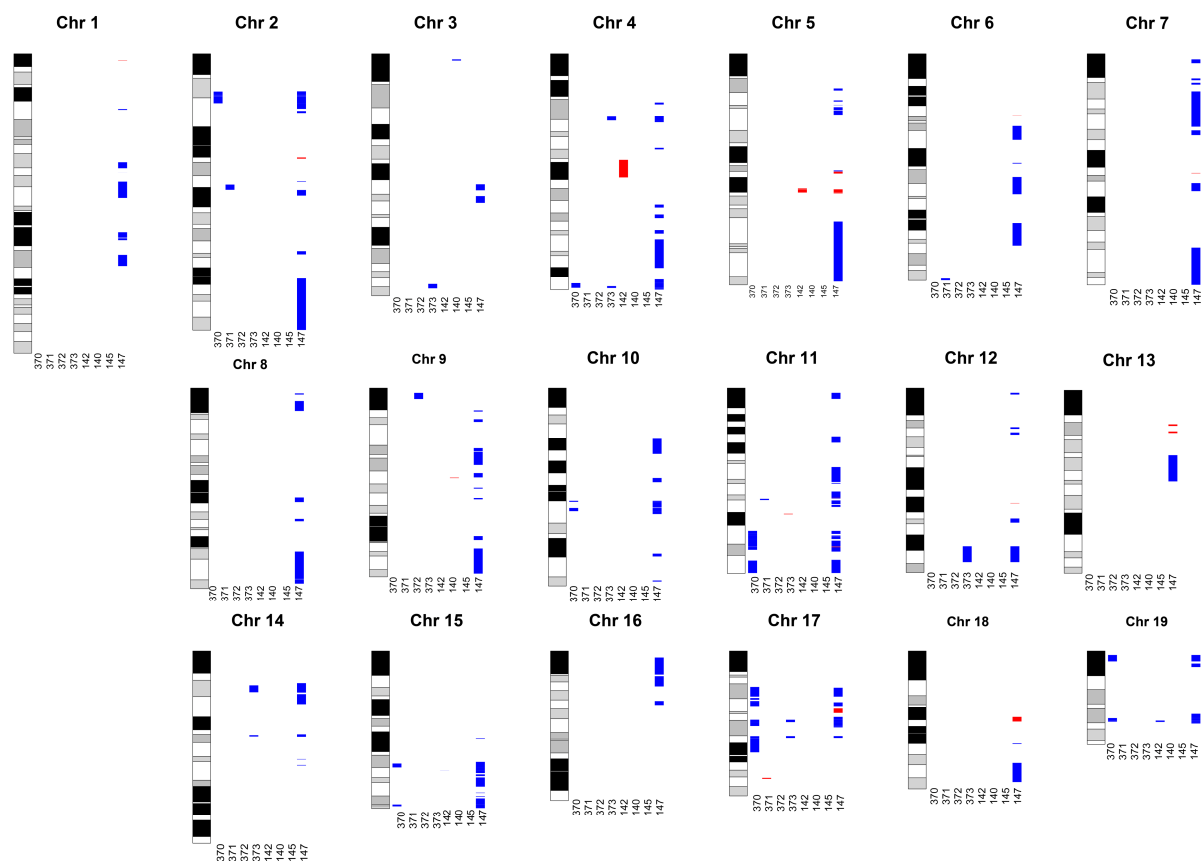


Figure 15: Array-based comparative genomic hybridization of tumors in the *nATF6^{IEC} tg/tg* mouse.

Karyogram summarizing array-based CGH results of 8 tumor samples derived from *nATF6^{IEC} tg/tg* mice (blue: loss; red: gain). Reference DNA was extracted from normal tissue of the respective mouse. CGH was performed at the Integrative Biology Group, Helmholtz Center Munich and analyzed by Dr. Kristian Unger.

4.3.2 Alterations in goblet cells and mucus barrier

Goblet cells and Paneth cells are secretory cells of the intestine known to be susceptible to altered ER functions [115, 121]. In light of this, they were in the focus of attention in the *nATF6^{IEC}* mice. Staining of mucin using PAS/AB showed significantly reduced numbers of mucin-filled goblet cells in the colonic epithelium of *nATF6^{IEC}* tg/tg mice already at a pre-tumor stage (5 wk) with increasing loss over time (Figure 16A). PAS/AB staining of tg/wt and fl/fl mice confirmed normal appearance of mucin-filled goblet cells at 5, 12, and 20 wk of age. To further examine alterations in mucus composition, mucin sulfation, sialylation and glycosylation were assessed. Despite a loss of mucin-filled goblet cells, high-iron diamine (HID) and AB staining showed that the ratio between sialo- and sulfomucins (represented as % sulfomucins) was similar between all three genotypes (Figure 16B). Furthermore, biochemical assays revealed that both sialic acid and O-glycan concentrations in *nATF6^{IEC}* tg/tg mice at a pre- (5 wk) and late-tumor stage (20 wk) remained unaltered (Figure 16C). qRT PCR-based analysis of goblet cell markers revealed a significant downregulation of early, intermediate and mature markers in *nATF6^{IEC}* tg/tg and tg/wt mice (Figure 16D).

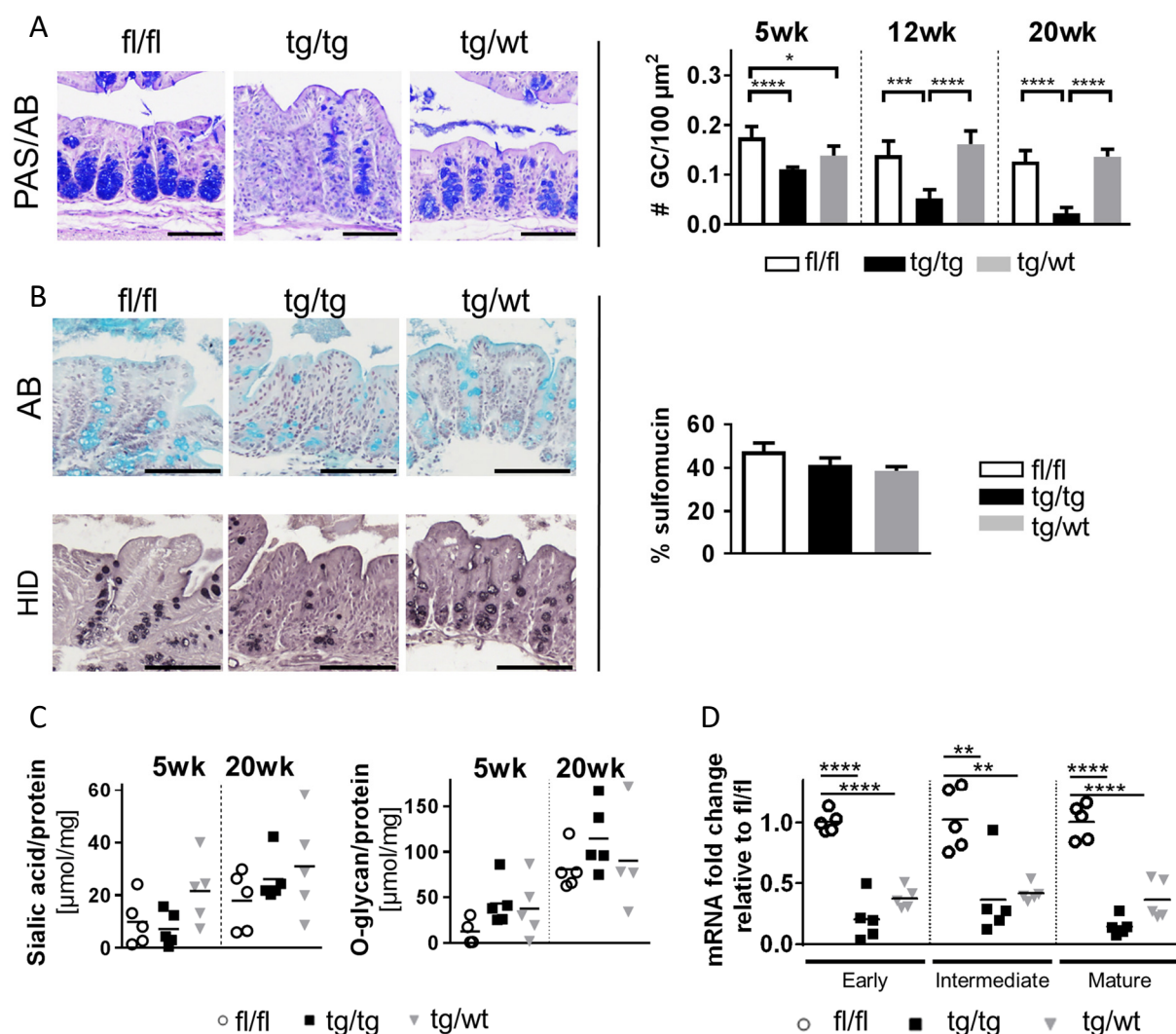


Figure 16: Goblet cell alterations in *nATF6*^{IEC} tg/tg mice.

(A) Representative PAS/AB staining for mucin-filled goblet cells in the colon at the age of 20 wk (magenta/blue), with nuclei counterstained using hematoxylin (scale bars 100 μm). The graph shows the number of mucin-filled goblet cells per 100 μm^2 at 5, 12 and 20 wk. (B) Representative high-iron diamine and AB staining for sialo- and sulfomucins in the colon at the age of 12 wk (blue/brown), with nuclei counterstained using hematoxylin (scale bars 100 μm). The graph shows the percentage of sulfomucins of 12 wk-old mice. (C) Biochemical assays for sialic acid and O-glycan concentrations in colonic mucus of 5 wk- and 20 wk-old mice ($n = 4-5$ per genotype). (D) Detection of an early (*Tff3*), intermediate (*Oasis*) and mature (*Muc2*) goblet cell marker by qRT-PCR in colonic IEC at 12 wk of age. Statistics (A-D): ANOVA followed by Bonferroni correction for multiple testing.

To reveal consequences of the observed goblet cell phenotype, the functionality of the mucus barrier was measured. The intestinal mucus barrier in the colon has important functions in separating bacteria and the intestinal epithelial cells and can be divided in the stratified inner layer which is impenetrable and loose outer layer which is penetrable to bacteria. Fluorescence *in situ* hybridization and Mucin 2 (*Muc2*) immunofluorescence staining of Carnoy-fixed colon tissue allowed simultaneous visualization of bacteria (Eub338 probe) and mucus. In line with the loss of mucin-filled goblet cells, the mucus layer in *nATF6*^{IEC} tg/tg mice appeared less structured (no clear stratified inner layer (s) and loose outer layer (o)), and more permeable to bacterial penetration (Figure 17A). Quantitative

measurements in the distal colon of all three genotypes revealed a significantly shorter distance between bacteria and the epithelial surface in $nATF6^{IEC}$ tg/tg mice, already at a pre-tumor stage (Figure 17B). Furthermore, in the proximal colon of tg/tg mice, bacteria were observed in much closer contact to the intestinal epithelium compared to fl/fl mice, with sporadic penetration into the lower parts of the crypt regions (Figure 17C). $nATF6^{IEC}$ tg/wt mice displayed no significant difference compared to $nATF6^{IEC}$ fl/fl mice.

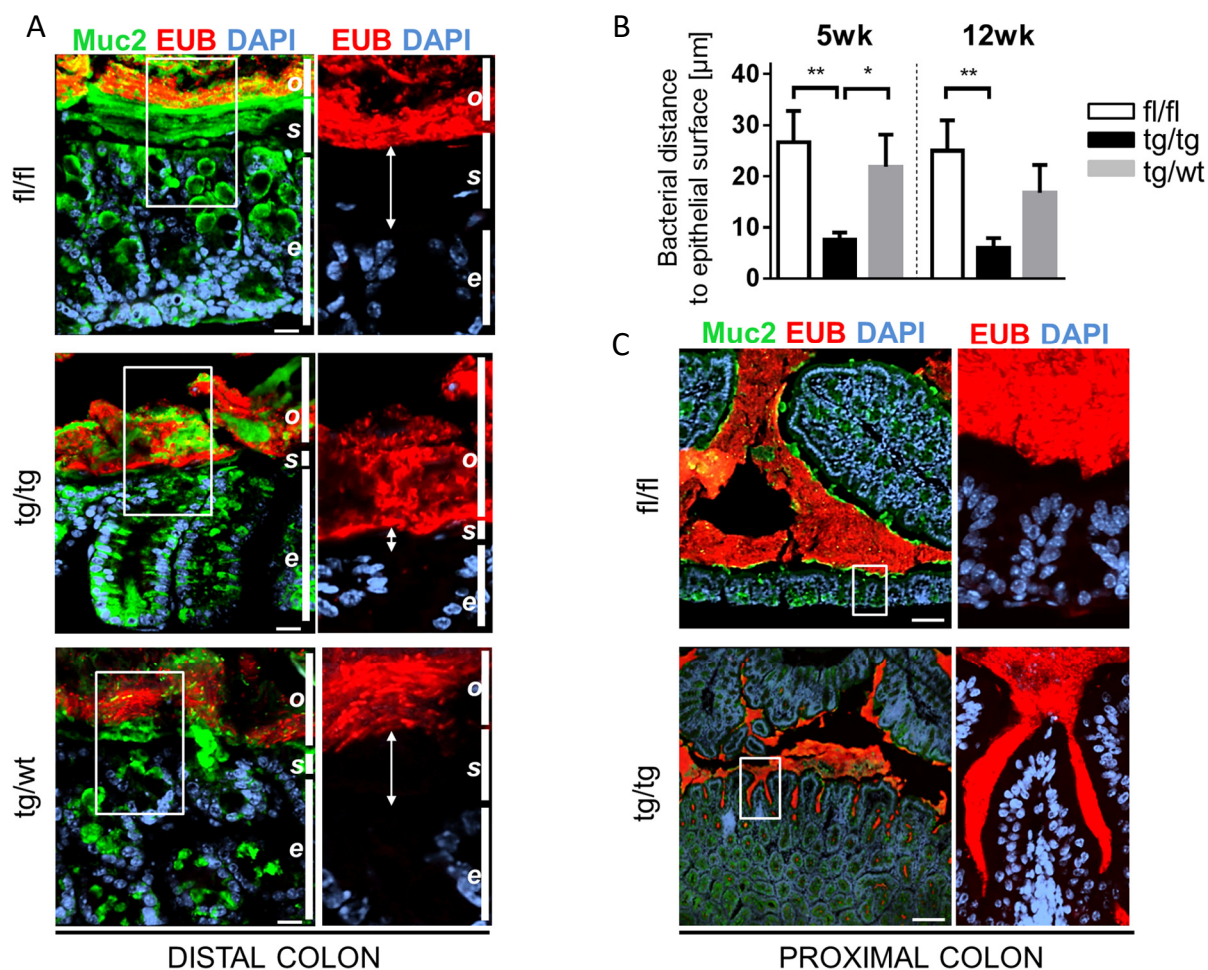


Figure 17: Higher bacterial penetration of colonic mucus in $nATF6^{IEC}$ tg/tg mice.

(A) FISH using the general bacterial probe Eub338 (red) in combination with immunostaining of Muc2 (green) in the distal colon. Nuclei were counterstained with DAPI (blue) (scale bars 100 μm). **(B)** Bacterial penetration of the mucus layer in the distal colon was quantified by measuring the distance between the bacteria and the epithelial surface ($n = 3-4$ per genotype). **(C)** FISH using the general bacterial probe Eub338 (red) in combination with immunostaining of Muc2 (green) in the proximal colon. Nuclei were counterstained with DAPI (blue) (scale bars 100 μm). Statistics **(B)**: ANOVA followed by Bonferroni correction for multiple testing.

A reduced overall number of mucin-filled goblet cells was also evident in the small intestine (data not shown). With respect to Paneth cells, no reduction in Paneth cell numbers were observed even at the age of 20 wk (Figure 18A and B). This was evaluated using Phloxin/Tartrazin stained sections of the distal ileum, mid jejunum and mid duodenum.

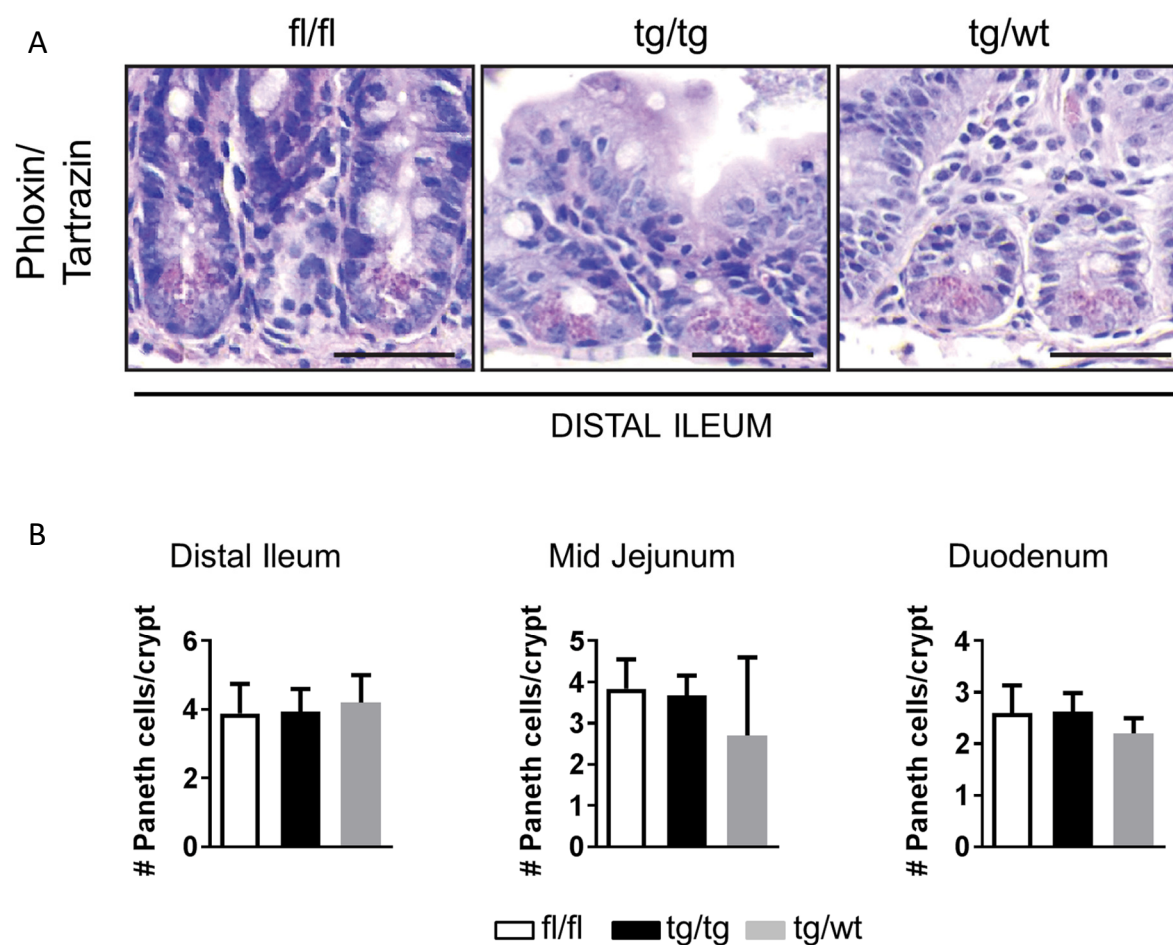


Figure 18: No alterations of Paneth cell numbers in $nATF6^{IEC}$ tg/tg mice.

(A) Representative images of Phloxin/Tartrazin stained distal ileum cross sections (scale bars 50 μ m). (B) Quantification of number of Paneth cells per crypt in the distal ileum, the mid jejunum and duodenum (n=4-6 per genotype, mean of 10 crypts per mouse). Statistics (B): ANOVA followed by pairwise comparison testing (Tukey).

4.3.3 Hyper-proliferative response of enterocytes

To get a deeper understanding of mechanisms that result in tumor formation proliferation was assessed at different time points by immunohistochemical detection of the marker of proliferation Ki67 (Ki67). Ki67 is detectable during all phases of cell cycle but is lacking in resting cells. In contrast to ER UPR activation, proliferation was only induced in $nATF6^{IEC}$ tg/tg mice and not in tg/wt mice (Figure 19A). This hyper-proliferative response was restricted to the large intestine (Figure 19A and B). Overtime evaluation revealed a small but significant increase in proliferating cells at the age of 5 wk, which was exacerbated at older ages in the tg/tg mice only. In tumor regions, proliferating cells were no longer restricted to the lower part of crypts, but were also found in upper crypt regions (magnification Figure 19A).

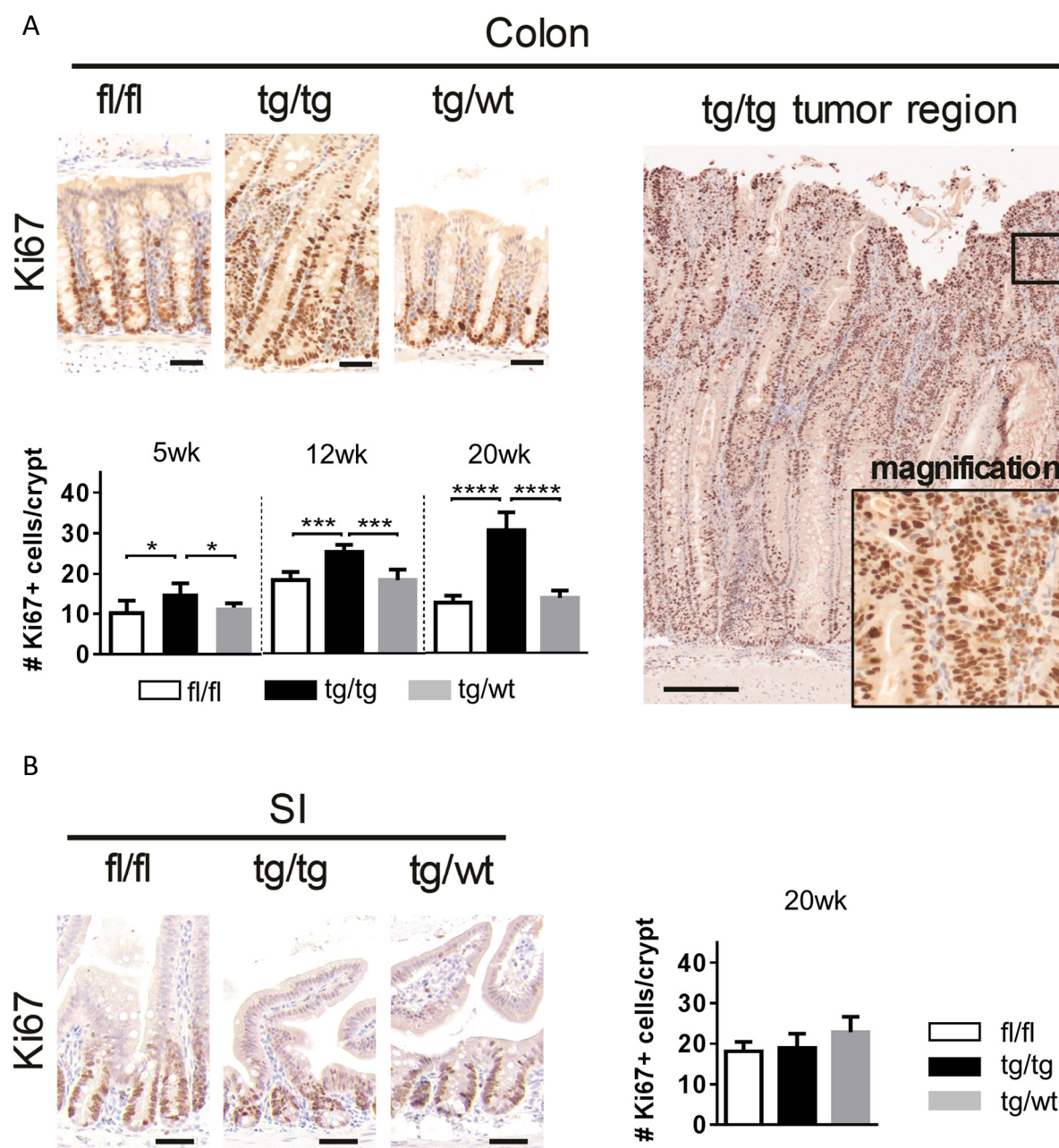


Figure 19: Hyper-proliferation of colonic but not small intestinal IEC in *nATF6^{IEC}* tg/tg mice.

(A) Representative immunohistochemically stained colonic swiss rolls for Ki67 at the age of 20 wk (left panel; scale bars 50 μ m). A colonic tumor region with magnification is given (right side, scale bar 200 μ m). The number of Ki67+ cells per crypt in non-tumor areas of the colon are shown for 5, 12 and 20 wk. **(B)** Representative images of Ki67+ cells are shown for the distal ileum at the age of 20 wk, with the number of Ki67+ cells per crypt quantified (scale bars 50 μ m). Statistics **(A, B)**: ANOVA followed by pairwise comparison testing (Tukey).

4.3.4 Endoplasmic reticulum dilatation in *nATF6^{IEC}* mice

Electron microscopy was performed to analyze the ultrastructure of IECs in the *nATF6^{IEC}* mice. As evident in Figure 20, both *nATF6^{IEC}* tg/tg and tg/wt mice at an age greater than 20 weeks show ER structure alterations defined by a swelling and shortening of the ER compared to *nATF6^{IEC}* fl/fl control mice. To quantify this, 3-4 electron microscopy pictures per mouse were evaluated for the presence of ER swelling. This quantification indicates frequent changes of the ER in *nATF6^{IEC}* tg/tg mice which are even more dominant in *nATF6^{IEC}* tg/wt mice. As evident in the microarray analysis, this goes along with major changes in the expression of genes important for the processing of proteins within the ER in both the tg/tg and tg/wt genotype as demonstrated by mapping of regulated genes in IEC of 5 wk old mice (Figure 21).

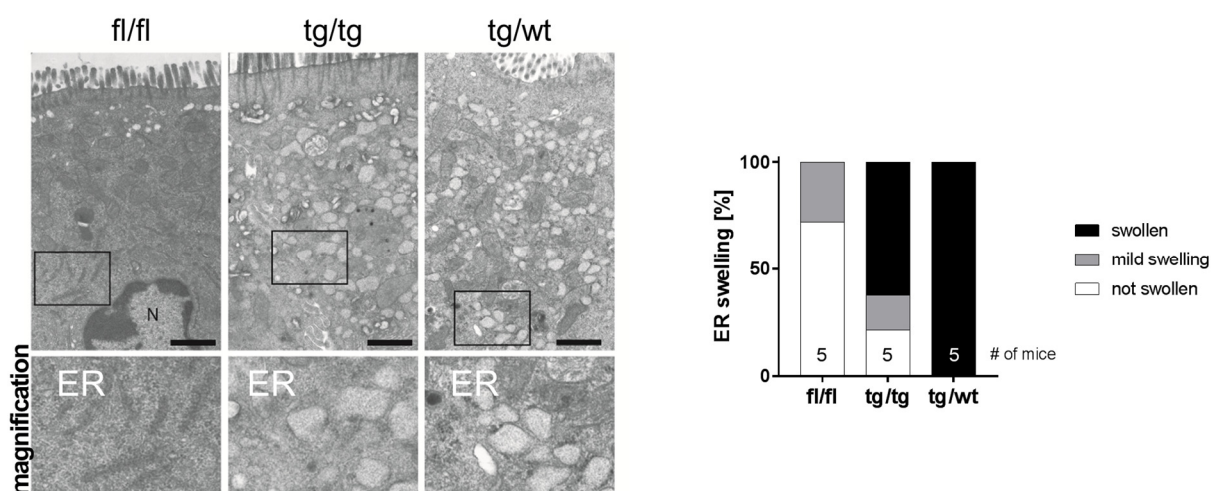


Figure 20: Dilatation of the endoplasmic reticulum in transgenic *nATF6^{IEC}* mice.

Electron microscopy of the proximal colon (>20 wk) was performed (n=5 per genotype). Representative pictures are given with magnified regions highlighting ER structures (N: nucleus; ER: endoplasmic reticulum; scale bar 1 μ m). ER swelling was evaluated for 4-5 pictures per mouse.

4.3.5 Intestinal inflammation as a late event of intestinal pathology

To elucidate whether intestinal tumorigenesis was driven by inflammation, colon tissue was subjected to cytokine expression analysis (Figure 22). Interestingly, none of the cytokines measured were induced at the age of 5 wk (pre-tumor) and at 12 wk (early tumor) with the exception of IL22. IL22 as a member of the IL10 superfamily, in contrast to the other cytokines measured, was significantly induced at the age of 12 wk in tg/tg mice and particularly increased in two mice. At late stages (>20 wk) no significant increase of IL22 was detected. In contrast to the 5wk and 12 wk time point, most cytokine mRNA levels were significantly increased at late stages (>20 wk).

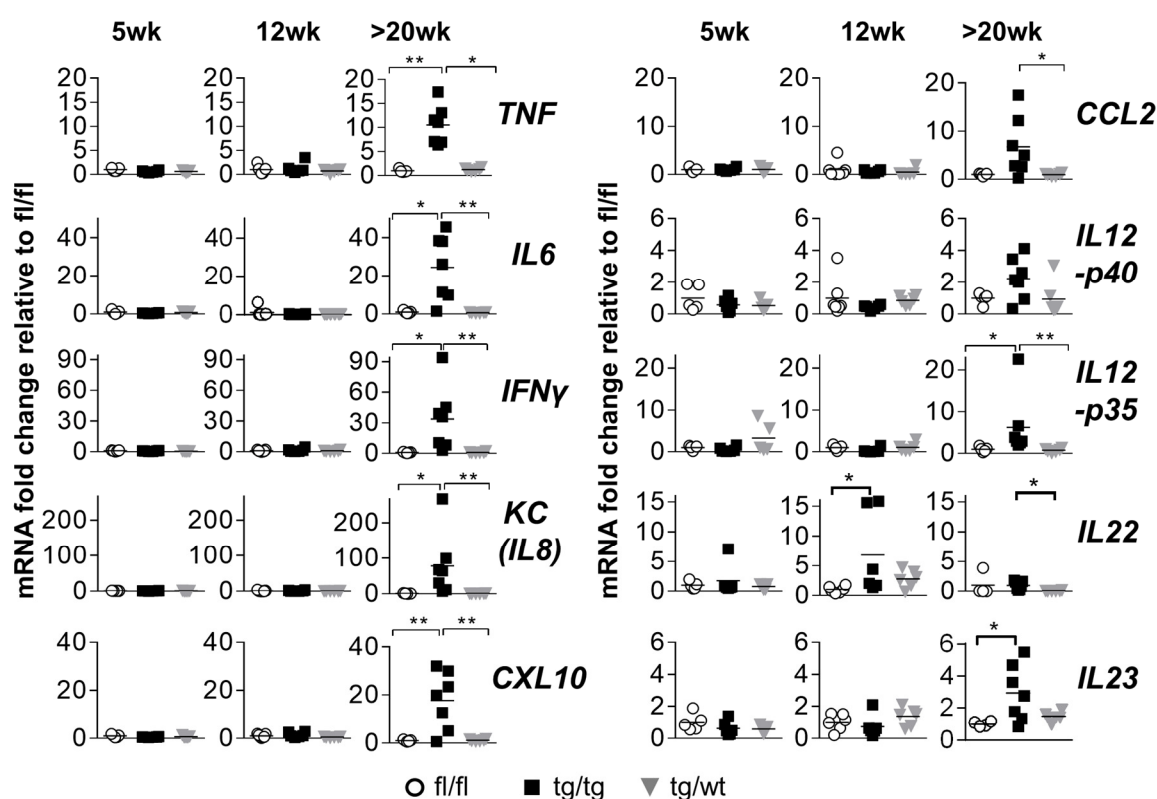


Figure 22: Intestinal inflammation does not precede tumorigenesis.

Cytokine mRNA levels in whole colonic tissue at 5 wk (pre-tumor stage), 12 wk (early tumor stage) and >20 wk (late tumor stage). Statistics: ANOVA followed by pairwise comparison testing (Tukey) or Kruskal-Wallis test followed by Dunn's multiple comparison test.

In line with no increase of most inflammatory cytokines at 5 wk and 12 wk, no histological colitis was detected at both time points assessing lamina propria mononuclear cell infiltration, crypt hyperplasia, goblet cell depletion and architectural distortion (data not shown). Consistent with this, the amount of T cells using CD3 as a marker and macrophages using F4/80 as a marker were not elevated at 12 wk in the colon (Figure 23). In contrast to the 12 wk time point, CD3 and F4/80 positive cells were more abundant in *nATF6^{IEC}* tg/tg mice at the >>20 wk time point. In detail, CD3-positive cells were significantly increased in tumor regions but showed only a trend to be increased in

non-tumor regions whereas the signal for F4/80 was significantly overrepresented in non-tumor and tumor regions (Figure 23A and B). These results in summary suggest that colitis is not a preconditioning factor but rather a consequence of ATF6-driven tumorigenesis in *nATF6^{IEC}* tg/tg mice.

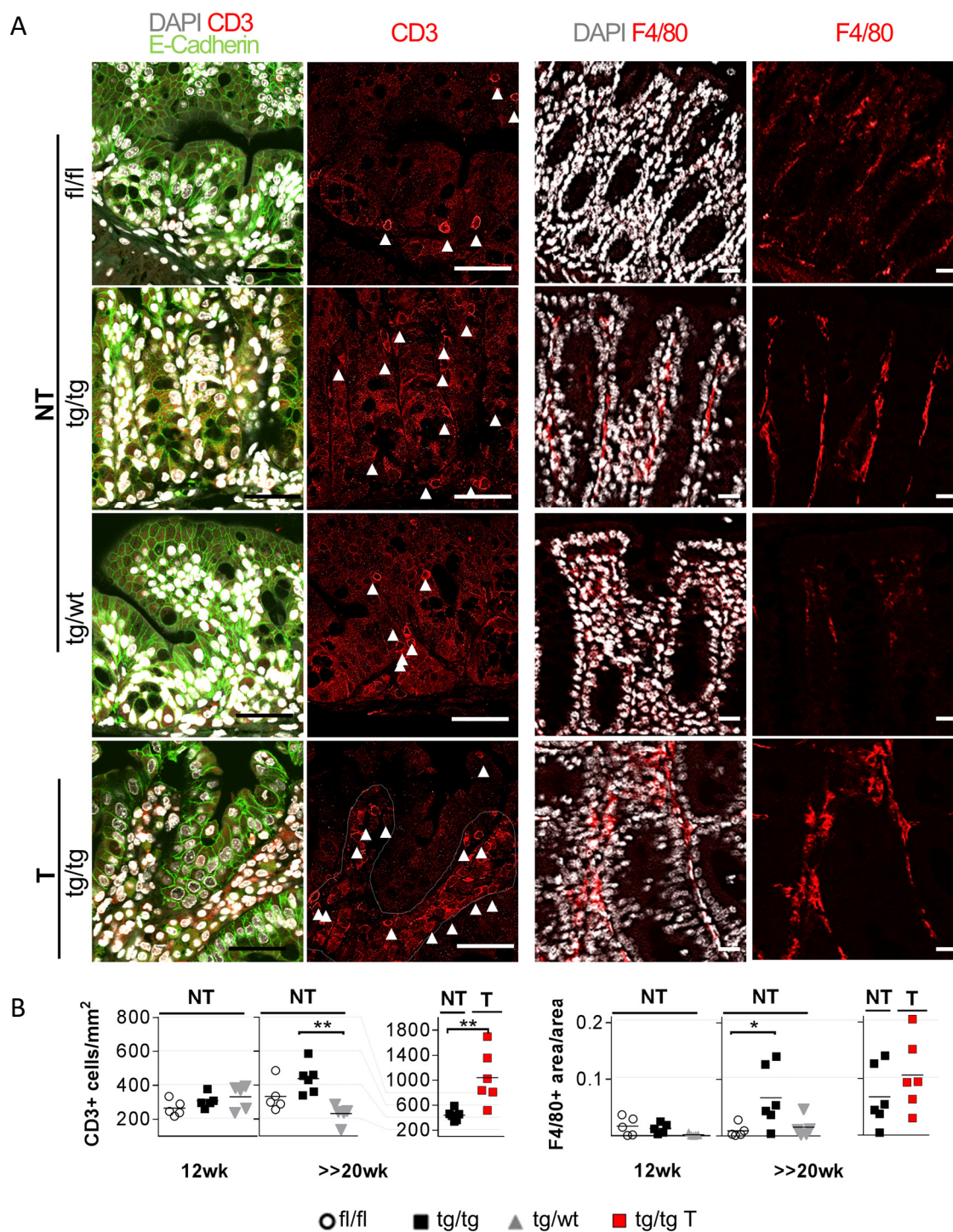


Figure 23: Infiltration of CD3+ and F4/80+ cells as a late event of intestinal pathology.

(A) Representative images of CD3+ cells (left panel) and F4/80+ cells (right panel) detected by immunofluorescent staining of colonic swiss rolls at the age of >>20 wk (scale bars 50 μ m). (B) Quantification of CD3+ cells and F4/80+ signal in the colon of 12 wk and >>20 wk old *nATF6^{IEC}* mice (n= 5-6 mice per genotype) in non-tumor (NT) and tumor (T) areas. Statistics (B): ANOVA followed by pairwise comparison testing (Holm-Sidak) or unpaired two-tailed T-test (T vs. NT comparison).

4.3.6 Effects of CHOP and RAG2 deficiency on tumor formation in *nATF6^{IEC}* mice

In the following, we wanted to gain a better understanding of tumor development and associated factors. Since the ATF6 target gene CHOP has been linked to hepatocellular tumor formation [217] and is overexpressed in *nATF6^{IEC}* tg/tg mice (Figure 11 A-C), the hypothesis of CHOP-dependent tumor growth was tested. CHOP-deficient *ATF6^{IEC}* mice housed under SPF conditions showed a phenotype similar to *nATF6^{IEC}* mice. Whereas the colon of *CHOP^{-/-}* *nATF6^{IEC}* tg/wt mice was tumor-free at the age of 1 year, *CHOP^{-/-}* *nATF6^{IEC}* tg/tg mice developed colonic tumors (Figure 24A). Although one out of 9 *CHOP^{-/-}* *nATF6^{IEC}* tg/wt mice showed a single tumor in the jejunum at the age of 1 year, the results suggest that CHOP does not have a strong impact on tumor formation in the *nATF6^{IEC}* tg/tg mice, since *CHOP^{-/-}* tg/tg mice recapitulate the tumor phenotype of *nATF6^{IEC}* tg/tg mice in the large intestine.

To further address the contribution of adaptive lymphocytes to the development of tumors in *nATF6^{IEC}* tg/tg mice, *nATF6^{IEC}* mice were bred to RAG2-deficient mice which lack these cells. Survival of most *RAG2* *nATF6^{IEC}* tg/tg mice was limited to the maximum age of 11 wk due to a low overall body weight and additional weight loss. At this early age, no tumors could be observed (Figure 24B). The small proportion of mice which survived longer developed tumors in all compartments of the intestinal tract (Figure 24B). In contrast to *nATF6^{IEC}* tg/wt mice sufficient for RAG2, *RAG2^{-/-}* *nATF6^{IEC}* tg/wt mice developed tumors in the intestine, both in the small and large intestine. These results indicate an impact of adaptive lymphocytes on tumor formation since RAG2 deficiency results in dominant small intestinal tumor contribution and tumor formation in tg/wt mice. Since only few colonic tumors were observed in this mice and the numbers are lower compared to *nATF6^{IEC}* tg/tg mice at similar ages, the role of adaptive lymphocytes in *nATF6*-driven colonic tumorigenesis are inconclusive.

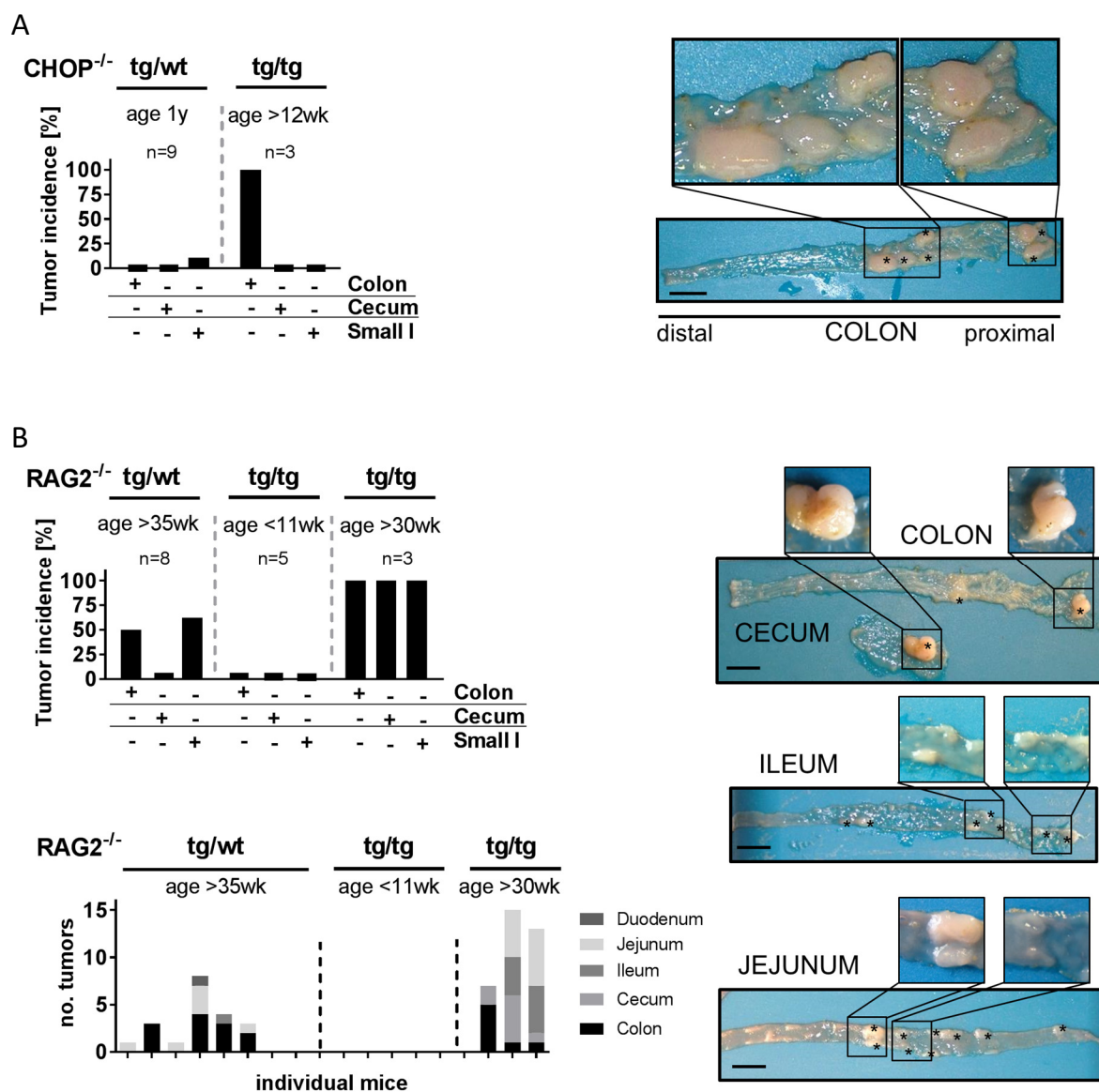


Figure 24: Tumor incidence in the intestine of *nATF6^{IEC}* mice deficient for CHOP or RAG2.

(A) Tumor incidence in percentage at different age time points for the CHOP deficient *nATF6^{IEC}* tg/tg and tg/wt genotypes in the colon, cecum and small intestine (Small I). A representative macroscopic image of the colon of a 12 wk old *CHOP^{-/-} nATF6^{IEC}* tg/tg mouse is given (tumors are highlighted with asterisks, scale bar 1 cm). **(B)** Tumor incidence in percentage and the number of tumors in the large and small intestine at different age time points for the RAG2 deficient *nATF6^{IEC}* tg/tg and tg/wt genotypes. Representative macroscopic images of the colon, cecum, ileum and jejunum are given of a >30 wk old *RAG2^{-/-} nATF6^{IEC}* tg/tg mouse (tumors are highlighted with asterisks, scale bar 1 cm).

4.4 Impact of timing and mode of nATF6 expression on intestinal phenotype

4.4.1 Presence of tumor development in *nATF6*^{IEC-OHT} tg/tg mice

The *nATF6*^{IEC} mouse model is a conditional model for tissue-specific expression of nATF6 in IEC. Recombination and thus expression of the transgene is under the control of the Villin-Promotor and therefore initiated at the embryonic day 9 in the visceral endoderm, and by E12.5 in the entire intestinal epithelium [218]. Accordingly, the observed phenotype in the *nATF6*^{IEC} mice could be a result of events during early embryogenesis. Further, only 25% of all *nATF6*^{IEC} offspring is tg/tg in breedings. Of note, the ratio should be 50:50, which suggests some disadvantage during embryonic development. On top of this, *nATF6*^{IEC} breeding pairs give on average less than two litters, although only male tg/tg mice are used for breeding and not females which might further affect the success rate. In light of possible effects of nATF6 expression during embryogenesis and breeding drawbacks, an inducible model for Villin-Cre-mediated recombination was investigated. This further allows to investigate initial effects of nATF6 expression. To achieve this, *nATF6* mice were bred to Vil-Cre^{ERT2} mice. Cre-ERT2 is a fusion protein of the Cre recombinase and a triple mutant form of the human estrogen receptor, which binds the synthetic estrogen receptor ligands 4-hydroxytamoxifen (OHT). The ERT2 moiety maintains the Cre recombinase in the cytoplasm but allows for translocation to the nucleus upon binding of OHT which results in the recombination of *loxP* sites. These *nATF6* x Vil-Cre^{ERT2} mice, referred to as *nATF6*^{IEC-OHT}, were used to induce recombination at an adult age. Mice were kept on phytoestrogen-reduced diet for three weeks before they were put on OHT-diet for one week at the age of 10 wk (Figure 25A, upper part). After the induction phase, feed was switched back to phytoestrogen-reduced diet. To study initial responses to nATF6 induction three mice per genotype were sampled four days after the end of OHT supplementation (4 d). A second cohort was sampled 15 weeks after the end of the induction phase (26 wk). In line with the results obtained for the constitutive *nATF6*^{IEC} tg/tg mice, induced *nATF6*^{IEC-OHT} tg/tg mice developed colonic tumors with an incidence of 100 % but no small intestinal tumors (Figure 25A). Transgene expression in the colonic epithelium was verified by HA-Tag detection already at the 4 d time point and indicated nuclear localization of the nATF6-HA in IECs (Figure 25B).

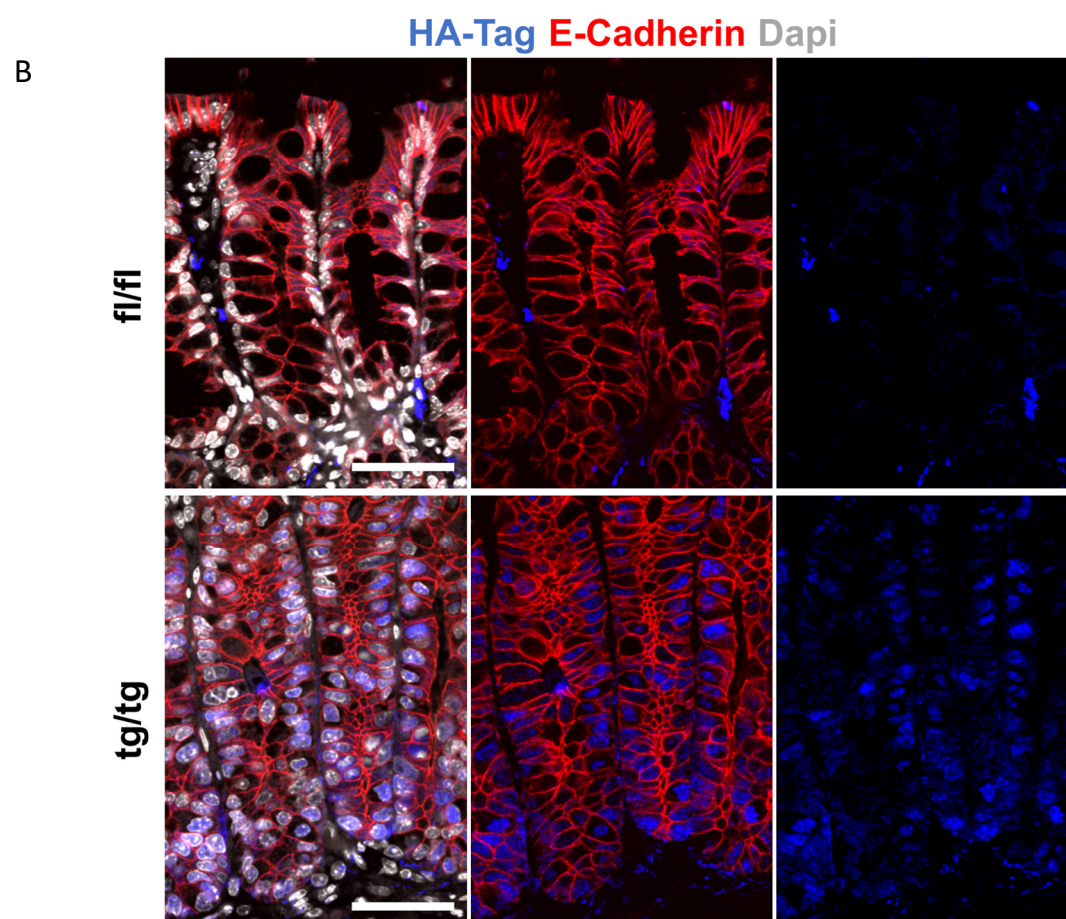
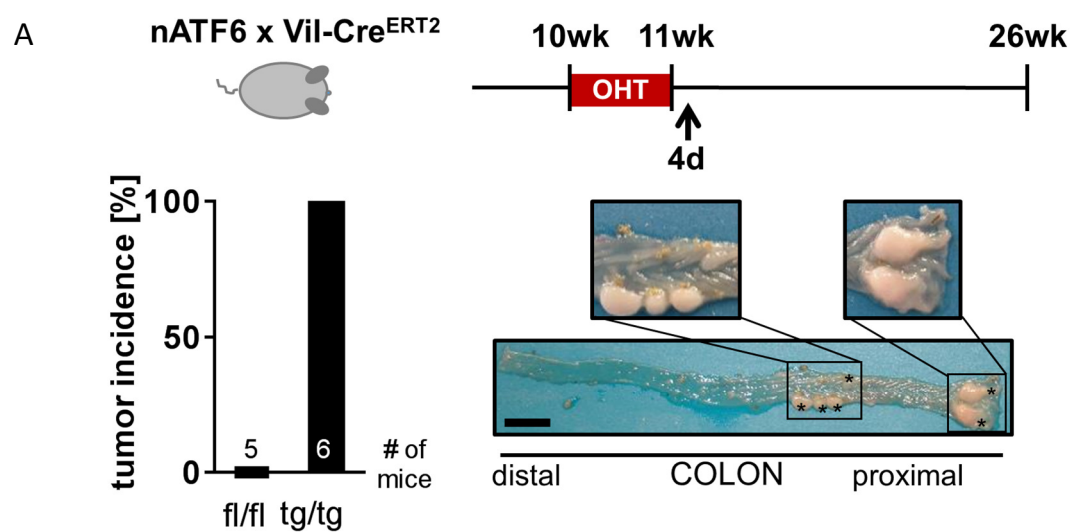


Figure 25: The *nATF6^{IEC-OHT}* mouse model: tumor incidence and *nATF6* expression.

(A) Experimental setup illustrating the induction of recombination in *nATF6^{IEC-OHT}* mice by oral feeding with OHT supplemented feed. Induced *fl/fl* and *tg/tg* mice were sacrificed either 4 days (4 d) or 15 weeks (age 26 wk) after end of OHT feeding. Colonic tumor incidence is given for the 26 wk time point. A representative macroscopic picture of the colon is shown (asterisks indicate tumors; scale bar 1 cm). **(B)** Transgene localization in the colon at the 4 d time point (scale bars 50 μ m) detected by immunofluorescence. Blue: HA-Tag; red: E-Cadherin; white: Dapi.

At the age of 26 wk – 15 wk after end of induction, $nATF6^{IEC-OHT}$ tg/tg mice showed significantly elevated numbers of Ki67+ cells in the colon demonstrating a general increase in proliferation (Figure 26A). This was associated with a trend for reduced numbers of mucin-filled goblet cells which did not reach significance (Figure 26B). At the 4 d time point, a tendency to elevated levels of Ki67+ cells and a reduced number of mucin-filled goblet cells was detected in the small group size. In conclusion, the inducible model of Villin-mediated nATF6 expression recapitulates the intestinal phenotype of the constitutive mouse, considering tumor formation and proliferation.

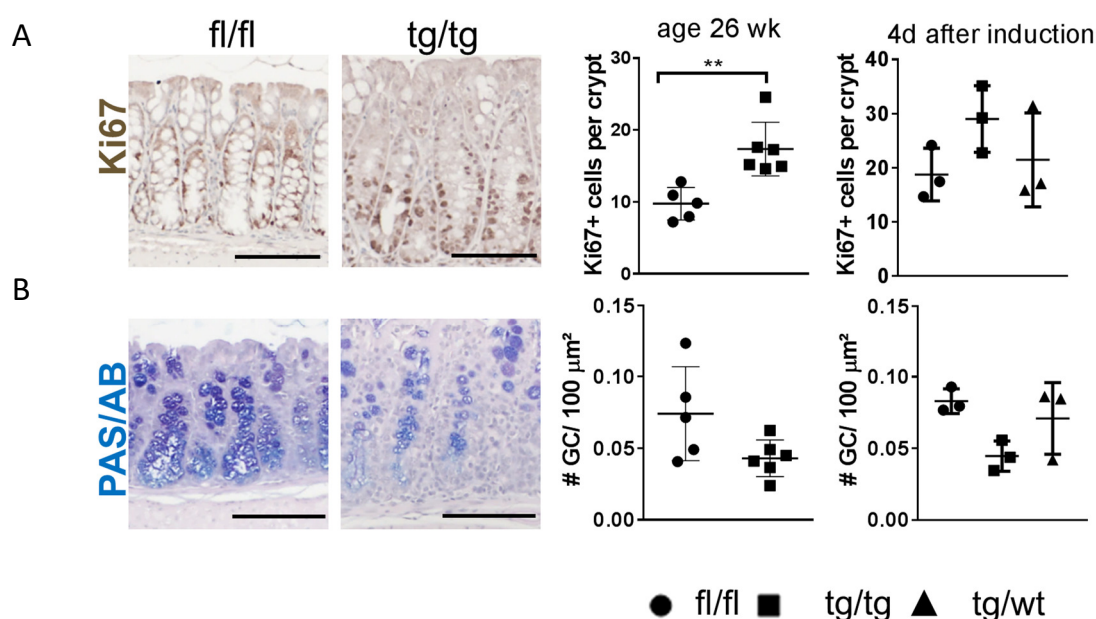


Figure 26: The $nATF6^{IEC-OHT}$ mouse: Hyper-proliferation and goblet cells.

(A) Representative immunohistochemical staining of colonic swiss rolls for Ki67 at the age of 26 wk (left panel; scale bars 100 μm). The number of Ki67+ cells per crypt in non-tumor areas of the colon are shown for the 26 wk and 4 d time point. (B) Representative PAS/AB staining of colonic swiss rolls at the age of 26 wk (left panel; scale bars 100 μm). The number of mucin-filled goblet cells per 100 μm² in non-tumor areas of the colon are shown for the 26 wk and 4 d time point. Statistics: ANOVA followed by pairwise comparison testing (Holm-Sidak).

4.4.2 Absence of tumor development in $nATF6$ x $LGR5-Cre^{ERT2}$ tg/tg mice

To elaborate the effects of the expression of nATF6 in the LGR5+ stem cell compartment, $nATF6$ mice were bred to $LGR5-Cre^{ERT2}$ ($LGR5-Cre^{ERT2-IRES-Egfp+}$) mice which express the Cre^{ERT2} fusion protein and the reporter gene *Egfp* under the control of the LGR5 promoter concurrently. EGFP allows for the detection of ISC which express the recombinase. The mice were induced alike to the $nATF6^{IEC-OHT}$ mice and samples at the corresponding 4 d and 26 wk time points were taken (Figure 27A, upper part). To be able to see EGFP positive ISCs also in control mice, OHT treated $LGR5-Cre^{ERT2}$ mice without modified *Rosa26* locus served as controls and are referred to as fl/fl. No tumor formation was detected in tg/tg mice at the age of 16 wk (Figure 27A). Already at the 4 d time point expression of

the transgene could be detected in nuclei of EGFP-positive colonic crypts but not in EGFP-negative crypts indicating successful recombination in ISCs (Figure 27B). Further, also IEC at the top of the crypt were positive for HA-Tag suggesting that the recombined ISCs were able to give rise to differentiated IECs.

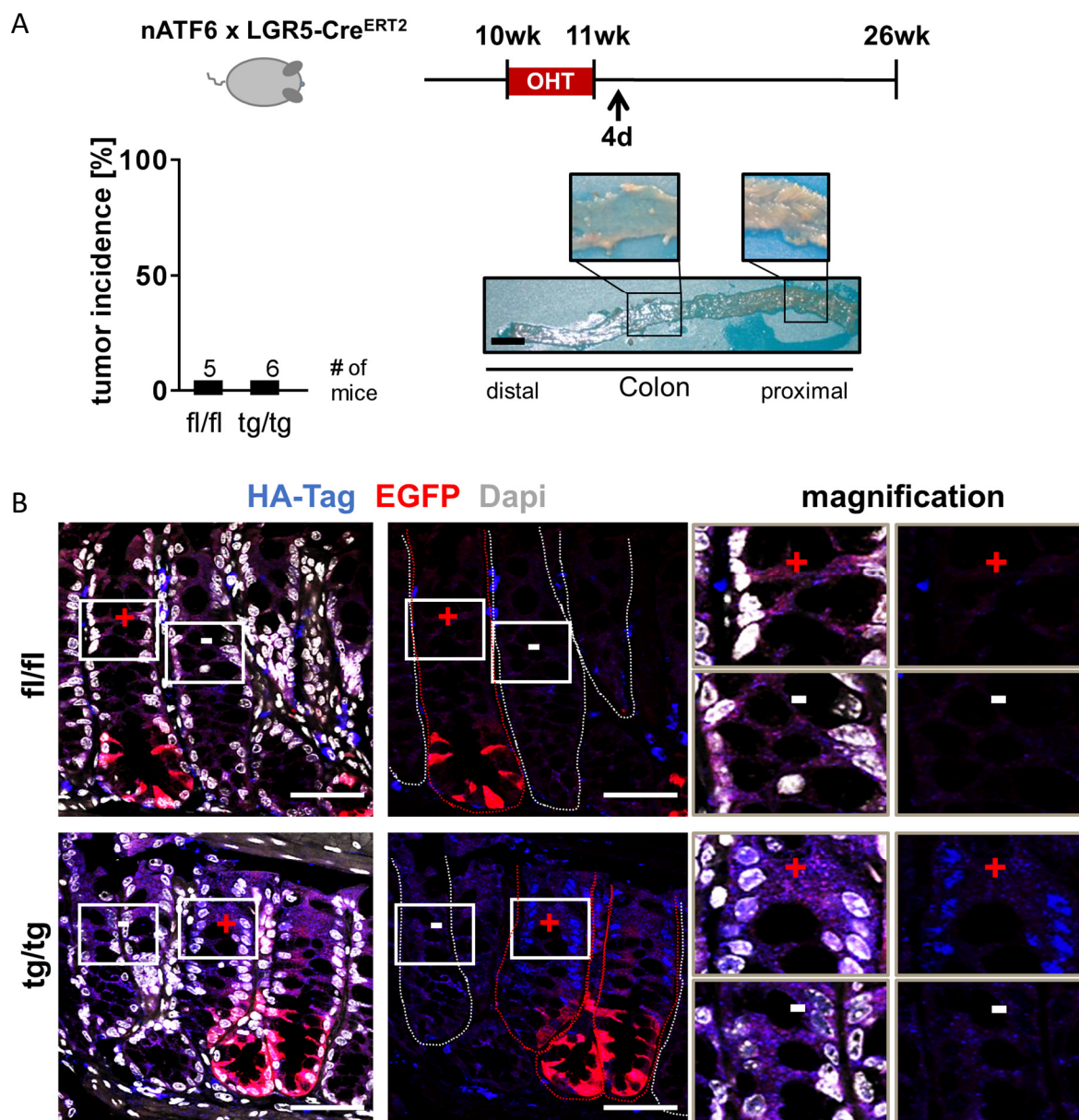


Figure 27: The *nATF6* x *LGR5-Cre^{ERT2}* mouse: tumor incidence and *nATF6* expression.

(A) Experimental setup illustrating the induction of recombination in *nATF6* x *LGR5-Cre^{ERT2}* mice by oral feeding with OHT supplemented feed. Induced fl/fl and tg/tg mice were sacrificed either 4 days (4 d) or 15 weeks (age 26 wk) after end of OHT feeding. Colonic tumor incidence is given for the 26 wk time point. A representative macroscopic picture of the colon is shown (scale bar 1 cm). **(B)** Transgene localization in the colon at the 26 wk age time point (scale bars 50 μ m) detected by immunofluorescence. Blue: HA-Tag; red: EGFP; white: Dapi; + EGFP-positive crypt; - EGFP-negative crypt.

The expression of nATF6 resulted in the up-regulation of Grp78 in the transgenic crypts as comparable to the constitutive *nATF6^{IEC}* model (Figure 28A). Using Grp78 as a surrogate marker for transgenic crypts, it is evident that roughly 30 % of all colonic crypts recombined as a result of limited Cre^{ERT2} expression in this model both at the 4 d and the 26 wk time point. To characterize proliferation (Figure 28B) and goblet cell appearance (Figure 28C) in the transgenic crypts of the colon, Grp78 was co-stained to identify transgenic crypts. The number of Ki67-positive cells is significantly increased in transgenic crypts compared to non-transgenic crypts of the same mouse and crypts of fl/fl mice. The number of mucin-filled goblet cells was significantly reduced in transgenic crypts compared to crypts in fl/fl mice but the comparison to non-transgenic crypts did only show a non-significant trend towards reduction of mucin-filled goblet cells.

In conclusion, nATF6 expression under the control of LGR5 resulted in recombination of Cre^{ERT2} expressing ISCs and subsequent population of the whole crypt with transgenic cells. This did not provoke tumor formation in the colon although transgenic crypts recapitulated the hyper-proliferative phenotype of crypts in the constitutive *nATF6^{IEC}* model.

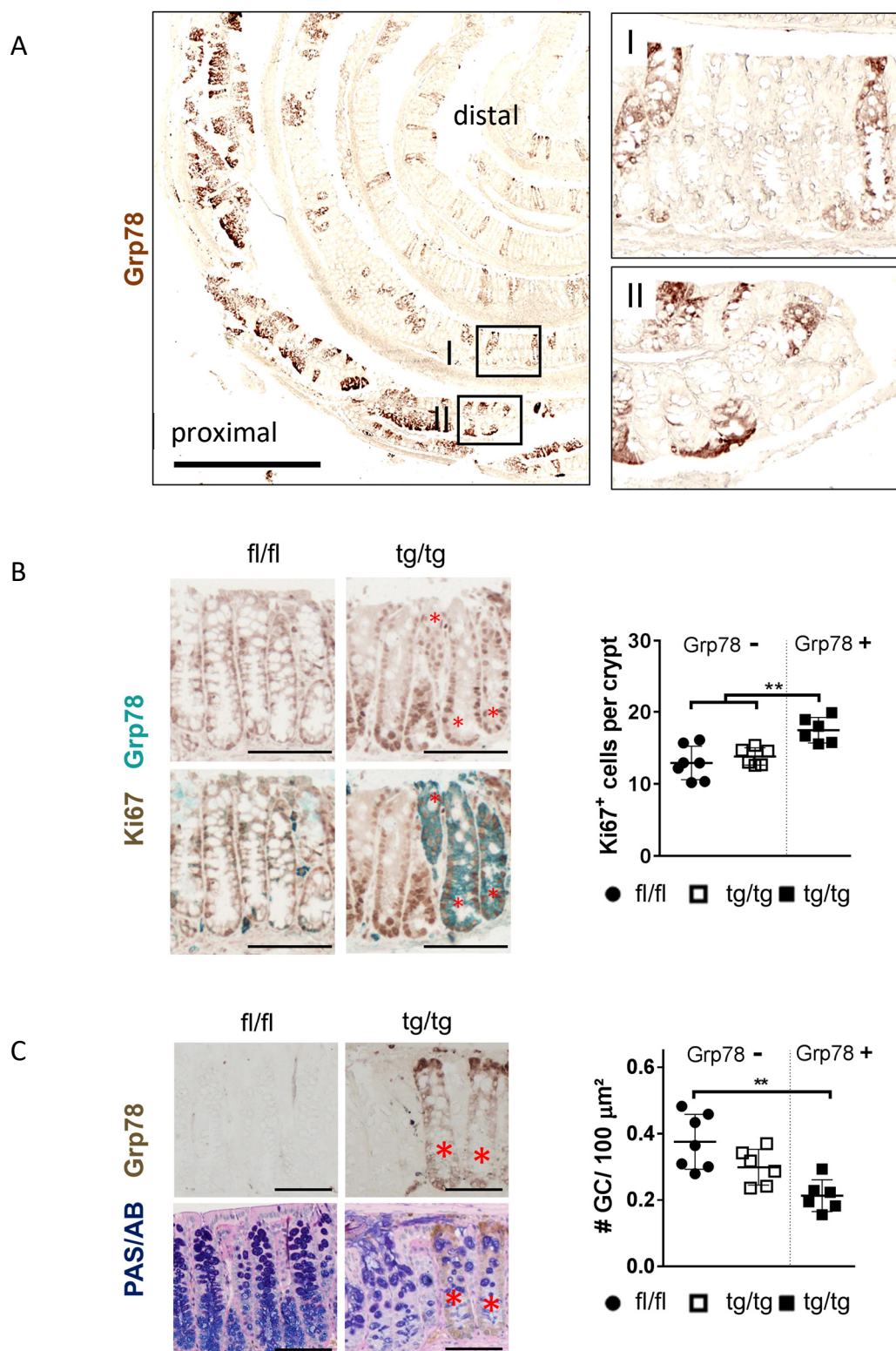


Figure 28: The *nATF6* x *LGR5-Cre^{ERT2}* mouse model: Proliferation and goblet cells in transgenic crypts.

(A) Immunohistochemical staining for Grp78 of a colonic swiss roll section of a tg/tg mouse at the 4 d time point (scale bar 1 mm). **(B)** Combined immunohistochemical staining for Grp78 (green) and Ki67 (brown) for the 26 wk time point (left panel; scale bar 100 μ m) and quantification of Ki67+ cells in Grp78- and Grp78+ crypts. **(C)** Representative PAS/AB stainings combined with immunohistochemical detection of Grp78 (brown) of colonic swiss rolls at the age of 26 wk (left panel; scale bars 100 μ m). The number of mucin-filled goblet cells per 100 μ m² in Grp78- and Grp78+ crypts of the colon are shown for the 26 wk time point. Statistics **(B, C)**: ANOVA followed by pairwise comparison testing (Holm-Sidak).

4.5 Inflammation, wounding and microorganisms as modulators of intestinal tumorigenesis in *nATF6^{IEC}* mice

4.5.1 Increased tumor susceptibility of *nATF6^{IEC}* tg/wt mice in response to chronic DSS

To address the question whether tissue injury and inflammation can promote tumorigenesis in the otherwise disease-free heterozygous model, we exposed *nATF6^{IEC}* tg/wt mice to four cycles of low dose, short-term dextran sodium sulfate (DSS) (Figure 29A, upper part). DSS treatment is used to chemically induce colitis and is a tool to induce acute and chronic inflammation. The mechanism of action of DSS is still under debate but might be connected to tissue injury and access of proinflammatory intestinal contents (*e.g.* bacteria and bacterial products) to underlying tissue [219]. In this protocol, the aim was to confront the mice with repetitive but low dose inflammatory triggers with sufficient time for recovery. The development of pathology was monitored by video colonoscopy and disease activity index (DAI). *nATF6^{IEC}* tg/wt mice responded the most to the first cycle of DSS, whereas *nATF6^{IEC}* fl/fl mice did not respond at all to this low dose of DSS. Cyclic DSS treatment resulted in tumor formation in four of five tg/wt mice (Figure 29A and B). As expected based on previous observations, none of the untreated *nATF6^{IEC}* tg/wt and fl/fl mice developed tumors. In contrast to the DSS-treated tg/wt mice, DSS treatment did not result in tumor formation in the fl/fl mice. This indicates that *nATF6^{IEC}* tg/wt, although disease-free under normal conditions, have an increased risk to develop tumors particularly in the context of inflammatory conditions and disruption of the intestinal barrier.

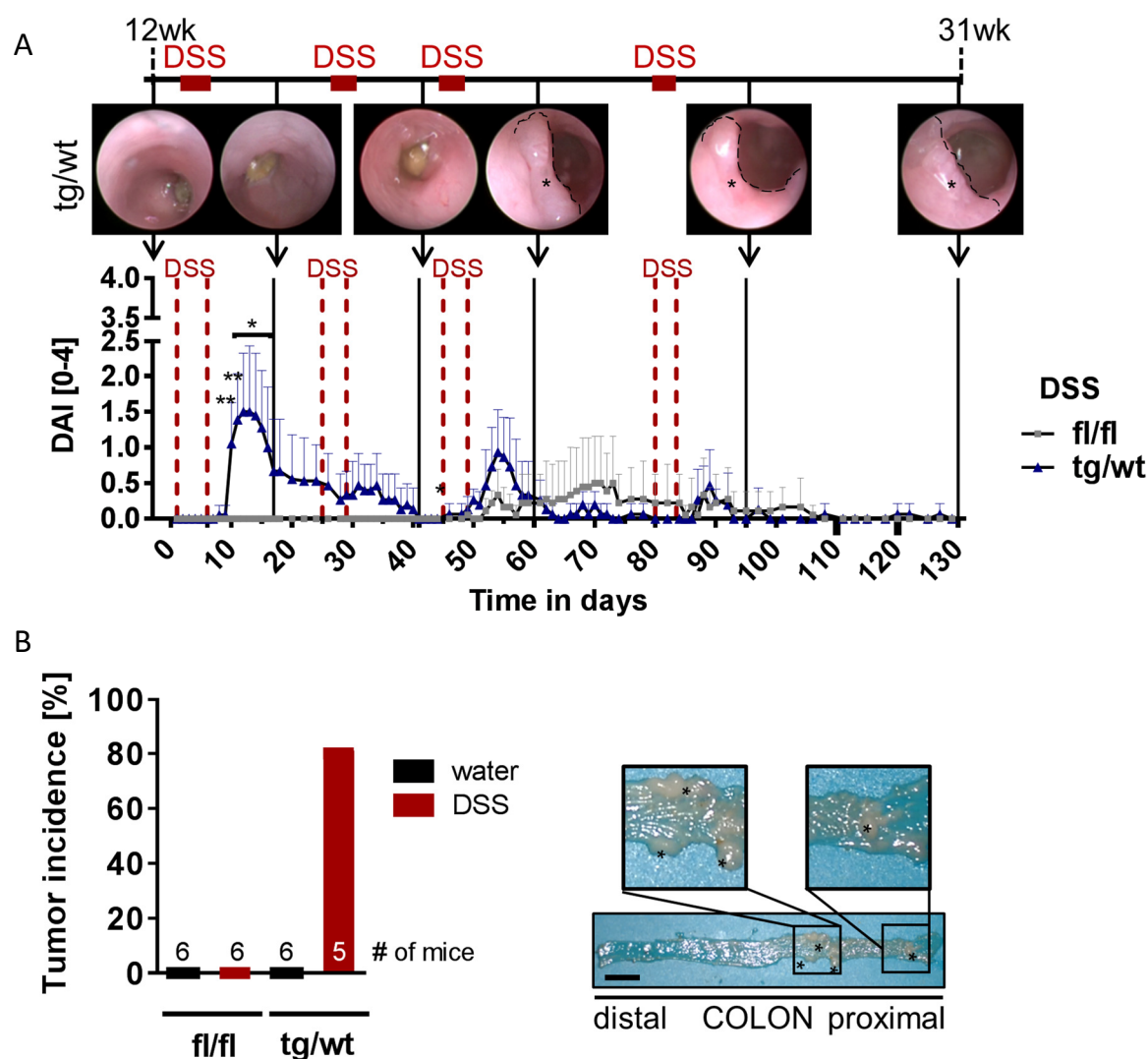


Figure 29: Increased tumor susceptibility of *nATF6*^{IEC} tg/wt mice in response to DSS.

(A) *nATF6*^{IEC} tg/wt and fl/fl mice were subjected to four cycles of dextran sodium sulfate (DSS), followed by normal drinking water phases as schematically represented. Representative colonoscopy images are given for one tg/wt mouse on DSS throughout the experiment (tumor indicated by asterisk and dashed line). Mice were scored according to the disease activity index (DAI). Weight was readjusted to 100 % before the onset of each individual DSS cycle. **(B)** Tumor incidence for the DSS-treated mice and respective water controls. The number for DSS treated tg/wt mice is 5 due to colonoscopy-related abortion of one mouse. Representative macroscopic images of the colon are given (asterisks indicate tumors; scale bar 1 cm). Statistics **(A)**: unpaired two-tailed T-test.

4.5.2 Increased tumor susceptibility of *nATF6*^{IEC} tg/wt mice on the genetic *IL10*^{-/-} background

Consistent with the observation in the DSS-mediated tissue injury model, heterozygous expression of *nATF6* in *IL10*-deficient mice as a model for colitis also induced tumors at the age of 12 wk (Figure 30A), substantiating the tumor-promoting effect of inflammatory triggers. Of interest, histopathology indicated only minor signs of intestinal inflammation in *IL10*^{-/-} mice without *nATF6* expression (Figure 30B) but increased scores in *IL10*^{-/-} tg/wt mice. This goes in line with changes in colonic TNF and

IL12-p40 expression (Figure 30C). Similar to the phenotype already described for $nATF6^{IEC} \times RAG2^{-/-}$ mice but more severe, $IL10^{-/-}$ mice expressing $nATF6$ homozygously showed an early phenotype of growth retardation, which resulted in abortion at the maximal age of 9 weeks. This phenotype was independent of tumor formation, since not all aborted mice had established macroscopically visible tumors at this early age.

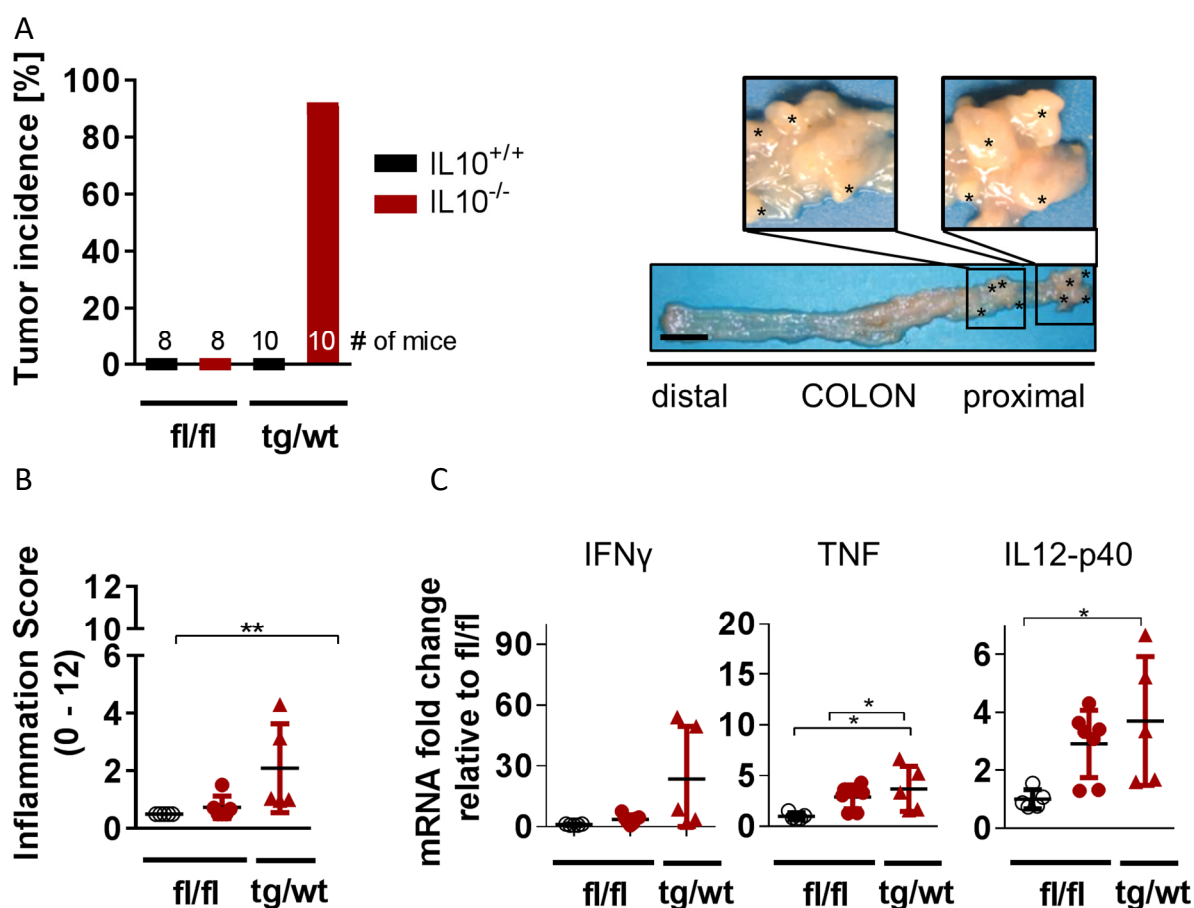


Figure 30: Increased tumor susceptibility of $nATF6^{IEC}$ tg/wt mice on the $IL10^{-/-}$ background.

(A) Tumor incidence for fl/fl and tg/wt mice and the respective genotypes bred to $IL10^{-/-}$ mice, at the age of 12 wk. Representative macroscopic images of the colon of a tg/wt $IL10^{-/-}$ mouse (asterisks indicate tumors; scale bar 1 cm). (B) Colon tissue of $nATF6^{IEC}$ fl/fl mice (black) and $nATF6^{IEC}$ fl/fl or tg/wt mice bred to $IL10^{-/-}$ mice (red) were scored histologically for inflammation at the age of 12 wk (range of score 0 (not inflamed) -12 (highly inflamed)). (C) Cytokine mRNA levels in whole colonic tissue at 12 wk of age of $nATF6^{IEC}$ fl/fl mice (black) and $nATF6^{IEC}$ fl/fl or tg/wt mice bred to $IL10^{-/-}$ mice (red). Statistics (B): Kruskal-Wallis test followed by Dunn's multiple comparison test; (C): ANOVA followed by pairwise comparison testing (Sidak).

4.5.3 Potential effect of mechanical stress on tumor formation

In order to follow tumor formation or other macroscopic changes in the colon over-time, one *nATF6^{IEC} tg/tg* and one *nATF6^{IEC} fl/fl* mouse repetitively underwent colonoscopy starting at the age of 8 wk until the age of 40 wk (treatment scheme Figure 31A). Of interest, this repetitive endoscopy, which goes along with mechanical manipulation of the distal colon by rinsing with water, dilation of the colonic tube by air and movement of the endoscope, affected the localization of the tumors in the investigated *nATF6^{IEC} tg/tg* mouse: In addition to the typical proximal and mid tumor site also distal colonic tumors were observed (Figure 31B). This was unique to the investigated *nATF6^{IEC} tg/tg* mouse, since no tumor formation in the distal colon was observed for any other *nATF6^{IEC} tg/tg* mice not undergoing colonoscopy. Further, the endoscopy had no impact on tumor risk in the respective fl/fl mouse.

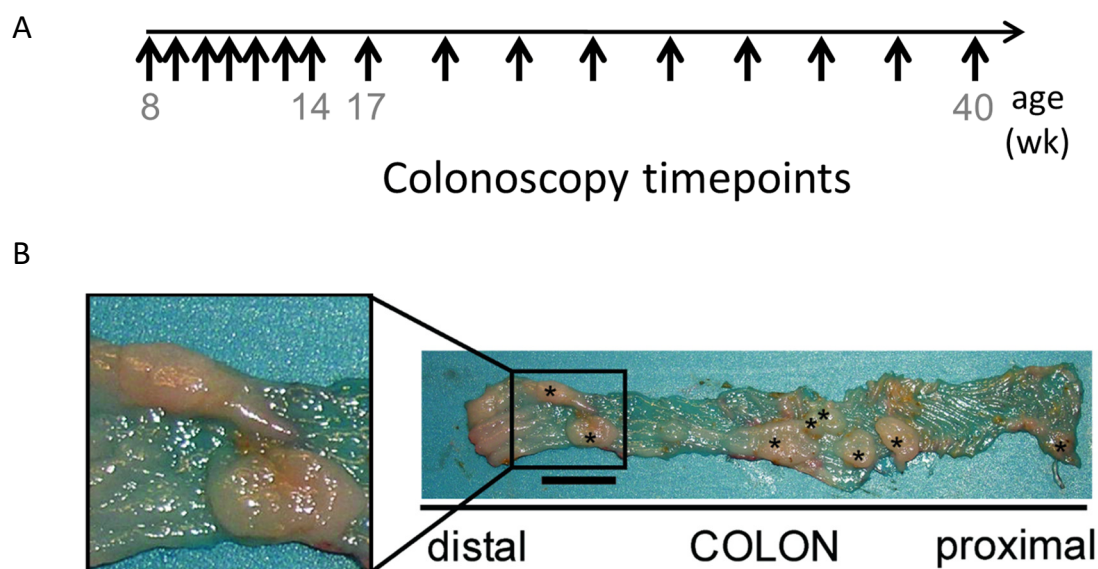


Figure 31: Colonoscopy-related effects on tumor formation.

(A) Scheme illustrating time frame and frequency of colonoscopic intervention. **(B)** Macroscopic image of the colon of a *nATF6^{IEC} tg/tg* mouse which underwent colonoscopy until the age of 40 wk (scale bar 1 cm).

4.5.4 Bacterial signals as trigger for tumorigenesis in the genetically susceptible host

To study a possible contribution of the gut microbiota to tumorigenic responses in $nATF6^{IEC}$ mice, 16S rRNA gene amplicon libraries from cecal microbiota in the pre- and late-tumor stage were sequenced. Beta-diversity analysis clearly indicated that the phylogenetic makeup of dominant bacterial communities was significantly altered in $nATF6^{IEC}$ tg/tg mice compared to their respective controls. These shifts were already evident at the age of 5 wk and further pronounced at a later age (Figure 32A). Independent of age, the cecal microbiota in $nATF6^{IEC}$ tg/tg mice was less diverse compared to fl/fl and tg/wt mice, as indicated by decreased numbers of observed species and Shannon effective counts (Figure 32B).

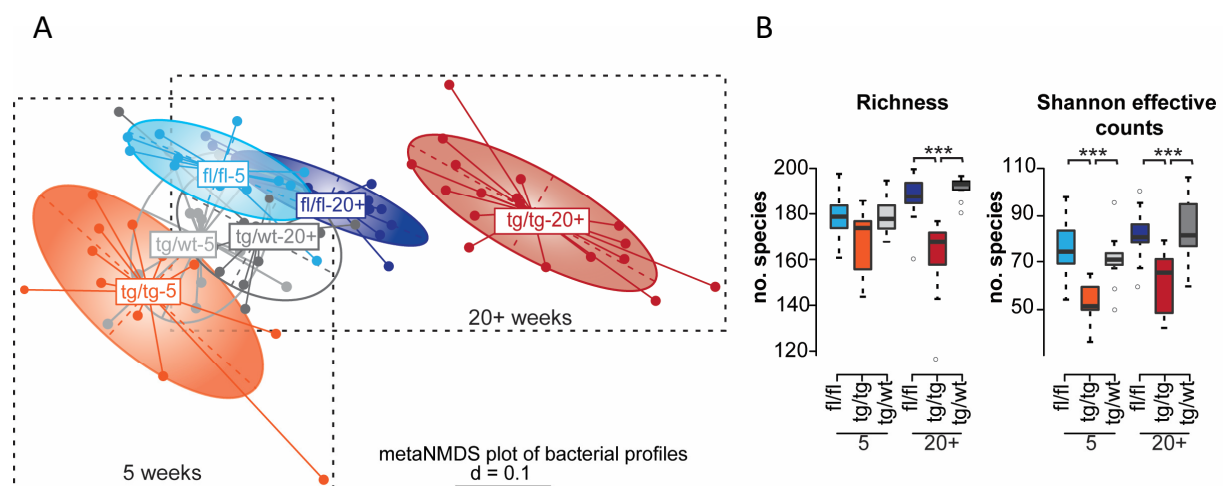


Figure 32: Microbial changes in $nATF6^{IEC}$ tg/tg mice precede tumorigenesis.

(A) Non-metric multidimensional scaling analysis plot of generalized UniFrac distances at 5 wk and >20 wk. (B) Alpha-diversity as represented by Richness and Shannon effective species counts in $nATF6^{IEC}$ mice at 5 wk and 20+ wk.

These alterations in diversity were accompanied by compositional changes: $nATF6^{IEC}$ tg/tg mice were characterized by a significantly decreased relative abundances of *Firmicutes* at the >20 wk age time point and by a significant increase in *Bacteroidetes* and *Proteobacteria* (Figure 33A and B). With respect to *Bacteroidetes*, the relative abundances of the families *Bacteroidaceae*, *Porphyromonadaceae* and *Rikenellaceae* were significantly increased at the >20 wk age time point. A similar increase was observed for the family *S24-7* at the >20 wk age time point, whereas a decreased abundance of this family was detected at the 5 wk time point. With respect to *Firmicutes*, *Lachnospiraceae* showed a significant drop at the >20 wk age time point. Further, *Lactobacillaceae* and *Ruminococcaceae* showed relative changes in abundance at the 5 wk time point, with increased abundances detected for *Lactobacillaceae* and decreased abundances for *Ruminococcaceae*.

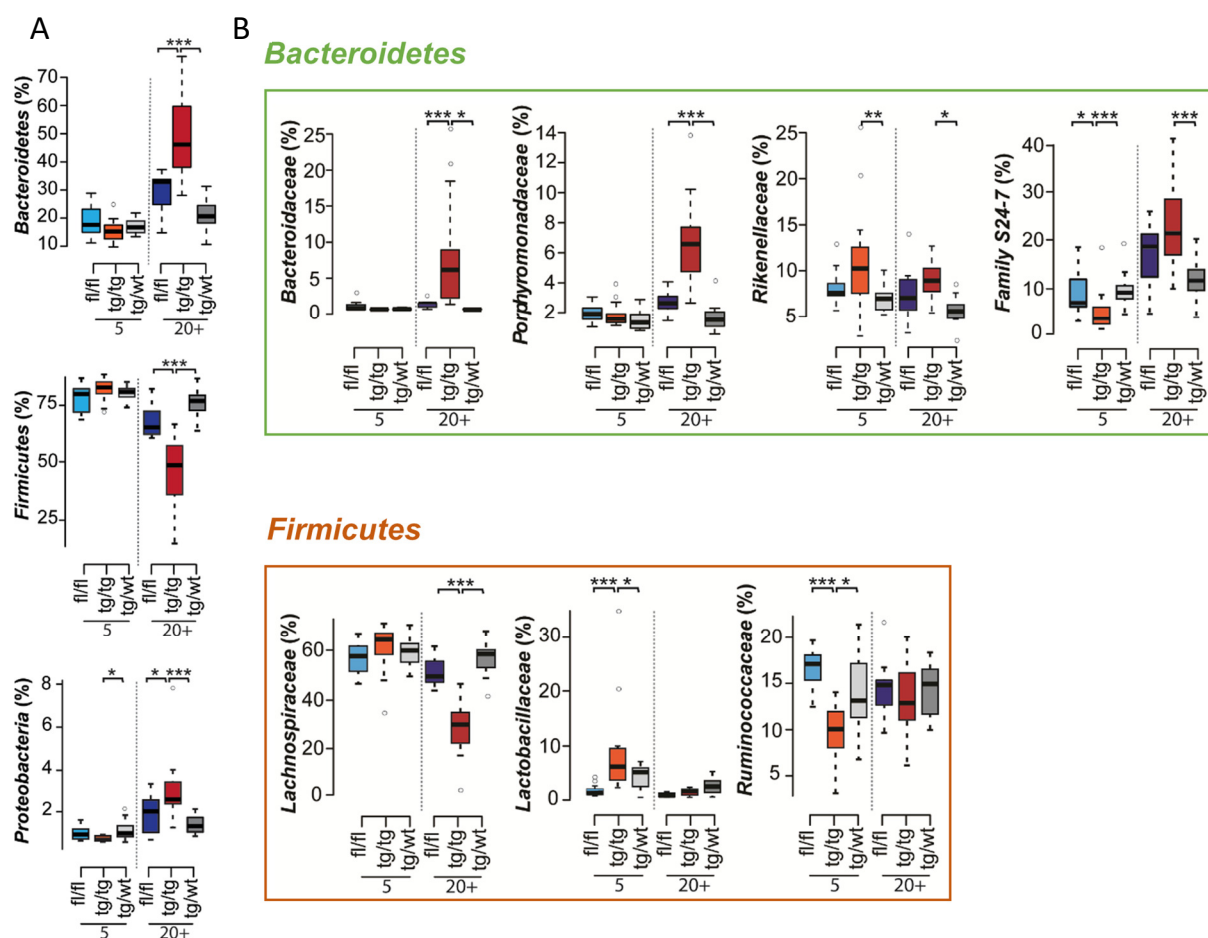


Figure 33: Relative abundances of phyla and families in the *nATF6^{IEC}* mice.

(A) Relative abundances of phyla after 16S rRNA gene sequencing of cecal contents from 5 wk and 20+ wk *nATF6^{IEC}* mice according to genotype and age. **(B)** Relative abundances of families.

Regarding the comparison of *nATF6^{IEC}* tg/tg and fl/fl, 42 OTUs were identified to be significantly different with respect to prevalence and 13 OTUs with respect to abundance in at least one time point. Prevalence was significantly different for 37 OTUs at the >20 wk time point and for 10 OTUs at the 5 wk time point. Abundance was changed for 10 OTUs and 4 OTUs, respectively. However, most of the significantly changed OTUs had low sequence similarity with known species as identified by EzTaxon [220]. Figure 34 illustrates the relative abundance of all OTUs assigned to known species at a similarity threshold >95 %. Additionally, the five OTUs which show similar changes in abundance or prevalence in the *nATF6^{IEC}* tg/tg genotype at both time points are illustrated (top 5 OTUs). Out of these five OTUs showing similar differences at both time points, one OTU was increased whereas four OTUs were decreased in the tg/tg genotype. Only one of the OTUs could be identified at the genus level and was assigned to *Flintibacter butyricus*, an amino-acid-degrading butyrate producer and a frequent colonizer of the murine gut [221].

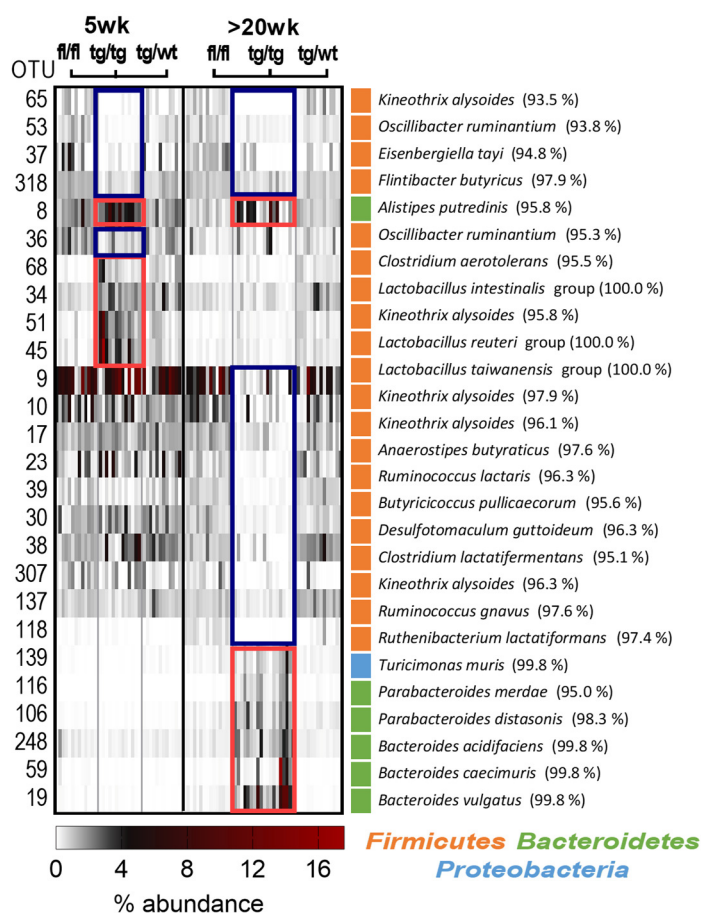


Figure 34: Significant OTUs different between *nATF6^{IEC}* tg/tg and fl/fl mice.

Heatmap illustration of selected OTUs color-coding % relative abundance. OTUs are selected based on significant differences ($p \leq 0.05$) in prevalence (Fisher's Exact Test) and abundance (Wilcoxon Rank Sum Test) for the comparison tg/tg and fl/fl for 5 wk and >20 wk. All OTUs with similar changes in the comparison between *nATF6^{IEC}* tg/tg and fl/fl at both age time points (top 5) and all OTUs identified by sequence similarity >95% are shown. OTUs were assigned to the closest known species using EzTaxon. The phylogenetic assignment of the respective OTU at the phylum level is indicated in orange, green or light blue. Red rectangles highlight increased, blue rectangles decreased prevalence or abundance of the respective OTU in the *nATF6^{IEC}* tg/tg mice.

To test the hypothesis that the microbiota promotes intestinal tumorigenesis, *nATF6^{IEC}* tg/tg mice were treated with antibiotics. Oral vancomycin/metronidazole (V/M) treatment was initiated at the pre-tumor stage (6 wk) and continued for six wk (until the early-tumor age of 12 wk). A second group of mice was given normal drinking water for additional four wk after the end of V/M treatment (treatment scheme Figure 35A). Antibiotics interfered with tumor formation as shown by significantly reduced tumor incidence (Figure 35B) and number (Figure 35C and D). In mice given water for 4 wk after end of V/M treatment, 3 out of 6 were tumor-free and the 3 other mice showed reduced numbers of colonic tumors compared to the control group receiving normal drinking water. The treatment impacted on proliferation and reduced numbers of Ki67+ cells to control level (Figure 35E). Further, there was no significant difference between the numbers of mucin-filled goblet cells when comparing the three genotypes in the treated mice in contrast to the non-treated water controls (Figure 35F).

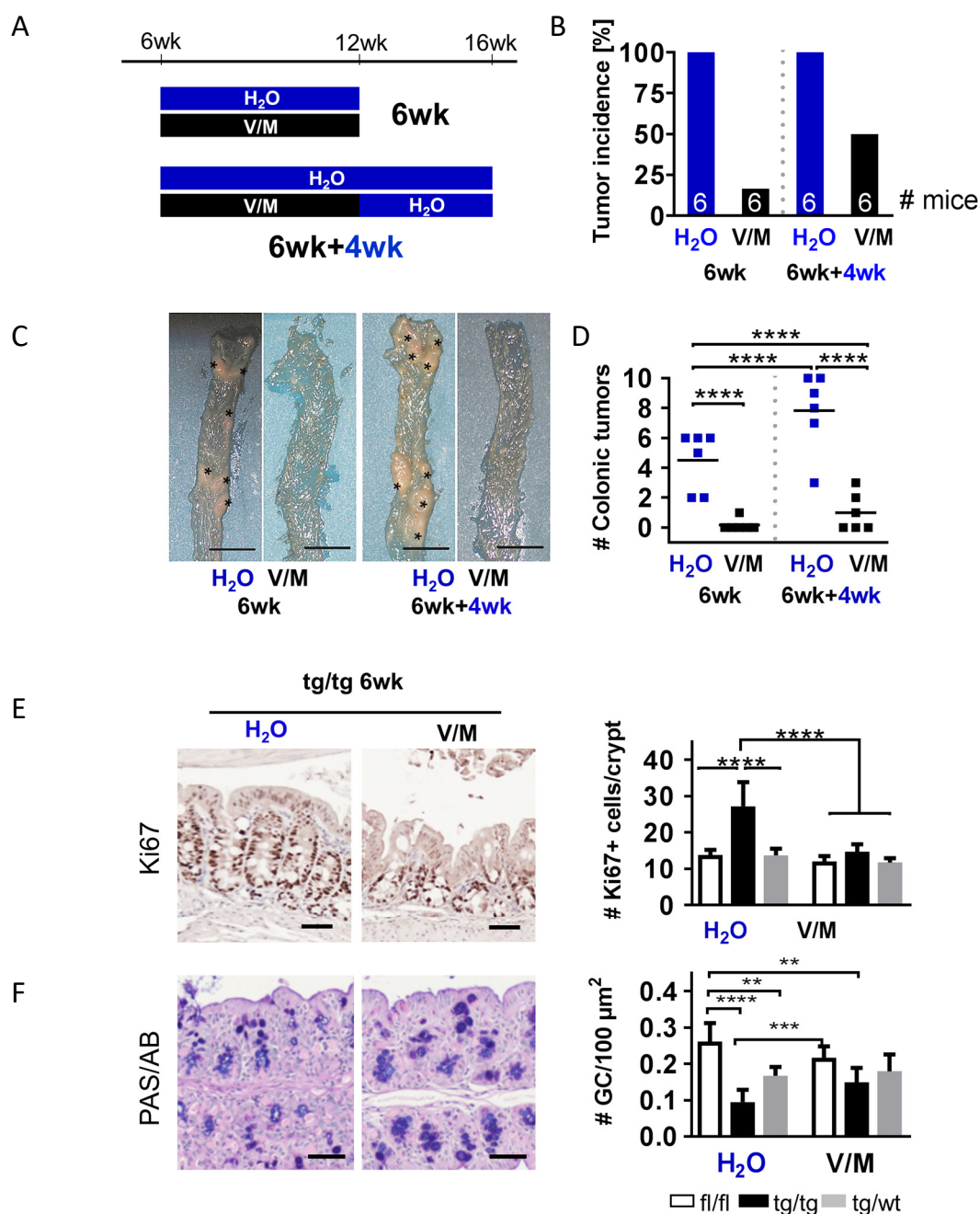


Figure 35: Antibiotic treatment affects tumor formation, hyper-proliferation and goblet cell counts.

(A) Schematic representation of the vancomycin/metronidazole (V/M) treatment of mice. Control mice were on normal drinking water, and V/M-treated mice were either treated for six weeks (6 wk) and sacrificed afterwards, or 6 weeks plus 4 wk on normal drinking water (6 wk+4 wk). (B) Tumor incidence in percentage of V/M-treated mice and water controls, with (C) representative macroscopic pictures of the colon of treated and untreated *nATF6^{IEC}* tg/tg mice (scale bar 1 cm). (D) Number of colonic tumors of V/M-treated mice and water controls. (E) Representative immunohistochemical staining of colonic swiss rolls for Ki67 at the 6 wk time point (left panel; scale bars 50 μm). The number of Ki67+ cells per crypt in non-tumor areas of the colon are shown for the 6 wk time point. (F) Representative PAS/AB staining of colonic swiss rolls at the 6 wk time point (left panel; scale bars 50 μm). The number of mucin-filled goblet cells per 100 μm² in non-tumor areas of the colon are shown for the 6 wk time point. Statistics (D, E, F): ANOVA followed by pairwise comparison testing (Tukey or Bonferroni correction).

Efficacy of the antibiotics was evident by a greatly enlarged cecum size (similar to GF mice; data not shown), a drop in α -diversity (Figure 36A) and shifts in bacterial community structures (Figure 36B).

In general, V/M treatment resulted in a relative decrease in *Bacteroidetes* and a relative increase in *Proteobacteria* (Figure 36C). As evident by both the distance in β -diversity and the taxonomic abundances, the V/M treated mice of the 6 wk+4 wk time point are more similar to the water controls than the treated mice of the 6 wk time point, suggesting a regeneration of the microbiota.

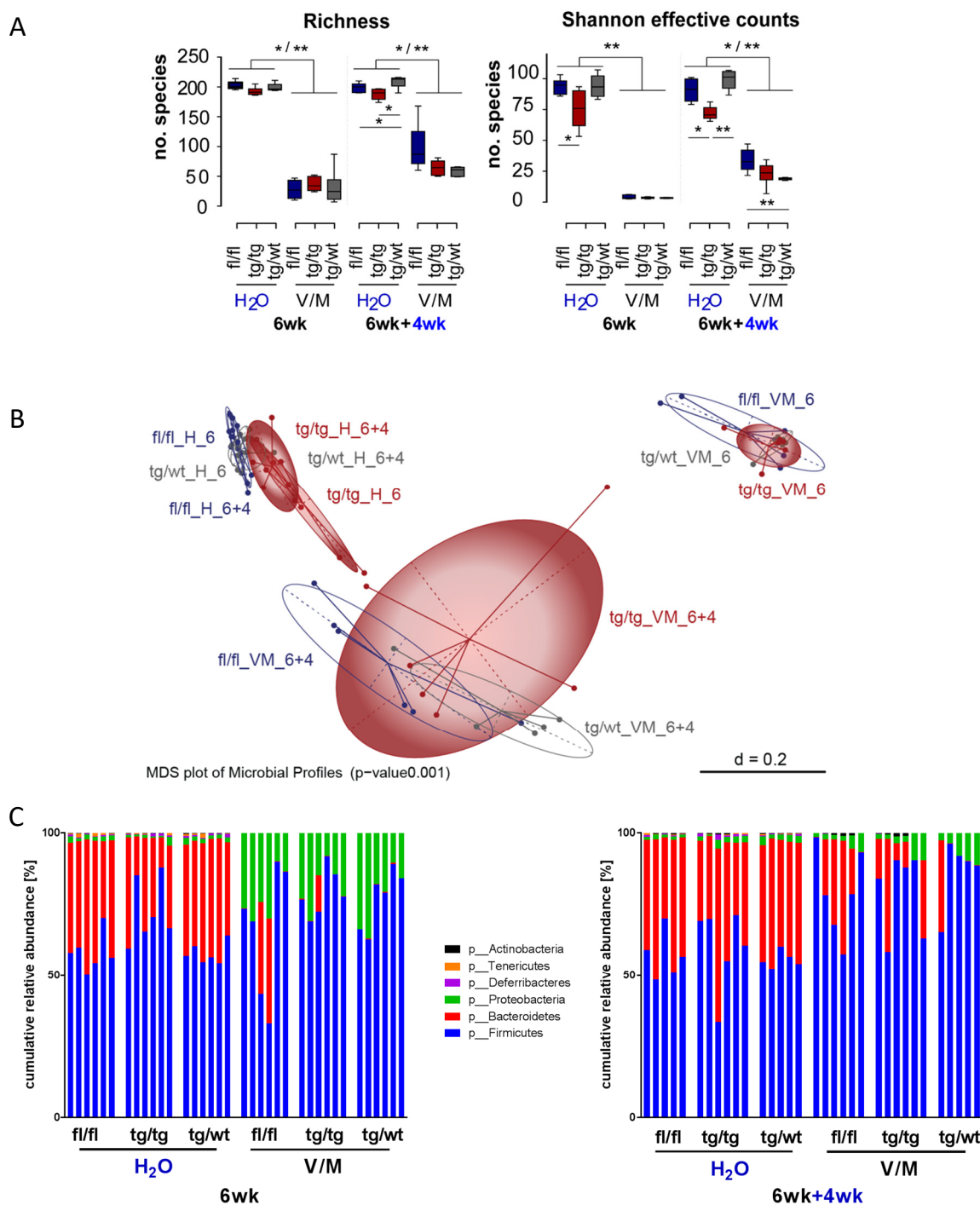


Figure 36: Cecal bacterial community structures are altered in V/M treated mice.

(A) Alpha-diversity (Richness and Shannon effective counts) in *nATF6^{EC}* mice subjected to V/M treatment or without antibiotics at the 6 wk or 6 wk+4 wk experimental time point based on 16S rRNA sequencing of cecal content. **(B)** Beta-diversity analysis of cecal microbiota in mice included in the V/M treatment experiment. **(C)** Cumulative relative abundances of taxa on phylum level for the 6 wk (left side) and 4 wk+6 wk time point (right side).

To elucidate whether a complete absence of the microbiota would prevent the tumorigenic phenotype, *nATF6^{IEC}* mice were made GF. Similar to SPF-housed mice, GF *nATF6^{IEC}* tg/tg and tg/wt mice showed an upregulation of the *nATF6* transgene (Figure 37A and B), the ER UPR chaperone Grp78 (Figure 37B and C), and other UPR target genes (Figure 37C, D, Figure 38).

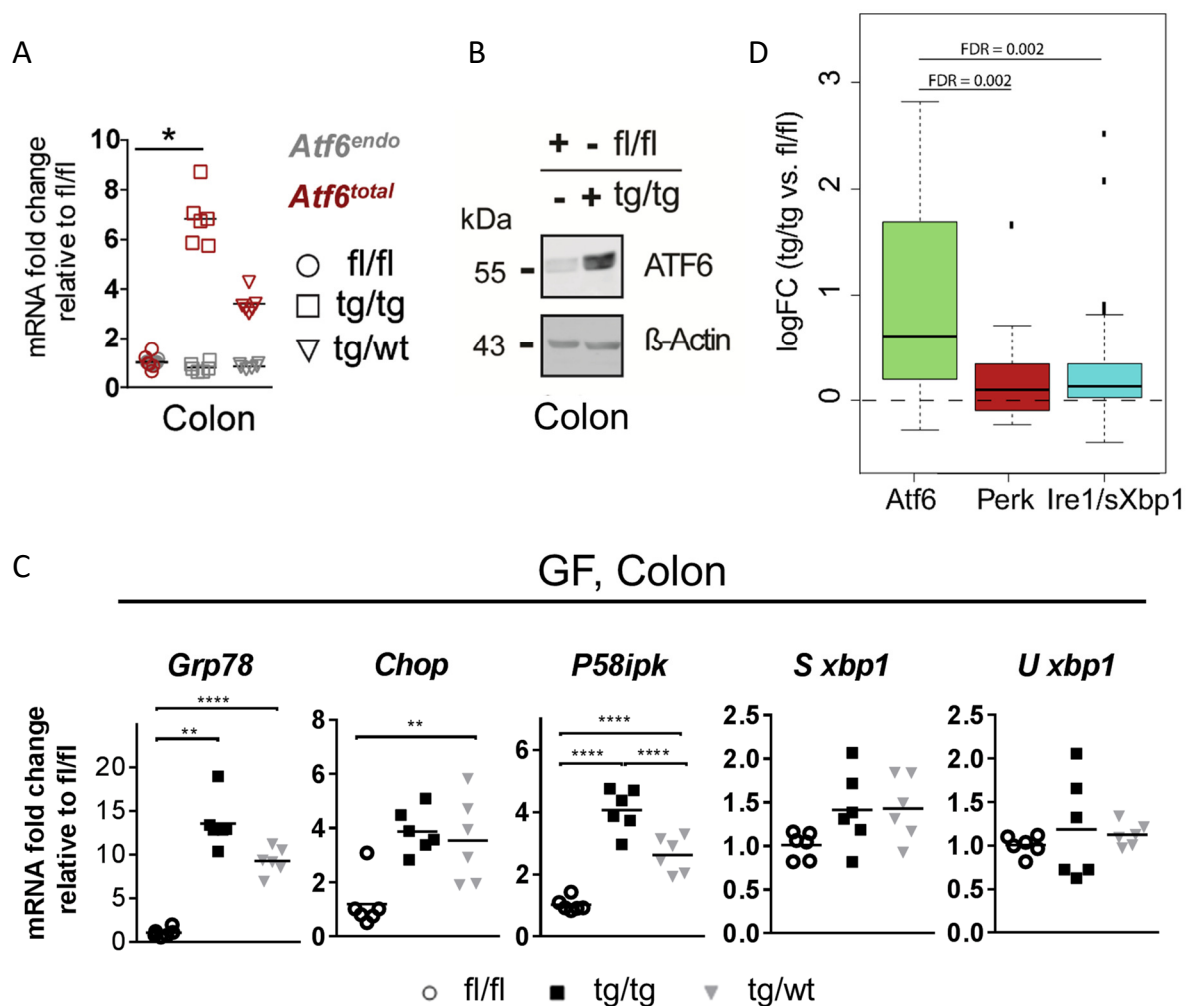


Figure 37: Transgene expression and ER UPR activation in GF *nATF6^{IEC}* mice.

(A) mRNA levels of colonic and small intestinal IEC for endo (endogenous) and total (transgene + endogenous) *Atf6* in GF housed *nATF6^{IEC}* mice. (B) Western blots of colonic IEC of GF *nATF6^{IEC}* mice for the activated form of ATF6 using specific antibodies against ATF6 and the HA-epitope. β -Actin served as loading control. (C) mRNA expression analysis of colonic IEC for UPR-relevant genes of GF *nATF6^{IEC}* mice at the age of 20 wk. (D) Median of the expression level of genes independent of significant regulation known to be involved in ATF6, PERK and IRE-1/sXbp1 driven UPR signaling [95] in microarray analysis of colonic IEC of GF *nATF6^{IEC}* mice at 5 wk of age. In the box plots, bold horizontal lines represent median values, and boxes highlight the corresponding interquartile ranges. Statistics (A, C): ANOVA followed by Bonferroni correction for multiple testing. (D) Two-sided Welch Two Sample t-test with p-values adjusted by Benjamini-Hochberg-Method.

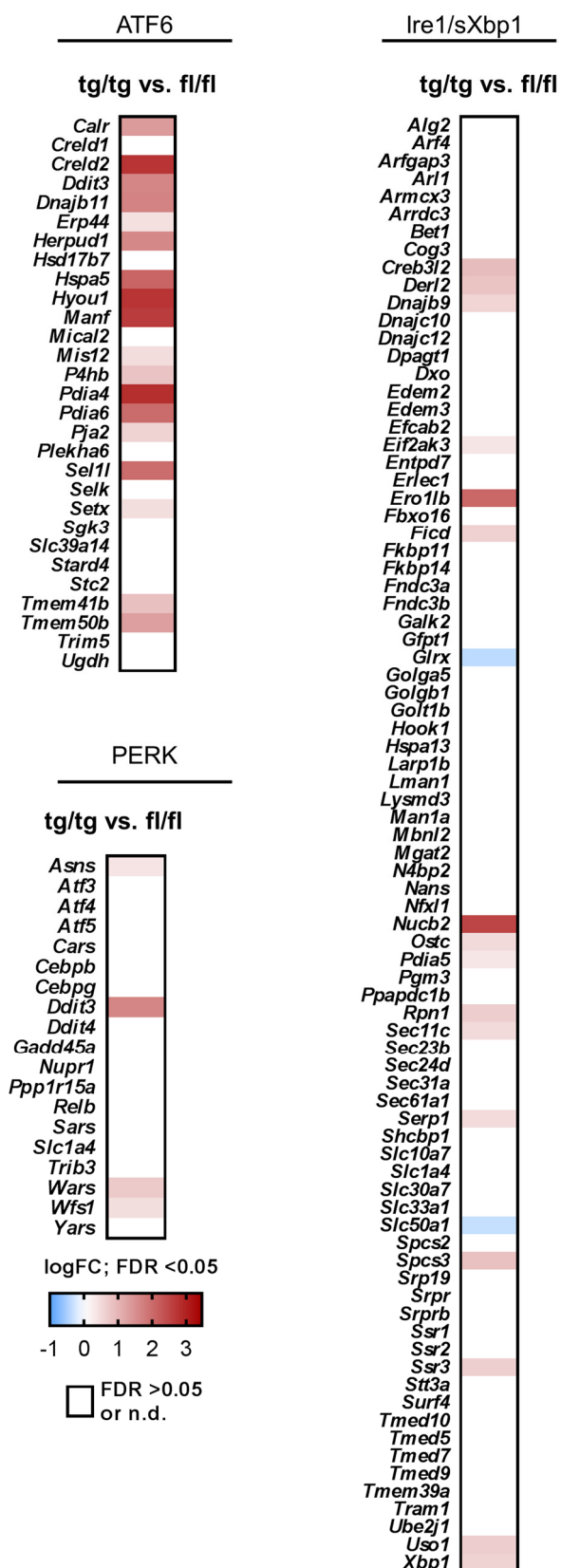


Figure 38: ATF6, PERK and IRE-1/sXBP1 signaling in GF *nATF6*^{EC} mice.

Heatmap illustration of genes involved in ATF6, PERK and IRE-1/sXBP1 signaling based on microarray analysis of GF mice. Gene sets are adapted from [95]. Each rectangle color-codes the logFC between tg/tg vs. fl/fl or tg/tg vs. tg/wt, respectively. Genes not significantly regulated (FDR < 0.05) or not detected are color-coded in white.

The absence of microbes had a pronounced effect on the expression profiles of *nATF6*^{IEC} mice, as evaluated by microarray analysis (Figure 39 B, Figure A 2). At a significance threshold of FDR <0.01, 147 genes were significantly regulated in both GF and SPF housing, but 940 genes were specific to SPF housing (Figure 39 B, Figure A 3). While the shared genes predominantly contribute to GO terms relevant for ER function, response to ER stress and protein folding (Figure 39 C), the SPF significant set of genes showed, besides others, an enrichment of the GO terms “nuclear cell division”, “chromosome segregation” and “cytokinesis” (Figure 39 D). Focusing on SPF housing, 291 genes were significantly (FDR <0.01) regulated in tg/tg mice compared to fl/fl and tg/wt mice (Figure 39 E). GO terms enriched for these genes compromise many terms relevant for cell cycle function (Figure 39 F). Based on the comparison of GF and SPF *nATF6*^{IEC} mice with induced *nATF6*^{IEC-OHT} mice 107 shared genes were identified with predominant roles in ER folding and function (Figure 40 B, C, Figure A 3).

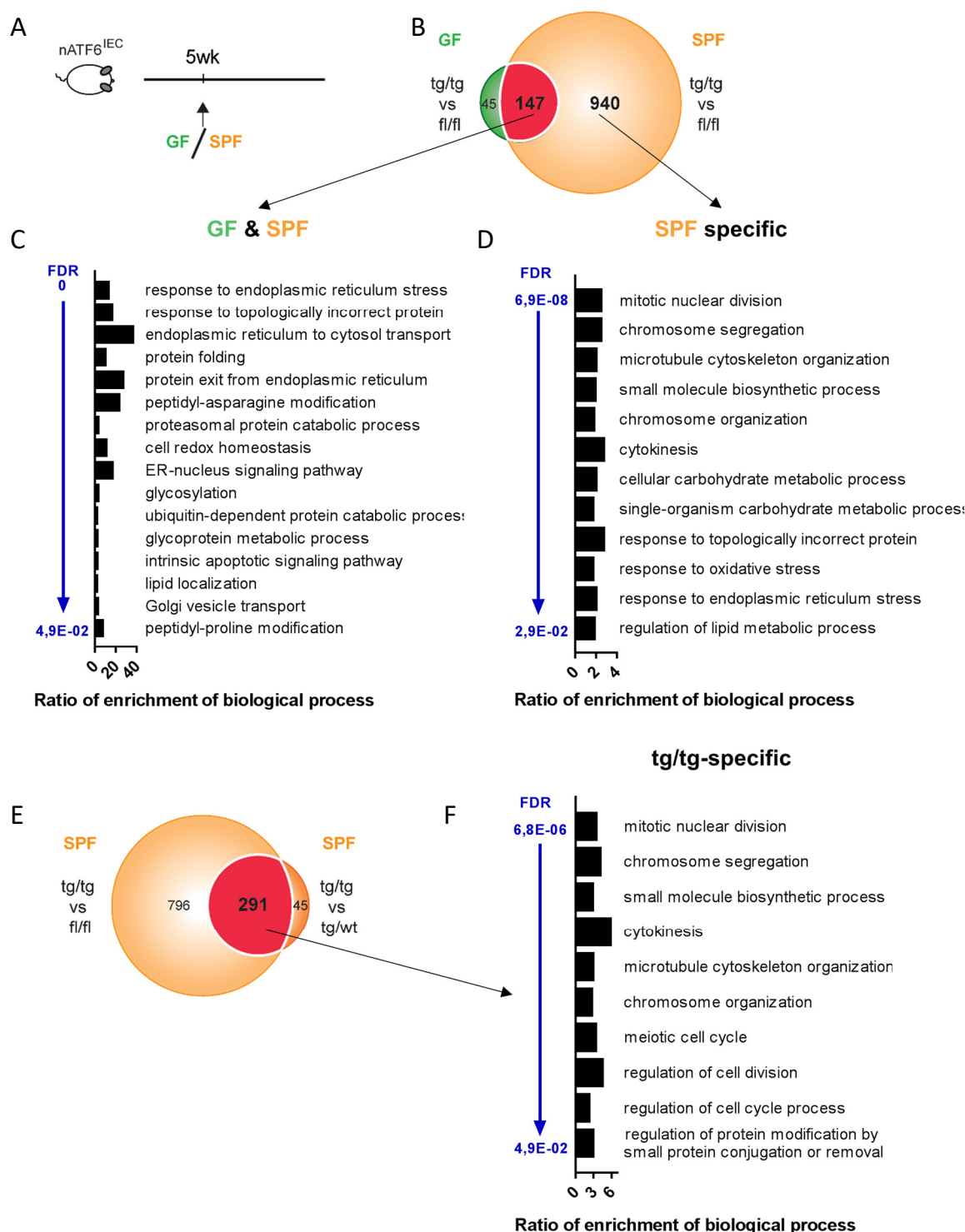


Figure 39: SPF housing of *nATF6^{IEC}* mice has a big impact on the set of regulated genes.

(A) Experimental setup for the generation of colonic IEC of SPF and GF housed *nATF6^{IEC}* mice for microarray analysis. **(B)** Venn-diagram illustration of the number of genes significantly differently expressed (FDR <0.01) between *tg/tg* and *fl/fl* mice under GF housing (green) or SPF housing (orange). 148 genes are shared between SPF and GF. **(C, D)** Gene set enrichment analysis of Biological processes (WebGestalt [222, 223], GO Terms only non-redundant, FDR <0.05). **(C)** Biological processes significantly enriched in the genes shared between GF and SPF. **(D)** Biological processes significantly enriched in the genes specific for the SPF dataset. **(E)** Venn-diagram illustration of the number of genes significantly differently expressed (FDR <0.01) between *tg/tg* and *fl/fl* mice or *tg/tg* and *tg/wt* mice in the SPF facility, respectively. 291 genes are shared between both comparisons. **(F)** Biological processes significantly enriched in the genes specific for the *tg/tg* genotype.

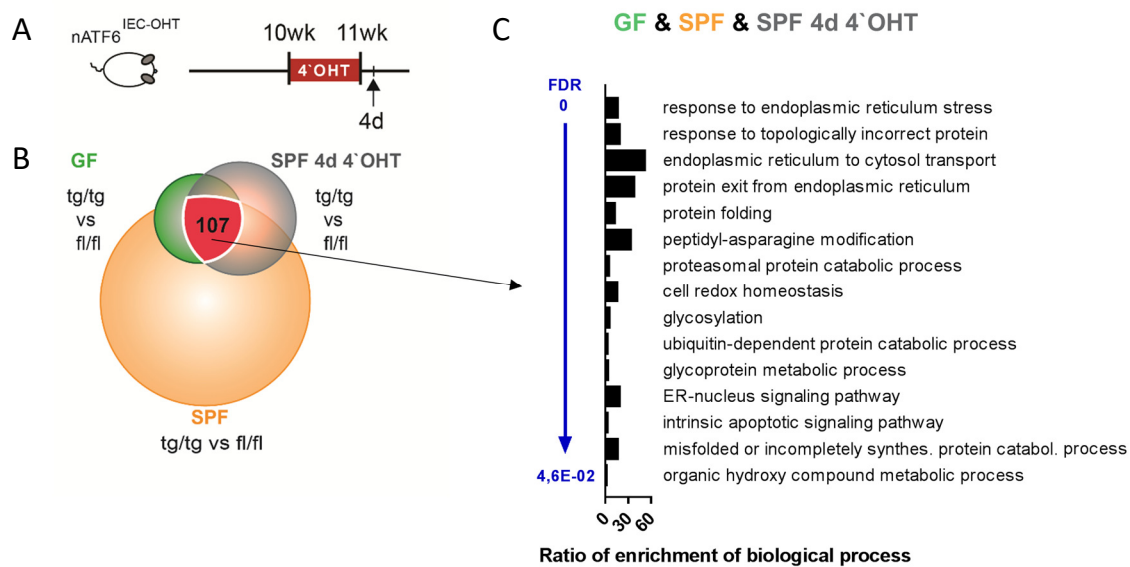


Figure 40: A set of genes is shared between SPF and GF $nATF6^{IEC}$ mice and $nATF6^{IEC-OHT}$ mice.

(A) Experimental setup for the generation of colonic whole tissue of SPF housed $nATF6^{IEC-OHT}$ mice for microarray analysis. **(B)** Venn-diagram illustration of the number of genes significantly differentially expressed (FDR <0.01) between tg/tg and fl/fl mice under GF housing (green), SPF housing (orange) or SPF housed $nATF6^{IEC-OHT}$ mice (grey). 107 genes are shared between all three datasets. **(C)** Gene set enrichment analysis of Biological processes (WebGestalt [222, 223], GO Terms only non-redundant, FDR <0.05). Biological processes significantly enriched in the genes shared between GF and SPF $nATF6^{IEC}$ mice and $nATF6^{IEC-OHT}$ mice.

Most significantly, GF $nATF6^{IEC}$ tg/tg mice did not develop adenomas even at the age of 20 wk (Figure 41A and C). To investigate whether a tumorigenic phenotype could be re-established via microbiota transfer, 4 wk old GF $nATF6^{IEC}$ tg/tg mice and fl/fl controls were gavaged with cecal content from either $nATF6^{IEC}$ tg/tg or fl/fl 5 wk old SPF mice (donors) (treatment scheme Figure 41B). Cecal microbiota from 3 different donors per genotype were each transferred to 3 recipient mice per genotype ($n = 9$ in total per genotype). The association of tg/tg mice with SPF microbiota resulted in abortion of the experiment for some mice due to weight loss (Figure 41B). Association of $nATF6^{IEC}$ tg/tg mice with cecal content from $nATF6^{IEC}$ fl/fl or tg/tg donors led to a tumor incidence of 20 % and 87.5 %, respectively (Figure 41C), suggesting a higher potential of the tg/tg microbiota to trigger the onset of tumorigenesis, even when collected from donors at the pre-tumor stage. In contrast, control mice (GF gavaged with PBS) did not develop adenomas (Figure 41C and D), and neither did fl/fl mice associated with any of the microbiota. The hyper-proliferative phenotype and loss of mucin-filled goblet cell previously observed in SPF housed $nATF6^{IEC}$ tg/tg mice was absent under GF conditions (Figure 41E, F, Figure 16, Figure 19). The transfer of the tg/tg donor microbiota into tg/tg mice was associated with an increase in proliferation (Figure 41E), and a pronounced reduction in mucin-filled goblet cell (Figure 41F). Interestingly, even the association with fl/fl donor microbiota caused a significant loss of mucin-filled goblet cell in tg/tg recipients but not in fl/fl recipients (Figure 41F).

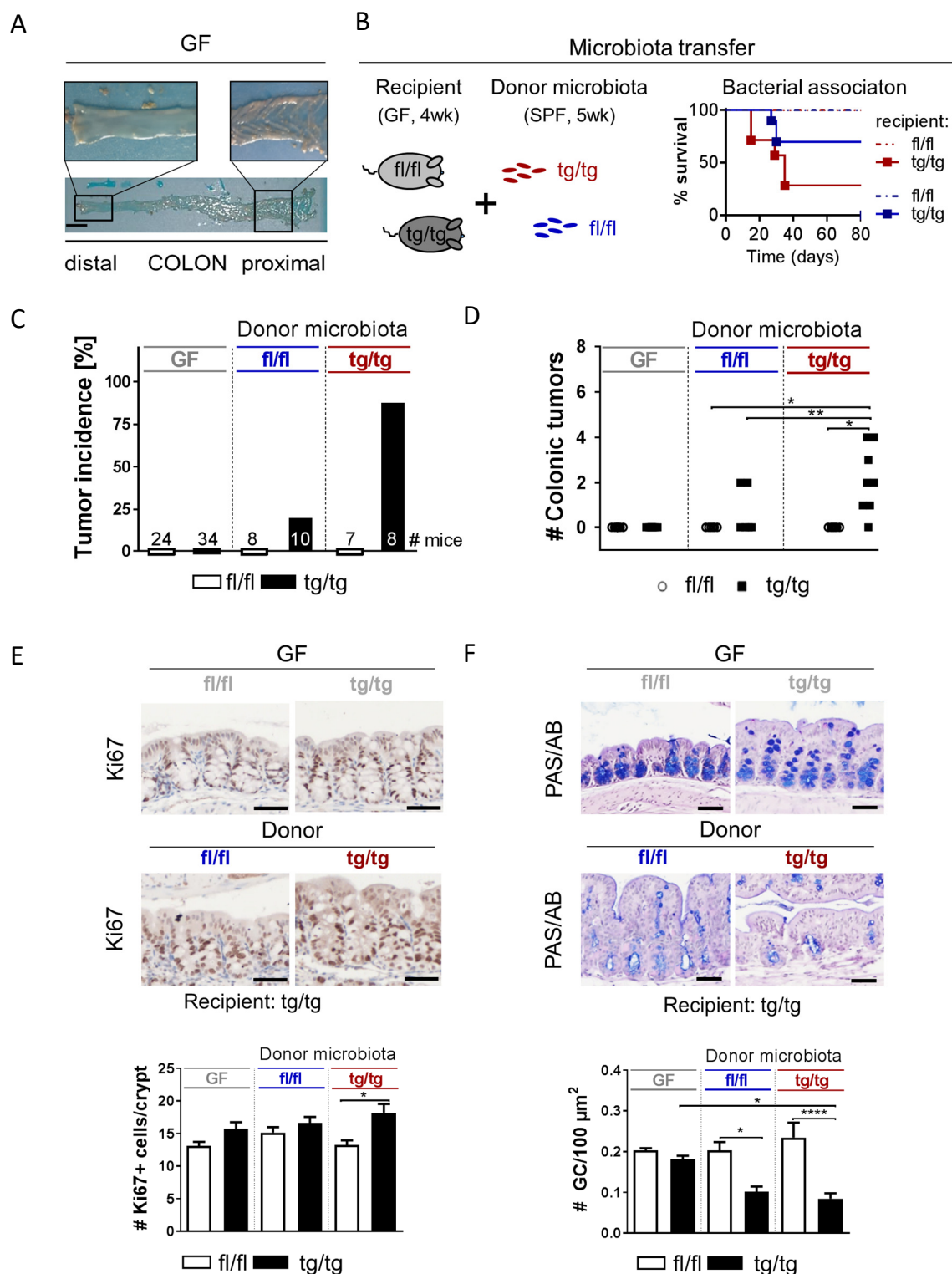


Figure 41: Microbial transfer re-establishes tumor development in GF $nATF6^{IEC}$ tg/tg mice.

(A) Representative macroscopic images of the appearance of a colon from a GF $nATF6^{IEC}$ tg/tg mouse at the age of 20 wk (scale bar 1 cm). (B) Schematic diagram illustrating the association experiment of GF recipient mice (age 4 wk) with cecal content from 5 wk old fl/fl and tg/tg SPF donor mice and survival curve observed for the experiment. (C) Tumor incidence in percentage in GF mice (12-20 wk) and associated $nATF6^{IEC}$ mice (7-16 wk). (D) Number of colonic tumors in GF mice (12-20 wk) and associated mice (7-16 wk). (E) Representative images and quantification of Ki67 positive cells in the colon of $nATF6^{IEC}$ PBS gavage controls and microbiota associated mice (scale bars 50 μ m). (F) Representative images and quantification of mucin-filled goblet cells in the colon of $nATF6^{IEC}$ PBS gavage controls and microbiota associated mice (scale bars 50 μ m). Statistics (D-F): ANOVA followed by pairwise comparison testing (Tukey or Bonferroni correction).

16S rRNA sequencing of cecal microbiota in recipient mice demonstrated a limited engraftment of diversity when comparing the alpha-diversity of donors and recipients (Figure 42A). This is further evident for taxonomic abundances in the tg/tg recipients (Figure 42C). However, β -diversity analysis confirmed the transfer of distinct bacterial communities since the microbiota of the recipients grouped significantly different according to the donor genotype (Figure 42B). When comparing tg/tg recipients associated with fl/fl or tg/tg donor microbiota (either remaining tumor-free (N) or developing tumors (T)), we identified 4 OTUs with significantly different prevalence in the comparison of all groups according to the Fisher test. These significant OTUs are illustrated in Figure 42D as a heatmap of relative abundances.

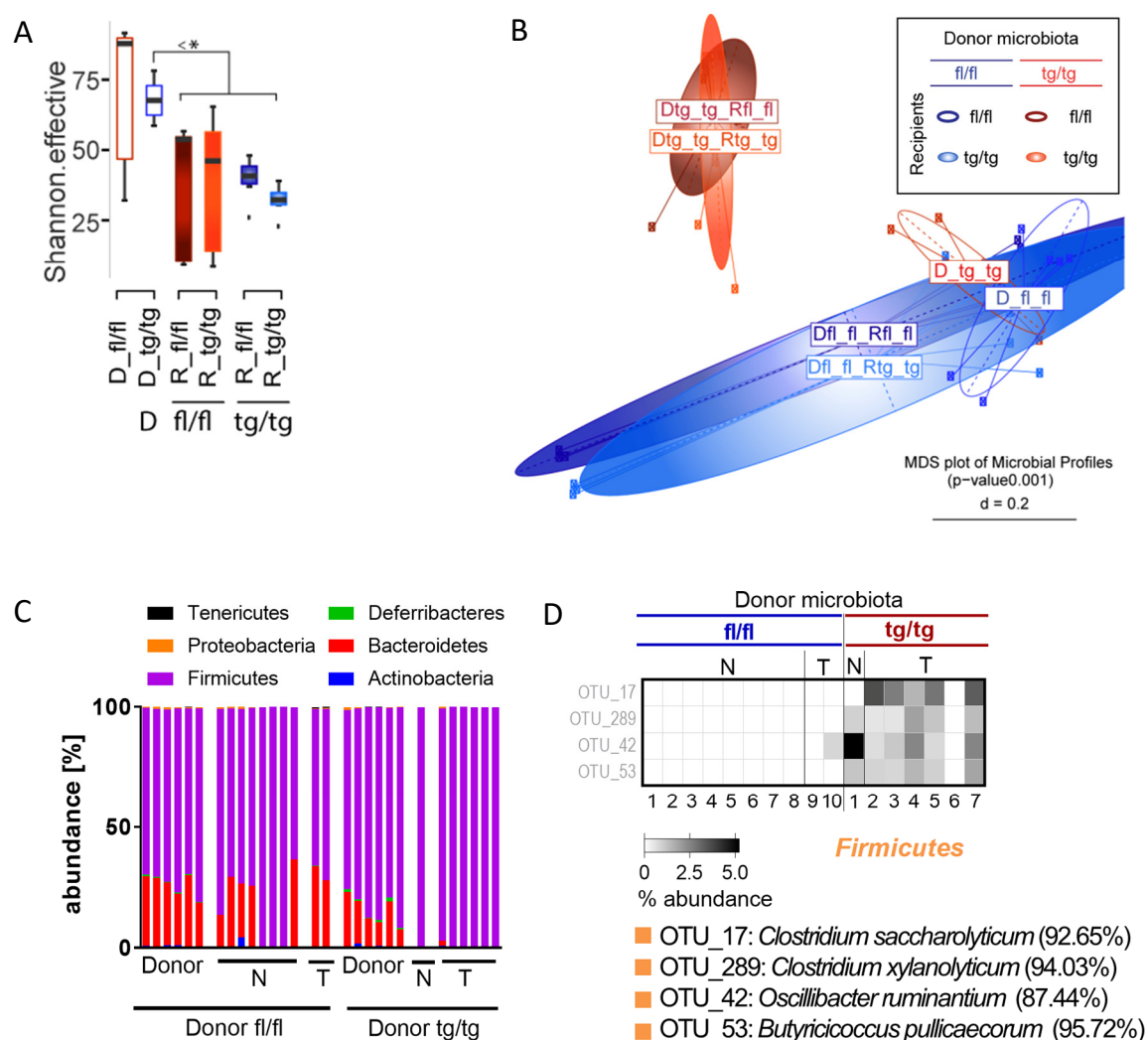


Figure 42: Cecal bacterial community structures after microbiota transfer.

(A) Alpha-diversity as represented by Shannon effective species counts in *nATF6*^{IEC} mice. Per donor sample both the original sample and the bacterial preparation transferred to the mouse is considered. (B) Multidimensional scaling analysis plot of generalized UniFrac of recipient and donor mice. (C) Taxonomic abundances of associated tg/tg mice with (T) or without (N) tumors and donors on phylum level. Per donor sample both the original sample and the bacterial preparation transferred to the mouse is considered. (D) Heatmap illustration of significantly altered OTUs with respect to prevalence for associated tg/tg mice with (T) or without (N) tumors. OTUs were assigned to the closest known species using EzTaxon.

Of relevance for the link between microbial colonization and the proliferative response in *nATF6^{IEC}* tg/tg mice, we did not observe a hyper-proliferative phenotype of organoids isolated from the colon of tg/tg mice housed either in SPF or GF conditions (Figure 43). This was assessed by measurement of cyst size at day 1 and day 7 and the number of budding crypts per cyst at day 7 after the start of the culture. Unexpectedly, organoids derived from *nATF6^{IEC}* tg/tg SPF mice showed a similar size than the respective fl/fl organoids at day 1 with a significantly decreased cyst size at day 7. Organoids isolated from GF *nATF6^{IEC}* tg/tg mice showed significantly smaller cysts at day 1 and day 7 and significantly less budding compared to the respective fl/fl control.

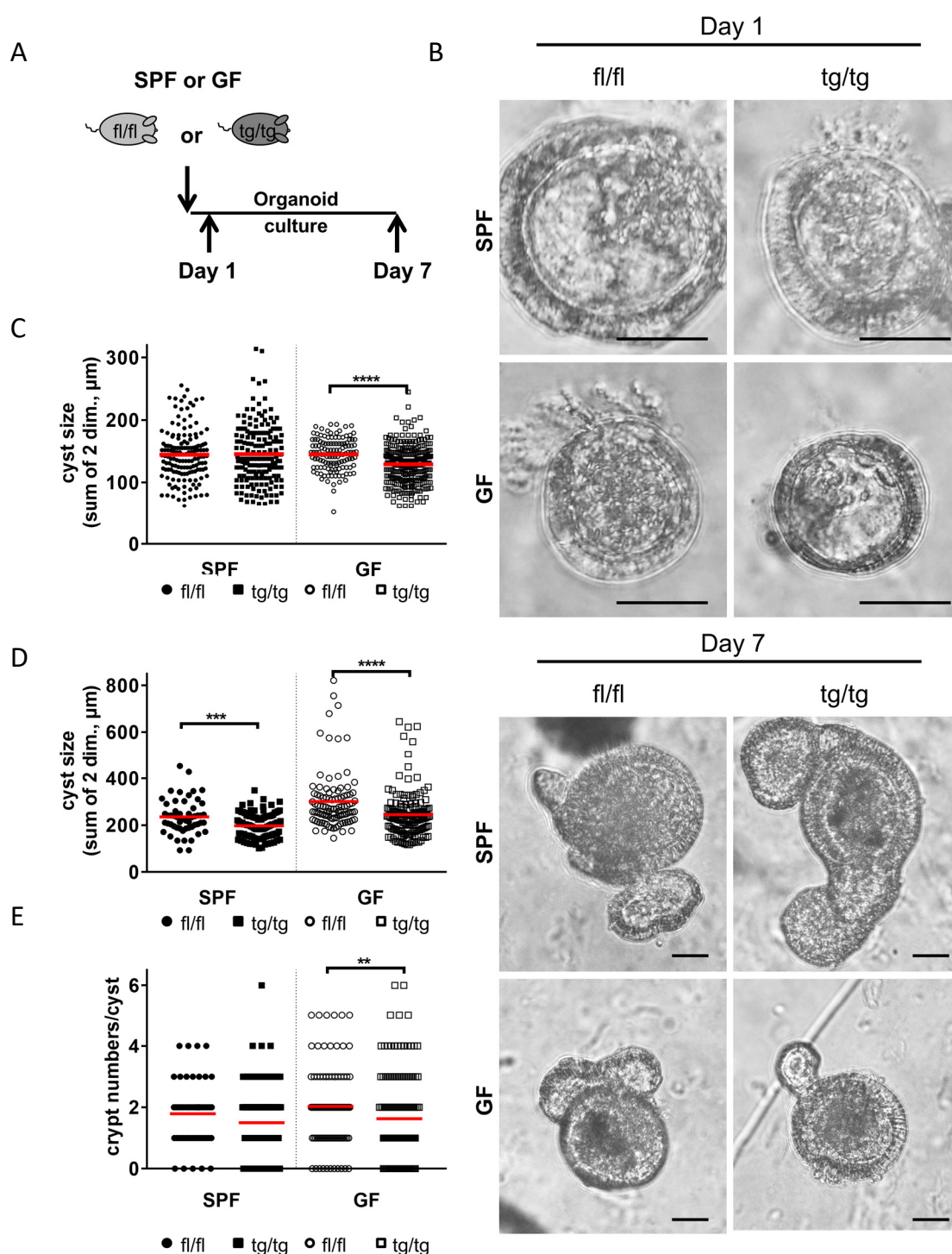


Figure 43: Growth characteristics of colonic organoids isolated from $nATF6^{\text{EC}}$ tg/tg mice is not increased in culture.

(A) Schematic representation of experimental setup. Organoids were isolated from the colon of $nATF6^{\text{EC}}$ fl/fl or tg/tg mice either housed in SPF or GF conditions at the age of 20 wk. (B) Exemplary pictures of organoids at day 1 and day 7 after start of culture (scale bars 50 μm). (C-D) Quantification of cyst size as the sum of two dimensions in μm at day 1 (C) and day 7 (D). (E) Quantification of the number of budding crypts per cyst. (C-E) The mean is indicated in red. For the analysis, four independent wells were evaluated per mouse genotype and housing condition with GF $nATF6^{\text{EC}}$ tg/tg organoids being represented by two individual mice. Statistics: Mann-Whitney test.

Since the signal transducer and activator of transcription (STAT) 3 signaling pathway is known to contribute to tumorigenesis we analyzed STAT3 activation in the *nATF6^{IEC}* mice (Figure 44). Immunohistochemical stainings of colonic swiss rolls for phosphorylated STAT3 indicated a dominant age-dependent increase in pSTAT3 with mild to distinct activation at 5 wk of age but strong and dominant activation at late ages in the *nATF6^{IEC} tg/tg* mice (Figure 44 A-C, in cooperation with Prof. Dr. Mathias Heikenwalder, Institute of Virology, German Research Center for Environmental Health, Helmholtz Center Munich). This activation was abrogated by GF housing and diminished by antibiotic treatment (Figure 44D, E). A similar increase in nuclear pSTAT3 in IEC was observed in the *nATF6^{IEC-OHT}* mice after induction (Figure 44F). Activation of pSTAT3 was already evident at the 4 d time point and distinct or frequent 15 wk after end of tamoxifen induction. To characterize the observed STAT3 activation further, potential STAT3 upstream regulators and targets were compared to the genes regulated in the *nATF6^{IEC}* mouse at 5 weeks (Figure 45). While many target genes were significantly regulated (Figure 45 B) at a FDR of 0.01, only few potential upstream regulators comprising STAT6, RAR Related Orphan Receptor C (*Rorc*) and STAT2 were significantly regulated at FDR < 0.05 (Figure 45A). In contrast to STAT3 activation, only a minor involvement of STAT1 activation was observed at early ages more distinct at later ages (Figure 46A-D, in cooperation with Prof. Dr. Mathias Heikenwalder, Institute of Virology, German Research Center for Environmental Health Helmholtz Center Munich). Further, no to mild activation of NFkB signaling as assessed by nuclear RelA in IEC was detected (Figure 46E-H).

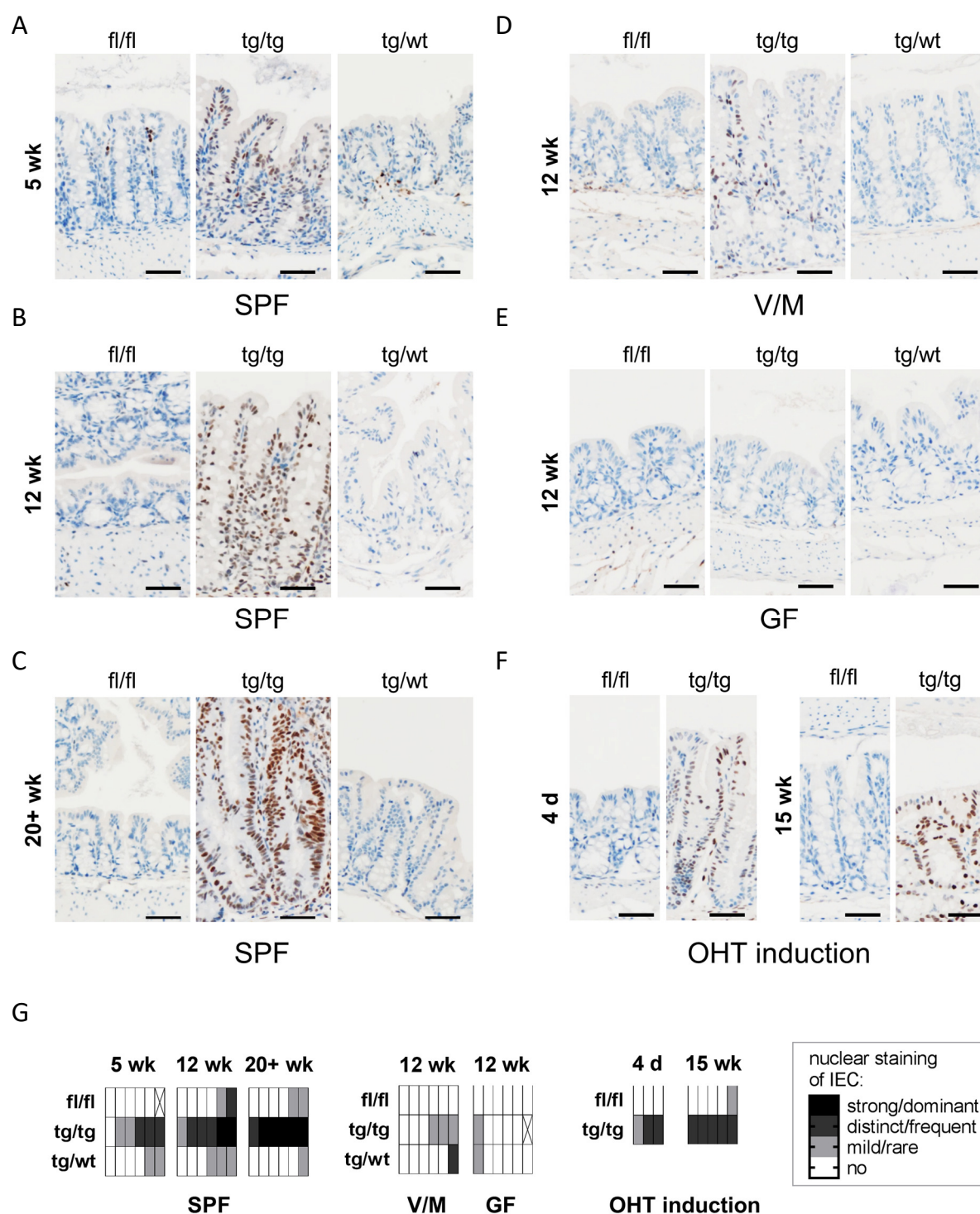


Figure 44: STAT3 signaling is activated in *nATF6* mice in a microbiota-dependent manner.

STAT3 signaling was evaluated by immunohistochemical staining of phospho-STAT3 in colonic swiss rolls of *nATF6*^{IEC} (A-E) and *nATF6*^{IEC-OHT} mice (F) (scale bars 50 μm). Stainings were performed by the Institute of Virology, German Research Center for Environmental Health, Helmholtz Center Munich. (A-C) Representative pictures of SPF housed mice at the age of 5 wk (A), 12 wk (B) and 20-30 wk (20w+ wk) (C). (D) Representative pictures of 12 wk old SPF-housed mice treated with V/M for 6 wk. (E) Representative pictures of GF mice at the age of 12 wk. (F) Representative pictures of *nATF6*^{IEC-OHT} mice sampled 4 d and 15 wk after end of OHT induction. (G) Heatmap illustration of the quantification of the stainings (A-F). Each square represents the final categorical score for an individual mouse. Categorical scores were assigned considering intensity and frequency of nuclear staining in IEC.

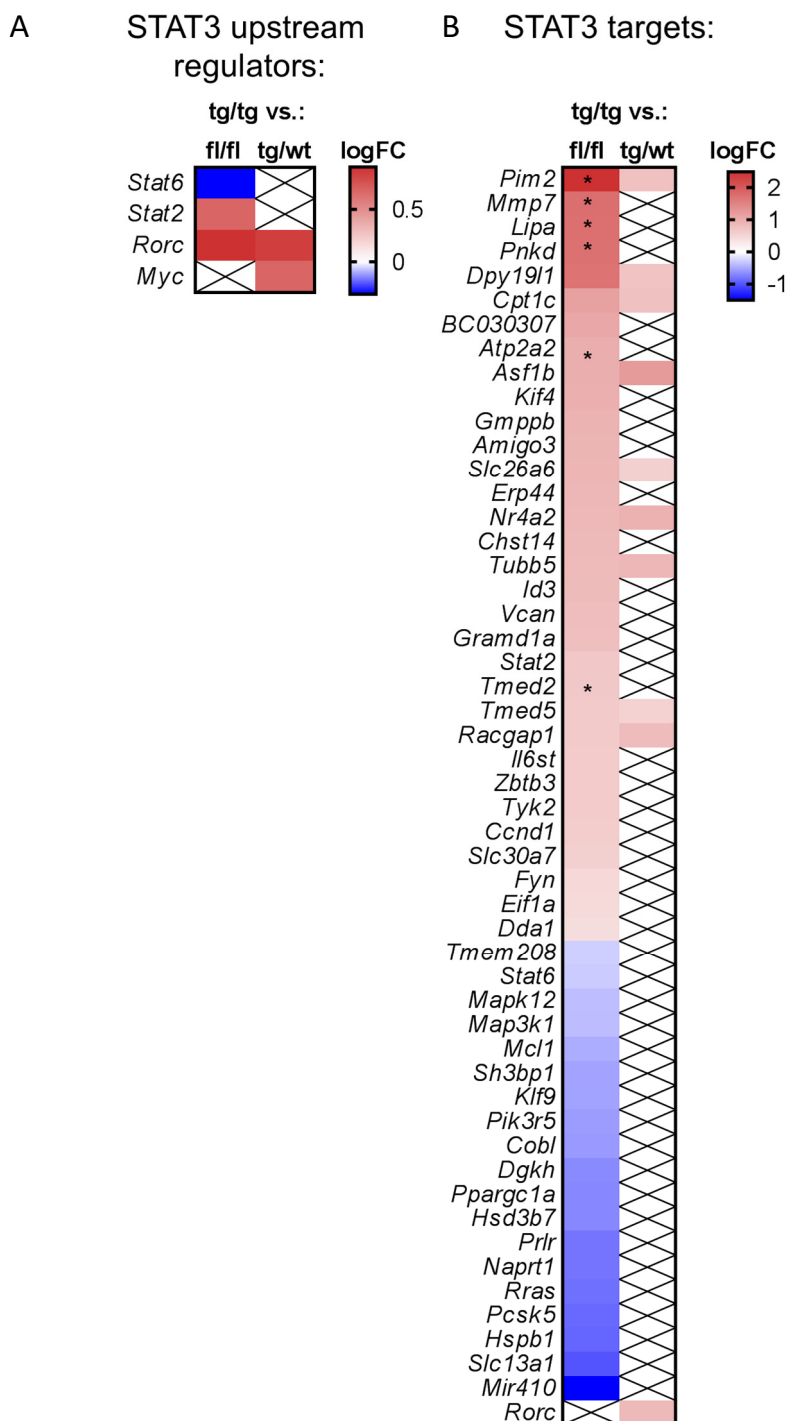


Figure 45: STAT3 upstream regulators and targets.

Analysis of STAT3 upstream regulators and targets based on the microarray analysis of *nATF6^{IEC}* SPF mice. Known regulators and targets for STAT3 were selected based on the RegNetwork database [224]. Upstream regulators (A) and targets (B) with a maximal FDR of 0.05 (regulators) and 0.01 (targets) are shown as heatmaps with the logFC color-coded. Asterisks indicate genes which are also significantly regulated in the GF dataset (same FDR threshold selected as for SPF).

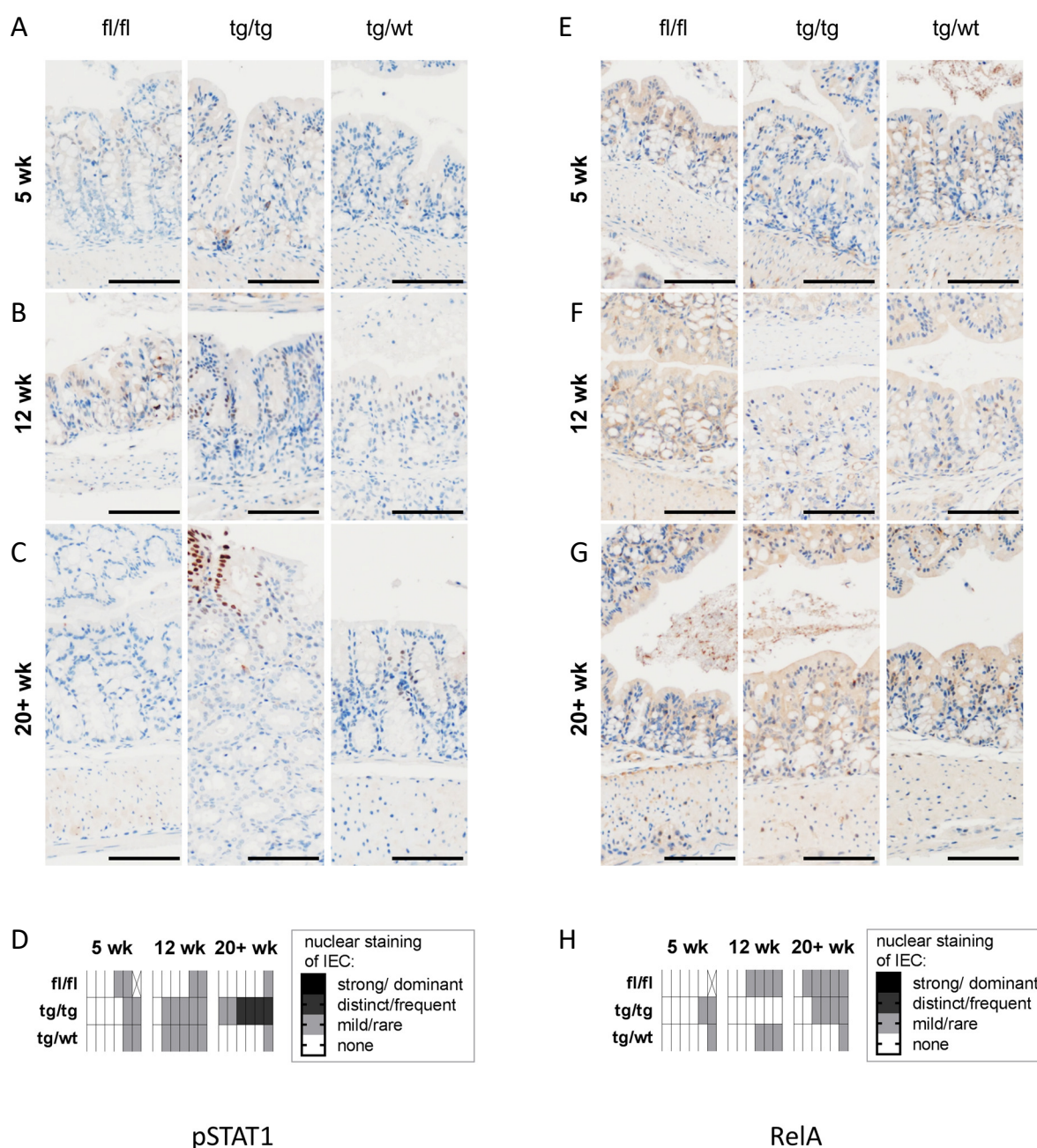


Figure 46: No activation of STAT1 and NF κ B signaling in *nATF6^{IEC} tg/tg* mice at early ages.

STAT1 and NF κ B signaling were evaluated by immunohistochemical staining of phospho-STAT1 (**A-D**) and RelA (**E-H**) in colonic swiss rolls of *nATF6^{IEC}* mice (scale bars 100 μ m). Stainings were performed by the Institute of Virology, German Research Center for Environmental Health, Helmholtz Center Munich. (**A-C**) Representative pictures of SPF housed mice for pSTAT1 at the age of 5 wk (**A**), 12 wk (**B**) and 20-30 wk (20+ wk) (**C**). (**D**) Heatmap illustration of the quantification of the data sets (**A-C**). Each square represents the final categorical score for an individual mouse. Categorical scores were assigned considering intensity and frequency of nuclear staining in IEC. (**E-G**) Representative pictures of SPF housed mice for RelA at the age of 5 wk (**E**), 12 wk (**F**) and 20+ wk (**G**). (**H**) Heatmap illustration of the quantification of the data sets (**E-G**). Each square represents the final categorical score for an individual mouse. Categorical scores were assigned considering intensity and frequency of nuclear staining in IEC.

Differences in microbial signaling are also evident in the microarray analysis and primarily observed in RNA isolated from colonic tissue of *nATF6^{IEC-OHT} tg/tg* mice (Figure 47A). Based on the median of the expression level of all genes assigned, the GO terms "REGULATION OF NLRP3 (NLR family pyrin

domain containing 3) INFLAMMASOME COMPLEX ASSEMBLY”, “MYD88 (myeloid differentiation primary response gene 88) DEPENDENT TOLL LIKE RECEPTOR SIGNALING PATHWAY” and the KEGG pathway “JAK (janus kinase) STAT SIGNALING PATHWAY” have a significantly decreased median expression in *nATF6^{IEC-OHT}* tg/tg mice compared to fl/fl mice. An opposite behavior is evident for the GO Term “MITOGEN ACTIVATED PROTEIN KINASE BINDING”. Focusing on microbial signaling in IEC of *nATF6^{IEC}* tg/tg mice, an increased median expression of genes involved in the GO terms “NEGATIVE REGULATION OF TOLL LIKE RECEPTOR SIGNALING PATHWAY” and “REGULATION OF CALCINEURIN NFAT (nuclear factor of activated T cells) SIGNALING PATHWAY” was found (Figure 47B).

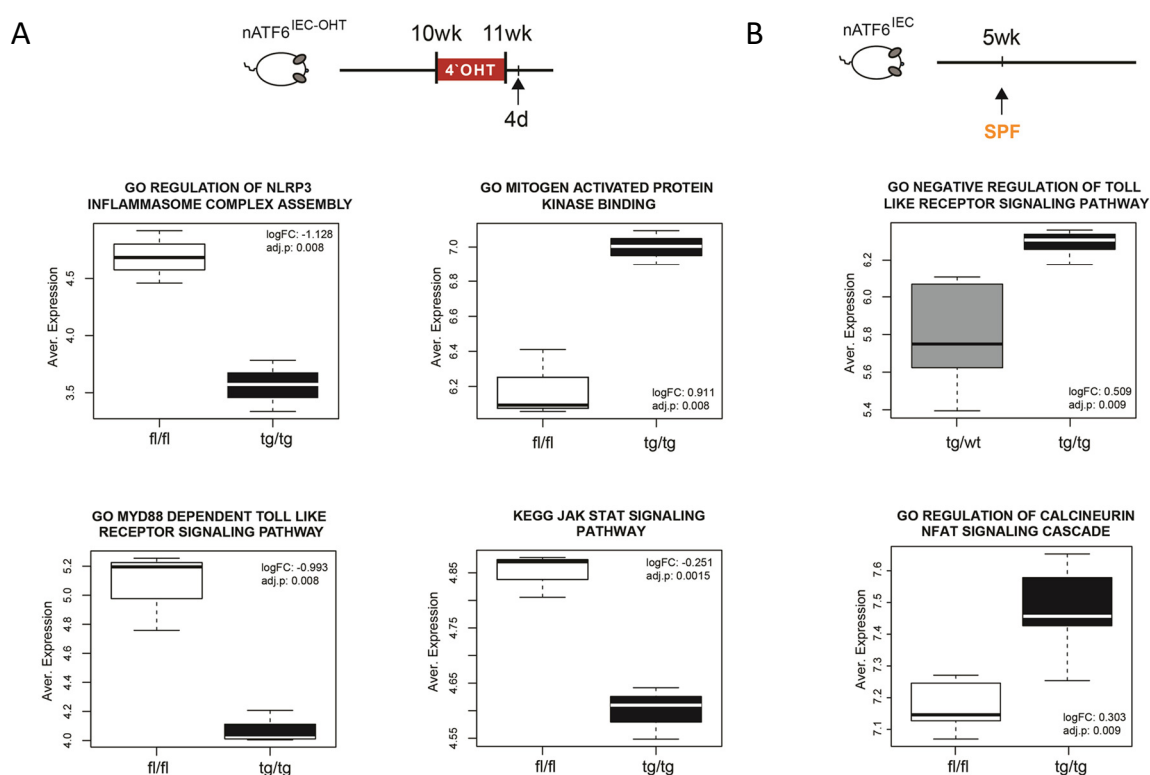


Figure 47: Evidence for differences in microbial signaling in *nATF6* mice based on microarray analysis.

GO Terms and KEGG pathways with significant differential activity based on the median of the expression level of all genes. Only pathways/GO terms were considered with a minimum mapping of 10 genes. Median expression alterations of GO terms and KEGG pathways relevant for microbial signaling enriched in *nATF6^{IEC-OHT}* mice (A) and *nATF6^{IEC}* mice (B). In the box plots, bold horizontal lines represent median values, and boxes highlight the corresponding interquartile ranges. The logFC and the adjusted p-value is given.

To address tumor-specific expression profiles, IEC isolated from tumor and non-tumor regions were analyzed by microarray (Figure 48). To allow for a biologically relevant interpretation of the results, genes with a FDR <0.05 were considered. In total, 376 genes were downregulated compared to 268 upregulated genes. 14 and 32 GO terms were assigned to down- and upregulated genes, respectively (Figure 48 C, D). Among these 32 GO terms, the top significant GO terms comprise terms relevant for microbial interaction. Differences in the recognition of microbes in tumor IEC were further evident based on the median of the expression level of all genes assigned to KEGG pathways (Figure 49).

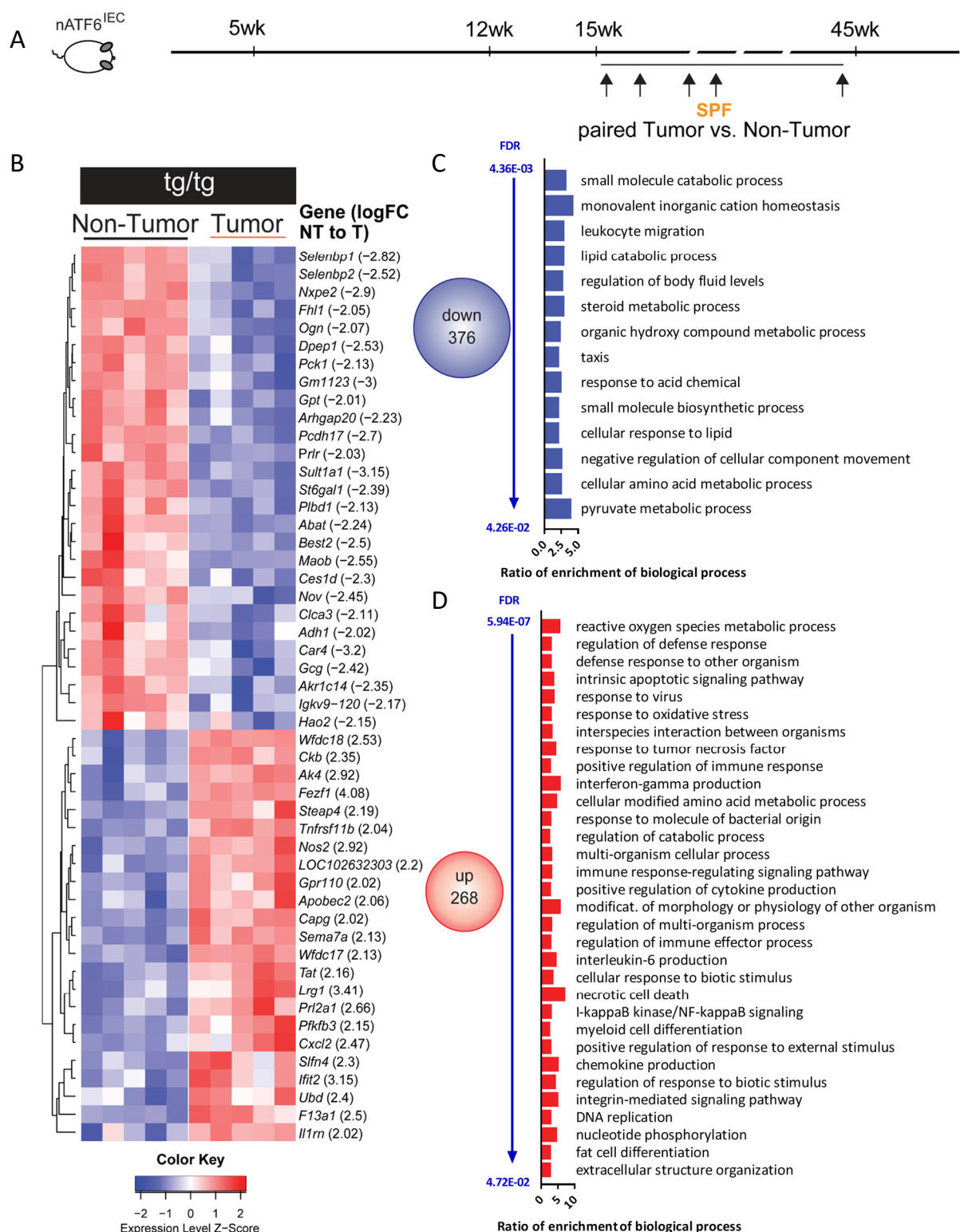


Figure 48: Microarray analysis of IEC isolated from tumor and paired non-tumor tissue of *nATF6*^{IEC} tg/tg mice.

(A) Experimental setup for the generation of colonic IEC of tumor and paired non-tumor tissue of *nATF6*^{IEC} tg/tg mice by Laser Microdissection. Tumor and non-tumor IEC were isolated from the same mouse (paired). **(B)** Top 50 most differentially regulated genes between tumor and non-tumor IEC (FDR <0.05). Each square represents the color-code of the respective Z-Score of a tumor or non-tumor sample. **(C)** Number of significantly downregulated (down) genes (FDR <0.05). Gene set enrichment analysis of Biological processes (WebGestalt [222, 223], GO Terms only non-redundant, FDR <0.05) of downregulated genes. **(D)** Number of significantly upregulated (up) genes (FDR <0.05). Gene set enrichment analysis of Biological processes (WebGestalt [222, 223], GO Terms only non-redundant, FDR <0.05) of upregulated genes.

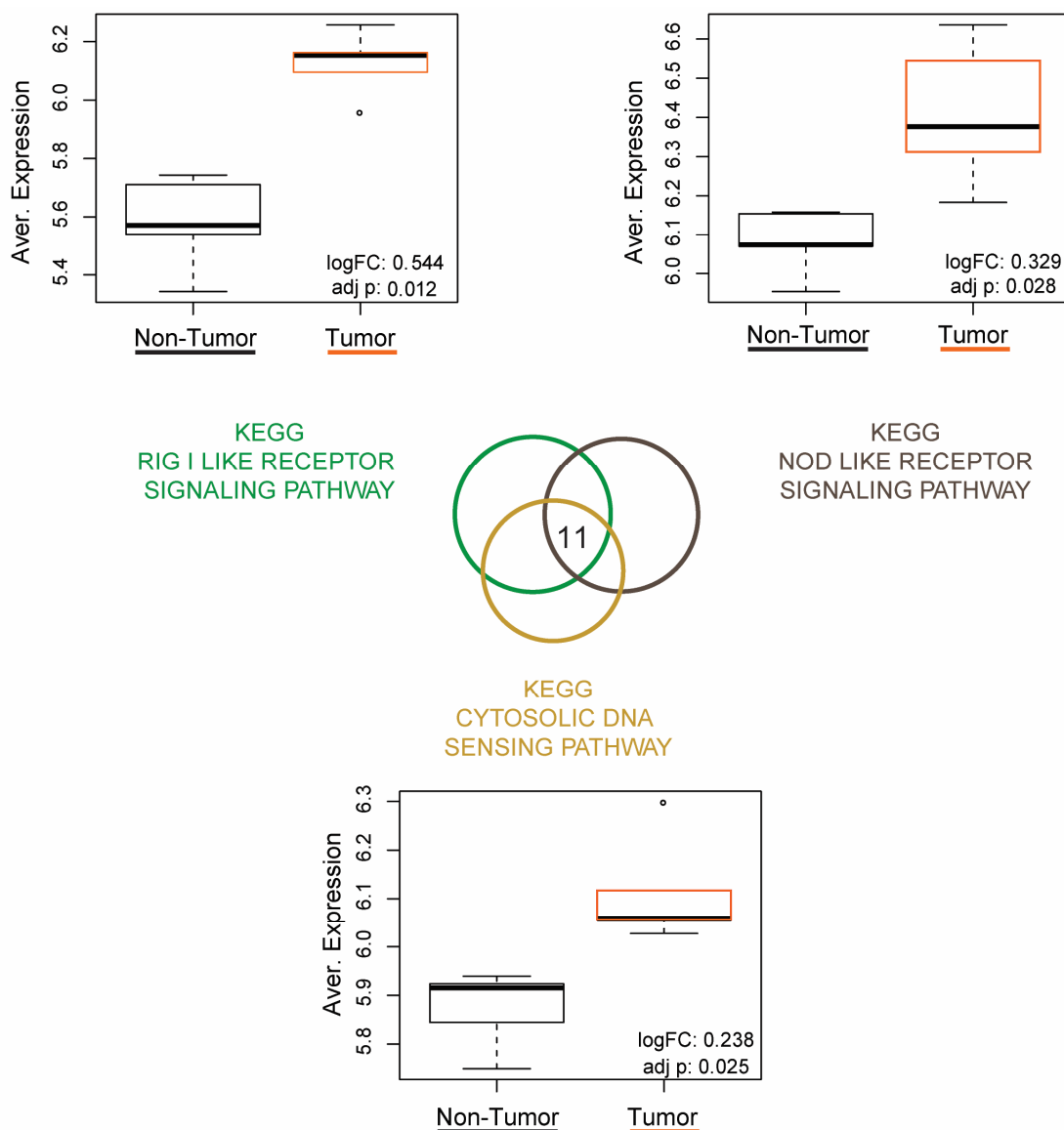


Figure 49: Differences in microbial recognition in tumor vs. non-tumor IEC based on microarray analysis.

Significantly enriched KEGG pathways relevant for microbial recognition based on the median of the expression level of all genes. Only pathways were considered with a minimum mapping of 10 genes. In the box plots, bold horizontal lines represent median values, and boxes highlight the corresponding interquartile ranges. The logFC and the adjusted p-value is given. 11 genes are mapped to all three KEGG pathways: Chuk (conserved helix-loop-helix ubiquitous kinase); Ikbkb (inhibitor of kappaB kinase beta); Ikbkg (inhibitor of kappaB kinase gamma); Nfkb1 (nuclear factor of kappa light polypeptide gene enhancer in B cells 1, p105); Nfkb2 (nuclear factor of kappa light polypeptide gene enhancer in B cells 2, p49/p100); Nfkbia (nuclear factor of kappa light polypeptide gene enhancer in B cells inhibitor, alpha); Nfkbib (nuclear factor of kappa light polypeptide gene enhancer in B cells inhibitor, beta); Rel (reticuloendotheliosis oncogene); Rela (v-rel reticuloendotheliosis viral oncogene homolog A (avian)); Relb (avian reticuloendotheliosis viral (v-rel) oncogene related B); Cxcl15 (chemokine (C-X-C motif) ligand 15)

Taken together, gene expression analysis reveal differences in the interaction of microbes and host, particularly in IECs isolated from tumor areas, further highlighting the involvement of microbes in nATF6-driven tumorigenesis.

5. DISCUSSION

The present study aimed to increase our knowledge of UPR in intestinal homeostasis and disease pathogenesis with a special focus on the ATF6 pathway. The results on the $nATF6^{IEC}$ mouse reveal a yet undescribed potential of ATF6 to promote colonic tumorigenesis in combination with microbiota-derived signals and establishes the $nATF6^{IEC}$ mouse as the first UPR model which spontaneously develops large intestinal tumors.

Preceding studies at the Chair of Nutrition and Immunology (Technical University Munich) and by others on the role of UPR in intestinal disease suggest that UPR activation in IEC is relevant for the development of intestinal inflammation in mouse models [108, 115, 120]. So far, most models with genetic manipulation of specific components of UPR do not spontaneously develop inflammation but have an altered susceptibility towards perturbations in intestinal homeostasis [123-127]. Spontaneous inflammation was predominantly observed if the highly secretory cells comprising Paneth cells and goblet cells exhibited ER stress as evident in $XBP1^{-/-}$, $AGR2^{-/-}$, Winnie and Eeyore mice [115, 122, 128]. The fact that ER stress and UPR signaling are also evident in IEC of IBD patients fosters the link between UPR and intestinal inflammation [108, 128]. Of relevance, unaffected mucosal tissue of UC patients showed decreased levels of eIF2 α phosphorylation and thus UC patients might be compromised in integrating stress responses at the mucosal surface [225]. Considering the current literature, there is good evidence that inappropriate ER stress handling can contribute to intestinal inflammation, particularly if goblet cell and Paneth cells are involved.

It is widely accepted that inflammation and cancer are interrelated pathologies considering epidemiological data, gene expression profiles which share inflammatory signatures, histopathological appearance, and the efficacy of anti-inflammatory drugs in prophylaxis [196]. Many examples show that chronic inflammation has the potential to predispose for dysplasia. Inversely, many tumors for which inflammation is not suggested to be an essential predisposing factor show an inflammatory signature and immune cell infiltration [196]. The association between inflammation and cancer is also apparent for the intestine [226]. With respect to IBD, UC patients with extensive and prolonged colitis have an increased risk to develop colon cancer [197, 198]. While there is significant evidence for a role of UPR signaling in IEC in intestinal inflammation, only few mouse studies have addressed the link between UPR in IEC and intestinal tumorigenesis. Particularly noteworthy are studies on IEC-specific $XBP1^{-/-}$ mice. These have revealed that ER stress can promote tumorigenesis, since $XBP1^{-/-}$ mice are prone to develop tumors in the genetically modified $Apc^{Min/+}$ mouse model and in the DSS/azoxymethane (AOM) model of colitis associated cancer [227]. Further,

a role of UPR in the control of intestinal stem cell properties is shown, since ER stress in ISC results in a PERK-eIF2 α dependent loss of stem cell signatures. Vice versa, PERK-eIF2 α activation is essential for the transition of ISC to TA cells [228]. Considering that XBP1 deficiency in IEC was first described to promote intestinal inflammation [115, 120], UPR signaling might be relevant for both inflammation and intestinal cancer. Irrespective of mouse studies establishing this connection, UPR activation is observed in a variety of cancers and has been linked to many tumor-promoting mechanisms [172].

5.1 The *nATF6*^{IEC} mouse – a model to mimic ATF6-specific activation of UPR in IEC

Activated, potentially pathological UPR signaling is frequently observed in IEC of IBD patients and in colon cancer, raising the question which properties and particularly which of the three UPR arms contribute to the disruption of intestinal homeostasis culminating in disease. To allow for in depth *in vivo* studies on the role of the UPR arm mediated by ATF6 in this context, a mouse model – referred to as the *nATF6* mouse – was generated at the Chair of Nutrition and Immunology (Technical University Munich).

The *nATF6* mouse can be used to express nATF6 in a tissue-specific manner. Tissue-specificity is achieved by breeding to distinct Cre-recombinase encoding strains. Villin-driven Cre-expression was used to accomplish expression of nATF6 in IEC in the *nATF6*^{IEC} mouse. Conceptually, the expression of the activated form of ATF6 should circumvent the need for activation of ATF6 and thus result in the expression of downstream transcriptional targets of ATF6. This approach to overexpress the activated form of ATF6 has already been used in *in vitro* studies and in heart- and podocyte- specific mouse models [62, 81, 181]. In line with our expectation, the HA-tagged nATF6 transgene is detected in IEC isolates of mice expressing the Cre-recombinase under the control of Villin showing clear nuclear localization as predicted for the activated form. Analysis of ATF6 targets clearly indicates functional activation of ATF6 mediated transcription in IEC in the small and large intestine. The expression of target genes shows a clear signature of predominant UPR signaling via ATF6 with only minor contribution of the PERK/ATF4 and IRE-1/XBP1 arm. With respect to the expression levels of nATF6 observed in the *nATF6*^{IEC} tg/tg mouse, a subset of human large intestinal tumor samples showed a similarly increased expression of nATF6 in relation to normal adjacent tissue. Thus, the *nATF6*^{IEC} mouse can serve as a model to study the contribution of IEC-specific activation of ATF6 to the pathogenesis of CRC. The prognostic significance of ATF6 alterations and increased ATF6 expression for colon cancer patients demonstrated in this study reinforces the hypothesis that ATF6 could be relevant for malignant conversion in CRC patients [187].

Reflecting on the IEC-specificity of the *nATF6*^{IEC} mouse, it is important to be aware of potential off-site effects of this genetic model. Known off-site effects of the Villin-Cre based expression mode comprise acinar cells of the pancreas and Villin-positive progenitor cells in the gastric antrum [229, 230]. Further, gradient-like expression of Villin is relevant to define the epithelial stomach/intestinal border during embryogenesis [231]. Indications for the involvement of stomach (proliferative metaplastic and dysplastic alterations of the antrum) and pancreas (signs for pancreatitis and reduced presence of host-derived proteases in the small intestine) are also observed in the *nATF6*^{IEC} mouse but are beyond the scope of this work. Extra-intestinal expression of nATF6 could be particularly relevant in light of the observed handicaps of *nATF6*^{IEC} tg/tg mice during embryogenesis which are one possible reasons for inadequate numbers of birth of this genotype.

Irrespective of these extra-intestinal off-site effects, the *ATF6*^{IEC} mouse can be used to investigate specific effects of ATF6-mediated UPR on IEC function and to study its contribution to intestinal disease.

5.2 The impact of *nATF6* expression on IEC function

The role of ATF6 signaling and its effect on cellular functions in current literature is based on knockout or forced expression studies of ATF6 in cell culture and *in vivo* models, respectively. Overall, ATF6 is primarily involved in the expression of ER quality control proteins. This results in an increase of ER protein folding capacity and ER-associated degradation of misfolded proteins particularly during chronic stress [64, 67]. Consequentially, ATF6 signaling was shown to be important for cell survival under diverse conditions of stress [232]. For instance, ATF6 deficiency results in decreased survival in response to Tunicamycin-mediated ER stress [64]. Inhibition of ATF6 decreases ER stress-induced apoptotic death of cardiomyocytes in the heart in response to ischemic stress. Vice versa, forced activation of ATF6 has protective effects on cardiomyocytes after myocardial infarction [181]. Yet, increased signaling via ATF6 and thus differential activation of the three UPR arms was also recently linked to maladaptive function of podocytes resulting in exacerbated pathology of diabetic nephropathy [81].

In the *nATF6*^{IEC} mouse, alterations in cellular functions of IEC are evident in goblet cell properties and increased epithelial proliferation. *nATF6*^{IEC} tg/tg mice show an early reduction in the number of mucin-filled goblet cells in the SPF housing. In trend, this is also recapitulated in the OHT-inducible mice but not under GF conditions. While the biochemical properties of the produced mucus was not changed with respect to the ratio of sialo- or sulfomucins and O-glycan concentrations, we observe functional consequences on the penetrability of the mucus layer by bacteria. The reduction of the

number of mucin-filled goblet cells raises the question which mechanisms are involved and what is the precise nature of this loss. Since ER stress is known to have a particular effect on highly secretory cells in the intestine, one hypothesis is that nATF6 expression interferes with the ER protein processing machinery and consequentially with mucus production and secretion. This hypothesis at the first glance seems contradictory to the role of ATF6 in regulating ER quality control, but might be plausible in light of the high macromolecular crowding within the ER – a phenomenon which was shown to affect the activity of the folding machinery [233]. Compared to the cytoplasm, macromolecular densities in the ER are 3-6-fold higher under normal conditions [50]. As evident in the *nATF6*^{IEC} mouse, nATF6 induces a multitude of ER resident proteins comprising the chaperones such as Grp78, Grp94 and Calreticulin which could itself increase the densities and thus affect the folding milieu. This is particularly conceivable considering the fact that chaperones themselves are not selectively degraded by translocational attenuation during acute ER stress in contrast to most other ER-targeted proteins [234]. This system has evolved to limit protein loading by cotranslocational degradation of selective ER proteins and is referred to as pre-emptive quality control (pQC) and complements eIF2 α -mediated translational attenuation and ERAD. Further, the chaperone-system depends on fine-tuned regulatory mechanisms. For instance, the activity of Grp78 is regulated by the equilibrium between oligomeric inactive Grp78, which serves as a short term accessible storage form of Grp78, and active monomeric Grp78 [235]. The monomeric form is further either bound to the UPR receptors or to unfolded proteins which itself is a major regulator of UPR activation.

Rather arguing against global ER stress is the fact that we see no prominent regulation of downstream targets of PERK and IRE-1 in IEC lysates. This would suggest no ER stress dependent activation but ER stress independent transcription induced by transgenic nATF6. However, since activation of the UPR sensors is repressed by their interaction with Grp78, the high levels of expression of Grp78 in IEC of *nATF6*^{IEC} mice might set a higher threshold for ER stress to trigger UPR activation. Further, a more detailed analysis focusing on goblet cell and not IEC isolates consisting of all subpopulations of IEC as done in this study might be necessary to increase the resolution. In favor of the presence of ER stress in the *nATF6*^{IEC} mouse are the morphological alterations of the ER observed in enterocytes at late ages. The ER is massively dilated and swollen which is often equated to ER stress [236, 237]. A deletion of the ERAD component SEL1L which disturbs ER homeostasis and activates ER stress for instance results in a similar swelling and shortening of the ER in the exocrine pancreas [238]. Of relevance, SEL1L deficiency also interfered with the secretory function of these cells. Independent of ER stress, specific ATF6 activation was shown to be important for ER

proliferation in response to ER membrane protein overload, thus linking membrane protein expression to ER expansion [98]. In line with this, expression of active ATF6 was shown to trigger ER expansion likely through the regulation of phosphatidylcholine synthesis [239].

In summary, high protein loading of the ER in the *nATF6*^{EC} mouse could impact on the folding machinery and thus the secretory capacity of the cell. This is supported by morphological swelling of the ER. Yet, the only mild activation of the PERK and IRE-1/XBP1 arm rather argues against the sensing of protein misfolding within the ER by the UPR sensors.

Another conceivable explanation for the reduced number of mucin-filled goblet cells could be a differentiation defect. Goblet cells are derived from the enterocyte lineage and shift into the secretory lineage in response to a block in Notch signaling [41]. For maturation, the E26 transformation-specific (ETS) domain transcription factor SPDEF (SAM-pointed domain-containing ETS-like factor) seems to be relevant [240]. Of importance, it was shown that the ATF6 orthologue OASIS (old astrocyte specifically induced substance) within the intestine is specifically expressed in goblet cells and deletion of OASIS interferes with goblet cell maturation [241]. In colonic IEC isolates of *nATF6*^{EC} mice housed under SPF conditions, both *Tff3* as an early, *Oasis* as an intermediate and *Muc2* as a late goblet cell maturation marker were decreased in tg/tg and tg/wt mice. This would support goblet cells to be diminished independently of the maturation stage rather than a loss in mucus secretory capacity of goblet cells. Yet, no reduction in mucin-filled goblet cell-numbers was observed in tg/wt mice, which also show a similar reduction in the expression of these goblet cell markers. Compared to SPF housing, no measurable reduction of mucin-filled goblet cells was evident in tg/tg mice under GF conditions linking the observed goblet cell alteration to the presence of bacteria. Recent scientific progress supports the functional connection between goblet cell secretion and microbial signaling. Mucus secretion as an important antimicrobial protective mechanism was shown to be regulated by the NLRP6 inflammasome [12], which itself is important for the steady-state regulation of the intestinal microbiota partly involving the secretion of IL-18 [242]. NLRP6 is highly expressed in IEC, particularly in goblet cells which supports the concept that goblet cells actively integrate signals from the host and its environment and serve as a component of the innate immune response [12]. In particular, a sentinel goblet cell was identified which nonspecifically endocytoses TLR ligands and activates the NLRP6 inflammasome in a TLR- and MYD88-specific manner. This results in Nox/Duox reactive oxygen species synthesis and *Muc2* exocytosis by the sentinel goblet cell. Via a gap junction signal *Muc2* secretion is orchestrated in adjacent goblet cells, directly coupling microbial pattern recognition to mucus secretion [40]. Of interest, the bacterial composition can shape the mucus barrier penetrability to bacteria, independent of an effect on

mucus thickness or mucus growth [243]. This is particularly evident in GF mice, which have an overall similar colon mucus organization compared to conventionally raised mice but a mucus layer which differs with respect to the penetrability to bacteria: In GF mice the mucus layer is completely permeable to bacteria and it takes 6 weeks after microbial association to establish an impenetrable mucus layer [244]. Thus, the regulation of mucus secretion and formation and bacteria is clearly bidirectional. The fact that we observe no detectable alterations of mucin-filled goblet cell in *nATF6^{IEC} tg/tg* mice housed under GF condition in contrast to the pronounced reduction under SPF conditions might be linked to this interaction. Further, there is a drastic reduction of mucin-filled goblet cells in *nATF6^{IEC} tg/tg* GF mice after association with cecal microbiota irrespective of the SPF donor genotype. This observation supports a functional connection between microbial signals and the genotype-specific loss of mucin-filled goblet cell. Since the mucus in GF mice is not equipped to serve as a barrier to bacteria, microbial signals acting on goblet cells might be very important in this model explaining the severe goblet cell loss. With respect to the hypothesis that goblet cell have Muc2 synthesis problems, the presence of bacteria might promote increased Muc2 exocytosis and thus result in increased need for mucus turnover, resulting in reduced numbers of mucin-filled goblet cells.

As addressed, it is evident that *nATF6* expression impacts on goblet cells in the *nATF6^{IEC}* model via a mechanism that is modulated by microbial-derived signals and could involve secretion or differentiation defects.

Focusing on the effects of mucus alterations, it is widely accepted that impairments in mucus properties can promote intestinal inflammation, a mechanism which is both relevant in DSS-induced colitis [245] and in the *IL10^{-/-}* model of colitis [246]. This is supported by the fact that a direct manipulation of mucus properties, *e.g.* in the Muc2-deficient mouse or in mice with defective mucus glycosylation, results in colitis [121, 128, 247-250]. Although we observe mucus alterations in the *nATF6^{IEC} tg/tg* mouse already at early ages, no early-onset inflammation is evident in these mice. Inflammatory changes are secondary to hyper-proliferation and tumor development and occur at late ages.

5.3 Microbial triggers – a prerequisite for the development of intestinal tumors in the *nATF6^{IEC} tg/tg* mouse?

Besides alterations in goblet cells, IEC in *nATF6^{IEC} tg/tg* mice have a clear hyper-proliferative phenotype. So far, no strong connection between ATF6-signaling and the control of proliferation has been shown in literature. Comparative studies between ATF6-transfected human HCC cells and HCC tissues suggest an overlap in cell cycle/proliferation relevant genes [190]. Nevertheless, no direct effect of ATF6 expression on proliferation was demonstrated and there is almost no overlap between these genes and significantly regulated genes in the *nATF6^{IEC} tg/tg* mouse under GF conditions. Another group suggested that ATF6 might act on carcinogen-induced HCC progression via regulation of CHOP [217], yet, we could show that CHOP deficiency in the *nATF6* model did not interfere with tumorigenesis. In breast cancer, anticipatory activation of UPR by estrogen via estrogen receptor $E\alpha$ is supposed to contribute to estrogen- $E\alpha$ -induced cell proliferation [77]. In this context, knockdown of ATF6 blocked estrogen-mediated induction of Grp78 and strongly inhibited E_2 - $E\alpha$ -stimulated cell proliferation. Recently, a connection between Yap (Yes-associated protein) and ATF6 has been established [251]. Yap is a transcriptional coactivator with oncogenic potential. Under homeostatic conditions, it is negatively regulated by the Hippo pathway and functions in the regulation of organ size and progenitor cell proliferation [252]. Active Yap signaling was shown to be important for IEC regeneration and intestinal cancer formation, whereas Yap deletion can interfere with adenoma formation in *APC^{Min/+}* mice [253]. This effect is at least in part mediated by an activation of the EGF pathway. Evidence in liver suggests that ATF6, but not IRE-1/XBP1, is highly activated upon activation of Yap signaling and might contribute to Yap-mediated tumorigenesis in HCC. ATF6 activation downstream of Yap was shown to regulate ER size and UPR activity and thus restores homeostasis during ER stress [251]. Overall, there are indications that ATF6 activation can contribute to cell proliferation but no direct regulation of cell cycle is described.

The potential of *nATF6* to drive hyper-proliferation and tumorigenesis in our model is clearly multifactorial. First, heterozygous mice do not spontaneously develop tumors, but show a clearly enhanced tumor susceptibility in the inflammation-conditioned host (DSS treatment and *IL10* deficiency). Of note, mucus alterations which go along with an increased interaction between bacteria and the host are involved in both DSS-induced colitis [245] and *IL10^{-/-}* mice [246]. Second, differences in the proliferative response are site-specific in *nATF6^{IEC} tg/tg* mice, being restricted to the large intestine, supporting the hypothesis that distinct UPR signal transducers and environmental conditions might differentially impact on the proliferation program.

Highly relevant in this context is the observation that the proliferative phenotype in the *nATF6^{IEC} tg/tg* mice requires the presence of intestinal microorganisms. This is supported by several lines of evidence: (1) Most importantly, expression of ATF6 in GF mice does not result in increased proliferation. In contrast (2), gnotobiotic transfer triggers tumorigenesis. Further (3), antibiotic treatment which significantly affects the microbial composition can dampen proliferation to a level observed in control mice. Of importance, colon organoids in sterile culture isolated from SPF *nATF6^{IEC} tg/tg* mice at the age of 20 wk show no growth benefits compared to fl/fl mice. This is similar to organoids isolated from GF *nATF6^{IEC} tg/tg* mice and supports the hypothesis that proliferation of IEC in *nATF6^{IEC} tg/tg* depends on both the expression of nATF6 and the environmental conditions. Either absence of microbial stimulation is important for the phenotypic switch, or growth factors in the organoid medium, which are essential to grow intestinal organoids *ex vivo*, mask the growth benefit of the tg/tg organoids by promoting growth in the fl/fl organoids.

Of note, we observe genotype-specific differences in microbial composition already at the pre-tumor stage. These compositional differences are not transferrable by simple co-housing since most *nATF6^{IEC} tg/tg* mice were co-housed with their fl/fl littermate controls. Interestingly, cecal content derived from 5 wk old tg/tg mice seems to be more potent in driving tumor formation in tg/tg mice compared to fl/fl donor microbiota, irrespective of the fact that not all bacterial taxa were transferred from the donor to the recipient. This suggests that intrinsic properties of the tg/tg microbiota were transferred, which are relevant to promote tumorigenesis in the susceptible *nATF6^{IEC} tg/tg* genotype only. This further supports the hypothesis that microbiota changes already at the pre-tumor stage of 5 wk are dysbiotic. Of note, the number of mucin-filled goblet cells was highly reduced after transfer of microbiota into tg/tg recipient mice independent of the donor-genotype. Since *nATF6^{IEC} fl/fl* mice undergoing microbial transfer did not show this loss of mucin-filled goblet cells, this could suggest an abnormal response of the goblet cells to intestinal microbes. Despite the similar reaction of *nATF6^{IEC} tg/tg* mice to microbes on goblet cell level, only donor microbiota derived from tg/tg resulted in a significant increase in IEC proliferation. Nevertheless, the fl/fl microbiota retains a residual capacity to induce tumor formation, since 20 % of the transferred *nATF6^{IEC} tg/tg* mice developed tumors upon the transfer of fl/fl microbiota. Analysis of bacterial communities after transfer in *nATF6^{IEC} tg/tg* mice identified four OTUs that were significantly altered in tg/tg recipients, which either remained tumor-free or developed tumors. One molecular species, with the closest relative *Clostridium saccharalyticum*, was exclusively associated with the tumor transmitting phenotype. Of note, the majority of discriminative OTUs identified in the present study (including the one

mentioned above) represent unknown taxa, which highlight the urgent need to cultivate bacteria for further description, and most of all precludes performing targeted colonization studies in this model. Reflecting on the potential causes for a distinct microbial composition in the *nATF6^{IEC} tg/tg* mice, it is known that the host and the microbes are in a bidirectional relation, with the host regulating the microbes and the microbiota modulating host physiology. This relationship is for instance evident in the IEC-specific *Myd88^{-/-}* (IEC-*Myd88^{-/-}*) mouse which has defective signaling through the interleukin-18 and -1 receptor and to microbe-associated molecular patterns through most TLRs [254]. IEC-*Myd88^{-/-}* mice suffer from insufficient production of AMP and goblet cell mediators in response to infection [254], highlighting the importance for microbial recognition to modulate AMPs and goblet cell-specific responses. The same mouse model in a different animal facility showed differences in transmucosal electrical resistance, mucus-associated antimicrobial activity and the expression of polymeric immunoglobulin receptor, *Muc2* and antimicrobial peptides [255]. This was coincident with changes in gut microbiota composition. Genotype induced alterations in bacterial composition were further evident in *NOD2^{-/-}* mice and linked to the predisposition for colitis and colorectal cancer [256]. With respect to other potential reasons for the differences in bacterial composition observed in the *nATF6^{IEC}* mouse, off-site expression of *nATF6*, e.g. in the pancreas, might impact on bacterial composition, since pancreatitis was shown to have an effect on the intestinal microbiota since it was associated with intestinal bacterial overgrowth [257].

IEC proliferation is modified by microbial signals [34, 35] and abnormal control of proliferation is part of tumorigenic transformation. Relevant with respect to a control of IEC proliferation by microbes is the observation that IEC proliferation is significantly reduced in whole body knockouts of *MyD88* [20, 258]. In contrast, in IEC-*Myd88^{-/-}* mice IEC proliferation is not reduced, suggesting that the proliferative status of IECs is driven by *MyD88*-dependent signaling in other cell types, rather than IEC. Besides recognition of microbial patterns, also bioactive molecules produced by microbes can modulate host proliferation. Prominent examples are short chain fatty acids (SCFA), unabsorbed carbohydrates and bile acids metabolized by microbes [259]. The SCFA butyrate has various health-promoting and antineoplastic properties in the colon: it serves as the preferred energy source for colonocytes, is involved in the maintenance of mucosal integrity and suppresses inflammation and carcinogenesis [259]. A recent study provides experimental evidence for a fine-tuned counterbalanced action of microbial-derived butyrate and pericrypt myofibroblast-derived *Wnt-5a* in the control of colonic epithelial proliferation [260]. In detail, butyrate induces the expression of intestinal epithelial heat shock proteins such as *Hsp25*, a protein which was shown to contribute to cellular protection, maintenance of barrier function, inhibition of proliferation and differentiation of

colonic epithelial cells [261-263]. In the crypt, Wnt-5a promotes canonical β -catenin signaling. While butyrate-driven expression of Hsp25 is greatest in surface epithelia, Wnt5a inhibits butyrate-induced Hsp25 in the proliferative compartment [260]. In SPF housed *nATF6^{IEC} tg/tg* mice, microarray analysis revealed a reduction of Hsp25 to 54 % of fl/fl expression level, supporting the link between proliferative control and Hsp25. Paradoxically, butyrate can both dampen proliferation and stimulate proliferation – a relation likely dependent on the local concentration of butyrate. While high concentrations of butyrate spill into the nucleus and inhibit histone deacetylases which results in increased differentiation and apoptosis, low colonic crypt concentrations of butyrate are completely consumed for cellular energetics [259, 264].

As discussed before, microbial-derived signals impact on goblet cells in the *nATF6^{IEC}* model and affect mucus barrier. Further, the presented data suggest that microbial-derived signals impact on IEC proliferation in the *nATF6^{IEC} tg/tg* mouse. It is conceivable that mucus barrier defects can amplify the hyper-proliferative response of IEC to microbial signals. Consequentially, impairments of goblet cell function could increase penetrability of the mucus barrier to microbes. This increased microbe-host interaction in consequence could amplify both microbially-triggered goblet cell dysfunction and IEC hyper-proliferation. This hypothesis could explain different outcomes in the inducible models of nATF6 expression. Villin-driven expression of nATF6 results in large intestinal tumorigenesis in both the constitutive and the inducible model suggesting that tumor formation is independent of events during embryogenesis and adolescence. This is in contrast to the absence of tumor formation in the inducible model using LGR5-Cre^{ERT2}-mediated recombination. One possible explanation for this discrepancy could be differences in the extent of mucus barrier alteration in both models. In the Villin-mediated model, *nATF6^{IEC-OHT} tg/tg* mice show universal expression of the nATF6 transgene in IEC and a reduction in mucin-filled goblet cells in all crypts. Analogous to the observations in *nATF6^{IEC}* mice, this likely results in a general perturbation of mucus barrier and increased host-microbial interaction. Since microbial signals impact on both goblet cell function and proliferation one can hypothesize that this augments both the goblet cell phenotype and IEC hyper-proliferation resulting in tumorigenesis. In contrast to the Villin-mediated model, Lgr5-driven Cre^{ERT2} expression is only detected in stem cells of a few crypts and thus recombination is restricted to a few crypts. As shown by HA-Tag and Grp78 staining of the colon of *nATF6 x LGR5-Cre^{ERT2} tg/tg* mice, this results in the formation of few but completely transgenic crypts. In the Lgr5-mediated model only few crypts are transgenic and thus show a trend towards reduced numbers of mucin-filled goblet cells. As a consequence, the mucus barrier is predominantly built up by wildtype goblet cells and thus likely less penetrable to bacteria compared to the mucus barrier in the *nATF6^{IEC-OHT} tg/tg* mice. The barrier is

able to limit host-microbial interactions. This results in local and only mild hyper-proliferative responses triggered by microbial signals. In this hypothetical model, the lack of tumor formation in the LGR5-driven model is in summary explained by local nATF6 expression and thus locally restricted goblet cell dysfunction. A globally intact mucus barrier dampens the effect of microbial signals on both goblet cell dysfunction and IEC hyper-proliferation.

Microbiota-host communication might be particularly relevant for the development of colon cancer, and metagenome-wide association studies (MGWAS) in humans identified bacterial risk profiles (oncobiome) potentially involved in generating a hostile intestinal milieu that promotes carcinogenesis [265, 266]. In human colorectal cancer patients *Fusobacterium nucleatum*, *Peptostreptococcus stomatis* and *Porphyromonas asaccharalytica*, were recently identified to contribute to a risk oncobiome [265]. Although a number of different pathogens trigger carcinogenesis, there are little mechanistic insights for a direct cancer-promoting role of a symbiotic microbiota (reviewed by [267]). Most evidence for a causal role of the intestinal microbiota in tumorigenesis is based on GF housing of adequate models. One of the few literature examples are the *Apc*^{Min/+} mice showing reduced tumor numbers under GF compared to SPF conditions [268, 269]. Furthermore, epithelial-specific deletion of the T-cell activating phosphatase calcineurin reduced tumor formation in the *Apc*^{Min/+} model [270]. Microbiota- and TLR-related signaling were shown to be involved in this nuclear factor of activated T cells (NFAT)-dependent mechanism [270], confirming early work by Rakoff-Nahoum and Medzhitov using MyD88-deficient *Apc*^{Min/+} mice [271]. Again, epithelial-specific deletion of the autophagy regulator ATG7 reduced tumor formation in *APC*^{Min/+} mice. Interestingly, loss of ATG 7 in the epithelium induced changes in the microbial environment associated with the generation of a tumor protective immune response [272]. Still, inflammation is inherently enrolled in the process of oncogenic transformation in mouse models. In line with the well-established hypothesis that infectious and chronic inflammation impact on oncogenic tissue transformation, mucus-defects at the intestinal interface have been suggested to provoke inflammation-associated cancer, mediated by microbiota-dependent mechanisms [65, 273, 274]. An earlier publication using *Muc2*-deficient mice on a mixed genetic background even demonstrated inflammation-independent tumor development with predominant small intestinal tumor formation (68 %) at late ages (1 year) [275]. In contrast, tumor development in *nATF6*^{IEC} tg/tg mice is restricted to the large intestine, with 100 % prevalence at an early age (12 wk). Consistent with previously published studies on ER stress-induced disruption of mucus barrier function, we showed a reduction in mucin-filled goblet cell at early life stages, clearly preceding tumor formation in *nATF6*^{IEC} tg/tg mice. Despite a mucus composition similar to fl/fl mice, bacterial penetration into the stratified inner

mucus layer was clearly advanced in tg/tg mice, reaching close proximity to the epithelial surface, yet lacking signs of inflammation.

The obvious dissociation of microbial signaling and inflammation-independent tumorigenesis in the *nATF6^{IEC}* model is surprising, considering the fact that TLR activation collaborates with IRE-1 to promote a pro-inflammatory response in macrophages [276]. In addition, the selective expression of TLR4 in intestinal crypts induced UPR activation and enterocolitis in mice, supporting a direct connection between pattern recognition receptor signaling and ER stress-associated inflammation in the intestine [277, 278].

A pathway which is downstream of many cytokines, growth factors and TLR signaling and was shown to substantially contribute to tumorigenesis is the signal transducer and activator of transcription 3 (STAT3) pathway [279]. STAT3 as a transcription factor regulates a variety of genes involved in diverse cellular responses, comprising differentiation, proliferation, apoptosis, and wound healing [280, 281]. Of interest, we observe increased phosphorylation and nuclear localization of STAT3 in IEC of *nATF6^{IEC}* tg/tg mice. This activation of STAT3 clearly depends on the presence of bacteria, since GF mice in contrast to SPF housed mice do not show elevated levels. In line with the protective effects of antibiotic treatment on tumor formation, STAT3 phosphorylation is diminished in the treated animals. Importantly, a similar activation of STAT3 is observed in the *nATF6^{IEC-OHT}* tg/tg mice.

STAT3 signaling is often discussed to contribute to intestinal inflammation and colitis-associated cancer [282-284]. Yet, we see no increased expression of inflammatory cytokines and histological inflammation preceding tumorigenesis and at early stages of tumorigenesis, with exception of a transient increase of IL22 at 12 wk of age. Further, no dominant changes in RelA nuclear localization are evident, suggesting no inflammatory activation of the canonical NFκB pathway. However, STAT3 activation in T cells was shown to promote host defense against microbes and intestinal inflammation. In contrast, STAT3 activation in IEC and myeloid cells is believed to contribute to protective and anti-inflammatory functions of the intestinal mucosa [285].

With respect to timing, STAT3 activation precedes macroscopic tumor formation, since both *nATF6^{IEC}* tg/tg mice at the age of 5 wk and *nATF6^{IEC-OHT}* tg/tg mice at an early time point show mildly/rarely to distinctly/frequently increased STAT3 activation. Major cytokines known to activate STAT3 in the intestine comprise Interleukin 6 (IL6) and Interleukin 22 (IL22) [285]. Since IL6 was only increased at late ages it is not likely to be relevant for STAT3 activation at early time points. As addressed, IL22 is increased at 12 wk of age and could thus be a candidate for STAT3 activation. However, the observation that it is neither increased at 5 wk nor at old ages argues against this. To

consider known regulatory STAT3 networks, the microarray data were queried for known regulators or downstream targets of STAT3. While several significantly regulated downstream targets were identified, only few STAT3 regulators were regulated on mRNA level. It is important to note that these analysis have to be interpreted with caution due to several aspects. First of all, the young age of the mice analyzed by microarray needs to be considered. As described, STAT3 activation is evident in 5 wk old mice but only observed in a small number of IEC. Thus, STAT3 activation may not be dominant in whole colon IEC lysates at this age. Second, regulation on mRNA level might not be appropriate to identify upstream regulators. Further, downstream targets of STAT3 are diverse and regulated by different signaling pathways. With respect to a potential direct regulation of STAT3 by ATF6, STAT3 was described to be a potential direct ATF6 target. This assumption, made by Belmont *et al.*, is based on the upregulation of STAT3 in nATF6 transgenic hearts and the presence of a consensus UPRE elements within the 2 kB promoter region of STAT3 [286]. UPRE elements are *cis* regulatory elements which can be bound by nATF6, yet, to a weaker extent than ERSE and ERSE-II [60]. In contrast to heart, no regulation of STAT3 on transcriptional level was observed in nATF6 transgenic IEC, rather questioning this direct interaction in the intestine. In light of all data presented arguing for a role of microbial signals in tumor formation in *nATF6*^{IEC} tg/tg mice, it is important to highlight the link between TLR signaling and STAT3 activation: Some studies claim that TLR signaling can activate the JAK-STAT3 pathway [283, 287]. Of interest, STAT3 in turn positively regulates the expression of certain TLRs [288, 289]. Of importance, in our mouse model, STAT3 activation is clearly dependent on both the presence of bacteria and the homozygous expression of nATF6. With respect to the role of TLR signaling in mediating inflammatory responses, it is remarkable that STAT3-driven expression of TLR2 was shown to contribute to the oncogenic functions of STAT3 but does not affect inflammation in gastric tumorigenesis [288]. This was evident since genetic and therapeutic targeting of TLR2 inhibited gastric tumorigenesis, but not inflammation. A dissociation between the role of STAT3 in promoting inflammation and tumorigenesis is further evident in conditional knockout mice for STAT3, specifically in IEC. While these mice show a higher susceptibility to experimentally induced colitis [284, 290, 291], they are protected from tumor development upon carcinogenic challenge [284, 291].

Focusing on the connection between ER UPR and STAT3 signaling, STAT3 activation has already been described in IEC-specific XBP1^{-/-} mice. In these mice, both a role in promoting intestinal inflammation and in suppressing tumorigenesis was attributed to XBP1 [115, 120, 227]. With respect to the tumor-suppressive role, XBP1^{-/-} mice showed an expansion of intestinal stem cells and a hyper-proliferation of TSA cells which resulted in an increased propensity to develop colitis-associated and spontaneous

APC related tumors. While the stem cell expansion was dependent on IRE-1, the hyper-proliferative response of the TSA was driven by STAT3 but independent of IRE-1. The authors suggest that STAT3 is activated as a consequence of prolonged ER stress within IECs and triggered by NF κ B activation [227].

Irrespective of how bacteria particularly impact on the host and thus contribute to tumorigenesis in the *nATF6*^{EC} tg/tg mouse, all presented results support the hypothesis that microbial triggers are required for the development of tumors in this model. In summary, we suggest that ATF6 activation in IEC in concert with microbial triggers prepare the ground for intestinal transformation.

5.4 Conclusion and perspectives

In the intestinal tract IEC fulfill essential tasks and are simultaneously required to adapt to host and gut luminal signals to maintain proper cell function. Dysfunctionality can result in pathologic outcomes as a consequence of barrier defects, changes in host-microbial communication and inappropriate mucosal immune system responses. IEC function is highly dependent on proper protein production especially in the highly secretory Paneth and goblet cells and thus relies on proper UPR to counteract ER stress.

The present study aimed to increase our understanding of how the UPR effects on IEC homeostasis and thus contributes to intestinal disease. This study shows, that nATF6 expression can promote tumorigenesis in the large intestine. This novel finding is of particular importance considering that increased expression of ATF6 was recently shown to be a marker of dysplasia in CRC patients, both in UC-independent and UC-associated CRC [187]. This link between ATF6 signaling and CRC pathogenesis is supported by the results presented in this study showing that both alterations of ATF6 and the expression levels of ATF6 have a prognostic impact on the course of disease.

So far, only limited experimental evidence indicated that deregulated UPR in IEC can promote intestinal tumorigenesis. A modulatory function on intestinal tumor susceptibility was identified for the IRE-1/XBP1 arm in IEC [227], but no contribution of the ATF6 arm was suggested. If compared to the other two arms, so far only few studies point towards a role of the ATF6 arm in tumorigenesis [80], highlighting the novel aspect of our finding. Central to the spontaneous tumorigenesis in our model are altered interactions between the host and the microbiota, which are at least in part promoted by alterations in mucus barrier and bacterial composition. Figure 50 summarizes the mechanistic insights gained from the studies on GF, SPF and microbially associated *nATF6*^{IEC} mice. As evident in the GF mice, an ATF6-driven UPR program in IEC does not result in a disruption of homeostasis culminating in intestinal disease. In contrast, SPF-reared *nATF6*^{IEC} tg/tg mice show early changes in bacterial composition and a reduction in mucin-filled goblet cells which goes along with defects in mucus barrier function. Further, IEC undergo a hyper-proliferative program and STAT3 activation which culminates in the formation of dysplastic adenomas. While the induction of inflammatory conditions can promote tumorigenesis as evident in the *nATF6*^{IEC} tg/wt mice on the IL10^{-/-} background and in mice treated with DSS, antibiotic treatment can interfere with tumorigenesis. Particularly relevant are observations on GF *nATF6*^{IEC} tg/tg mice associated with SPF microbiota, which reveal that *nATF6*^{IEC} tg/tg mice show significant goblet cell impairment upon association with microbes irrespective of the donor genotype. This indicates that *nATF6*^{IEC} tg/tg mice have intrinsic problems to adapt and regain homeostasis once challenged by the presence of microbes. In contrast to the observed effect on goblet cells, only microbiota derived from

nATF6^{IEC} tg/tg mice has a high potential to drive tumorigenesis in the genetically susceptible *nATF6^{IEC}* tg/tg host. This argues for the acquirement of dysbiotic properties of the microbiota in the *nATF6^{IEC}* tg/tg mice.

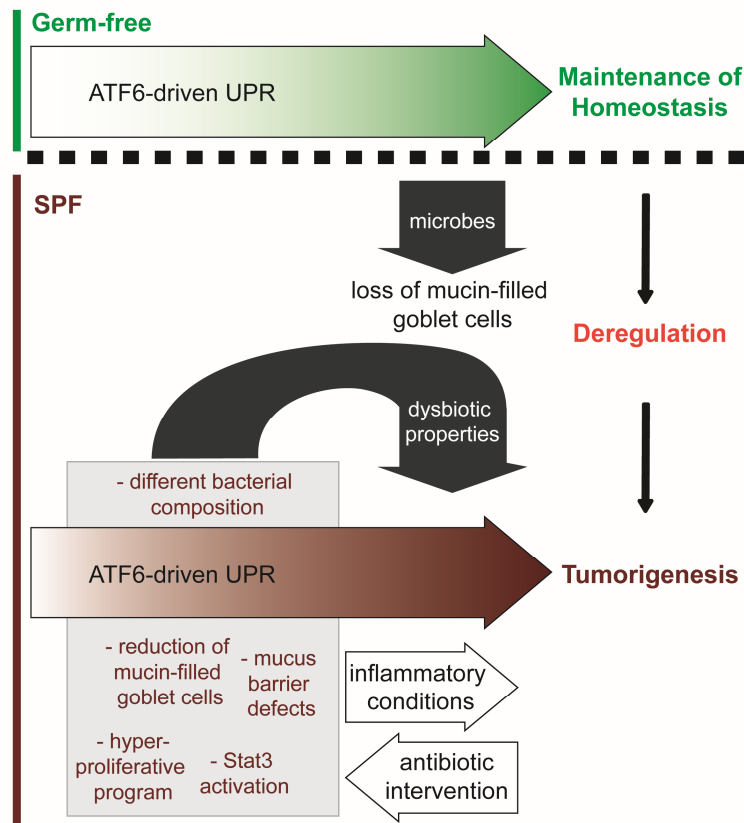


Figure 50: Mechanistic insights gained from the studies of GF, SPF and microbially associated *nATF6^{IEC}* mice.

ATF6-driven UPR does not negatively impact on homeostasis in the absence of microbes but culminates in tumorigenesis under SPF conditions. *nATF6^{IEC}* tg/tg mice show changes in bacterial composition, goblet cell and mucus barrier alterations, a hyper-proliferative program and STAT3 activation. Although inflammation is not preceding tumorigenesis in the *nATF6^{IEC}* model, inflammatory conditions can foster tumorigenesis. *Vice versa*, antibiotic treatment can interfere with tumor formation. Association of GF *nATF6^{IEC}* tg/tg mice with microbes results in the loss of mucin-filled goblet cells independent of the donor genotype of the microbiota. While microbiota derived from *nATF6^{IEC}* fl/fl donors only has a weak capacity to drive tumorigenesis, *nATF6^{IEC}* tg/tg microbiota harbors dysbiotic properties able to promote tumorigenesis in the *nATF6^{IEC}* tg/tg genotype.

The reduction of mucin-filled goblet cells in both the constitutive and the inducible models of *nATF6* expression indicates an impairment of goblet cells in response to *nATF6*-driven UPR. As evident in the GF situation, this impairment needs to be triggered by microbial signals. Goblet cell alterations increase the penetrability of the mucus barrier which in turn could negatively impact on the presence of mucus-filled goblet cells. Considering the dependence of both the hyper-proliferative response and the goblet cell impairment on microbial signals one can hypothesize that tumorigenesis in the *nATF6^{IEC}* mouse depends on the amplification of microbe-host interactions which in turn promote hyper-proliferation in *nATF6* expressing IECs (Figure 51).

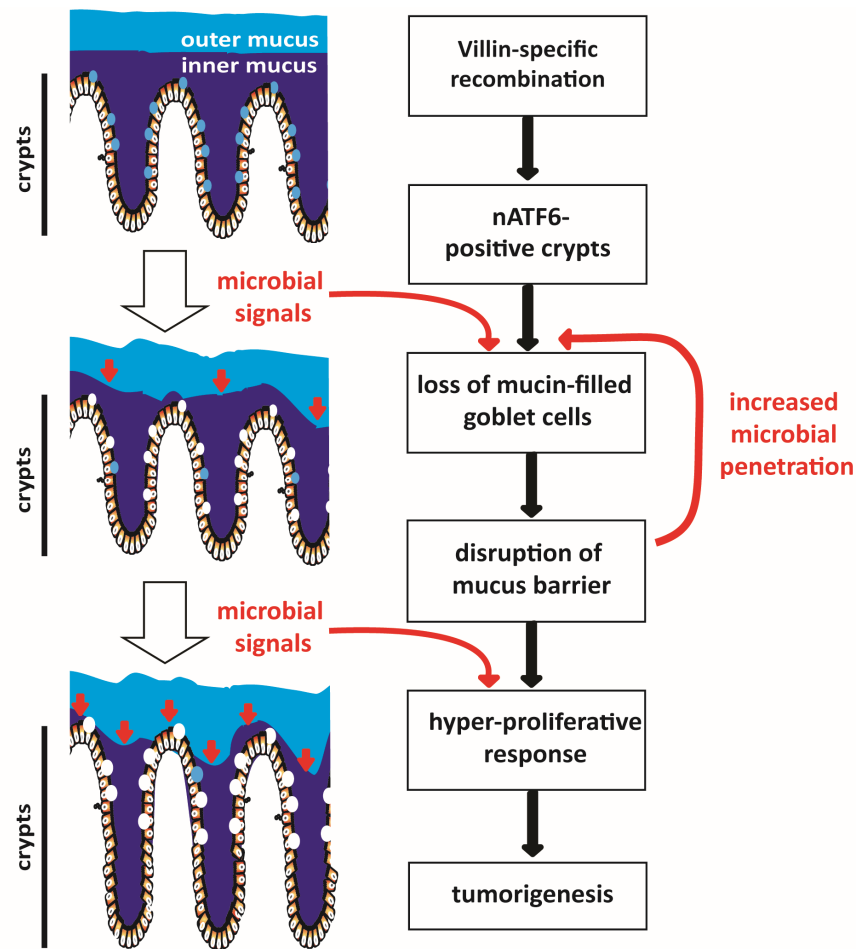


Figure 51: Amplification of loss of mucus barrier by microbial signals promotes IEC hyper-proliferation

Microbial signals trigger the loss of mucus-filled goblet cells in genetically susceptible $nATF6^{IEC}$ tg/tg mice. Increased microbe-host interactions are the consequence of an increased mucus barrier penetrability and further amplify microbially-triggered goblet cell impairment. $nATF6$ -expressing IEC hyper-proliferate in response to augmented microbial signals culminating in tumorigenesis.

The presented data proof the potential of ATF6 to promote large intestinal tumorigenesis and suggest that genetic alterations and elevated expression of ATF6 are associated with a poor prognosis in CRC. In the distant future, the ATF6 pathway, might be used both as a diagnostic marker of dysplastic changes and as a target of treatment for colorectal malignancies. This study sets the stage for future research. Questions to be answered gather around two major topics: The nature of the microbial signals and what is required to uncover the tumorigenic potential of ATF6 *in vivo*.

Alterations in mucus barrier function foster host-bacterial interactions in the $nATF6^{IEC}$ tg/tg mouse. Both, the loss of mucin-filled goblet cells and tumor formation are only observed in response to bacterial stimulation. Many host responses to bacteria, including the exocytosis of Mucus by goblet cells [40], are mediated by TLR-based recognition of bacterial ligands. Thus, TLR signaling could contribute to microbiota-driven tumorigenesis in our model. To address this, $nATF6^{IEC}$ mice are

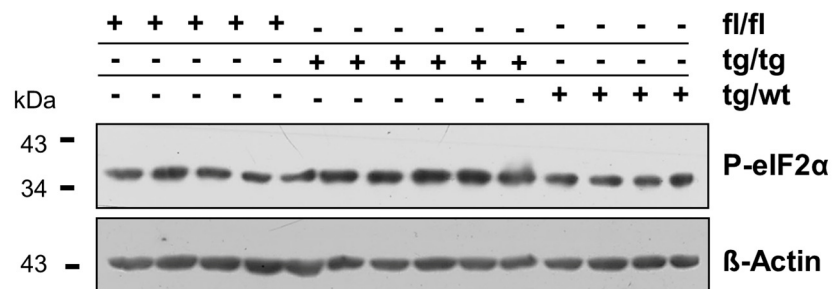
currently bred to knockout mice for the TLR adaptors Myd88 and TICAM1 (toll like receptor adaptor molecule 1), which allows for the blockage of TLR signaling. The intestinal phenotype of these mice in synergy with organoid stimulation experiments with microbial ligands will increase our understanding which microbial signal promote tumorigenesis. This might further elucidate how microbial signals and nATF6 expression affect the numbers of mucin-filled goblet cells and whether TLR signaling is involved in the activation of STAT3. In addition, the administration of inhibitors of STAT3 will unravel the contribution of this signaling pathway to the tumorigenic response in *nATF6^{IEC}* tg/tg mice. As an independent approach, a goblet cell-specific Cre mouse could be used to achieve goblet cell-restricted expression of nATF6. This would allow to study the effects on goblet cells in more detail and to dissect the contribution of mucus barrier alteration from the tumorigenic response. This is particularly relevant since defective mucus production was shown to promote tumorigenesis, yet in a predominantly inflammation-associated context [273-275, 292]. However, since no goblet cell-specific Cre model has been developed so far, the specific targeting of goblet cells would require the generation of a new mouse model.

Besides the unknown nature of the microbial signal, it is unclear which mechanisms activate ATF6 and unravel its tumorigenic potential? Is a specific activation of the ATF6 arm isolated of the other arms required for tumor formation or is global UPR activation of all three arms sufficient to promote tumor formation? ATF6-specific responses independent of global UPR activation have already been described in literature. For example, ATF6 is specifically activated downstream of Ormdl3 [183, 184], in response to chemical compounds [95] and as a consequence of increased membrane protein load [98]. The data presented by Hanoaka *et al.* suggest that ATF6 is discriminatively elevated between low-grade dysplastic lesions and the inflammatory regenerative epithelium in UC patients [187]. This further raises the question what particularly triggers ATF6 in this very important phase of malignant conversion. To address this, the endogenous activation of ATF6 should be studied in more detail in relevant tumor models, like the DSS/AOM model and APC^{Min/+} mice. Further, and currently ongoing for the Pvillin-Kras^{V12G} mice, the *nATF6^{IEC}* mice could be bred to established tumor models to unravel if this can model all steps of oncogenic transformation including tumor invasion and metastasis. These experiments will give valuable insights into the role of ATF6 during oncogenic tissue transformation and provide the basis for targeting the UPR as a potential anti-cancer therapy.

6. APPENDIX

Table A 1: Clinical data of human cohort used for Western Blot analysis.

Parameter		Total: n=83*
Age (mean \pm SD)		65 \pm 12 y
Gender (n)	Male	50
	Female	33
Tumor TNM stage distribution (UICC/AJCC)	I	4
	II	25
	III	45
	IV	9
Anatomical Localization	Colon	76
	Rectum	7

**Figure A 1: ER UPR activation in *nATF6^{IEC}* mice.**

Western Blot of colonic IEC of *nATF6^{IEC}* mice at the age of 5 wk for phosphorylated eIF2 α . β -Actin serves as a control for protein loading.

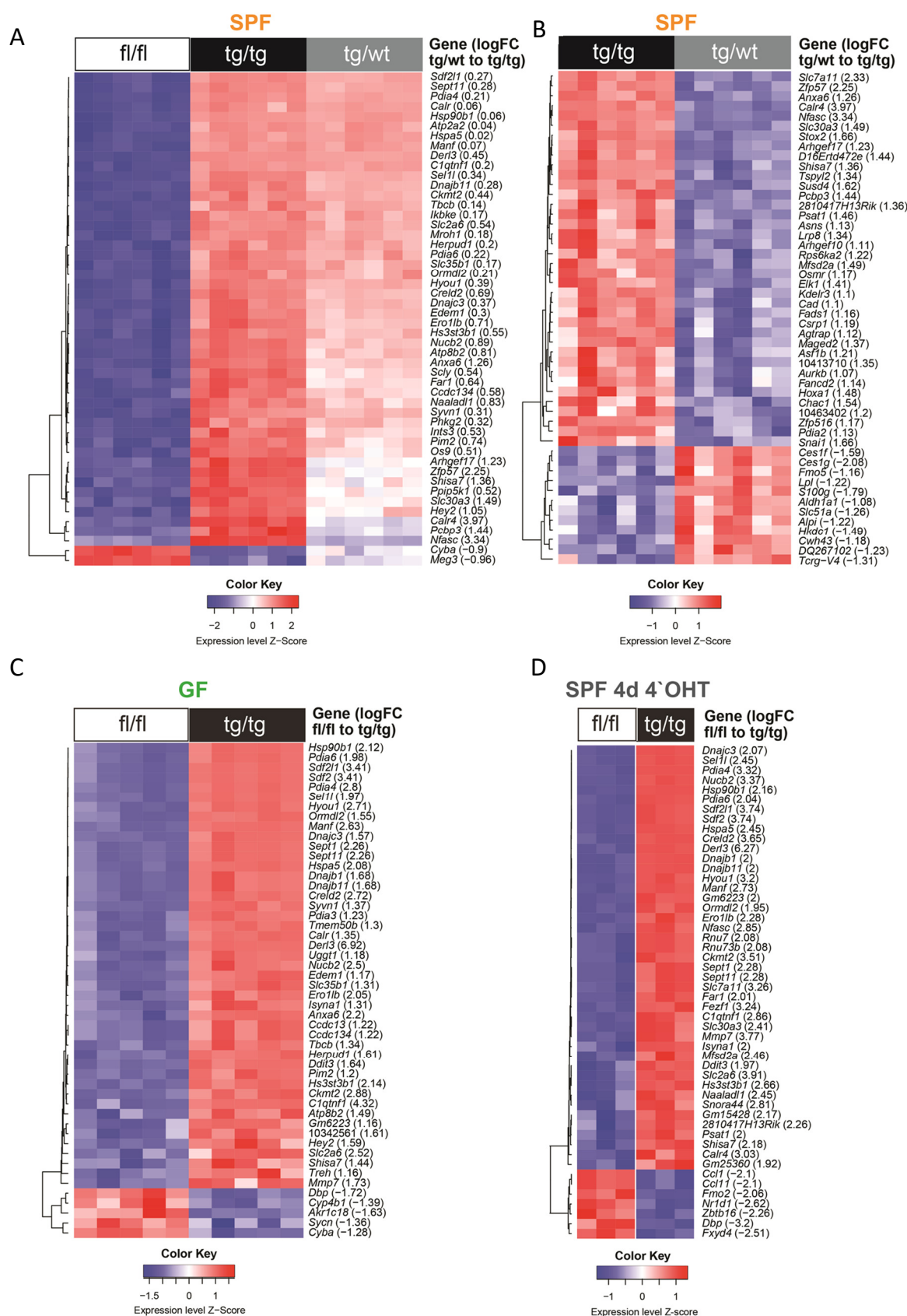


Figure A 2: Heatmap illustration of top regulated genes in the microarray analysis.

Top 50 most differentially regulated genes are illustrated for SPF (A, B), the GF (E) and *nATF6*^{IEC-OHT} mice at the 4 day time point (D) (FDR <0.01). Each square represents the color-code of the respective Z-Score of an individual mouse.

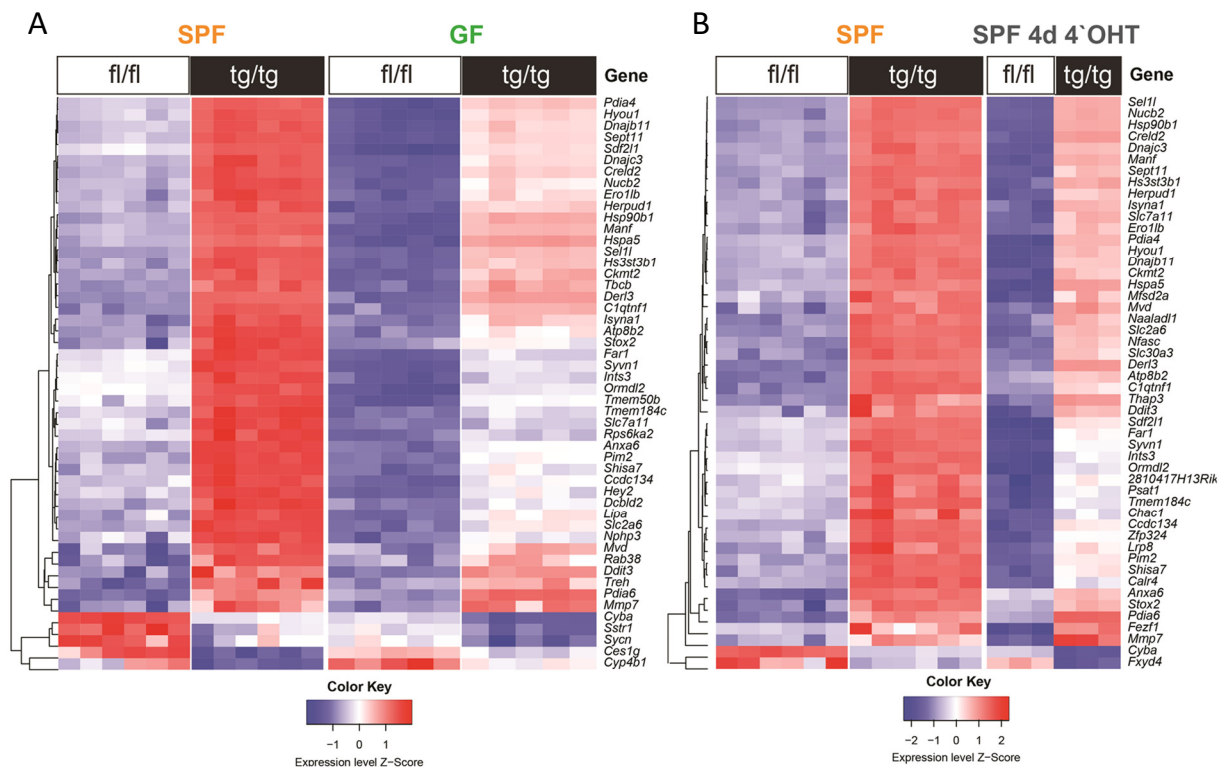


Figure A 3: Heatmap illustration of top genes with similar regulation in two datasets in the microarray analysis.

Top 50 most differentially regulated genes shared between the SPF and the GF dataset (**A**) and the SPF and *nATF6*^{IEC-OHT} dataset (**B**), respectively (FDR < 0.01). Significant genetic probes which could not be mapped onto known genes are represented by their original Affymetrix probe identifiers. No significant genes (FDR < 0.01) showed dissimilar regulation. Each square represents the color-code of the respective Z-Score of an individual mouse.

LIST OF FIGURES

Figure 1: Intestinal homeostasis - an interplay between environment, microbiota and host.....	3
Figure 2: Intestinal organization and cell types of intestinal epithelial cells.....	5
Figure 3: Main principle of ER UPR signaling and detailed signaling.....	9
Figure 4: The anticipatory mode of ER UPR.	10
Figure 5: Mechanisms of regulation of ATF6 activation and ATF6-driven target gene expression.....	13
Figure 6: Summary of the role of UPR in cancer.....	20
Figure 7: ATF6 alterations have prognostic significance in the TCGA CRC dataset.....	42
Figure 8: High nATF6 levels have prognostic significance in human colon cancer.....	43
Figure 9: The nATF6 ^{IEC} mouse model: genetics and ATF6 expression.....	46
Figure 10: Expression levels of nATF6 in the nATF6 ^{IEC} mouse and tumor tissues.	47
Figure 11: The nATF6 ^{IEC} mouse model: ATF6-driven ER UPR activation in IEC.....	48
Figure 12: ATF6, PERK and IRE-1/sXBP1 signaling in nATF6 ^{IEC} mice.....	49
Figure 13: Spontaneous large intestinal tumor formation in nATF6 ^{IEC} tg/tg mice.	50
Figure 14: Histopathological characterization of tumors in the nATF6 ^{IEC} tg/tg mouse as adenomas with low to focal high grade dysplasia.....	52
Figure 15: Array-based comparative genomic hybridization of tumors in the nATF6 ^{IEC} tg/tg mouse. ...	53
Figure 16: Goblet cell alterations in nATF6 ^{IEC} tg/tg mice.....	55
Figure 17: Higher bacterial penetration of colonic mucus in nATF6 ^{IEC} tg/tg mice.....	56
Figure 18: No alterations of Paneth cell numbers in nATF6 ^{IEC} tg/tg mice.	57
Figure 19: Hyper-proliferation of colonic but not small intestinal IEC in nATF6 ^{IEC} tg/tg mice.	58
Figure 20: Dilatation of the endoplasmic reticulum in transgenic nATF6 ^{IEC} mice.	59
Figure 21: Upregulation of the pathway “Protein Processing In Endoplasmic Reticulum” in nATF6 ^{IEC} tg/tg and tg/wt mice.....	60
Figure 22: Intestinal inflammation does not precede tumorigenesis.....	61
Figure 23: Infiltration of CD3+ and F4/80+ cells as a late event of intestinal pathology.....	62
Figure 24: Tumor incidence in the intestine of nATF6 ^{IEC} mice deficient for CHOP or RAG2.	64
Figure 25: The nATF6 ^{IEC-OHT} mouse model: tumor incidence and nATF6 expression.	66
Figure 26: The nATF6 ^{IEC-OHT} mouse: Hyper-proliferation and goblet cells.	67
Figure 27: The nATF6 x LGR5-Cre ^{ERT2} mouse: tumor incidence and nATF6 expression.	68
Figure 28: The nATF6 x LGR5-Cre ^{ERT2} mouse model: Proliferation and goblet cells in transgenic crypts.	70

Figure 29: Increased tumor susceptibility of <i>nATF6</i> ^{IEC} tg/wt mice in response to DSS.....	72
Figure 30: Increased tumor susceptibility of <i>nATF6</i> ^{IEC} tg/wt mice on the <i>IL10</i> ^{-/-} background.....	73
Figure 31: Colonoscopy-related effects on tumor formation.	74
Figure 32: Microbial changes in <i>nATF6</i> ^{IEC} tg/tg mice precede tumorigenesis.....	75
Figure 33: Relative abundances of phyla and families in the <i>nATF6</i> ^{IEC} mice.	76
Figure 34: Significant OTUs different between <i>nATF6</i> ^{IEC} tg/tg and fl/fl mice.....	77
Figure 35: Antibiotic treatment affects tumor formation, hyper-proliferation and goblet cell counts.	78
Figure 36: Cecal bacterial community structures are altered in V/M treated mice.....	79
Figure 37: Transgene expression and ER UPR activation in GF <i>nATF6</i> ^{IEC} mice.	80
Figure 38: ATF6, PERK and IRE-1/sXBP1 signaling in GF <i>nATF6</i> ^{IEC} mice.....	81
Figure 39: SPF housing of <i>nATF6</i> ^{IEC} mice has a big impact on the set of regulated genes.....	83
Figure 40: A set of genes is shared between SPF and GF <i>nATF6</i> ^{IEC} mice and <i>nATF6</i> ^{IEC-OHT} mice.	84
Figure 41: Microbial transfer re-establishes tumor development in GF <i>nATF6</i> ^{IEC} tg/tg mice.	85
Figure 42: Cecal bacterial community structures after microbiota transfer.....	86
Figure 43: Growth characteristics of colonic organoids isolated from <i>nATF6</i> ^{IEC} tg/tg mice is not increased in culture.	88
Figure 44: STAT3 signaling is activated in <i>nATF6</i> mice in a microbiota-dependent manner.	90
Figure 45: STAT3 upstream regulators and targets.	91
Figure 46: No activation of STAT1 and NFκB signaling in <i>nATF6</i> ^{IEC} tg/tg mice at early ages.....	92
Figure 47: Evidence for differences in microbial signaling in <i>nATF6</i> mice based on microarray analysis.	93
Figure 48: Microarray analysis of IEC isolated from tumor and paired non-tumor tissue of <i>nATF6</i> ^{IEC} tg/tg mice.....	94
Figure 49: Differences in microbial recognition in tumor vs. non-tumor IEC based on microarray analysis.....	95
Figure 50: Mechanistic insights gained from the studies of GF, SPF and microbially associated <i>nATF6</i> ^{IEC} mice.....	111
Figure 51: Amplification of loss of mucus barrier by microbial signals promotes IEC hyper- proliferation	112
Figure A 1: ER UPR activation in <i>nATF6</i> ^{IEC} mice.....	114
Figure A 2: Heatmap illustration of top regulated genes in the microarray analysis.	115

Figure A 3: Heatmap illustration of top genes with similar regulation in two datasets in the microarray analysis.....116

LIST OF TABLES

Table 1: Mouse breedings (SPF).	26
Table 2: Dehydration and paraffin embedding of FFPE tissue.	29
Table 3: Deparaffinization, rehydration and H&E staining.	30
Table 4: Primary and secondary antibodies used for immunochemical stainings.	33
Table 5: Primer combinations and PCR product sizes for genotyping.	35
Table 6: Sequence of genotyping primers.	36
Table 7: PCR program settings for genotyping.	36
Table 8: Primer sequences used for qRT-PCR analyses.	37
Table 9: Primary and secondary antibodies used for Western Blot analysis.	40
Table A 1: Clinical data of human cohort used for Western Blot analysis.	114

LIST OF ABBREVIATIONS

Abbreviation	Full term
AMP	Antimicrobial peptide
AOM	Azoxymethane
APC	Adenomatous polyposis coli
APC ^{Min/+}	Mouse model for human familial adenomatous polyposis
ATF	Activating transcription factor
ATF6	ATF6 alpha
CD	Crohn's disease
CFU	Colony forming units
CGH	Comparative genomic hybridization
CHOP	CCAAT/enhancer-binding protein homologous protein
CRC	Colorectal cancer
Cre	Cre recombinase
CRT	Calreticulin
d	Day / days
DAI	Disease activity index
dpc	Days post coitum
DSS	Dextran sodium sulfate
eIF	Eukaryotic translation initiation factor
ER	Endoplasmic reticulum
ERAD	ER associated degradation
ERSE	ER stress response element
ERT2	Estrogen receptor (tamoxifen binding variant 2)
Fl/Fl	Floxed/floxed; no transgene expression due to no recombination
Flox/ fl	Flanked by loxP sites
GADD	Growth arrest and DNA-damage inducible protein
GALT	Gut associated lymphoid tissue
GAPDH	Glycerinaldehyd-3-phosphat-Dehydrogenase
GC	Goblet cells
gDNA	Genomic desoxyribonucleic acid
GF	Germ-free
GO	Gene ontology
GRP	Glucose-regulated protein
GWAS	Genome wide association study
H&E	Hematoxylin and eosin
HA	Hemagglutinin
IBD	Inflammatory bowel diseases
IEC	Intestinal epithelial cell(s)
IEL	Intraepithelial lymphocytes
IF	Immunofluorescence
IFN	Interferon

LIST OF ABBREVIATIONS

Abbreviation	Full term
Ig	Immunoglobulin
IHC	Immunohistochemistry
IL	Interleukin
IP3R	Inositol 1,4,5-triphosphate receptor
IRE	Inositol requiring enzyme
ISC	Intestinal stem cell(s)
KEGG	Kyoto Encyclopedia of Genes and Genomes
KO / -/-	Knockout
LGR5	Leucine-rich repeat-containing G-protein coupled receptor 5
MAPK	Mitogen-activated protein kinase
MEK	MAPK/ERK kinase
miRNA	Micro ribonucleic acid
mRNA	Messenger ribonucleic acid
Muc2	Mucin2
nATF6	Nuclear ATF6
<i>nATF6</i> ^{IEC}	<i>nATF6</i> x Vil-Cre mice
<i>nATF6</i> ^{IEC-OHT}	<i>nATF6</i> x Vil-Cre ^{ERT2}
OHT	4'-Hydroxy-Tamoxifen
p-/phospho-	Phosphorylated
PDI	Protein disulfide isomerase
PERK	PKR-like ER kinase
RAG	Recombination activating gene
Rcf, g	Relative centrifugal force
ROS	Reactive oxygen species
rRNA	Ribosomal ribonucleic acid
S1P	Site-1 protease
S2P	Site-2 protease
SDS-PAGE	Sodium dodecyl sulfate polyacrylamide gel electrophoresis
SPF	Specific pathogen-free
SREBP	Sterol Regulatory Element-Binding Protein
STAT	Signal transducer and activator of transcription
TA (cells)	Transit amplifying (cells)
Tg	Transgenic
Tg/tg	Homozygous for transgene expression
Tg/wt	Heterozygous for transgene expression
TLR	Toll-like receptor
UC	Ulcerative colitis
UPR	Unfolded protein response
UPRE	UPR response element
Vil	Villin
w/o	without
wk	Week/ weeks
wt	Wild type

REFERENCES

1. Helander, H.F. and L. Fandriks, *Surface area of the digestive tract - revisited*. Scand J Gastroenterol, 2014. **49**(6): p. 681-9.
2. Sommer, F. and F. Backhed, *The gut microbiota--masters of host development and physiology*. Nat Rev Microbiol, 2013. **11**(4): p. 227-38.
3. Lozupone, C.A., et al., *Diversity, stability and resilience of the human gut microbiota*. Nature, 2012. **489**(7415): p. 220-30.
4. Greenhalgh, K., et al., *The human gut microbiome in health: establishment and resilience of microbiota over a lifetime*. Environ Microbiol, 2016. **18**(7): p. 2103-16.
5. Eckburg, P.B., et al., *Diversity of the human intestinal microbial flora*. Science, 2005. **308**(5728): p. 1635-8.
6. Ley, R.E., et al., *Obesity alters gut microbial ecology*. Proc Natl Acad Sci U S A, 2005. **102**(31): p. 11070-5.
7. Lozupone, C.A., et al., *Meta-analyses of studies of the human microbiota*. Genome Res, 2013. **23**(10): p. 1704-14.
8. Cannon, W.B., *Physiological Regulation of Normal States: Some Tentative Postulates Concerning Biological Homeostatics*. Paris: Editions Medicales, 1926.
9. *homeostasis*, in *Collins English Dictionary - Complete & Unabridged 10th Edition*. Retrieved December 30, 2016.
10. Sonnenburg, J.L., et al., *Glycan foraging in vivo by an intestine-adapted bacterial symbiont*. Science, 2005. **307**(5717): p. 1955-9.
11. LeBlanc, J.G., et al., *Bacteria as vitamin suppliers to their host: a gut microbiota perspective*. Curr Opin Biotechnol, 2013. **24**(2): p. 160-8.
12. Wlodarska, M., et al., *NLRP6 inflammasome orchestrates the colonic host-microbial interface by regulating goblet cell mucus secretion*. Cell, 2014. **156**(5): p. 1045-59.
13. Camp, J.G., et al., *Microbiota modulate transcription in the intestinal epithelium without remodeling the accessible chromatin landscape*. Genome Res, 2014. **24**(9): p. 1504-16.
14. Olszak, T., et al., *Microbial exposure during early life has persistent effects on natural killer T cell function*. Science, 2012. **336**(6080): p. 489-93.
15. Candela, M., et al., *Interaction of probiotic Lactobacillus and Bifidobacterium strains with human intestinal epithelial cells: adhesion properties, competition against enteropathogens and modulation of IL-8 production*. Int J Food Microbiol, 2008. **125**(3): p. 286-92.
16. Fukuda, S., et al., *Bifidobacteria can protect from enteropathogenic infection through production of acetate*. Nature, 2011. **469**(7331): p. 543-7.
17. Ubeda, C., A. Djukovic, and S. Isaac, *Roles of the intestinal microbiota in pathogen protection*. Clin Transl Immunology, 2017. **6**(2): p. e128.
18. Juge, N., *Microbial adhesins to gastrointestinal mucus*. Trends Microbiol, 2012. **20**(1): p. 30-9.
19. Derrien, M., et al., *Mucin-bacterial interactions in the human oral cavity and digestive tract*. Gut Microbes, 2010. **1**(4): p. 254-268.
20. Rakoff-Nahoum, S., et al., *Recognition of commensal microflora by toll-like receptors is required for intestinal homeostasis*. Cell, 2004. **118**(2): p. 229-41.
21. Kobayashi, K.S., et al., *Nod2-dependent regulation of innate and adaptive immunity in the intestinal tract*. Science, 2005. **307**(5710): p. 731-4.
22. Brandl, K., et al., *MyD88-mediated signals induce the bactericidal lectin RegIII gamma and protect mice against intestinal Listeria monocytogenes infection*. J Exp Med, 2007. **204**(8): p. 1891-900.

23. Vaishnava, S., et al., *Paneth cells directly sense gut commensals and maintain homeostasis at the intestinal host-microbial interface*. Proc Natl Acad Sci U S A, 2008. **105**(52): p. 20858-63.
24. Vaishnava, S., et al., *The antibacterial lectin RegIIIgamma promotes the spatial segregation of microbiota and host in the intestine*. Science, 2011. **334**(6053): p. 255-8.
25. Arnoldi, J.F., M. Loreau, and B. Haegeman, *Resilience, reactivity and variability: A mathematical comparison of ecological stability measures*. J Theor Biol, 2016. **389**: p. 47-59.
26. Sommer, F., et al., *The resilience of the intestinal microbiota influences health and disease*. Nat Rev Microbiol, 2017. **15**(10): p. 630-638.
27. David, L.A., et al., *Diet rapidly and reproducibly alters the human gut microbiome*. Nature, 2014. **505**(7484): p. 559-63.
28. Walker, A.W., et al., *Dominant and diet-responsive groups of bacteria within the human colonic microbiota*. ISME J, 2011. **5**(2): p. 220-30.
29. Barker, N., *Adult intestinal stem cells: critical drivers of epithelial homeostasis and regeneration*. Nat Rev Mol Cell Biol, 2014. **15**(1): p. 19-33.
30. Lee, Y.K., *Effects of diet on gut microbiota profile and the implications for health and disease*. Biosci Microbiota Food Health, 2013. **32**(1): p. 1-12.
31. Rao, J.N. and J.Y. Wang, in *Regulation of Gastrointestinal Mucosal Growth*. 2010: San Rafael (CA).
32. van der Flier, L.G. and H. Clevers, *Stem cells, self-renewal, and differentiation in the intestinal epithelium*. Annu Rev Physiol, 2009. **71**: p. 241-60.
33. Burrin, D.G., et al., *Glucagon-like peptide 2 dose-dependently activates intestinal cell survival and proliferation in neonatal piglets*. Endocrinology, 2005. **146**(1): p. 22-32.
34. Williams, J.M., et al., *Epithelial cell shedding and barrier function: a matter of life and death at the small intestinal villus tip*. Vet Pathol, 2015. **52**(3): p. 445-55.
35. Shirkey, T.W., et al., *Effects of commensal bacteria on intestinal morphology and expression of proinflammatory cytokines in the gnotobiotic pig*. Exp Biol Med (Maywood), 2006. **231**(8): p. 1333-45.
36. Bowcutt, R., et al., *Heterogeneity across the murine small and large intestine*. World J Gastroenterol, 2014. **20**(41): p. 15216-32.
37. Tanaka, M., et al., *Spatial distribution and histogenesis of colorectal Paneth cell metaplasia in idiopathic inflammatory bowel disease*. J Gastroenterol Hepatol, 2001. **16**(12): p. 1353-9.
38. Mabbott, N.A., et al., *Microfold (M) cells: important immunosurveillance posts in the intestinal epithelium*. Mucosal Immunol, 2013. **6**(4): p. 666-77.
39. Chang, S.Y., et al., *Colonic patches direct the cross-talk between systemic compartments and large intestine independently of innate immunity*. J Immunol, 2008. **180**(3): p. 1609-18.
40. Birchenough, G.M., et al., *A sentinel goblet cell guards the colonic crypt by triggering Nlrp6-dependent Muc2 secretion*. Science, 2016. **352**(6293): p. 1535-42.
41. Birchenough, G.M., et al., *New developments in goblet cell mucus secretion and function*. Mucosal Immunol, 2015. **8**(4): p. 712-9.
42. Johansson, M.E., et al., *The inner of the two Muc2 mucin-dependent mucus layers in colon is devoid of bacteria*. Proc Natl Acad Sci U S A, 2008. **105**(39): p. 15064-9.
43. Assimakopoulos, S.F., I. Papageorgiou, and A. Charonis, *Enterocytes' tight junctions: From molecules to diseases*. World J Gastrointest Pathophysiol, 2011. **2**(6): p. 123-37.
44. Kim, M., et al., *Bacterial interactions with the host epithelium*. Cell Host Microbe, 2010. **8**(1): p. 20-35.
45. McDole, J.R., et al., *Goblet cells deliver luminal antigen to CD103+ dendritic cells in the small intestine*. Nature, 2012. **483**(7389): p. 345-9.

46. He, B., et al., *Intestinal bacteria trigger T cell-independent immunoglobulin A(2) class switching by inducing epithelial-cell secretion of the cytokine APRIL*. *Immunity*, 2007. **26**(6): p. 812-26.
47. Brandtzaeg, P., *Function of mucosa-associated lymphoid tissue in antibody formation*. *Immunol Invest*, 2010. **39**(4-5): p. 303-55.
48. Peterson, L.W. and D. Artis, *Intestinal epithelial cells: regulators of barrier function and immune homeostasis*. *Nat Rev Immunol*, 2014. **14**(3): p. 141-53.
49. Colaco, H.G. and L.F. Moita, *Initiation of innate immune responses by surveillance of homeostasis perturbations*. *FEBS J*, 2016. **283**(13): p. 2448-57.
50. Dayel, M.J., E.F. Hom, and A.S. Verkman, *Diffusion of green fluorescent protein in the aqueous-phase lumen of endoplasmic reticulum*. *Biophys J*, 1999. **76**(5): p. 2843-51.
51. Hwang, C., A.J. Sinskey, and H.F. Lodish, *Oxidized redox state of glutathione in the endoplasmic reticulum*. *Science*, 1992. **257**(5076): p. 1496-502.
52. Montero, M., et al., *Monitoring dynamic changes in free Ca²⁺ concentration in the endoplasmic reticulum of intact cells*. *EMBO J*, 1995. **14**(22): p. 5467-75.
53. Wang, M., et al., *Role of the unfolded protein response regulator GRP78/BiP in development, cancer, and neurological disorders*. *Antioxid Redox Signal*, 2009. **11**(9): p. 2307-16.
54. Rutkowski, D.T. and R.J. Kaufman, *A trip to the ER: coping with stress*. *Trends Cell Biol*, 2004. **14**(1): p. 20-8.
55. Lee, A.S., *The ER chaperone and signaling regulator GRP78/BiP as a monitor of endoplasmic reticulum stress*. *Methods*, 2005. **35**(4): p. 373-81.
56. Harding, H.P., Y. Zhang, and D. Ron, *Protein translation and folding are coupled by an endoplasmic-reticulum-resident kinase*. *Nature*, 1999. **397**(6716): p. 271-4.
57. Urano, F., et al., *Coupling of stress in the ER to activation of JNK protein kinases by transmembrane protein kinase IRE1*. *Science*, 2000. **287**(5453): p. 664-6.
58. Yoshida, H., et al., *XBP1 mRNA is induced by ATF6 and spliced by IRE1 in response to ER stress to produce a highly active transcription factor*. *Cell*, 2001. **107**(7): p. 881-91.
59. Hollien, J., et al., *Regulated Ire1-dependent decay of messenger RNAs in mammalian cells*. *J Cell Biol*, 2009. **186**(3): p. 323-31.
60. Yamamoto, K., et al., *Differential contributions of ATF6 and XBP1 to the activation of endoplasmic reticulum stress-responsive cis-acting elements ERSE, UPRE and ERSE-II*. *J Biochem*, 2004. **136**(3): p. 343-50.
61. Ye, J., et al., *ER stress induces cleavage of membrane-bound ATF6 by the same proteases that process SREBPs*. *Mol Cell*, 2000. **6**(6): p. 1355-64.
62. Haze, K., et al., *Mammalian transcription factor ATF6 is synthesized as a transmembrane protein and activated by proteolysis in response to endoplasmic reticulum stress*. *Mol Biol Cell*, 1999. **10**(11): p. 3787-99.
63. Shen, J., et al., *ER stress regulation of ATF6 localization by dissociation of BiP/GRP78 binding and unmasking of Golgi localization signals*. *Dev Cell*, 2002. **3**(1): p. 99-111.
64. Wu, J., et al., *ATF6alpha optimizes long-term endoplasmic reticulum function to protect cells from chronic stress*. *Dev Cell*, 2007. **13**(3): p. 351-64.
65. Kouroku, Y., et al., *ER stress (PERK/eIF2alpha phosphorylation) mediates the polyglutamine-induced LC3 conversion, an essential step for autophagy formation*. *Cell Death Differ*, 2007. **14**(2): p. 230-9.
66. Talloczy, Z., et al., *Regulation of starvation- and virus-induced autophagy by the eIF2alpha kinase signaling pathway*. *Proc Natl Acad Sci U S A*, 2002. **99**(1): p. 190-5.
67. Adachi, Y., et al., *ATF6 is a transcription factor specializing in the regulation of quality control proteins in the endoplasmic reticulum*. *Cell Struct Funct*, 2008. **33**(1): p. 75-89.

68. Reid, D.W., et al., *The unfolded protein response triggers selective mRNA release from the endoplasmic reticulum*. *Cell*, 2014. **158**(6): p. 1362-74.
69. Sano, R. and J.C. Reed, *ER stress-induced cell death mechanisms*. *Biochim Biophys Acta*, 2013. **1833**(12): p. 3460-70.
70. Sovolyova, N., et al., *Stressed to death - mechanisms of ER stress-induced cell death*. *Biol Chem*, 2014. **395**(1): p. 1-13.
71. Walter, P. and D. Ron, *The unfolded protein response: from stress pathway to homeostatic regulation*. *Science*, 2011. **334**(6059): p. 1081-6.
72. Shapiro, D.J., et al., *Anticipatory UPR Activation: A Protective Pathway and Target in Cancer*. *Trends Endocrinol Metab*, 2016. **27**(10): p. 731-41.
73. Hu, C.C., et al., *XBP-1 regulates signal transduction, transcription factors and bone marrow colonization in B cells*. *EMBO J*, 2009. **28**(11): p. 1624-36.
74. van Anken, E., et al., *Sequential waves of functionally related proteins are expressed when B cells prepare for antibody secretion*. *Immunity*, 2003. **18**(2): p. 243-53.
75. Karali, E., et al., *VEGF Signals through ATF6 and PERK to promote endothelial cell survival and angiogenesis in the absence of ER stress*. *Mol Cell*, 2014. **54**(4): p. 559-72.
76. Yu, L., et al., *Anticipatory activation of the unfolded protein response by epidermal growth factor is required for immediate early gene expression and cell proliferation*. *Mol Cell Endocrinol*, 2016. **422**: p. 31-41.
77. Andruska, N., et al., *Anticipatory estrogen activation of the unfolded protein response is linked to cell proliferation and poor survival in estrogen receptor alpha-positive breast cancer*. *Oncogene*, 2015. **34**(29): p. 3760-9.
78. Andruska, N.D., et al., *Estrogen receptor alpha inhibitor activates the unfolded protein response, blocks protein synthesis, and induces tumor regression*. *Proc Natl Acad Sci U S A*, 2015. **112**(15): p. 4737-42.
79. Kurosaki, T., et al., *Regulation of the phospholipase C-gamma2 pathway in B cells*. *Immunol Rev*, 2000. **176**: p. 19-29.
80. Chevet, E., C. Hetz, and A. Samali, *Endoplasmic reticulum stress-activated cell reprogramming in oncogenesis*. *Cancer Discov*, 2015. **5**(6): p. 586-97.
81. Madhusudhan, T., et al., *Defective podocyte insulin signalling through p85-XBP1 promotes ATF6-dependent maladaptive ER-stress response in diabetic nephropathy*. *Nat Commun*, 2015. **6**: p. 6496.
82. Back, S.H. and R.J. Kaufman, *Endoplasmic reticulum stress and type 2 diabetes*. *Annu Rev Biochem*, 2012. **81**: p. 767-93.
83. Hong, M., et al., *Underglycosylation of ATF6 as a novel sensing mechanism for activation of the unfolded protein response*. *J Biol Chem*, 2004. **279**(12): p. 11354-63.
84. Nadanaka, S., et al., *Role of disulfide bridges formed in the luminal domain of ATF6 in sensing endoplasmic reticulum stress*. *Mol Cell Biol*, 2007. **27**(3): p. 1027-43.
85. Higa, A., et al., *Endoplasmic reticulum stress-activated transcription factor ATF6alpha requires the disulfide isomerase PDIA5 to modulate chemoresistance*. *Mol Cell Biol*, 2014. **34**(10): p. 1839-49.
86. Luo, S. and A.S. Lee, *Requirement of the p38 mitogen-activated protein kinase signalling pathway for the induction of the 78 kDa glucose-regulated protein/immunoglobulin heavy-chain binding protein by azetidine stress: activating transcription factor 6 as a target for stress-induced phosphorylation*. *Biochem J*, 2002. **366**(Pt 3): p. 787-95.
87. Yoshida, H., et al., *ATF6 activated by proteolysis binds in the presence of NF-Y (CBF) directly to the cis-acting element responsible for the mammalian unfolded protein response*. *Mol Cell Biol*, 2000. **20**(18): p. 6755-67.
88. Luo, R., et al., *CBF/NF-Y controls endoplasmic reticulum stress induced transcription through recruitment of both ATF6(N) and TBP*. *J Cell Biochem*, 2008. **104**(5): p. 1708-23.

89. Li, M., et al., *ATF6 as a transcription activator of the endoplasmic reticulum stress element: thapsigargin stress-induced changes and synergistic interactions with NF-Y and YY1*. *Mol Cell Biol*, 2000. **20**(14): p. 5096-106.
90. Yamamoto, K., et al., *Transcriptional induction of mammalian ER quality control proteins is mediated by single or combined action of ATF6alpha and XBP1*. *Dev Cell*, 2007. **13**(3): p. 365-76.
91. Yoshida, H., et al., *Endoplasmic reticulum stress-induced formation of transcription factor complex ERSF including NF-Y (CBF) and activating transcription factors 6alpha and 6beta that activates the mammalian unfolded protein response*. *Mol Cell Biol*, 2001. **21**(4): p. 1239-48.
92. Shoulders, M.D., et al., *Stress-independent activation of XBP1s and/or ATF6 reveals three functionally diverse ER proteostasis environments*. *Cell Rep*, 2013. **3**(4): p. 1279-92.
93. Thuerauf, D.J., et al., *Coordination of ATF6-mediated transcription and ATF6 degradation by a domain that is shared with the viral transcription factor, VP16*. *J Biol Chem*, 2002. **277**(23): p. 20734-9.
94. Elimam, H., et al., *Calcium-independent phospholipase A2gamma enhances activation of the ATF6 transcription factor during endoplasmic reticulum stress*. *J Biol Chem*, 2015. **290**(5): p. 3009-20.
95. Plate, L., et al., *Small molecule proteostasis regulators that reprogram the ER to reduce extracellular protein aggregation*. *Elife*, 2016. **5**.
96. Gallagher, C.M., et al., *Ceapins are a new class of unfolded protein response inhibitors, selectively targeting the ATF6alpha branch*. *Elife*, 2016. **5**.
97. Gallagher, C.M. and P. Walter, *Ceapins inhibit ATF6alpha signaling by selectively preventing transport of ATF6alpha to the Golgi apparatus during ER stress*. *Elife*, 2016. **5**.
98. Maiuolo, J., et al., *Selective activation of the transcription factor ATF6 mediates endoplasmic reticulum proliferation triggered by a membrane protein*. *Proc Natl Acad Sci U S A*, 2011. **108**(19): p. 7832-7.
99. Oglesby, I.K., et al., *miRNA-221 is elevated in cystic fibrosis airway epithelial cells and regulates expression of ATF6*. *Mol Cell Pediatr*, 2015. **2**(1): p. 1.
100. Belmont, P.J., et al., *Regulation of microRNA expression in the heart by the ATF6 branch of the ER stress response*. *J Mol Cell Cardiol*, 2012. **52**(5): p. 1176-82.
101. Wang, S. and R.J. Kaufman, *The impact of the unfolded protein response on human disease*. *J Cell Biol*, 2012. **197**(7): p. 857-67.
102. Hu, P., et al., *Autocrine tumor necrosis factor alpha links endoplasmic reticulum stress to the membrane death receptor pathway through IRE1alpha-mediated NF-kappaB activation and down-regulation of TRAF2 expression*. *Mol Cell Biol*, 2006. **26**(8): p. 3071-84.
103. Eferl, R. and E.F. Wagner, *AP-1: a double-edged sword in tumorigenesis*. *Nat Rev Cancer*, 2003. **3**(11): p. 859-68.
104. Tam, A.B., et al., *ER stress activates NF-kappaB by integrating functions of basal IKK activity, IRE1 and PERK*. *PLoS One*, 2012. **7**(10): p. e45078.
105. Zhang, Y., et al., *Peroxynitrite-induced neuronal apoptosis is mediated by intracellular zinc release and 12-lipoxygenase activation*. *J Neurosci*, 2004. **24**(47): p. 10616-27.
106. Yamazaki, H., et al., *Activation of the Akt-NF-kappaB pathway by subtilase cytotoxin through the ATF6 branch of the unfolded protein response*. *J Immunol*, 2009. **183**(2): p. 1480-7.
107. Nakajima, S., et al., *Selective abrogation of BiP/GRP78 blunts activation of NF-kappaB through the ATF6 branch of the UPR: involvement of C/EBPbeta and mTOR-dependent dephosphorylation of Akt*. *Mol Cell Biol*, 2011. **31**(8): p. 1710-8.

108. Shkoda, A., et al., *Interleukin-10 blocked endoplasmic reticulum stress in intestinal epithelial cells: impact on chronic inflammation*. *Gastroenterology*, 2007. **132**(1): p. 190-207.
109. Kaser, A., S. Zeissig, and R.S. Blumberg, *Inflammatory bowel disease*. *Annu Rev Immunol*, 2010. **28**: p. 573-621.
110. Goldsmith, J.R. and R.B. Sartor, *The role of diet on intestinal microbiota metabolism: downstream impacts on host immune function and health, and therapeutic implications*. *J Gastroenterol*, 2014. **49**(5): p. 785-98.
111. Sheehan, D., C. Moran, and F. Shanahan, *The microbiota in inflammatory bowel disease*. *J Gastroenterol*, 2015. **50**(5): p. 495-507.
112. Jostins, L., et al., *Host-microbe interactions have shaped the genetic architecture of inflammatory bowel disease*. *Nature*, 2012. **491**(7422): p. 119-24.
113. Liu, J.Z., et al., *Association analyses identify 38 susceptibility loci for inflammatory bowel disease and highlight shared genetic risk across populations*. *Nat Genet*, 2015. **47**(9): p. 979-986.
114. Uniken Venema, W.T., et al., *The genetic background of inflammatory bowel disease: from correlation to causality*. *J Pathol*, 2017. **241**(2): p. 146-158.
115. Kaser, A., et al., *XBP1 links ER stress to intestinal inflammation and confers genetic risk for human inflammatory bowel disease*. *Cell*, 2008. **134**(5): p. 743-56.
116. Zheng, W., et al., *Evaluation of AGR2 and AGR3 as candidate genes for inflammatory bowel disease*. *Genes Immun*, 2006. **7**(1): p. 11-8.
117. McGovern, D.P., et al., *Genome-wide association identifies multiple ulcerative colitis susceptibility loci*. *Nat Genet*, 2010. **42**(4): p. 332-7.
118. Barrett, J.C., et al., *Genome-wide association defines more than 30 distinct susceptibility loci for Crohn's disease*. *Nat Genet*, 2008. **40**(8): p. 955-62.
119. Kaser, A., E. Martinez-Naves, and R.S. Blumberg, *Endoplasmic reticulum stress: implications for inflammatory bowel disease pathogenesis*. *Curr Opin Gastroenterol*, 2010. **26**(4): p. 318-26.
120. Adolph, T.E., et al., *Paneth cells as a site of origin for intestinal inflammation*. *Nature*, 2013. **503**(7475): p. 272-6.
121. Zhao, F., et al., *Disruption of Paneth and goblet cell homeostasis and increased endoplasmic reticulum stress in Agr2^{-/-} mice*. *Dev Biol*, 2010. **338**(2): p. 270-9.
122. Park, S.W., et al., *The protein disulfide isomerase AGR2 is essential for production of intestinal mucus*. *Proc Natl Acad Sci U S A*, 2009. **106**(17): p. 6950-5.
123. Bertolotti, A., et al., *Increased sensitivity to dextran sodium sulfate colitis in IRE1 β -deficient mice*. *J Clin Invest*, 2001. **107**(5): p. 585-93.
124. Cao, S.S., et al., *The unfolded protein response and chemical chaperones reduce protein misfolding and colitis in mice*. *Gastroenterology*, 2013. **144**(5): p. 989-1000 e6.
125. Waldschmitt, N., et al., *C/EBP homologous protein inhibits tissue repair in response to gut injury and is inversely regulated with chronic inflammation*. *Mucosal Immunol*, 2014. **7**(6): p. 1452-66.
126. Namba, T., et al., *Positive role of CCAAT/enhancer-binding protein homologous protein, a transcription factor involved in the endoplasmic reticulum stress response in the development of colitis*. *Am J Pathol*, 2009. **174**(5): p. 1786-98.
127. Brandl, K., et al., *Enhanced sensitivity to DSS colitis caused by a hypomorphic Mbtps1 mutation disrupting the ATF6-driven unfolded protein response*. *Proc Natl Acad Sci U S A*, 2009. **106**(9): p. 3300-5.
128. Heazlewood, C.K., et al., *Aberrant mucin assembly in mice causes endoplasmic reticulum stress and spontaneous inflammation resembling ulcerative colitis*. *PLoS Med*, 2008. **5**(3): p. e54.
129. Wang, M. and R.J. Kaufman, *The impact of the endoplasmic reticulum protein-folding environment on cancer development*. *Nat Rev Cancer*, 2014. **14**(9): p. 581-97.

130. Forbes, S.A., et al., *COSMIC (the Catalogue of Somatic Mutations in Cancer): a resource to investigate acquired mutations in human cancer*. *Nucleic Acids Res*, 2010. **38**(Database issue): p. D652-7.
131. Greenman, C., et al., *Patterns of somatic mutation in human cancer genomes*. *Nature*, 2007. **446**(7132): p. 153-8.
132. Gutierrez, T. and T. Simmen, *Endoplasmic reticulum chaperones and oxidoreductases: critical regulators of tumor cell survival and immunorecognition*. *Front Oncol*, 2014. **4**: p. 291.
133. Koritzinsky, M., et al., *Two phases of disulfide bond formation have differing requirements for oxygen*. *J Cell Biol*, 2013. **203**(4): p. 615-27.
134. Hanahan, D. and R.A. Weinberg, *Hallmarks of cancer: the next generation*. *Cell*, 2011. **144**(5): p. 646-74.
135. Tang, C.H., et al., *Inhibition of ER stress-associated IRE-1/XBP-1 pathway reduces leukemic cell survival*. *J Clin Invest*, 2014. **124**(6): p. 2585-98.
136. Wek, R.C. and D.R. Cavener, *Translational control and the unfolded protein response*. *Antioxid Redox Signal*, 2007. **9**(12): p. 2357-71.
137. Zhang, P., et al., *The GCN2 eIF2alpha kinase is required for adaptation to amino acid deprivation in mice*. *Mol Cell Biol*, 2002. **22**(19): p. 6681-8.
138. Tameire, F., Verginadis, I., and C. Koumenis, *Cell intrinsic and extrinsic activators of the unfolded protein response in cancer: Mechanisms and targets for therapy*. *Semin Cancer Biol*, 2015. **33**: p. 3-15.
139. Ozcan, U., et al., *Loss of the tuberous sclerosis complex tumor suppressors triggers the unfolded protein response to regulate insulin signaling and apoptosis*. *Mol Cell*, 2008. **29**(5): p. 541-51.
140. Hart, L.S., et al., *ER stress-mediated autophagy promotes Myc-dependent transformation and tumor growth*. *J Clin Invest*, 2012. **122**(12): p. 4621-34.
141. Denoyelle, C., et al., *Anti-oncogenic role of the endoplasmic reticulum differentially activated by mutations in the MAPK pathway*. *Nat Cell Biol*, 2006. **8**(10): p. 1053-63.
142. Corazzari, M., et al., *Oncogenic BRAF induces chronic ER stress condition resulting in increased basal autophagy and apoptotic resistance of cutaneous melanoma*. *Cell Death Differ*, 2015. **22**(6): p. 946-58.
143. Nam, S., et al., *A pathway-based approach for identifying biomarkers of tumor progression to trastuzumab-resistant breast cancer*. *Cancer Lett*, 2015. **356**(2 Pt B): p. 880-90.
144. Arteaga, C.L., et al., *Treatment of HER2-positive breast cancer: current status and future perspectives*. *Nat Rev Clin Oncol*, 2011. **9**(1): p. 16-32.
145. Oromendia, A.B. and A. Amon, *Aneuploidy: implications for protein homeostasis and disease*. *Dis Model Mech*, 2014. **7**(1): p. 15-20.
146. Clarke, H.J., et al., *Endoplasmic reticulum stress in malignancy*. *Cancer Cell*, 2014. **25**(5): p. 563-73.
147. Bi, M., et al., *ER stress-regulated translation increases tolerance to extreme hypoxia and promotes tumor growth*. *The EMBO Journal*, 2005. **24**(19): p. 3470-3481.
148. Blais, J.D., et al., *Perk-dependent translational regulation promotes tumor cell adaptation and angiogenesis in response to hypoxic stress*. *Mol Cell Biol*, 2006. **26**(24): p. 9517-32.
149. Atkins, C., et al., *Characterization of a Novel PERK Kinase Inhibitor with Antitumor and Antiangiogenic Activity*. *Cancer Research*, 2013. **73**(6): p. 1993-2002.
150. Axten, J.M., et al., *Discovery of 7-Methyl-5-(1-{[3-(trifluoromethyl)phenyl]acetyl}-2,3-dihydro-1H-indol-5-yl)-7H-pyrrolo[2,3-d]pyrimidin-4-amine (GSK2606414), a Potent and Selective First-in-Class Inhibitor of Protein Kinase R (PKR)-like Endoplasmic Reticulum Kinase (PERK)*. *Journal of Medicinal Chemistry*, 2012. **55**(16): p. 7193-7207.

151. Yu, L., et al., *Anticipatory activation of the unfolded protein response by epidermal growth factor is required for immediate early gene expression and cell proliferation*. *Molecular and Cellular Endocrinology*, 2016. **422**: p. 31-41.
152. Pereira, E.R., et al., *Transcriptional and post-transcriptional regulation of proangiogenic factors by the unfolded protein response*. *PLoS One*, 2010. **5**(9).
153. Wang, Y., et al., *The Unfolded Protein Response Induces the Angiogenic Switch in Human Tumor Cells through the PERK/ATF4 Pathway*. *Cancer Research*, 2012. **72**(20): p. 5396-5406.
154. Pereira, E.R., et al., *Endoplasmic reticulum (ER) stress and hypoxia response pathways interact to potentiate hypoxia-inducible factor 1 (HIF-1) transcriptional activity on targets like vascular endothelial growth factor (VEGF)*. *J Biol Chem*, 2014. **289**(6): p. 3352-64.
155. Wang, Z.V., et al., *Spliced X-box binding protein 1 couples the unfolded protein response to hexosamine biosynthetic pathway*. *Cell*, 2014. **156**(6): p. 1179-92.
156. Denzel, M.S., et al., *Hexosamine pathway metabolites enhance protein quality control and prolong life*. *Cell*, 2014. **156**(6): p. 1167-78.
157. Hazari, Y.M., et al., *Emerging tale of UPR and cancer: an essentiality for malignancy*. *Tumour Biol*, 2016. **37**(11): p. 14381-14390.
158. Acosta-Alvear, D., et al., *XBP1 Controls Diverse Cell Type- and Condition-Specific Transcriptional Regulatory Networks*. *Molecular Cell*, 2007. **27**(1): p. 53-66.
159. Bobrovnikova-Marjon, E., et al., *PERK promotes cancer cell proliferation and tumor growth by limiting oxidative DNA damage*. *Oncogene*, 2010. **29**(27): p. 3881-3895.
160. Duplan, E., et al., *ER-stress-associated functional link between Parkin and DJ-1 via a transcriptional cascade involving the tumor suppressor p53 and the spliced X-box binding protein XBP-1*. *J Cell Sci*, 2013. **126**(Pt 9): p. 2124-33.
161. Mlynarczyk, C. and R. Fahraeus, *Endoplasmic reticulum stress sensitizes cells to DNA damage-induced apoptosis through p53-dependent suppression of p21(CDKN1A)*. *Nat Commun*, 2014. **5**: p. 5067.
162. Thomas, S.E., et al., *p53 and translation attenuation regulate distinct cell cycle checkpoints during endoplasmic reticulum (ER) stress*. *J Biol Chem*, 2013. **288**(11): p. 7606-17.
163. Zhang, F., et al., *Ribosomal stress couples the unfolded protein response to p53-dependent cell cycle arrest*. *J Biol Chem*, 2006. **281**(40): p. 30036-45.
164. Aguirre-Ghiso, J.A., *Models, mechanisms and clinical evidence for cancer dormancy*. *Nat Rev Cancer*, 2007. **7**(11): p. 834-846.
165. Yadav, R.K., et al., *Endoplasmic Reticulum Stress and Cancer*. *Journal of Cancer Prevention*, 2014. **19**(2): p. 75-88.
166. Thorpe, J.A. and S.R. Schwarze, *IRE1 α controls cyclin A1 expression and promotes cell proliferation through XBP-1*. *Cell Stress and Chaperones*, 2010. **15**(5): p. 497-508.
167. Brewer, J.W. and J.A. Diehl, *PERK mediates cell-cycle exit during the mammalian unfolded protein response*. *Proc Natl Acad Sci U S A*, 2000. **97**(23): p. 12625-30.
168. Hamanaka, R.B., et al., *PERK and GCN2 contribute to eIF2 α phosphorylation and cell cycle arrest after activation of the unfolded protein response pathway*. *Mol Biol Cell*, 2005. **16**(12): p. 5493-501.
169. Schewe, D.M. and J.A. Aguirre-Ghiso, *ATF6 α -Rheb-mTOR signaling promotes survival of dormant tumor cells in vivo*. *Proc Natl Acad Sci U S A*, 2008. **105**(30): p. 10519-24.
170. Mahadevan, N.R., et al., *Transmission of endoplasmic reticulum stress and pro-inflammation from tumor cells to myeloid cells*. *Proc Natl Acad Sci U S A*, 2011. **108**(16): p. 6561-6.
171. Mahadevan, N.R., et al., *Cell-Extrinsic Effects of Tumor ER Stress Imprint Myeloid Dendritic Cells and Impair CD8 $^+$ T Cell Priming*. *PLOS ONE*, 2012. **7**(12): p. e51845.

172. Urra, H., et al., *Endoplasmic Reticulum Stress and the Hallmarks of Cancer*. Trends in Cancer, 2016. **2**(5): p. 252-262.
173. Mahadevan, N.R. and M. Zanetti, *Tumor Stress Inside Out: Cell-Extrinsic Effects of the Unfolded Protein Response in Tumor Cells Modulate the Immunological Landscape of the Tumor Microenvironment*. The Journal of Immunology, 2011. **187**(9): p. 4403-4409.
174. Senft, D. and Z.E. Ronai, *Adaptive Stress Responses During Tumor Metastasis and Dormancy*. Trends Cancer, 2016. **2**(8): p. 429-442.
175. Feng, Y.-x., et al., *Epithelial-to-Mesenchymal Transition Activates PERK-eIF2 α and Sensitizes Cells to Endoplasmic Reticulum Stress*. Cancer Discovery, 2014. **4**(6): p. 702-715.
176. Lee, A.H., et al., *Proteasome inhibitors disrupt the unfolded protein response in myeloma cells*. Proc Natl Acad Sci U S A, 2003. **100**(17): p. 9946-51.
177. Obeid, M., et al., *Calreticulin exposure dictates the immunogenicity of cancer cell death*. Nat Med, 2007. **13**(1): p. 54-61.
178. Senovilla, L., et al., *An immunosurveillance mechanism controls cancer cell ploidy*. Science, 2012. **337**(6102): p. 1678-84.
179. Gomez, J.A., et al., *Synthetic embryonic lethality upon deletion of the ER cochaperone p58(IPK) and the ER stress sensor ATF6alpha*. Biochem Biophys Res Commun, 2014. **443**(1): p. 115-9.
180. Martindale, J.J., et al., *Endoplasmic reticulum stress gene induction and protection from ischemia/reperfusion injury in the hearts of transgenic mice with a tamoxifen-regulated form of ATF6*. Circ Res, 2006. **98**(9): p. 1186-93.
181. Toko, H., et al., *ATF6 is important under both pathological and physiological states in the heart*. J Mol Cell Cardiol, 2010. **49**(1): p. 113-20.
182. Kaser, A., T.E. Adolph, and R.S. Blumberg, *The unfolded protein response and gastrointestinal disease*. Semin Immunopathol, 2013. **35**(3): p. 307-19.
183. Miller, M., et al., *ORMDL3 transgenic mice have increased airway remodeling and airway responsiveness characteristic of asthma*. J Immunol, 2014. **192**(8): p. 3475-87.
184. Miller, M., et al., *ORMDL3 is an inducible lung epithelial gene regulating metalloproteases, chemokines, OAS, and ATF6*. Proc Natl Acad Sci U S A, 2012. **109**(41): p. 16648-53.
185. Li, Z. and Z. Li, *Glucose regulated protein 78: a critical link between tumor microenvironment and cancer hallmarks*. Biochim Biophys Acta, 2012. **1826**(1): p. 13-22.
186. Shuda, M., et al., *Activation of the ATF6, XBP1 and grp78 genes in human hepatocellular carcinoma: a possible involvement of the ER stress pathway in hepatocarcinogenesis*. J Hepatol, 2003. **38**(5): p. 605-14.
187. Hanaoka, M., et al., *Expression of ATF6 as a marker of pre-cancerous atypical change in ulcerative colitis-associated colorectal cancer: a potential role in the management of dysplasia*. J Gastroenterol, 2017.
188. Ginos, M.A., et al., *Identification of a gene expression signature associated with recurrent disease in squamous cell carcinoma of the head and neck*. Cancer Res, 2004. **64**(1): p. 55-63.
189. Lin, Y.H., et al., *Multiple gene expression classifiers from different array platforms predict poor prognosis of colorectal cancer*. Clin Cancer Res, 2007. **13**(2 Pt 1): p. 498-507.
190. Arai, M., et al., *Transformation-associated gene regulation by ATF6alpha during hepatocarcinogenesis*. FEBS Lett, 2006. **580**(1): p. 184-90.
191. Wu, X., et al., *A missense polymorphism in ATF6 gene is associated with susceptibility to hepatocellular carcinoma probably by altering ATF6 level*. Int J Cancer, 2014. **135**(1): p. 61-8.

192. Kresse, S.H., et al., *Mapping and characterization of the amplicon near APOA2 in 1q23 in human sarcomas by FISH and array CGH*. Mol Cancer, 2005. **4**: p. 39.
193. Guan, M., et al., *Nelfinavir induces liposarcoma apoptosis through inhibition of regulated intramembrane proteolysis of SREBP-1 and ATF6*. Clin Cancer Res, 2011. **17**(7): p. 1796-806.
194. Schepeler, T., et al., *Diagnostic and prognostic microRNAs in stage II colon cancer*. Cancer Res, 2008. **68**(15): p. 6416-24.
195. Chai, J., et al., *MicroRNA-455 inhibits proliferation and invasion of colorectal cancer by targeting RAF proto-oncogene serine/threonine-protein kinase*. Tumour Biol, 2015. **36**(2): p. 1313-21.
196. Rakoff-Nahoum, S., *Why cancer and inflammation?* Yale J Biol Med, 2006. **79**(3-4): p. 123-30.
197. Jess, T., C. Rungoe, and L. Peyrin-Biroulet, *Risk of colorectal cancer in patients with ulcerative colitis: a meta-analysis of population-based cohort studies*. Clin Gastroenterol Hepatol, 2012. **10**(6): p. 639-45.
198. Castano-Milla, C., M. Chaparro, and J.P. Gisbert, *Systematic review with meta-analysis: the declining risk of colorectal cancer in ulcerative colitis*. Aliment Pharmacol Ther, 2014. **39**(7): p. 645-59.
199. Berger, E.C., *Impact of unfolded protein responses on intestinal epithelial homeostasis in genetically modified mouse models*, in *Chair of Nutrition and Immunology*. 2014, Technical University Munich.
200. de Almeida, S.F., et al., *Chemical chaperones reduce endoplasmic reticulum stress and prevent mutant HFE aggregate formation*. J Biol Chem, 2007. **282**(38): p. 27905-12.
201. Grossmann, J., et al., *New isolation technique to study apoptosis in human intestinal epithelial cells*. Am J Pathol, 1998. **153**(1): p. 53-62.
202. Sato, T., et al., *Single Lgr5 stem cells build crypt-villus structures in vitro without a mesenchymal niche*. Nature, 2009. **459**(7244): p. 262-5.
203. Sato, T., et al., *Paneth cells constitute the niche for Lgr5 stem cells in intestinal crypts*. Nature, 2011. **469**(7330): p. 415-8.
204. Livak, K.J. and T.D. Schmittgen, *Analysis of relative gene expression data using real-time quantitative PCR and the 2(-Delta Delta C(T)) Method*. Methods, 2001. **25**(4): p. 402-8.
205. Irizarry, R.A., et al., *Summaries of Affymetrix GeneChip probe level data*. Nucleic Acids Res, 2003. **31**(4): p. e15.
206. Smyth, G.K., *Linear models and empirical bayes methods for assessing differential expression in microarray experiments*. Stat Appl Genet Mol Biol, 2004. **3**: p. Article3.
207. Benjamini, Y. and Y. Hochberg, *Controlling the False Discovery Rate: A Practical and Powerful Approach to Multiple Testing*. Journal of the Royal Statistical Society. Series B (Methodological), 1995. **57**(1): p. 289-300.
208. Ihaka, R. and R. Gentleman, *R: A Language for Data Analysis and Graphics*. Journal of Computational and Graphical Statistics, 1996. **5**(3): p. 299-314.
209. Lagkouvardos, I., et al., *Gut metabolites and bacterial community networks during a pilot intervention study with flaxseeds in healthy adult men*. Mol Nutr Food Res, 2015. **59**(8): p. 1614-28.
210. Edgar, R.C., *UPARSE: highly accurate OTU sequences from microbial amplicon reads*. Nat Methods, 2013. **10**(10): p. 996-8.
211. Edgar, R.C., et al., *UCHIME improves sensitivity and speed of chimera detection*. Bioinformatics, 2011. **27**(16): p. 2194-200.
212. Nitsche, U., et al., *Mucinous and signet-ring cell colorectal cancers differ from classical adenocarcinomas in tumor biology and prognosis*. Ann Surg, 2013. **258**(5): p. 775-82; discussion 782-3.

-
213. Nitsche, U., et al., *Integrative marker analysis allows risk assessment for metastasis in stage II colon cancer*. *Ann Surg*, 2012. **256**(5): p. 763-71; discussion 771.
214. Zeestraten, E.C., et al., *Specific activity of cyclin-dependent kinase 1 is a new potential predictor of tumour recurrence in stage II colon cancer*. *Br J Cancer*, 2012. **106**(1): p. 133-40.
215. Gao, J., et al., *Integrative analysis of complex cancer genomics and clinical profiles using the cBioPortal*. *Sci Signal*, 2013. **6**(269): p. p1.
216. Cerami, E., et al., *The cBio cancer genomics portal: an open platform for exploring multidimensional cancer genomics data*. *Cancer Discov*, 2012. **2**(5): p. 401-4.
217. Scaiewicz, V., et al., *CCAAT/enhancer-binding protein homologous (CHOP) protein promotes carcinogenesis in the DEN-induced hepatocellular carcinoma model*. *PLoS One*, 2013. **8**(12): p. e81065.
218. el Marjou, F., et al., *Tissue-specific and inducible Cre-mediated recombination in the gut epithelium*. *Genesis*, 2004. **39**(3): p. 186-93.
219. Chassaing, B., et al., *Dextran sulfate sodium (DSS)-induced colitis in mice*. *Curr Protoc Immunol*, 2014. **104**: p. Unit 15 25.
220. Yoon, S.H., et al., *Introducing EzBioCloud: a taxonomically united database of 16S rRNA gene sequences and whole-genome assemblies*. *Int J Syst Evol Microbiol*, 2017. **67**(5): p. 1613-1617.
221. Lagkouvardos, I., et al., *The Mouse Intestinal Bacterial Collection (miBC) provides host-specific insight into cultured diversity and functional potential of the gut microbiota*. 2016. **1**: p. 16131.
222. Zhang, B., S. Kirov, and J. Snoddy, *WebGestalt: an integrated system for exploring gene sets in various biological contexts*. *Nucleic Acids Res*, 2005. **33**(Web Server issue): p. W741-8.
223. Wang, J., et al., *WEB-based GENE SeT AnaLYsis Toolkit (WebGestalt): update 2013*. *Nucleic Acids Res*, 2013. **41**(Web Server issue): p. W77-83.
224. Liu, Z.P., et al., *RegNetwork: an integrated database of transcriptional and post-transcriptional regulatory networks in human and mouse*. *Database (Oxford)*, 2015. **2015**.
225. Treton, X., et al., *Altered endoplasmic reticulum stress affects translation in inactive colon tissue from patients with ulcerative colitis*. *Gastroenterology*, 2011. **141**(3): p. 1024-35.
226. Clevers, H., *At the crossroads of inflammation and cancer*. *Cell*, 2004. **118**(6): p. 671-4.
227. Niederreiter, L., et al., *ER stress transcription factor Xbp1 suppresses intestinal tumorigenesis and directs intestinal stem cells*. *J Exp Med*, 2013. **210**(10): p. 2041-56.
228. Heijmans, J., et al., *ER stress causes rapid loss of intestinal epithelial stemness through activation of the unfolded protein response*. *Cell Rep*, 2013. **3**(4): p. 1128-39.
229. Means, A.L., et al., *Pancreatic epithelial plasticity mediated by acinar cell transdifferentiation and generation of nestin-positive intermediates*. *Development*, 2005. **132**(16): p. 3767-76.
230. Li, Q., et al., *Disruption of Klf4 in villin-positive gastric progenitor cells promotes formation and progression of tumors of the antrum in mice*. *Gastroenterology*, 2012. **142**(3): p. 531-42.
231. Braunstein, E.M., et al., *Villin: A marker for development of the epithelial pyloric border*. *Dev Dyn*, 2002. **224**(1): p. 90-102.
232. Bobrovnikova-Marjon, E. and J.A. Diehl, *Coping with stress: ATF6alpha takes the stage*. *Dev Cell*, 2007. **13**(3): p. 322-4.
233. Totani, K., et al., *Effects of macromolecular crowding on glycoprotein processing enzymes*. *J Am Chem Soc*, 2008. **130**(6): p. 2101-7.

-
234. Kadowaki, H., et al., *Pre-emptive Quality Control Protects the ER from Protein Overload via the Proximity of ERAD Components and SRP*. Cell Rep, 2015. **13**(5): p. 944-56.
235. Preissler, S., et al., *Physiological modulation of BiP activity by trans-protomer engagement of the interdomain linker*. Elife, 2015. **4**: p. e08961.
236. Quan, W., Y.M. Lim, and M.S. Lee, *Role of autophagy in diabetes and endoplasmic reticulum stress of pancreatic beta-cells*. Exp Mol Med, 2012. **44**(2): p. 81-8.
237. Kelly, K.R., et al., *Reovirus therapy stimulates endoplasmic reticular stress, NOXA induction, and augments bortezomib-mediated apoptosis in multiple myeloma*. Oncogene, 2012. **31**(25): p. 3023-38.
238. Sun, S., et al., *Sel1L is indispensable for mammalian endoplasmic reticulum-associated degradation, endoplasmic reticulum homeostasis, and survival*. Proc Natl Acad Sci U S A, 2014. **111**(5): p. E582-91.
239. Bommasamy, H., et al., *ATF6alpha induces XBP1-independent expansion of the endoplasmic reticulum*. J Cell Sci, 2009. **122**(Pt 10): p. 1626-36.
240. Gregorieff, A., et al., *The ets-domain transcription factor Spdef promotes maturation of goblet and paneth cells in the intestinal epithelium*. Gastroenterology, 2009. **137**(4): p. 1333-45 e1-3.
241. Asada, R., et al., *The endoplasmic reticulum stress transducer OASIS is involved in the terminal differentiation of goblet cells in the large intestine*. J Biol Chem, 2012. **287**(11): p. 8144-53.
242. Elinav, E., et al., *Regulation of the antimicrobial response by NLR proteins*. Immunity, 2011. **34**(5): p. 665-79.
243. Jakobsson, H.E., et al., *The composition of the gut microbiota shapes the colon mucus barrier*. EMBO Rep, 2015. **16**(2): p. 164-77.
244. Johansson, M.E., et al., *Normalization of Host Intestinal Mucus Layers Requires Long-Term Microbial Colonization*. Cell Host Microbe, 2015. **18**(5): p. 582-92.
245. Johansson, M.E., et al., *Bacteria penetrate the inner mucus layer before inflammation in the dextran sulfate colitis model*. PLoS One, 2010. **5**(8): p. e12238.
246. Schwerbrock, N.M., et al., *Interleukin 10-deficient mice exhibit defective colonic Muc2 synthesis before and after induction of colitis by commensal bacteria*. Inflamm Bowel Dis, 2004. **10**(6): p. 811-23.
247. Fu, J., et al., *Loss of intestinal core 1-derived O-glycans causes spontaneous colitis in mice*. J Clin Invest, 2011. **121**(4): p. 1657-66.
248. Lu, P., et al., *Colonic gene expression patterns of mucin Muc2 knockout mice reveal various phases in colitis development*. Inflamm Bowel Dis, 2011. **17**(10): p. 2047-57.
249. Van der Sluis, M., et al., *Muc2-deficient mice spontaneously develop colitis, indicating that MUC2 is critical for colonic protection*. Gastroenterology, 2006. **131**(1): p. 117-29.
250. Wenzel, U.A., et al., *Spontaneous colitis in Muc2-deficient mice reflects clinical and cellular features of active ulcerative colitis*. PLoS One, 2014. **9**(6): p. e100217.
251. Wu, H., et al., *Integration of Hippo signalling and the unfolded protein response to restrain liver overgrowth and tumorigenesis*. Nat Commun, 2015. **6**: p. 6239.
252. Avruch, J., D. Zhou, and N. Bardeesy, *YAP oncogene overexpression supercharges colon cancer proliferation*. Cell Cycle, 2012. **11**(6): p. 1090-6.
253. Gregorieff, A., et al., *Yap-dependent reprogramming of Lgr5(+) stem cells drives intestinal regeneration and cancer*. Nature, 2015. **526**(7575): p. 715-8.
254. Bhinder, G., et al., *Intestinal epithelium-specific MyD88 signaling impacts host susceptibility to infectious colitis by promoting protective goblet cell and antimicrobial responses*. Infect Immun, 2014. **82**(9): p. 3753-63.
255. Frantz, A.L., et al., *Targeted deletion of MyD88 in intestinal epithelial cells results in compromised antibacterial immunity associated with downregulation of polymeric immunoglobulin receptor, mucin-2, and antibacterial peptides*. Mucosal Immunol, 2012. **5**(5): p. 501-12.

-
256. Couturier-Maillard, A., et al., *NOD2-mediated dysbiosis predisposes mice to transmissible colitis and colorectal cancer*. J Clin Invest, 2013. **123**(2): p. 700-11.
257. Trespi, E. and A. Ferrieri, *Intestinal bacterial overgrowth during chronic pancreatitis*. Curr Med Res Opin, 1999. **15**(1): p. 47-52.
258. Gibson, D.L., et al., *MyD88 signalling plays a critical role in host defence by controlling pathogen burden and promoting epithelial cell homeostasis during Citrobacter rodentium-induced colitis*. Cell Microbiol, 2008. **10**(3): p. 618-31.
259. O'Keefe, S.J., *Diet, microorganisms and their metabolites, and colon cancer*. Nat Rev Gastroenterol Hepatol, 2016. **13**(12): p. 691-706.
260. Uchiyama, K., et al., *Butyrate and bioactive proteolytic form of Wnt-5a regulate colonic epithelial proliferation and spatial development*. Sci Rep, 2016. **6**: p. 32094.
261. Comalada, M., et al., *The effects of short-chain fatty acids on colon epithelial proliferation and survival depend on the cellular phenotype*. J Cancer Res Clin Oncol, 2006. **132**(8): p. 487-97.
262. Ren, H., et al., *Short-chain fatty acids induce intestinal epithelial heat shock protein 25 expression in rats and IEC 18 cells*. Gastroenterology, 2001. **121**(3): p. 631-9.
263. Hu, S., et al., *Regional differences in colonic mucosa-associated microbiota determine the physiological expression of host heat shock proteins*. Am J Physiol Gastrointest Liver Physiol, 2010. **299**(6): p. G1266-75.
264. Donohoe, D.R., et al., *The Warburg effect dictates the mechanism of butyrate-mediated histone acetylation and cell proliferation*. Mol Cell, 2012. **48**(4): p. 612-26.
265. Zeller, G., et al., *Potential of fecal microbiota for early-stage detection of colorectal cancer*. Mol Syst Biol, 2014. **10**: p. 766.
266. Feng, Q., et al., *Gut microbiome development along the colorectal adenoma-carcinoma sequence*. Nat Commun, 2015. **6**: p. 6528.
267. Schwabe, R.F. and C. Jobin, *The microbiome and cancer*. Nat Rev Cancer, 2013. **13**(11): p. 800-12.
268. Li, Y., et al., *Gut microbiota accelerate tumor growth via c-jun and STAT3 phosphorylation in APCMin/+ mice*. Carcinogenesis, 2012. **33**(6): p. 1231-8.
269. Dove, W.F., et al., *Intestinal neoplasia in the ApcMin mouse: independence from the microbial and natural killer (beige locus) status*. Cancer Res, 1997. **57**(5): p. 812-4.
270. Peucker, K., et al., *Epithelial calcineurin controls microbiota-dependent intestinal tumor development*. Nat Med, 2016. **22**(5): p. 506-15.
271. Rakoff-Nahoum, S. and R. Medzhitov, *Regulation of spontaneous intestinal tumorigenesis through the adaptor protein MyD88*. Science, 2007. **317**(5834): p. 124-7.
272. Levy, J., et al., *Intestinal inhibition of Atg7 prevents tumour initiation through a microbiome-influenced immune response and suppresses tumour growth*. Nat Cell Biol, 2015. **17**(8): p. 1062-73.
273. Bergstrom, K., et al., *Defective Intestinal Mucin-Type O-Glycosylation Causes Spontaneous Colitis-Associated Cancer in Mice*. Gastroenterology, 2016.
274. Bao, Y., et al., *MicroRNA profiling in Muc2 knockout mice of colitis-associated cancer model reveals epigenetic alterations during chronic colitis malignant transformation*. PLoS One, 2014. **9**(6): p. e99132.
275. Velcich, A., et al., *Colorectal cancer in mice genetically deficient in the mucin Muc2*. Science, 2002. **295**(5560): p. 1726-9.
276. Martinon, F., et al., *TLR activation of the transcription factor XBP1 regulates innate immune responses in macrophages*. Nat Immunol, 2010. **11**(5): p. 411-8.
277. Sodhi, C.P., et al., *Intestinal epithelial Toll-like receptor 4 regulates goblet cell development and is required for necrotizing enterocolitis in mice*. Gastroenterology, 2012. **143**(3): p. 708-18 e1-5.

-
278. Afrazi, A., et al., *Toll-like receptor 4-mediated endoplasmic reticulum stress in intestinal crypts induces necrotizing enterocolitis*. J Biol Chem, 2014. **289**(14): p. 9584-99.
279. Yu, H., et al., *Revisiting STAT3 signalling in cancer: new and unexpected biological functions*. Nat Rev Cancer, 2014. **14**(11): p. 736-46.
280. Zhong, Z., Z. Wen, and J.E. Darnell, Jr., *Stat3: a STAT family member activated by tyrosine phosphorylation in response to epidermal growth factor and interleukin-6*. Science, 1994. **264**(5155): p. 95-8.
281. Stepkowski, S.M., et al., *STAT3: an important regulator of multiple cytokine functions*. Transplantation, 2008. **85**(10): p. 1372-7.
282. Sugimoto, K., *Role of STAT3 in inflammatory bowel disease*. World J Gastroenterol, 2008. **14**(33): p. 5110-4.
283. Eyking, A., et al., *Toll-like receptor 4 variant D299G induces features of neoplastic progression in Caco-2 intestinal cells and is associated with advanced human colon cancer*. Gastroenterology, 2011. **141**(6): p. 2154-65.
284. Grivennikov, S., et al., *IL-6 and Stat3 are required for survival of intestinal epithelial cells and development of colitis-associated cancer*. Cancer Cell, 2009. **15**(2): p. 103-13.
285. Hruz, P., S.M. Dann, and L. Eckmann, *STAT3 and its activators in intestinal defense and mucosal homeostasis*. Curr Opin Gastroenterol, 2010. **26**(2): p. 109-15.
286. Belmont, P.J., et al., *Roles for endoplasmic reticulum-associated degradation and the novel endoplasmic reticulum stress response gene Derlin-3 in the ischemic heart*. Circ Res, 2010. **106**(2): p. 307-16.
287. Kortylewski, M., et al., *Toll-like receptor 9 activation of signal transducer and activator of transcription 3 constrains its agonist-based immunotherapy*. Cancer Res, 2009. **69**(6): p. 2497-505.
288. Tye, H., et al., *STAT3-driven upregulation of TLR2 promotes gastric tumorigenesis independent of tumor inflammation*. Cancer Cell, 2012. **22**(4): p. 466-78.
289. Herrmann, A., et al., *TLR9 is critical for glioma stem cell maintenance and targeting*. Cancer Res, 2014. **74**(18): p. 5218-28.
290. Pickert, G., et al., *STAT3 links IL-22 signaling in intestinal epithelial cells to mucosal wound healing*. J Exp Med, 2009. **206**(7): p. 1465-72.
291. Bollrath, J., et al., *gp130-mediated Stat3 activation in enterocytes regulates cell survival and cell-cycle progression during colitis-associated tumorigenesis*. Cancer Cell, 2009. **15**(2): p. 91-102.
292. An, G., et al., *Increased susceptibility to colitis and colorectal tumors in mice lacking core 3-derived O-glycans*. J Exp Med, 2007. **204**(6): p. 1417-29.

CURRICULUM VITAE

Personal information:

Surname / First name	Lobner, Elena Maria
Nationality	German
E-mail	elena.lobner@tum.de

Work experience:

01/2012-03/2017	Research associate Department for Nutrition and Immunology (Technical University Munich)
Title of PhD thesis	Epithelial Cell-Specific Induction of Activating Transcription Factor 6 Signaling Promotes Intestinal Dysbiosis and Colonic Tumorigenesis

Education:

10/2009-11/2011	Master program Molecular Biotechnology (Technical University of Munich) Degree: Master of Science; with distinction
Title of Master thesis	Role of mitochondrial creatine kinase in mitochondrial unfolded protein response and during intestinal inflammation
10/2006-09/2009	Bachelor program Biochemistry (University of Ulm) Degree: Bachelor of Science
Title of Bachelor thesis	New interaction partners of Cla4p, a PAK-Kinase of the yeast <i>Saccharomyces cerevisiae</i>

PUBLICATIONS AND PRESENTATIONS

Peer-reviewed manuscripts

E. M. Lobner, Coleman, O. I., S. Bierwirth, A. Sorbie, N. Waldschmitt, E. Rath, E. Berger, I. Lagkourdos, T. Clavel, K. D. McCoy, A. Weber, M. Heikenwalder, K. P. Janssen and D. Haller (2018). "Activated ATF6 Induces Intestinal Dysbiosis and Innate Immune Response to Promote Colorectal Tumorigenesis." Gastroenterology.

Berger, E., E. Rath, D. Yuan, N. Waldschmitt, S. Khaloian, M. Allgauer, O. Staszewski, E. M. Lobner, T. Schottl, P. Giesbertz, O. I. Coleman, M. Prinz, A. Weber, M. Gerhard, M. Klingenspor, K. P. Janssen, M. Heikenwalder and D. Haller (2016). "Mitochondrial function controls intestinal epithelial stemness and proliferation." Nat Commun **7**: 13171.

Published abstracts

Lobner, E., O. Kober, E. Berger, T. Clavel, I. Lagkourdos, A. Weber and D. Haller "403 Tissue-Specific Induction of Activating Transcription Factor 6 Signaling Promotes Intestinal Dysbiosis and Colonic Tumorigenesis." Gastroenterology **148**(4): S-86.

Lobner, E., O. Kober, E. Berger, T. Clavel, I. Lagkourdos, A. Weber and D. Haller "435 Microbiota-Dependent Signals Link ATF6-driven Unfolded Protein Response to Colonic Tumorigenesis." Gastroenterology **150**(4): S90-S91.

Oral presentations

Annual meeting of German Nutrition Society (DGE) 2015 in Halle, Germany

Digestive Disease Week (DDW) 2015 in Washington, D.C., USA

International Congress of Mucosal Immunology (ICMI) 2015 in Berlin, Germany

Digestive Disease Week (DDW) 2016 in San Diego, USA

9th Seeon Conference "Microbiota, Probiota and Host", 2016 in Seeon, Germany

Poster presentations

5th Seeon Conference „Microbiota, Probiota and Host“, 2012 in Seeon, Germany

Keystone conference “Gut Microbiota Modulation of Host Physiology: The Search for Mechanism”, 2015 in Keystone, USA

8th Seeon Conference „From sequencing to function“, 2015 in Seeon, Germany

Grants

Young Investigators Travel Award International Congress of Mucosal Immunology (ICMI) 2015

Poster price 8th Seeon Conference „From sequencing to function“

Certificate of Recognition for “scientific accomplishment as an early stage investigator”, Digestive Disease Week (DDW) 2015

Memberships

TUM Graduate School since 2014

Associated fellow of the DFG-Graduate college 1482 “Interface functions of the intestine between luminal factors and host signals” since 2013

EIDESSTATTLICHE ERKLÄRUNG

Ich erkläre an Eides statt, dass ich die bei der promotionsführenden Einrichtung
Wissenschaftszentrum Weihenstephan für Ernährung, Landnutzung und Umwelt

der TUM zur Promotionsprüfung vorgelegte Arbeit mit dem Titel:
Epithelial Cell-Specific Induction of Activating Transcription Factor 6 Signaling Promotes Intestinal Dysbiosis and Colonic
Tumorigenesis

in Fakultät Wissenschaftszentrum Weihenstephan, Lehrstuhl für Ernährung und Immunologie
Fakultät, Institut, Lehrstuhl, Klinik, Krankenhaus, Abteilung

unter der Anleitung und Betreuung durch: Prof. Dirk Haller ohne sonstige Hilfe erstellt und bei der Abfassung nur die gemäß
§ 6 Ab. 6 und 7 Satz 2 angebotenen Hilfsmittel benutzt habe.

- Ich habe keine Organisation eingeschaltet, die gegen Entgelt Betreuerinnen und Betreuer für die Anfertigung von
Dissertationen sucht, oder die mir obliegenden Pflichten hinsichtlich der Prüfungsleistungen für mich ganz oder
teilweise erledigt.
- Ich habe die Dissertation in dieser oder ähnlicher Form in keinem anderen Prüfungsverfahren als Prüfungsleistung
vorgelegt.
- Die vollständige Dissertation wurde in _____
veröffentlicht. Die promotionsführende Einrichtung

_____ hat der Veröffentlichung zugestimmt.

- Ich habe den angestrebten Doktorgrad noch nicht erworben und bin nicht in einem früheren Promotionsverfahren für
den angestrebten Doktorgrad endgültig gescheitert.
- Ich habe bereits am _____ bei der Fakultät für _____
_____ der
Hochschule _____ unter
Vorlage einer Dissertation mit dem Thema _____
_____ die
Zulassung zur Promotion beantragt mit dem Ergebnis: _____

Die öffentlich zugängliche Promotionsordnung der TUM ist mir bekannt, insbesondere habe ich die Bedeutung von § 28
(Nichtigkeit der Promotion) und § 29 (Entzug des Doktorgrades) zur Kenntnis genommen. Ich bin mir der Konsequenzen
einer falschen Eidesstattlichen Erklärung bewusst.

Mit der Aufnahme meiner personenbezogenen Daten in die Alumni-Datei bei der TUM bin ich

- einverstanden, nicht einverstanden.

Eching, 14.11.2017, Unterschrift